TEMPERATURE AND PH-RESPONSIVE LAYER-BY-LAYER COATINGS FOR THE PREVENTION OF BACTERIAL COLONIZATION

A Dissertation

by

VICTORIA R. ALBRIGHT

Submitted to the Office of Graduate and Professional Studies of
Texas A&M University
in partial fulfillment of the requirements for the degree of

DOCTOR OF PHILOSOPHY

Chair of Committee,	Svetlana A. Sukhishvili
Committee Members,	Arul Jayaraman
	Jodie L. Lutkenhaus
	Daniel Alge
Head of Department,	Ibrahim Karaman

December 2019

Major Subject: Materials Science and Engineering

ABSTRACT

All biomaterials are prone to bacterial adhesion that can further lead to the development of biofilms, which are colonies of bacteria surrounded by extracellular polymeric substances that are notoriously difficult to treat. As a method to pre-emptively prevent biofilm formation, this dissertation research has focused on understanding how to create stimuli-responsive, layer-by-layer (LbL) polymer films that can controllably release antibiotics during the early stages of bacterial adhesion. Two complementary strategies have been explored for sequestering antibiotics in polymer films, namely (1) temperature-responsive micellar containers, which can trap hydrophobic small molecules, and (2) pH-responsive assemblies, which utilize changes in polymer ionization to uptake and release cationic small molecules. Recognizing that biomaterials often have complicated 3D structures, the LbL technique was chosen for constructing antimicrobial-hosting coatings as it enables uniform deposit on a variety of substrates and easily tunable antibiotic payload. My goal was to relate stimuli-responsive behavior of polymers in LbL films to their ability to selectively trigger release of small molecules and to establish methods to maximize antibiotic uptake while minimizing uncontrollably release, with a focus on preventing leaching at physiological pH (pH 7.5). Leaching antibiotics in normal physiological conditions is particularly undesirable as the presence of low levels of antibiotics has been shown to increase the chance for bacteria to develop resistance to that antibiotic. This goal was accomplished by studying the physicochemical characteristics of LbL coatings and correlating them with their antibiotic content and release profiles. My findings widen the fundamental knowledge about the functionality of temperature-

responsive micelles in LbL coatings and open the door to creating biocompatible LbL coatings *via* direct polymer assembly with antibiotics. Moreover, these results can be useful guidelines for designing antibiotic-loaded, stimuli-responsive LbL coatings and for developing the next generation of biomedical coatings.

ACKNOWLEDGEMENTS

I would like to thank my committee chair, Prof. Svetlana Sukhishvili, and my committee members, Prof. Arul Jayaraman, Prof. Jodie Lutkenhaus, and Prof. Daniel Alge, and my collaborators, Prof. Alexander Andrianov and Prof. Hongjun Wang for their guidance and support throughout the course of this research.

I would like to thank Svetlana for taking me along on this journey with her, with our relocation from NJ to TX, it has been quite an adventure over all of these years. Thank you to Svetlana for letting me explore many different scientific directions and always giving me an added dose of optimism. I would like to thank Svetlana for always allowing and encouraging me to multitask and work in many directions even if it didn't seem likely that I would be able to handle it all. Many thanks go to Svetlana for allowing me to have as many undergraduate students as I have had; I have really enjoyed this opportunity to develop my mentorship skills.

I would like to thank Prof. Jayaraman for providing me access to his bacterial research laboratory and his many insights on bacteria culture.

I would like to thank Professor Henny van der Mei and Professor Henk Busscher for giving me my first exposure to bacterial experiments and Professor Matthew Libera for allowing me to use his bacterial facilities back at Stevens and organizing the collaboration.

Many thanks to Prof. Hongjun Wang for all of the guidance over more skype meetings than I can count. Your expertise helped shape my research direction and your advice helped make our micelle coatings more practical for skin graft applications.

Thanks to Prof. Alexander Andrianov for giving us the opportunity to work with polyphosphazenes, I have really enjoyed exploring these novel materials.

Thanks to Prof. Christopher Quick and Andrew McNeely for organizing the Aggie Research Program; I am very grateful that I was given the chance to participate in it. Thanks to my undergraduates for being so curious and optimistic. You all were an inspiration to me and your energy helped to re-energize me when I was in doubt. Thank you all for helping me to grow into a much better mentor than I was when I started out.

Thanks to Jules Henry and Erin Bandza for helping me with all the academic paperwork and making my graduation become a reality. Thanks to Hanna Prichard, Sheri Stebenne, and Jules Henry for always being there to talk to and being so supportive of Women in Materials Science (WIMS), especially during our early years. Many thanks to Murat Kaynak for always helping our lab, especially for helping us during our move of the lab here. Without you, we would not have made it.

Thanks to the MSEN department head, Ibrahim Karaman, for his support. Your constant support in my future career and encouragement to push myself further helped me to succeed.

Thanks to Amy Bolon, Tim Brown, Hanna Hlushko, Natalie Benner, Christa Torrence, Mengying Liu, and many others for helping to establish Women in Materials Science (WIMS) and make it into a success. I really enjoyed the supportive network that we formed. I am forever grateful for all of your help participating in numerous outreach activities, without all of you, it would not have been possible.

Thanks to my lab mates including Yuhao Wang, Anbu Palanisamy, Victor Selin, Hanna Hlushko, Raman Hlushko, Alex Aliakseyeu, Parvin Karimineghlani, Diana Al Husseini, Adwait Gaikwad, and Qing Zhou.

Many thanks go out to all of my friends for their constant support and willingness to always lend an ear. A special thanks to Hanna Hlushko for always encouraging me and pushing me to go further than I thought I could. Thorough our time here we participated in very many activities together, many of which I am not sure I would have been brave enough to go to alone. Thank you Daniel Penarete for always making me laugh and smile even when I had a horribly elaborate experiment to do. Thanks to Christa Torrence for always being there to support and encourage me. Many thanks to my NJ friends for having flexible schedules and always making time to see when I would briefly come home.

Thanks to my parents for supporting me thorough all of my academic endeavors, my move across the country, and for never letting me give up on my dreams. Thank you for all of your continuous love and support. Thanks to my dad for always talking to me on my many long drives between Houston and College Station. Thanks to my mom for sending me countless care packages full of yummy baked goods and other special treats. Thanks to my soon-to-be mother- and father-in laws for their support and positivity. The excitement of all my parental figures about the potential of my work was much appreciated.

More thanks than I can count to my very soon to be Husband, Tim. Being in a long distance relationship thorough my Ph. D. time is not something that either of us thought we would manage, but we are so much stronger now because of it. Thank you. For all the

late nights when I wasn't home to be with you, for all the times I called you in a panic because I didn't know how I was going to finish everything on my plate, for all the times that I asked for your help for doing boring, tedious tasks like helping me revive endnote references that I killed or making sure all the fonts on my presentation slides matched. I would not have been able to make it through this program without your love and support. I love you so much and cannot wait to be Mr. and Mrs. Barbright.

CONTRIBUTORS AND FUNDING SOURCES

Contributors

This work was supervised by a dissertation committee consisting of Professor Svetlana Sukhishvili of the Department of Materials Science & Engineering, Professor Arul Jayaraman of the Departments of Chemical and Biomedical Engineering, Professor Jodie Lutkenhaus of the Department of Chemical Engineering and Professor Daniel Alge of the Department of Biomedical Engineering. Throughout the Ph.D. program, the student participated in two collaborations with Professor Hongjun Wang's group at Stevens Institute of Technology and Professor Andrianov Alexander's group at the University of Maryland.

Upper critical solution temperature micelles (Chapters 2-5) were synthesized by Anbazhagan (Anbu) Palanisamy, who was a post-doc in the Sukhishvili group. Also in chapter 4, Anbu also deposited the micelles on fibers, did SEM imaging of coatings, and performed degradation studies on flat substrates. Aliaksei (Alex) Aliakseyeu performed isothermal titration calorimetry studies and fitted neutron reflectrometry data in Chapter 3. Neutron measurements (Chapter 3) were performed by Victor Selin at the Spallation Neutron Source at the Oak Ridge National Laboratory. Electrospun fibers used in this work (Chapters 4 and 5) were provided by Dr. Hongjun Wang's group at Stevens Institute of Technology. Human cell studies in Chapter 4 were done by Meng Xu from Dr. Hongjun Wang's group at Stevens Institute of Technology. Tjitske Boekema from the University of Groningen Netherlands performed Petrifilm and flow experiments in Chapter 5. Yuhao Wang performed confocal microscopy imaging in Chapter 5.

All polyphosphazenes used in this work (Chapters 7 to 9) were synthesized by Prof. Andrianov's group at the University of Maryland. All hemocompatibility studies done in this work (Chapters 7 to 9) were done by Prof. Andrianov's group at the University of Maryland. Hanna Hlushko did the SEM imaging in Chapters 5, 8, and 9 and the XPS analysis in Chapter 7. Cell studies in Chapter 9 were done by Daniel Penarete from Dr. Jayaraman's group at Texas A&M University. LC-MS work (Chapter 9) was done by the Integrated Metabolomics Analysis Core at Texas A&M University.

Additionally, the student participated in the Aggie Research Program throughout her Ph.D. resulting in the mentoring of 17 undergraduate students. These students helped prepare various layer-by-layer coatings and measure some time points for various assays. Please note that while undergraduates helped to deposit films or collect data in various cases, all data was analyzed by the student. The names of the students, their majors, and time frame in which they worked in the lab are listed below.

1. Haley Nelson, Chemical Engineering (Summer 2016, Fall 2016, Spring 2017, Fall 2017)
2. Miranda Molina, Biomedical Sciences (Summer 2016, Fall 2016)
3. Steven Strack, Chemical Engineering (Summer 2016)
4. Jesse York, Chemical Engineering (Spring 2017)
5. Emily Janak, Biomedical Sciences and Nutrition, (Spring 2017)
6. Christopher Erb, General Engineering, (Spring 2017)
7. Anh Tran, Chemical Engineering (Fall 2017)
8. Shabba Armbrister, Biomedical Sciences (Fall 2017, Spring 2018, Summer 2018)

9. Cynthia Co, Biomedical Engineering (Fall 2017, Spring 2018);

10. Matthew Andreo, Biomedical Engineering (Spring 2018, Fall 2018)

11. Samantha Hernandez, Biomedical Sciences (Spring 2018, Summer 2018, Fall 2018, Spring 2019, Summer 2019, Fall 2019)

12. Christina Abraham, Materials Science & Engineering (Fall 2018)

13. Jayant Singh, General Engineering (Fall 2018)

14. Christian Frey, Biology (Fall 2018, Spring 2019, Summer 2019, Fall 2019)

15. Jeremy Zheng, Biomedical Engineering (Spring 2019, Summer 2019, Fall 2019)

16. Danielle Yarbrough, Chemical Engineering (Spring 2019, Summer 2019, Fall 2019)

17. Lillian Mortensen, Materials Engineering, (Summer REU 2019)

All other work conducted for the dissertation was completed by the student.

Funding Sources

Graduate study was supported by a fellowship from Texas A&M University/Association of Former Students Graduate Merit Fellowship and Texas A&M Engineering Experiment Station (TEES). This work was supported by the National Science Foundation under Award DMR-1808483 (S.S.) and 1808531 (A.A.). This work was also made possible in part by NSF-DMR award number 1610725. Its contents are solely the responsibility of the authors and do not necessarily represent the official views of the NSF or any other funding agency.

NOMENCLATURE

ABTS	(2,2'-azino-bis(3-ethylbenzothiazoline-6-sulphonic acid)
Abx	Antibiotics
ACT	1-(3-Dimethylaminopropyl)-3-ethylcarbodiimide hydrochloride
ATCC	American Type Culture Collection
BCM	Block Copolymer Micelle
BHI	Brain Heart Infusion
BL	Bilayer
BPEI	Branched polyethyleneimine
CA	Contact Angle
CFU	Colony Forming Units
CLSM	Confocal Laser Scanning Microscopy
DAPI	4′,6-diamidino-2-phenylindole
DMEM	Dulbecco's Modified Eagle Medium
DMSO	Dimethyl Sulfoxide
E. coli	*Escherichia coli*
ECM	Extracellular Matrix
EDA	Ethylene diamine
FBS	Fetal Bovine Serum
FESP	Polyphosphazene with p-sulfophenoxy-, ethylphenoxy- and trifluoroethoxy- side groups
FITC	Fluorescein isothiocyanate

FPSP	Polyphosphazene with p-sulfophenoxy-, ethylphenoxy- and trifluoromethylphenoxy- side groups
FPXX	Fluorinated Polyphosphazene with XX% of Fluorinated Groups
FTIR	Fourier-Transform Infrared Spectroscopy
Gent	Gentamicin
h	Hours (of culturing)
HAS	Human Serum Albumin
HEPES	(4-(2-hydroxyethyl)-1-piperazineethanesulfonic acid)
HFIP	Hexafluoroisopropanol
HPLC	High Pressure Liquid Chromatography
ITC	Isothermal Titration Calorimetry
LbL	Layer-by-Layer
LC-MS	Liquid Chromatography-Mass Spectrometry
LCST	Lower Critical Solution Temperature
MIC	Minimum Inhibitory Concentration
MRSA	Methicillin-Resistant *S. aureus*
MTT	(3-(4,5-dimethylthiazol-2-yl)-2,5-diphenyltetrazolium bromide)
Mw	Molecular Weight
NFs	Nanofibers
NHDFs	Normal Human Dermal Fibroblasts

NMR	Nuclear Magnetic Resonance
NR	Neutron Reflectometry
OD	Optical Density
P(Aam-co-AN)	poly(acrylamide-*co*-acrylonitrile)
PAA	Polyacrylic acid
PB	Phosphate Buffer
PBS	Phosphate Buffered Saline
PCL/Coll	Polycaprolactone-Collagen
PCPP	Poly[di(carboxylatophenoxy)phosphazene]
PDCP	Polydichlorophosphazene
PDI	Polydispersity Index
PEG	polyethylene glycol
PGMA	Poly(glycidyl methacrylate)
PMAA	Poly(methacrylic) acid
PNAGA	poly(N-acryloyl glycinamide)
PNIPAM	Poly(N-isopropylacrylamide)
Poly B	Polymyxin B
PPzs	Polyphosphazenes
PSS	Polystyrene Sulfonate
PTFEP	Poly[bis(trifluoroethoxy)phosphazene]
PVCL	Polyvinylcaprolactam

PVP	Polyvinylpyrrolidone
PVP-*b*-PUOL	Polyvinylpyrrolidone-*b*-polyureido(ornithine-*co*-lysine)
RAFT	Reversible Addition-Fragmentation Chain Transfer
RBC	Red Blood Cells
S. aureus	*Staphylococcus aureus*
S. epi	*Staphylococcus epidermidis*
SEM	Scanning Electron Microscopy
SNARF-1	SNARF-1 carboxylic acid, acetate, succinimidyl ester
SP	Poly[di(phenoxyphosphazenesulfonic acid)]
SRM	Selected Reaction Monitoring
TA	Tannic acid
TGF-β1	Transforming Growth Factor - Beta1
TRITC	Tetramethylrhodamine
TSB	Tryptic Soy Broth
UCST	Upper Critical Solution Temperature
UCSTM	Upper Critical Solution Temperature Micelles
VASE	Variable Angle Spectroscopic Ellipsometer
XPS	X-ray photoelectron spectroscopy
ZOI	Zone of Inhibition
α-SMA	Alpha Smooth Muscle Actin

TABLE OF CONTENTS

LIST OF FIGURES

Page

LIST OF TABLES

Page

1. INTRODUCTION

1.1. The Problem of Biofilm Formation

Bacterial colonization of biomedical devices is a common occurrence on a wide range of materials ranging from catheters to hip implants.[1] When bacteria attach to a surface, they tend to form communities, called biofilms[2] as shown in Figure 1-1. In biofilms, bacteria are surrounded by an extracellular polymeric substance matrix and have reduced metabolism rates. As such, bacteria in biofilms are notoriously hard to treat with conventional systemic antibiotics.[3-7] Moreover, biofilms-associated infections occur on a wide range of biomedical devices, increasing patient suffering and cost of treatment.[8] Such infection can even cause material failure; as an example, for skin grafts, infection with $>10^5$ colony forming units (CFU) per gram of tissue causes about 80% of skin grafts to fail.[9] If systemic antibiotics cannot stop the biomaterials-associated infection, the normal course of action is to remove and replace the implant entirely,[10] with the new implant having a much higher chance of infection.[1] Therefore, prevention of bacterial colonization of surfaces at early stages, *i.e.* upon adhesion of first few bacteria to the surface, is crucial.

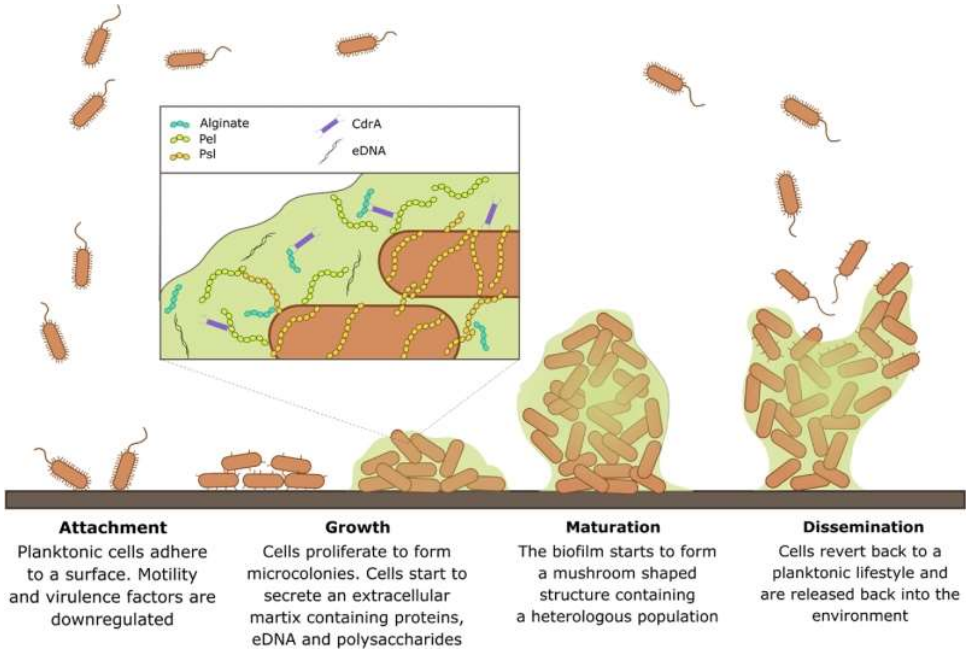

Figure 1-1. Diagram showing how bacterial adhesion to surfaces leads to biofilm formation. Reprinted with permission from[11] Copyright 2017 FEMS.

1.2. Methods to Prevent Biofilm Formation

Many strategies have been developed to combat bacterial attachment and biofilm formation on surfaces.[12-15] Two broad categories have been explored that focus on (1) preventing bacterial adhesion or (2) killing bacteria near/on surfaces. Anti-adhesive properties can be endowed to surfaces in a variety of ways including using highly hydrated polymers in the form of polymer brushes or coatings.[16-18] Similarly, antibacterial surfaces can be engineered by using cationic polymers as brushes[19,20] or in coatings to kill bacteria upon contact.[21] Alternatively, antibacterial coatings can be engineered to sequester small molecule antibiotics and release them in a large variety of profiles. Such coatings (*i.e.* antibiotic releasing) will be the focus of this work.

Many methods to controllable delivery antibiotics have been developed. One method has been to disperse drugs in a polymeric matrix to provide burst and continuous release of antimicrobial agents.[22] While such materials have shown promise in clinical applications, these materials often exhibit burst release followed by a long tail release with sub-lethal concentrations.[23] Exposure of bacterial strains to sub-lethal concentrations of antibiotics is correlated with increasing antibacterial resistance,[24] and therefore, should be avoided. A strategy to avoid such release is to design a stimuli-responsive polymeric material.[25] To that end, a large variety of materials that respond to various stimuli have been explored including pH, electrical pulses,[26] ultra-sound,[27,28] light,[29,30] and temperature.[31] My dissertation has focused on two practical, yet parallel, stimuli for releasing antibiotics: temperature and pH. Temperature is an easy to apply stimulus that is attractive for biomedical applications,[32] and is relevant to bacterial colonization as bacterial infections often cause an increase in temperature (*i.e.* fever). pH is an attractive stimulus as several bacterial strains, including *Staphylococcus aureus* and *Escherichia coli,* are known to acidify the medium in which they grow as a result of secretion of lactic and acetic acid, respectively.[33,34]

1.3. Stimuli-Responsive Layer-by-Layer Coatings

One convenient way to make stimuli responsive polymer coatings is to use the layer-by-layer assembly (LbL) technique, shown schematically in Figure 1-2. LbL was first established by Decher[35,36] and is a well-established method for attaching polymers and nanoparticles to surfaces that enables the retention of stimuli-responsive behavior for a wide range of biomedical applications.[37-40] Importantly, LbL assembly can be done on

materials of a variety of dimensions including nanoparticles,[41] nanopillars,[42] and nanofibers.[43,44] The LbL assembly technique will be used here to deposit both temperature and pH responsive coatings. Our goal is to engineer stimuli-responsive LbL films that are non-leachable in normal physiological conditions, yet deliver antibiotics on-demand when prompted. Such coatings can be used to endow biomedical surfaces such as sutures, stents, catheters, orthopedic implants, etc. with the ability to prevent biofilm formation as it is beginning. To achieve this goal, stimuli-responsive behavior of temperature- and pH-responsive polymers in LbL films will be correlated with their ability to selectively retain and release of small molecules. Two different strategies of temperature- and pH-stimulus will be used to sequester hydrophobic and hydrophilic antibiotics in micellar containers and through the use of electrostatic-interactions, respectively.

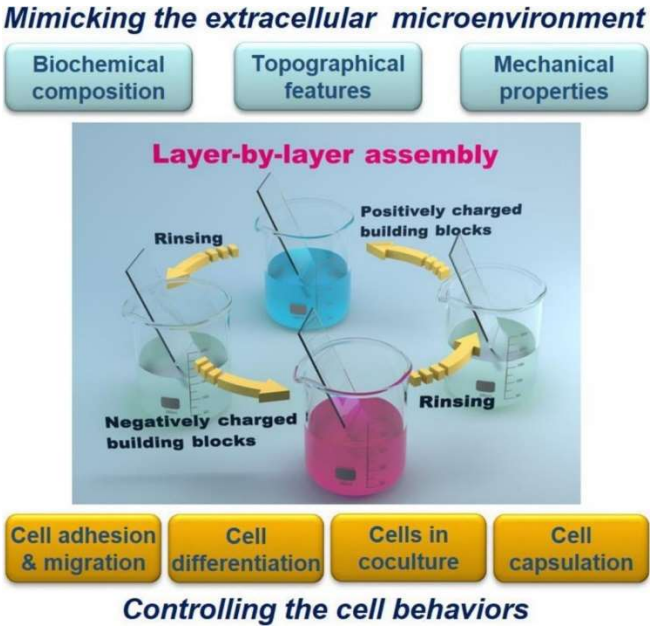

Figure 1-2. Schematic of layer-by-layer (LbL) assembly as well as features and properties endowed by LbL. Reprinted with permission from [45]. Copyright 2019 Elsevier B. V.

1.4. Strategies for Trapping Small Molecules in LbL Assemblies

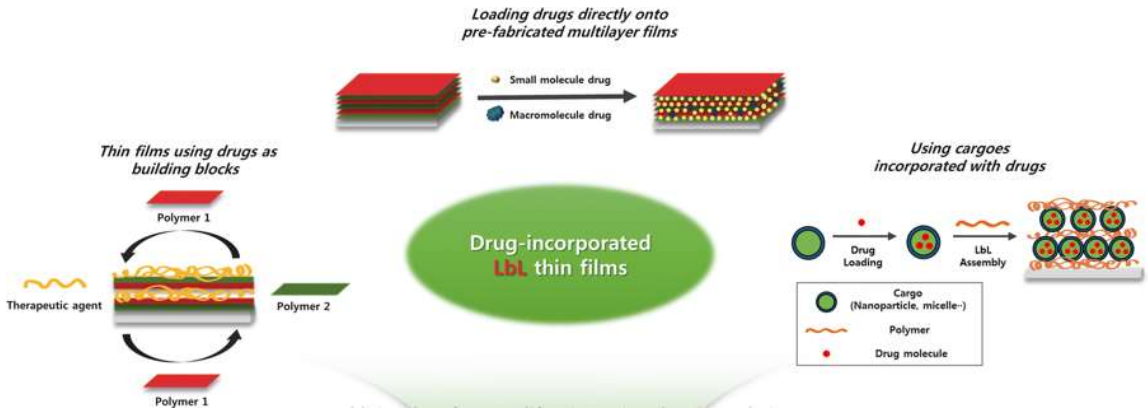

Figure 1-3. Different ways to incorporate drugs into LbL assemblies, modified and reprinted from [46]. Copyright 2018 The Author(s) (Park, Han, Choi, and Hong). http://creativecommons.org/licenses/by/4.0/

Depositing small molecules in LbL coatings is challenging, as small molecules have few binding points and low binding energy, which generally results in these molecules being easily washed out of films. To combat this, many strategies have been developed for trapping small molecules.[47] One method is to directly conjugate an antibiotic to a polymer chain.[48] However, this requires that the antibiotic has a chemical site that is reactive to enable conjugation. Moreover, conjugation may influence the efficacy of the antibiotic itself. An alternative strategy to trap small molecules, that works best for neutral, hydrophobic molecules, is inside nanocarriers such as micelles,[49] dendrimers,[50] or cyclodextrins.[51] This method can be and has been combined with LbL depositon. For example, biodegradable polyethyelene oxide-*block*-polycaprolcatone micelles were LbL assembled with polyacrylic acid and shown to trap triclosan, an uncharged antibitoic.[52] Moreover, Smith et al. showed that LbL assemblies of biodegradable poly(β-amino esters) with polymerized cyclodextrins give drug release profiles that were tunable by

degradation rate of the poly(β-amino esters).[53] Moreover, using nanocontainers that reversibly form due to a trigger such as pH or temperature is a facile way to combine the capture of hydrophobic small molecules with stimuli-response. Both pH and temperature micelles have been explored for encapsulation in LbL.[52,54-61]

In contrast to micellar coatings which trap a hydrophobic payload by partitioning, anionic polymers can be used to sequester cationic antibiotics through electrostatic interactions. This strategy can be applied by pre-building films and then loading them with drugs. In this case, surface-attached thin hydrogels are attractive.[62,63] These materials have been shown to trap cationic antimicrobials efficiently. This works well for charged classes of antibiotics such as aminoglycosides, polymyxins. However, one challenge with this approach is that antibiotics are retained through electrostatic-interactions that are susceptible to partial disruption upon immersion in salt solutions. To enhance antibiotic uptake, secondary interactions can be endowed to the polymers to increase binding strength.

In another strategy, antibiotics can be directly assembled as one of the layers of the LbL assembly. Only a few reports of coatings of this type exist to date. Quadlayers of polyacrylic acid, poly(beta-amino esters), and gentamicin were reported, which showed tunable release of gentamicin driven by the degradation of the polyesters.[64] While such coatings showed efficacy against *Staphylococcus aureus* in a rabbit bone model,[65] the release was continuous and not "on-demand". In contrast, multilayers of tannic acid, a small polyphenol, with cationic antibiotics (tobramycin, gentamicin, and polymyxin B), were recently reported with pH-responsive release. [66]

For the trapping of hydrophobic molecules, this work explores the use of temperature-responsive micelle coatings. Here, we explore a new kind of temperature triggered release: release of molecules in response to an increase in temperature or upper critical solution temperature (UCST) behavior. Temperature-responsive micelles will be deposited in hydrogen-bonding LbL films on planar, Si wafers, and 3D nanofiber (NF) substrates with both synthetic polymers and small molecules. The influence of binding partner ionization on film growth and temperature-responsive properties will be studied. Specifically, temperature-responsive swelling of micelle films will be quantified with *in situ* ellipsometry and correlated with their ability to uptake and release small molecules as measured by spectrofluorimetry. The deposition of micellar films on polycaprolactone-collagen (PCL/Coll) nanofiber surfaces will be explored as a way to introduce secondary topographic features, which may modulate cellular responses, bring antioxidant capabilities, and offer the ability to deliver therapeutic molecules on-demand. The ability of such coatings loaded with antibiotics to prevent infection will be assessed with *Staphylococcus aureus*.

To trap hydrophilic, cationic antibiotics, both strategies of loading antibiotics into pre-assembled films and depositing antimicrobials as a layer component will be explored. For loading, pre-assembled films, a hydrogel-like, crosslinked poly(methacrylic acid) (PMAA) film will be constructed. To better understand the release mechanism of these films, a pH-responsive fluorescent probe will be attached to the film and imaged with confocal microscopy after exposure to various pH conditions and *Staphylococcus aureus* bacterial cultures. To verify that local pH acidification is the mechanism of release,

coatings will be exposed to flowing, large volume, highly buffered solutions, which prevent changes of bulk culture pH. For this experiment, pH-responsive hydrogels are exposed to high numbers of *S. aureus* in flowing buffer and then imaged to quantify bacterial adhesion as well as live/dead ratio of bacteria.

Next, we explore the assembly of polyphosphazenes first with polymeric partners, to better understand the material behavior, and then with small molecules to understand their potential for biomedical coatings. Polyphosphazenes (PPzs) are unique class of polymers with an inorganic backbone and organic side groups. PPzs display a high degree of flexibility of their backbone,[67,68] facile tunability of their degradation rate with physiologically benign degradation products,[69-71] and have a proven record of preclinical and clinical safety.[72-77] The ease of varying the side groups of PPzs makes them excellent candidates for systemically exploring the combined effects of electrostatic and hydrophobic interactions on antibiotic retention and release.

First, we study the influence of fluorination degree and ionic group type on PPz assembly with cationic, branched polyethylene imine in terms of layer growth, contact angle, swelling, and importantly, hemocompatibility. Specifically, ionic, non-fluorinated poly[di(carboxylatophenoxy)phosphazene] (PCPP) and ionic, fluorinated PPzs of fluorinated degrees varying from 20% to 86% are explored to understand how hydrophobic microenvironments may influence charge-charge interactions. Additionally, sulfonated and fluorinated PPzs are explored to understand the influence of ionic pair strength. Lastly, we explore the direct assembly of cationic small molecules (Polymyxin B, Gentamicin, Neomycin, Colistin) in LbL with ionic, fluorinated PPzs and ionic, non-

fluorinated poly[di(carboxylatophenoxy)phosphazene] (PCPP). The influence of fluorination degree on film growth, film swelling, and antibiotic content, and pH-responsive release will be measured through spectroscopic ellipsometry (dry and *in situ*) and liquid chromatography-mass spectrometry (LC-MS), respectively. After showing that fluorination degree of coatings modulates pH-responsive release, we aim to explore the hemocompatibility, cytocompatibility, and long term antibacterial efficacy of these coatings. Antibacterial performance of coatings will be assessed with *S. aureus* and *Escherichia coli*.

2. FUNCTIONAL SURFACES THROUGH CONTROLLED ASSEMBLIES OF UPPER CRITICAL SOLUTION TEMPERATURE BLOCK COPOLYMERS[1]

2.1. Introduction

Stimuli-responsive polymeric materials are highly desirable for advanced biomedical,[25] actuation,[79,80] and sensing devices. Among various stimuli that can be applied to polymeric materials, (e.g. pH,[81,82] electrical pulses,[26] ultra-sound,[27,28] light,[29] and temperature[31]), temperature is one of the most important triggers for materials in biomedical,[32] food packaging,[83] and smart textile applications.[84] Therefore, significant effort has been focused on the development of temperature-responsive polymers, especially those that can demonstrate temperature response in aqueous environments.

The application of a temperature stimulus to polymers results in changes in their degree of hydration degree and conformational state.[85] In the simplest case of linear polymer chains in solution, such changes lead to phase separation occurring *via* several stages of coil-to-globule collapse and inter-chain aggregation.[86] The mode of temperature response of polymers in water, *i.e.* LCST or UCST behavior, is defined by a delicate balance of temperature-dependent enthalpic and entropic contributions associated with water-water, water-polymer, and polymer-polymer interactions.[87,88] Since water has a strong tendency to form water-water hydrogen bonds, the overall phase behavior of

[1] Reprinted in part with permission from Albright, V.; Palanisamy, A.; Zhou, Q.; Selin, V.; Sukhishvili, S. A. Functional Surfaces through Controlled Assemblies of Upper Critical Solution Temperature Block and Star Copolymers. *Langmuir* **2019**, *35*, 10677-10688. Copyright 2019 American Chemical Society. Please note in the original article, ucst micelles vs. star polymers were discussed, as I have only worked on micelles and not on stars, stars have been removed from this copy of the text.

polymers in aqueous solutions is governed by the competitive bonding of polymer functional groups with self-associating water molecules. Water can solvate hydrophobic groups of polymers by forming low-entropy solvation shells,[89,90] or can directly hydrogen bond to proton-accepting polymers groups.[87,91] It is generally accepted that hydrophobic hydration largely contributes to LSCT-type transitions in polymer solutions, which are typically endothermic because of the heat absorbed during restructuring of the solvation shell of collapsing coils[91-93] and breakage of polymer-water hydrogen bonds.[94] Note that the contribution of dehydration of methyl groups of PNIPAM during LCST transitions was directly shown spectroscopically.[95] Because of their strong association to the energetics of the hydration, LCST transitions in aqueous solutions are weakly dependent of polymer concentration and/or molecular weight.[96] Interestingly, the addition of an organic solvent can destroy the low-entropy hydration shells, and first eliminate and then even invert temperature response from LCST to UCST.[95]

Unlike LCST, UCST behavior is mostly governed by polymer-polymer binding, while also depending on polymer-solvent hydrogen bonding.[97] For UCST systems, the entropy term is mostly defined by the distribution of chains in solution rather than formation of the hydration shell, and phase separation is associated with a decrease in entropy of mixing upon cooling and the resulting domination of the enthalpy term.[98] However, the absolute values of enthalpies of UCST transitions are at least one order of magnitude lower than those measured for LCST transitions.[99,100] Additionally, UCST transitions are usually much broader, sometimes spanning over tens of degrees in the

temperature scale, than LCST transitions.[54,101-103] The breadth of UCST transitions is due to gradual changes in hydration of polymer functional groups as directly observed by nuclear magnetic resonance (NMR), Fourier Transform Infrared (FTIR) and Raman spectroscopies.[95,98] This is in striking contrast to the sharp cooperative rearrangements in hydration shell for LCST polymer chains.[104] Beyond chain dehydration, slow polymer chain dynamics due to the formation of polymer-polymer hydrogen bonds accompany UCST transitions. Such polymer-polymer hydrogen bonding results in a strong dependence of UCST transitions on polymer concentration, especially in the low concentration region.[105,106]

Among temperature-responsive systems, those that exhibit LCST behavior have been extensively explored. One of the most studied LCST polymers, poly(N-isopropylacrylamide) (PNIPAM), with LCST transition of 32 °C,[96,107] has been incorporated within thin films to leverage temperature-triggered film swelling to control protein adsorption, drug release,[108,109] or enable the formation of removable cellular sheets.[110,111] In contrast, polymeric systems that exhibit UCST behavior are much rarer. To date, UCST behavior is most often observed in organic solvents or water-organic solvent mixtures.[112-116] However, advances in synthetic techniques have enabled the creation of several types of polymers that display UCST transitions in aqueous solutions.[117] In water, UCST behavior is endowed generally through the introduction of two types of polymer-polymer interactions: (1) electrostatic[118,119] and (2) hydrogen-bonding.[105,120-125] UCST behavior driven by electrostatic interactions commonly involves zwitterionic polymers, with polysulfobetaines as the most prominent example.[118,126]

Alternatively, interaction of polycations with small ions such as NaCl,[93] lithium bis(trifluoromethane)sulfonamide,[93] or potassium persulfate[119,127] can be also used to induce UCST transitions. Yet, most of those systems are limited to salt-free environments, since electrostatic interactions between polymer chains are very sensitive to the presence of small ions, which excludes their use in biological applications.[128] Therefore, hydrogen-bonding polymers are seen as a more promising class of polymers to engineer UCST responsive systems for aqueous environments.[100,121] The most commonly employed hydrogen-bonding UCST polymers are based on poly(N-acryloyl glycinamide) (PNAGA),[100,121,125] poly(acrylamide-*co*-acrylonitrile), P(AAm-*co*-AN),[102,125] or ureido-modified polymers, such as poly(L-citrulline)[105] or poly(allyl urea).[105] The UCST of the aforementioned nonionic polymers can be tuned in a wide temperature range from 6 to 80°C by introducing hydrophobic groups *via* co-polymerization, (such as in copolymers of P(NAGA-*co*-butyl acrylate), P(NAGA-*co*-styrene) and P(AAm-*co*-AN)), or by varying polymer molecular weight.[125]

The prospect of using temperature-responsive polymers for drug delivery, soft actuation, and adaptive surface coatings prompted the development of several types of functional UCST nanocontainers. In one strategy, UCST polymers were used to decorate gold nanoparticles to enable their on-demand dispersion/aggregation in aqueous condition.[129-131] In another strategy, UCST-containing diblock copolymers were synthesized, which underwent reversible micellization and could serve as depots for small molecules. The latter strategy follows the steps of a much more mature area of LCST-type block polymer micelles and enables a more practical route of triggering delivery of small

molecules *via* an increase rather a decrease in temperature. UCST-exhibiting micelles have been synthesized with electrostatic interactions[99,132-134] or hydrogen bonding[102,135,136] driving core formation. Finally, very recently star-shaped polymers were explored as another type of UCST nanocontainer and enabled control over UCST transitions *via* their molecular architecture and high local polymer concentration.[137,138] The capability of star-shaped polymers to host small molecules, earlier demonstrated for non-responsive polymers in solution,[139] can be also leveraged to support temperature-triggered delivery from surface assemblies.

This feature article will focus on the recent development of UCST block copolymer micelles (BCMs). UCST behavior of our interest (a) occurs in aqueous medium and (b) involves the formation of hydrogen-bonded micellar cores, which are addressable *via* temperature variations. Our focus on responsive nanocontainers is explained by the capability of UCST containers to serve as depots for loading functional cargo, which can be then delivered by increasing temperature above UCST. Triggered release upon increase in temperature (as in UCST), as compared to LCST systems, is advantageous as most therapeutic molecules need to be delivered at physiological temperatures. Moreover, attaching UCST nanocontainers to surfaces will enable controlled water uptake, mechanical compliance, and delivery of small molecules. The ability to control these behaviors by deposition conditions of films and molecular parameters such as chemical composition, and polymer architecture will be discussed.

2.2. UCST-like Behavior of Nanocontainers in Solution

UCST-exhibiting block copolymers that have been synthesized to date are summarized in Table 2-1. The most studied UCST polymer for hydrogen-bond driven micellization has been P(AAm-*co*-AN), which has robust UCST transitions in water and electrolyte solutions[125] driven by hydrogen bond formation between carbonyl and amide groups. P(AAm-*co*-AN) can be polymerized using the Reversible Addition-Fragmentation Chain Transfer (RAFT) technique using commercially available monomers.[102,135,136] One of the first studies to report UCST micellization was based on a block/graft copolymer of P(AAm-*co*-AN)-*g*-poly(ethylene glycol) (PEG).[102] These micelles were able to load and release doxorubicin to reduce tumor size in mice upon application of an external temperature stimulus. Later, a series of P(AAm-*co*-AN)-based amphiphilic BCMs with either UCST core, corona or 'schizophrenic' behavior was reported.[136] Importantly, the UCST transition of these systems could be controlled within a wide temperature range by varying the content of acrylonitrile (AN) in the temperature-responsive block (*i.e.* the transition temperature increased ~50 °C with AN content increase from ~8 to 17 % in mol).[125] Using the above robust UCST block, we synthesized P(AAm-*co*-AN)-*b*-polyvinylpyrrolidone (P(AAm-*co*-AN)-*b*-PVP)) diblock copolymers *via* RAFT polymerization using a switchable RAFT agent, and demonstrated that the resultant polymer exhibited UCST-triggered reversible micellization between ~27 °C to 55 °C.[135] The temperature-governed assembly was highly repeatable, showing only minimal hysteresis, and occurred in phosphate buffer in a wide range of pH and sodium chloride concentrations.[135]

Table 2-1. Reported UCST Block Copolymers *(Modified from original by removal of UCST Stars). Reprinted in part with permission from [78] Copyright 2019 American Chemical Society.

	UCST Transition	Ref.
UCST Block Copolymers		
Poly(acrylamide-*co*-acrylonitrile) (P(AAm-*co*-AN))-*g*-poly(ethylene glycol)	43 °C, in water, 0.05 to 1 mg/mL	[102]
$P(AAm_{231}$-*co*-$AN_{78})$-*b*-$polystyrene_{42}$	48 to 50 °C, in PBS, 0.5 mg/mL	[136]
$P(AAm_{231}$-*co*-$AN_{78})$-*b*-$poly(dimethylacrylamide)_{425}$	14 to 15 °C, in PBS, 5 mg/mL	[136]
$P(AAm_{231}$-*co*-$AN_{78})$-*b*- poly(N,N-dimethylaminoethyl $methacrylate)_{319}$	21 °C, in PBS, 5 mg/mL	[136]
P(AAm-*co*-AN)-*b*-polyvinylpyrrolidone (PVP)	27 °C to 55 °C, in PBS, 2 mg/mL	[135]
poly(2-methacryloyloxyethyl phosphorylcholine)-*block*-poly(2-ureidoethyl methacrylate)	36 to 40 °C, in 0.1 M NaCl, 1 mg/mL	[140]
PVP-*b*-polyureido(ornithine-*co*-lysine) (PUOL)	14 °C to 33 °C, in PBS, 5 mg/mL	[120]

With biomedical applications in mind, biocompatible BCM nanocontainers were assembled from poly(2-ureidoethyl methacrylate) cores with phosphorylcholine-based corona, which enabled the encapsulation of hydrophobic guest molecules and endowed anti-biofouling characteristics, respectively.[140] To enable degradable nanocontainers, we recently synthesized a diblock copolymer composed of core-forming poly(amino-acid) and corona-forming PVP blocks.[120] Formation of BCMs in this case was driven by hydrogen bonding among ureido groups on the polyureido(ornithine-*co*-lysine) (PUOL)

block (Appendix B).[105] By tuning the length of the PUOL block, the UCST transition of PVP-*b*-PUOL could be controlled within a range between 14 °C and 33 °C. Additionally, hydrophobicity of amino acid could be used to tune the transition temperature. For instance, when the ratio of ornithine to lysine changed from 70:30 to 30:70 (for PVP_{162}-*b*-$PUOL_{216}$ and PVP_{162}-*b*-$PUOL_{168}$, respectively), the UCST transition increased from 14 to 21°C. Prior studies of ureido-modified polymers, such as poly(2-ureidoethyl methacrylate) and poly(L-ornithine)-*co*-poly(L-citrulline), have similarly demonstrated that UCST was strongly dependent on ureido group content, polymer molecular weight, and concentration.[105,106] Finally, our experiments with PVP-*b*-PUOL BCMs pointed to the large degree of hydration of the micellar cores below PUOL's UCST transition temperature, with large differences in BCM diameters when wet (~140 nm) and dry (~35 nm), suggesting larger content of water than in collapsed PNIPAM, which contains up to 60% of water.[141,142] This highly hydrated environment facilitated restructuring of polypeptide cores, which progressively transformed to β-sheets upon temperature cycling. Formation of β-sheets is commonly associated with polypeptide aggregation,[143-145] and eventually resulted in irreversible precipitation of PVP-*b*-PUOL micelles from solution.[120]

2.3. UCST-Responsive Nanocontainers at Surfaces

While LCST polymers have been widely used for building functional interfacial assemblies, exploration of UCST polymers at surfaces is still in its infancy. UCST polymers can be attached to surfaces in a variety of ways, for example by grafting polymer brushes to solid a substrate or through incorporation in thin films. To date, only a few

studies on UCST brushes have been published using both the grafting-to[131,146] and grafting-from methods.[147,148] Such studies have shown that grafting density strongly affected polymer response.[147,148] Specifically, sparsely grafted brushes did not exhibit UCST behavior, as their interfacial spacing suppressed intermolecular association. While polymer brushes present a promising way to engineer temperature-responsive interfacial layers, reactive chemical groups are required for their synthesis.[149]

In contrast, the layer-by-layer (LbL) technique, first established by Decher,[35] enables noncovalent immobilization of polymers at substrates, thus forming films of controllable thickness with programmable stratification perpendicular to the substrate.[150] Additionally, using the LbL technique, polymers can be deposited from aqueous solutions for on a wide variety of substrates with various chemistries and shapes.[108] An additional attractive feature of LbL coatings is that the amount of antibiotics included in the film can be easily adjusted by modulating the thickness of the films.[63,82,151] Earlier, we have explored several strategies to design temperature-responsive LbL coatings.[31,55,59,60,152-154] One strategy relied on polymers which exhibited UCST behavior only after their assembly, as in the case of PAAm/poly(methacrylic acid) (PMAA) LbL films.[31] Another strategy involved LbL assembly of intrinsically temperature-responsive nanocontainers of BCMs.[55,59,60,152]

Earlier, LCST micellar containers were incorporated into LbL films *via* hydrogen-bonding[59,60] or electrostatic[153,154] interactions between micellar coronae and a binding partner. Those LCST-responsive films have been studied extensively and demonstrated many parameters that control film assembly and responsiveness to external

stimuli.[55,59,60,152] For example, it was shown that upon deposition, micelles spread over the surface and "flatten" out, resulting in a bilayer thickness smaller than their dry diameter.[55,57,60] Additionally, micelles do not completely cover a surface after a single deposition cycle,[57] but instead require two deposition cycles to achieve a full monolayer.[154] Importantly, by binding micellar corona with a partner, micellar morphology could be retained and disintegration above LCST prevented, enabling reversible film swelling.[57,60] Furthermore, swelling degree of the film can be controlled by the nature and strength of interactions between the micellar coronae and the binding partner in the film. Binding of micelles within films must be strong enough to prevent disintegration of micelles after exposure to temperatures at which dissociation in solution is expected, yet, weak enough to prevent loss of temperature response by the assembled films.[153]

With this knowledge in mind, we recently assembled, for the first time, UCST BCMs in LbL films with tannic acid (TA).[120] TA has a high pKa of ~ 8.5,[155,156] which enables stability of hydrogen-bonded films at physiological pH. Moreover, TA is attractive for biomedical coatings as it possesses antiradical properties and has relatively low toxicity.[157] Assembly of P(AAm-*co*-AN)*b*-PVP BCMs with TA readily occurred at acidic and neutral pH, with higher amounts deposited at lower pHs.[135] In dense layers constructed at low pH (pH 3), where TA was not ionized, micelles displayed crumpled morphology due to enhanced hydrogen-bonding interactions. In contrast, micelles deposited at pH 5 and 7 maintained micellar morphology, likely due to the presence of small amount of charge in TA within this pH range, which was critical for preserving

temperature response of the film. Unlike in solution, binding with a partner molecule within the film prevented micellar dissociation to individual polymer chains, and UCST transitions within micellar cores resulted in extraordinarily reversible, large-amplitude swelling transitions in films, which could be repeated for 40 - 50 cycles. In addition to the effect of pH, the swelling amplitude and transition temperature for UCST-BCM-containing films was strongly dependent on film thickness, with both increasing for thicker films, in which micelles were no longer pinned to the surface and had more freedom for swelling. As a result, thick films displayed transition temperatures close to the onset of micellar disintegration in solution.

Beyond reversibility, degradability is attractive feature to endow to micellar LbL films. To that end, we reported the LbL assembly of polypeptide-based UCST BCMs (PVP-*b*-PUOL) with TA.[120] Such assembly resulted in films that were stable for at least a week in physiological pH at elevated temperatures and could be potentially removed enzymatically.[120,158] Importantly, LbL assembly of polypeptide micelles not only prevented micellar disintegration to unimers but also suppressed formation of β-sheets, whose formation in solution compromised temperature response. This suppression occurred due to binding of BCM corona with TA, which decreased the conformational freedom that was needed for arrangement of PUOL within β-sheets. As a result, cores of assembled BCMs preserved the capability to hydrate and dehydrate in response to temperature, and the films retained the ability to reversibly swell in PBS. With biomedical applications in mind, we also deposited degradable PVP-*b*-PUOL BCM/TA layers on polycaprolactone (PCL)-collagen nanofibers (See Chapter 4).[158] Micellar diameter on flat

and nanofiber surfaces remained almost constant (36 ± 14 nm *vs.* 34 ± 19 nm), suggesting that nanofiber geometry had little effect on micellar flattening upon adhesion to the surface. Moreover, micellar films on curved nanofibers still exhibited temperature responsive behavior,[158] suggesting that this system can be used for the development of functional wound healing materials.

One of the most important properties of responsive LbL films is their capability to support controlled release of functional molecules from surfaces. It is well established that LCST micelles in LbL films enable temperature-controlled release of therapeutic molecules from surfaces.[55,59,60] However, UCST-induced release is significantly less studied. The first robust system recently reported by our group is based on LbL films of degradable UCST BCMs (chemical structure in Appendix A) and TA,[120] which supported both pulsated (Figure 2-1a) and continuous pyrene release (Figure 2-1a).[120] Control experiments with films of PVP homopolymer and TA indicated that pyrene loading primarily occurred within the functional micellar cores. Furthermore, BCM/TA films were reloadable and non-toxic to human cells.[158]

BCM/TA films were able to load not only the model drug pyrene but also antibiotics, namely, gentamicin and clindamycin.[158] Gentamicin-loaded and unloaded 3.5 bilayer films were challenged with *Staphylococcus aureus*, and the growth of bacteria counted after 48 h. For a high number of bacteria (10^5 CFU cm^{-2}), gentamicin-containing BCM/TA films were able to kill >99.99% of *S. aureus*, while control films without micelles (PVP/TA) showed negligible effect on bacterial counts. Further work showed that clindamycin could be uptaken into micellar films and used to prevent the growth of *S.*

aureus on nanofiber matrices. Taken together, these results indicate that micellar cores can act as cargo holders for antibiotics and that such cargo can be controllably released on demand using temperature as a trigger.

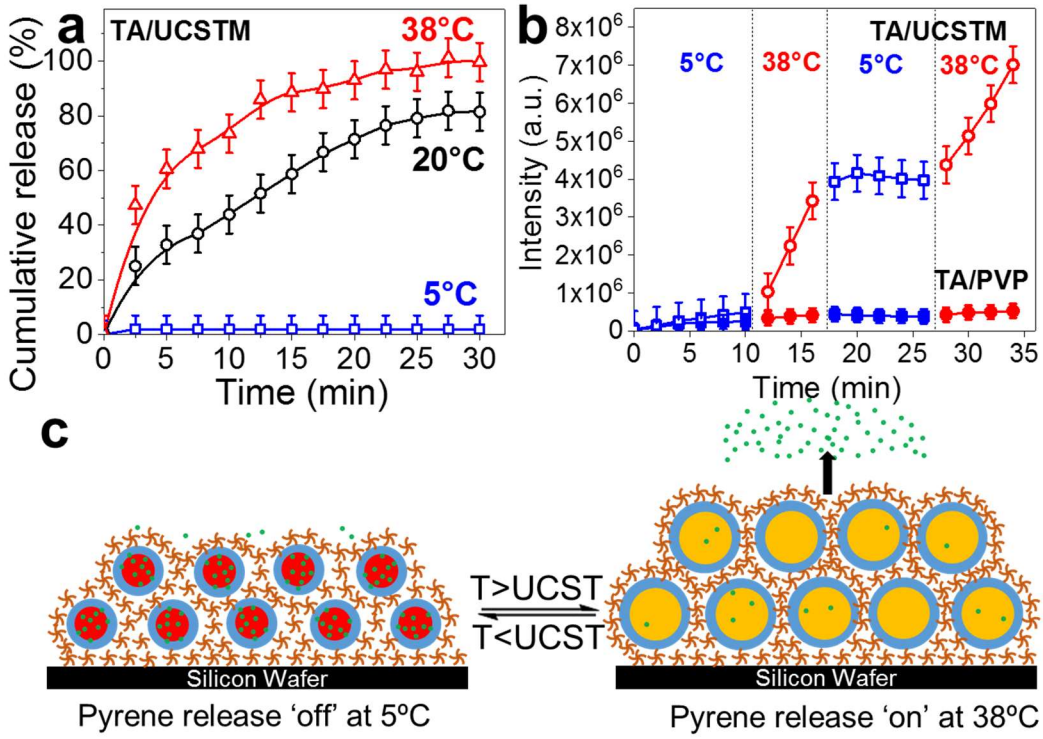

Figure 2-1. Release profile of model drug pyrene from 2.5-bilayer PVP-*b*-PUOL BCM/TA films is temperature-dependent (a) and can be turned on and off by changing temperature (b) as shown in schematically (c). Adapted with permission from ref [120]. Copyright 2017 American Chemical Society.

2.4. Conclusions

Recent studies of UCST responsive polymers revealed rich opportunities to use various molecular architectures (such as amphiphilic block copolymers) and preassembled solution structures (such as BCMs) as promising building blocks for the development of new generations of functional surface coatings for soft actuation, antifouling, and

controlled delivery applications. Such surface coatings exhibit temperature-triggered film swelling, which can be used to manipulate film compliance and for the retention/release of small molecules. Functionality of UCST films is strongly affected by molecular parameters and chain architecture of UCST polymers, as well as by the binding partner molecules, assembly conditions, and even by the overall film thickness.

Yet, non-covalent association of polymer chains in responsive LbL films intrinsically comes with challenges from both practical and fundamental perspectives. One practical challenge is repeatability of the film response to the application of stimuli. So far, this challenge was most pronounced for the case of LbL films build with BCMs containing poly(amino acid)-based cores, which were prone to irreversible formation of β-sheet motifs. While this challenge was largely overcome recently by the application of star rather than linear architecture of UCST polymers,[159] the effect of poly(amino acid) architecture on the formation of secondary structures, and their consequences for functionality of responsive film still need to be understood. For linear micelle-forming UCST polymers, the use of triblock in place of diblock copolymers for constructing UCST films has not be yet explored, while knowledge from LCST films indicated that the use of triblock copolymers can significantly suppress film restructuring.[153] Understanding the role of molecular architecture and binding strength of binding partner on functionality and internal structure of assemblies is yet to be developed. A broader, fundamental question important for all UCST systems, including films, is elucidating at the molecular level the intricate details of UCST response in aqueous systems and applying this knowledge to control the UCST transition temperature and its breadth.

For the specific case of delivery applications, it will be intriguing to explore the effect of molecular architecture (BCM vs star polymer) on overall drug loading capacity and retention. Yet, a challenge common for both LCST and UCST systems is controlling premature release of functional cargo when assembled functional containers are in their "closed" state. Further progress in molecular-level research on UCST polymers as well as involvement of theoretical modelling approaches may enable rational design of microenvironments for optimal retention and controlled, triggered release of functional small molecules from the films. As drug delivery platforms, UCST films offer the advantage that functional cargo is not released at low temperatures (such as in ambient and storage conditions), yet the release can be triggered by the exposure to higher physiological temperatures. This property, convenient for applications, could not be achieved with LCST functional coatings, which demonstrated the opposite behavior.

3. UNDERSTANDING RESPONSIVE SWELLING BEHAVIOR OF LAYER-BY-LAYER FILMS OF UPPER CRITICAL SOLUTION TEMPERATURE MICELLES

3.1. Introduction

Stimuli-responsive micelles are attractive nanocontainers for drug delivery applications.[160] In solution, stimuli-responsive block copolymers transition between either soluble polymer chains or aggregated micelles in which one block of the copolymer is "non-soluble". This transition can be utilized to sequester and release hydrophobic small molecules. By attaching such containers to a surface, stimuli-responsive polymer coatings can easily be made. One facile way to attach micellar containers to surface is to use the layer-by-layer technique. Both pH and temperature-responsive micelles in LbL assemblies have been previously explored. For example, lower critical solution temperature (LCST) block copolymer micelles (BCMs) in LbL films have been successfully shown to enable temperature-controlled release of drug molecules from surfaces.[55,59,60,152,161-163]

Past work on LCST micelle containing LbL films has made progress in correlating micellar features and deposition conditions with overall characteristics and temperature-responsive behavior of films. Studies have found that micelles spread out upon deposition and that micellar coverage can be tuned by number of bilayers deposited.[55,57,60,154] Additionally, if the micelles are covered with a top layer of another polymer, reversible film swelling can be achieved, with the nature and strength of interactions between the binding partner and micelle being the deciding factor in responsiveness of micelles.[57,60] While binding must be strong enough to prevent disintegration of micelles above transition

temperature, it must be weak enough to enable breathing of micelles. Past work has shown that if the binding strength between the coronae and LbL partner is too strong, the temperature response within the film can be lost.[153]

Recently, our group has developed a family of upper critical solution temperature (UCST) block copolymer micelles (BCM) and reported their incorporation in hydrogen-bonded layer-by-layer (LbL) films.[164] We have shown that UCST BCMs can be deposited on flat[120,165] and 3D substrates,[43] while retaining functionality in terms of temperature-triggered swelling and drug release. While these coatings were able to release antibiotics to prevent bacterial colonization, a fundamental understanding of how to control the drug loading capacity and release profile at the deposition step has yet to be explored. Towards understanding how interactions in the film control film properties of UCST BCM containing LbL, Palanisamy *et al.* explored the effect ionization of tannic acid on micellar morphology. They found that the in strong hydrogen-bonding conditions, micelles collapsed, while the presence of charge enabled preservation of micellar morphology.[165] However, how such stabilization influences the drug loading and release capabilities was unexplored.

Here, we explore the effect of poly(methacrylic acid) (PMAA) ionization on LbL film growth, swelling, and drug release capabilities with UCST micelles made of poly(acrylamide-*co*-acrylonitrile) cores and polyvinylpyrrolidone (PVP) coronae. We hypothesized that by changing the ionization of the binding polymer, we could control the strength of hydrogen bonding between the BCMs and PMAA, thus controlling the morphology of the micellar nanocontainers, temperature-responsive swelling, and the

loading capacity and temperature-triggered release of drugs from such containers. By monitoring dry film thickness and film swelling with spectroscopic ellipsometry, film internal structure with neutron reflectometry, and enthalpy of binding of PMAA with PVP micellar coronae by isothermal titration calorimetry, we identified the main factors that contribute to preserving temperature responsiveness of UCST cores of assembled BCMs. Using this temperature-responsive swelling behavior to uptake and release model drugs from micellar layers in response to a temperature stimulus is discussed.

3.2. Materials

Branched polyethylenimine (BPEI, weight-average molecular weight M_w of 750,000 g/mol), and sodium phosphate monobasic dihydrate were purchased from Sigma-Aldrich (Allentown, PA). Poly(methacrylic acid) (PMAA) (M_w 163 kDa, PDI <1.20) was purchased from polymer standard services. Hydrochloric acid, sodium hydroxide, pyrene, and sulfuric acid were obtained from Alfa Aesar (Tewksbury, MA). Ultrapure water from a Milli-Q system (Merck Millipore, Burlington, MA, USA) with a resistivity of 18.2 MΩ was used in all experiments. Boron-doped silicon (Si) wafers were purchased from University Wafer, Inc. All chemicals were purchased from Sigma-Aldrich and used without further modification. PVP-*b*-P(AAm-co-AN) micelles were synthesized as reported earlier.[165]

3.3. Methods

3.3.1. Layer-by-Layer Deposition

LbL films of UCST micelles (UCST BCMs, PVP-*b*-P(AAm-co-AN)) and poly(methacrylic acid) (PMAA) were deposited using the dip-deposition technique. For LbL growth, swelling, and drug loading studies, samples were deposited on Si wafers. To prime all samples, a layer of BPEI (pH 9, 0.2 mg/mL) was deposited for 15 minutes followed by a layer of PMAA (pH 3 or 4, 0.2 mg/mL) for 5 minutes as the prime layer. To deposition micelles, alternating layers of UCSTMs (pH 3 or 4, 1 mg/mL, 0.01 M phosphate buffer with 0.15 M NaCl) and PMAA (pH 3 or 4, 0.2 mg/mL, water) were deposited for 5 mins at room temperature to ensure deposition of micelles. Control coatings of PVP and PMAA were deposited in an analogous manner with PVP solution (pH 3 or 4, 0.5 mg/mL) replacing the BCM solution.

3.3.2. Spectroscopic Ellipsometry

Thicknesses and optical constants of films in dry states were characterized by a variable angle spectroscopic ellipsometer (M-2000 UV−visible−NIR (240−1700 nm) J. A. Woollam Co., Inc., Lincoln, NE, USA) at four angles of incidence: 45°, 55°, 65° and 75°. Swelling measurements were done on the same ellipsometer equipped with a temperature-controlled liquid cell. For data fitting, polymeric layers were treated as a Cauchy material. More details of specific fitting models can be found in a previously published paper.[44]

3.3.3. Isothermal Titration Calorimetry

Solutions of polyvinylpyrrolidone, polyacrylamide-co-acetonitrile, and micelles in PBS were titrated with PMAA.

3.3.4. Neutron Reflectometry (NR)

Neutron Reflectometry studies were performed at Oak Ridge National Lab. For NR studies, LbL films were constructed in the following format: $((hPMAA/UCSTM)_4(dPMAA/UCSTM))_3(hPMAA/UCSTM)_4$. Molecular weights of 163 kDa PMAA and 180 for dPMAA were used.

3.3.5. Pyrene Loading and Release

8 bilayer samples were prepared for drug release studies on 1 x 1 cm^2 Si wafers. Films were loaded by soaking in 1 mg/mL of pyrene in ethanol at 50 C for 1 h. Afterwards, samples were washed with cold phosphate buffer adjusted to deposition pH (3 or 4) and dried. All spectra were collected using a Shimadzu Scientific Instruments RF-6000 fluorescence spectrometer. All release data was collected with λex = 320 nm and measured λem = 371 nm. To collect release over time, a 3 mL aliquot of the total 5 mL release solution was taken, measured, and quickly put back.

3.4. Results and Discussion

Previously, we reported synthesis of upper critical solution temperature block copolymer micelles (UCST BCMs) with poly(acrylamide-co-acrylonitrile) (poly(AAm-

co-AN)) cores and polyvinylpyrrolidone (PVP) coronae.[135] In that work, we showed that micelles have a broad transition temperature, with disassembly starting at temperatures greater than 40 °C. Below transition temperature, micelles had hydrodynamic sizes of ~150 nm regardless of salt concentration and pH. In that work, we studied micelles with 260 AAm and 80 AN units in the temperature responsive block and 260 VP units in the PVP block. Here, UCST BCMs were synthesized in an analogous manner, had the same formula of temperature block but 390 VP units in the PVP block (Chemical Structure in Figure 3-1). Such a difference in PVP block did not cause much of a difference in overall micelle (~ 150 nm) size nor transition temperature (~45 °C) (data not shown).

3.4.1. Layer-by-Layer Assembly

UCST BCMs were deposited in layer-by-layer films with poly(methacrylic acid) *via* hydrogen-bonding interactions in a variety of acidic pHs (Figure 3-1). At more acidic pHs, PMAA is less ionized and therefore, hydrogen-bonding interactions between the components are stronger and more mass is deposited per layer-by-layer cycle. As pH increases, PMAA becomes more ionized and at pH 5, films are unable to grow. We previously observed a similar trend with tannic acid and UCST BCMs growth.[165]

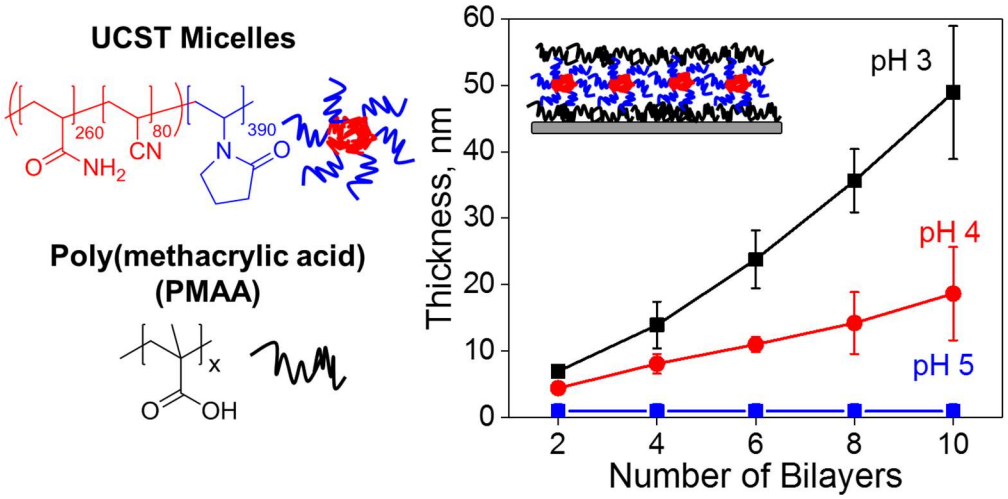

Figure 3-1. (Left) Chemical structures of micelles and PMAA. (Right) Dry thickness, as measured by spectroscopic ellipsometry, of micelle/PMAA films deposited in different pH at RT for 5 minutes per layer from 1 mg/mL micelles in PBS and 0.2 mg/mL PMAA in water.

3.4.2. Isothermal Titration Calorimetry (ITC)

To get a deeper understanding of fundamental interactions in the system, isothermal titration calorimetry was performed with the film components. To first understand how PMAA and the corona or core of the micelles interact, solution studies of homopolymers of PVP or polyacrylamide-*co*-acetonitrile (P(AAm-*co*-AN)), respectively, were studied separately. PVP was found to interact enthalpically with PMAA at both pHs and have a slightly higher binding energy at pH 4 (Figure 3-2). In contrast, P(AAm-*co*-AN), interacts very differently with PMAA at pH 3 and 4. At pH 3, a large negative enthalpy is observed, while at pH 4, only a small negative enthalpy is observed. This suggests that at pH 3, PMAA is strongly interacting with both PVP and P(AAm-*co*-AN)), while at pH 4, PMAA is mainly interacting with PVP. When micelles are titrated with PMAA, the enthalpy of reaction appears to be the sum of the interactions of the two

micellar components. Taken together, this suggests that during micellar assembly at pH 3, PMAA is penetrating the core of the micelle, which could prevent temperature-responsive swelling of micelles. In contrast, at pH 4, the micellar morphology is likely intact and available for temperature-triggered swelling and drug loading/release.

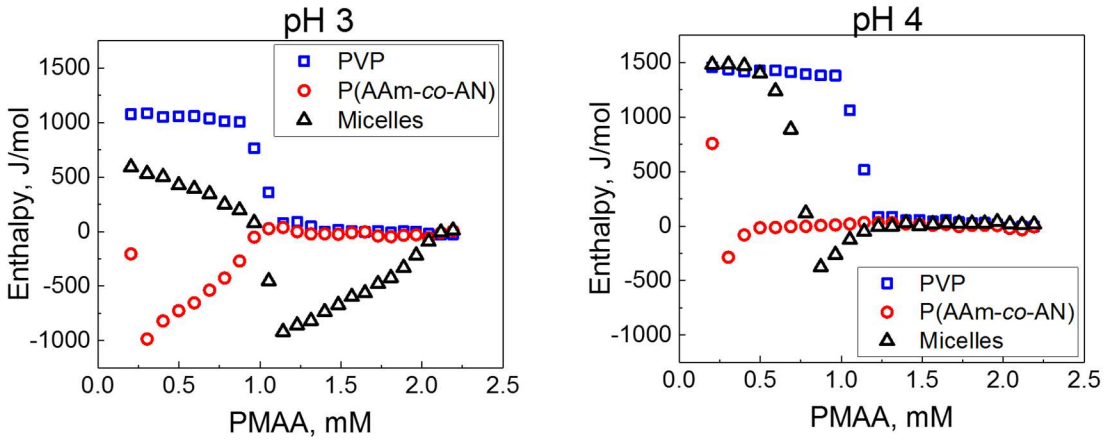

Figure 3-2. Isothermal titration calorimetry at pH 3 (A) and pH 4 (B) of PVP (Corona), polyacrylamide-*co*-acetonitrile (Core), and micelles (poly(AAm-*co*-AN)-*b*-PVP) as measured at room temperature with PMAA.

3.4.3. Neutron Reflectometry Studies

Since ITC suggests that PMAA is penetrating the micellar cores, we wondered whether the stratification of the LbL would be corrupted. To understand whether or not micelles were strongly layered or intermixed, we performed neutron reflectometry studies using deuterated PMAA to provide significant contrast. LbL films were constructed in the following format: $((hPMAA/UCSTM)_4(dPMAA/UCSTM))_3(hPMAA/UCSTM)_4$. M_ws of 163 kDa PMAA and 180 for dPMAA were used. Surprisingly, there is no significant difference in overall film stratification between pH 3 and pH 4 (Figure 3-3). Instead, these

results indicate that both films are significantly stratified to support temperature-responsive behavior.

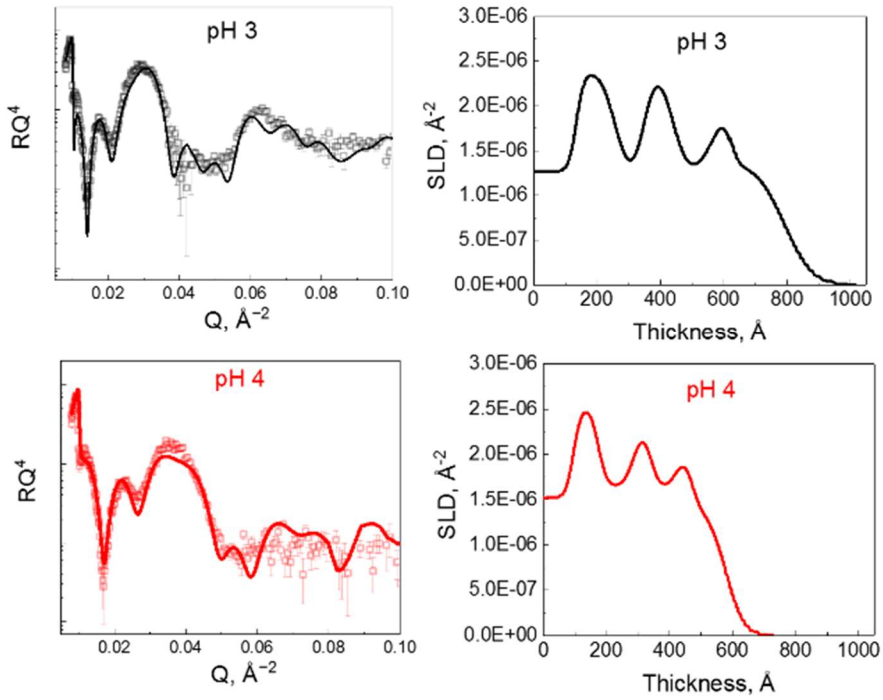

Figure 3-3. Neutron reflectometry results of micelle/PMAA films.

3.4.4. Temperature-Responsive Film Swelling

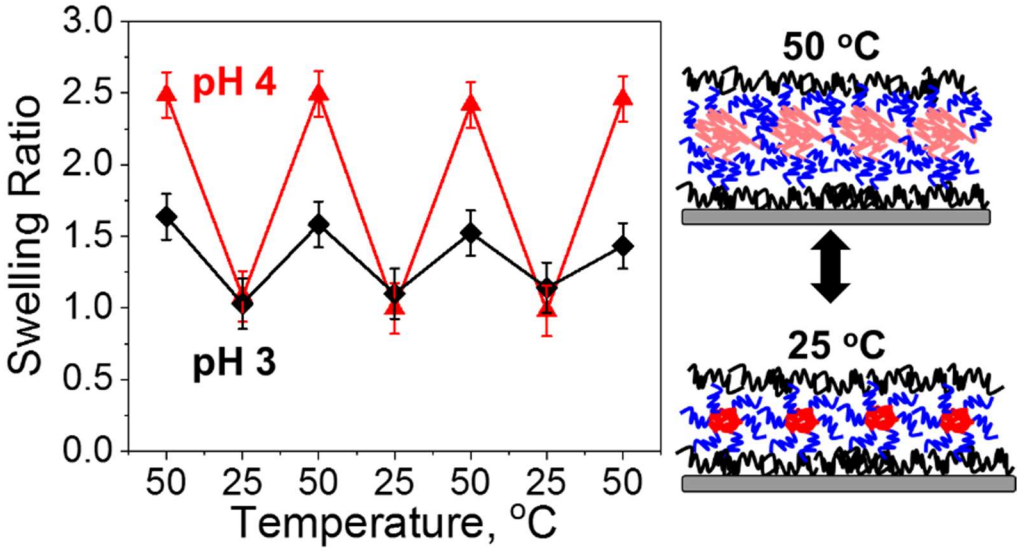

Figure 3-4. Swelling ratio of 8 bilayer micelle/PMAA films deposited at either pH 3 or 4 in 0.01 M phosphate buffer (matching deposition pH) as measured by *in situ* spectroscopic ellipsometry. Schematic representing micelle swelling-deswelling.

We then aimed to find out how different degrees of penetration of polymer chains in micellar cores affected film swelling and functionality. To that end, swelling of 8 bilayer UCST BCM/PMAA films was measured in 0.01 M phosphate buffer, matching the pH of deposition (Figure 3-4). Films were exposed to repeated cycles between 25 and 50 °C. Interestingly, swelling ratios with PMAA were highly dependent on deposition pH of the film, with films deposited at pH 4 swelling significantly more than films deposited at pH 3. This highlights the strong influence of PMAA penetration into the core of the micelles and the importance of binding strength of the partner molecule on the functionality of the film. Importantly, the swelling ratio of the films remained consistent even when films were exposed to pH not matching the deposition pH, indicating that the difference in swelling

ratios is established for films during deposition, not due to external changes in pH. Moreover, swelling ratios with PMAA (1.0 to 1.7 or 2.5) were much lower than previously reported with tannic acid (2 to 7).[135] The lower overall swelling degree is likely due to stronger binding between PMAA and UCSTMs than between UCSTMs and tannic acid.

3.4.5. Temperature-Responsive Small Molecule Release

After establishing the influence of PMAA penetration into the core of micelles on temperature-triggered film swelling, we wondered whether the ability of these films to uptake and release of small molecules would be hindered. To explore this question, pyrene was loaded into the films and its release measured at temperatures below (25 °C) and above (50 °C) UCST as shown schematically in Figure 3-5. Both films were able to uptake and release pyrene (Figure 3-5), however films deposited at pH 4 showed much more robust temperature responsive release, correlating well with temperature-responsive swelling data. In contrast, films deposited at pH 3 showed very similar release profiles for films released at both temperatures. Taken together, this shows that binding partner penetration into the micellar core prevents temperature-responsive behavior of micelles.

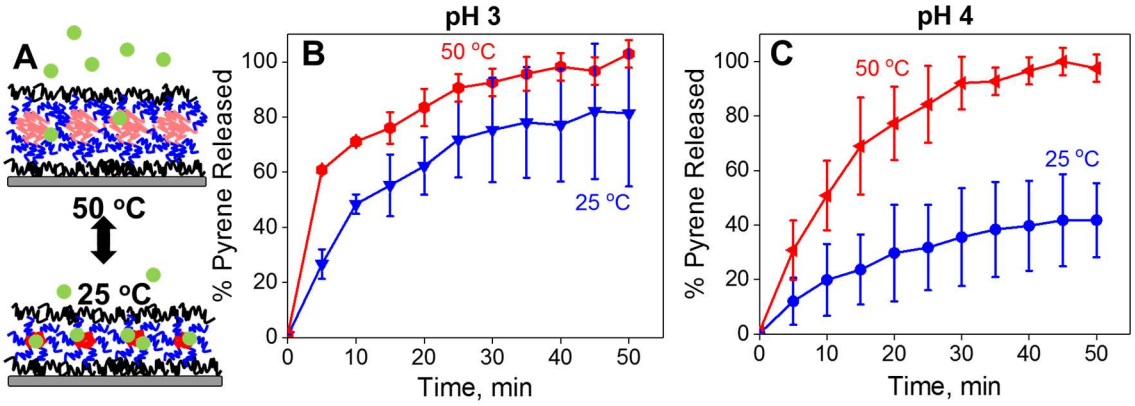

Figure 3-5. (A) Schematic representation of pyrene release at temperatures below (25 °C) and above (50 °C) UCST. Temperature responsive release of pyrene as measured from 10 BL films deposited at pH 3 (B) or pH 4 (C).

3.5. Conclusions

In conclusion, we have shown that the strength of the interaction between micelles and binding partner is critical for maintaining temperature-responsive behavior of micelles. By simply changing the deposition pH and, therefore, the ionization degree of PMAA, penetration of PMAA into the core can be prevented and the functionality of the micelles can be preserved. We showed that not only does penetration of PMAA into the core increase thickness of films but also reduces overall ability of the film to swell and release small molecules.

4. MICELLE-COATED, HIERARCHICALLY STRUCTURED NANOFIBERS WITH DUAL-RELEASE CAPABILITY FOR ACCELERATED WOUND HEALING AND INFECTION CONTROL[2]

4.1. Introduction

Chronic wounds are an important medical problem that affect approximately 6.5 million people and cost 6 to 15 billion dollars annually in the United States alone.[166,167] Chronic wounds display prolonged stages of inflammation and delayed wound healing, due to an imbalance of cytokines and growth factors in the wound site.[168,169] Many scaffolding materials have been developed to facilitate chronic wound closure,[170,171] with nanofibrous matrices (NFs) showing much potential and numerous advantages. NFs can morphologically and dimensionally mimic the native extracellular matrix (ECM) fibers[172] due to the tunability of fiber diameter, spatial fiber organization, and interfiber distance (i.e., pore size).[173] Moreover, NFs can create a stimulatory microenvironment that can enhance wound healing through the local release of biomolecules.[174,175]

NFs can be fabricated from a large variety of polymeric materials (e.g., synthetic, natural, or polyblended) via electrospinning.[176-178] Polyblended nanofibers of bioresorbable polycaprolactone (PCL) and collagen (Coll) have shown promise for wound healing applications. PCL/Coll NFs support the attachment, spreading, and proliferation

---

[2]Reprinted with permission from "Micelle-coated, Hierarchically Structured Nanofibers with Dual-release Capability for Accelerated Wound Healing and Infection Control" by Victoria Albright, Meng Xu, Anbazhagan Palanisamy, Jun Cheng, Mary Stack, Beilu Zhang, Arul Jayaraman, Svetlana A. Sukhishvili, and Hongjun Wang, 2018, Advanced Healthcare Materials, 7, 1800132. Copyright 2018 John Wiley & Sons, Inc.

of normal human dermal fibroblasts (NHDFs) and the formation of dermal substitutes.[179-181] Moreover, anisotropically aligned PCL/Coll nanofibers are able to not only enhance cell migration along the oriented nanofibers, but also promote cellular differentiation.[181] Furthermore, stacking of NHDF-seeded PCL/Coll fibrous matrices can lead to the formation of a 3D tissue construct that closely mimics the layered structure of native dermis within a short culture period.[180] Considering that compromised wounds have imbalanced growth factors and cytokines, incorporating growth factors into PCL/Coll nanofibers for locally modulating the regenerative capacity of skin cells is an appealing strategy.

To that end, we explore the incorporation of transforming growth factor-β1 (TGF-β1) into PCL/Coll NFs. TGF-β1 is a multifunctional growth factor involved in wound healing by recruiting inflammatory cells and enhancing angiogenesis in wounds while stimulating wound closure.[182,183] Deficiency in TGF-β1 has shown delayed wound healing in mice.[184] Interestingly, NHDFs cultured on PCL/Coll NFs with TGF-β1 supplemented in media exhibit decreased proliferation, increased migration, and increased expression of α-smooth muscle actin (α-SMA).[185] α-SMA is a well-known marker of myofibroblastic differentiation, and its high-level expression is correlated with high fibroblast contractile activity.[186-188] Here, we investigate the effects of TGF-β1 incorporated directly into PCL/Coll nanofibers on cellular adhesion, migration, and differentiation.

Healing of wounds may be hampered by bacterial infection, most commonly of *Staphylococcus aureus*, with a rate of ~6% for skin grafts.[189-194] Moreover, upon infection with $>10^5$ colony forming units (CFU) per gram of tissue, about 80% of skin grafts fail.[195]

Post-operative antibiotic treatment has been associated with the survival of skin grafts.[194,196] However, systemic delivery of antibiotics can cause undesirable side effects, especially with the most potent antibiotics, which may be mitigated with local delivery. More importantly, local delivery may help avoid overexposure of bacterial strains to antibiotics, which is correlated with increasing antibacterial resistance,[197] as well as the deleterious consequences of systemic administration of antibiotics. In this regard, incorporating antibacterial agents into NFs is an attractive option for local delivery of antibiotics, and has been implemented with varying degrees of success.[198-201] Water-soluble antibiotics such as tetracycline,[202,203] gentamicin,[199] and ciproflaxin[199,201] among others have been successfully incorporated into NFs via direct addition to electrospinning solution. Although these NFs showed the ability to prevent infection, no evidence indicated they could enhance wound healing.

In another approach to deliver drugs from NFs, large antibiotic-containing polylactic-*co*-glycolic acid micropatterns (~75 micron) were printed on top of NF membranes for local release.[204] Alternatively, to achieve time-programmed multi-agent release upon dissolution, hydrophilic, biodegradable micelles, loaded with anticancer agents, were included within hydrophilic NFs via electrospinning.[205,206] However, the aforementioned efforts focused either on bone regeneration or anti-cancer applications and did not involve topographical modification of NF surfaces through micellar attachment. Furthermore, bioactive agents incorporated into NFs via electrospinning are exposed to harsh organic solvents and control over their release kinetics is limited. In recognition of the advantages of micelle-enabled, localized drug release from surface coatings,[207] we explore the

decoration of nanofiber surfaces with micelles for release of antibiotics with a particular interest in wound healing. Additionally, immobilization of micellar nanocarriers on NF surfaces introduces secondary topographic features on NFs which could also modulate cellular responses.

To immobilize micellar nanocarriers onto NF surfaces, we use the well-established layer-by-layer (LbL) technique, enabling the construction of stimuli-responsive films for drug delivery.[36,38,39,41,55,58,60,61,161,207-212] In this study, PCL/Coll NFs with large surface area and versatile surface chemistry were used as a 3D structural support to host micelles. Polypeptide-based block copolymer micelles (BCMs) were assembled with tannic acid (TA) to achieve robust films with swelling/deswelling behavior for release of small molecules.[120] TA is an attractive binding partner due to its antibacterial, anti-inflammatory, and pro-wound healing effects.[213] Specifically, TA has been shown to suppress the synthesis of tumor necrosis factor-α cytokine,[214] known for its involvement in chronic inflammation and high levels in chronic wound fluids.[215] Here we show that LbL coatings of BCM/TA on PCL/Coll NFs created a favorable topography for fibroblasts with regard to cellular attachment, spreading, proliferation, and wound gap closure. Moreover, BCM/TA-coated PCL/Coll NFs could be loaded with antibiotic cargo to prevent bacterial infection, with facile control over timing of delivery. Through the use of a modular system, these BCM/TA-coated PCL/Coll NFs can be combined with TGF-β1 loaded PCL/Coll NFs to create a multifunctional platform for simultaneous infection prevention and accelerated wound healing as illustrated schematically in Figure 4-1.

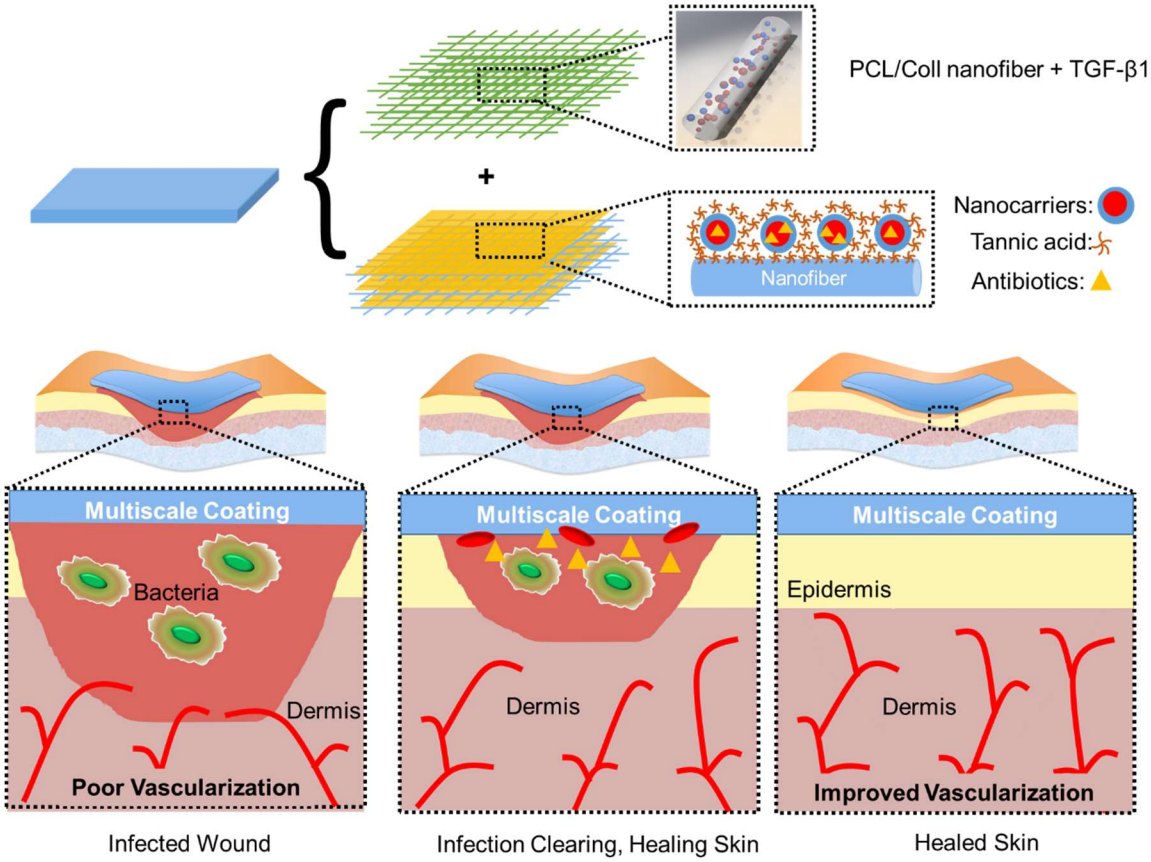

Figure 4-1. Schematic representation of a modular system to simultaneously stimulate wound healing and mitigate infection. TGF-β1 was incorporated into PCL/Coll nanofibers to stimulate fibroblast-to-myofibroblast differentiation. Micellar nanocarriers were deposited on the surface of PCL/Coll nanofibers and loaded with antibiotics to prevent infection. Reprinted with permission from [43] Copyright 2018 John Wiley & Sons, Inc.

4.2. Materials

Tannic acid (TA) was purchased from Alfa Aesar chemicals (Tewksbury, MA). Clindamycin hydrochloride was obtained from TCI chemicals (Portland, OR). Collagenase was obtained from Worthington Biomedical Corporation (Lakewood, NJ). Tryptic soy broth (TSB) powder was obtained from MP biomedicals (Solon, OH). Difco™ Technical Agar was obtained from BD Biosciences (San Jose, CA). Branched

polyethylenimine (BPEI, weight-average molecular weight M_w of 750,000 g mol^{-1}), sodium phosphate monobasic dihydrate, poly(epsilon-caprolactone) (PCL, M_w = 80,000 g mol^{-1}), and trypsin were purchased from Sigma-Aldrich (Allentown, PA). 1,1,1,3,3,3-hexafluoro-2-propanol (HFIP) was obtained from Oakwood products Inc. (West Columbia, SC). Type I collagen (Coll) was obtained from Elastin Products Inc. (Owensville, MO). All other solvents were obtained in anhydrous form and used without further purification. Boron-doped silicon (Si) wafers were purchased from University Wafer, Inc. Recombinant human transforming growth factor-β1 (TGF-β1) was purchased from Invitrogen (Invitrogen, Carlsbad, CA).

4.3. Methods

4.3.1. Fabrication of Nanofibers

NFs of PCL and Coll at a weight ratio of 3:1 were fabricated using electrospinning as previously described.[216] Briefly, 8% (w/v) solution of 3:1 PCL/Coll was prepared by dissolving PCL and Coll in HFIP. Then, the solution was loaded into a 3-mL syringe with a 20-gauge stainless steel blunt-tip needle and electrospun at 10 kV using a custom electrospinning apparatus. The polymer solution was dispensed using a syringe pump (Kdscientific, Holliston, MA) at 10 μL min^{-1}. PCL/Coll NFs for micellar modification were electrospun onto 12-well-plate-sized paper rings (filter paper, inner diameter 0.5" and outer diameter 0.75") or metal rings (diameter 0.6") with a collecting surface of aluminum foil. Before NF spinning, rings were pre-coated with BPEI (0.2 mg mL^{-1}, pH 9) for 20 min. PCL/Coll NFs with TGF-β1 were prepared by electrospinning PCL/Coll

solution mixed with reconstituted TGF-β1 at a final concentration of 500 ng mL^{-1} onto glass coverslips. The estimated amount of TGF-β1 in each sample was 5 ng. Once sufficient NFs were collected, the NFs were cut along the edges of the coverslip to assure full coverage of the entire coverslip surface.

4.3.2. Preparation of Biocompatible Micellar Nanocontainers and Their Deposition on Substrate Surfaces

A block copolymer of polyvinylpyrrolidone-*b*-polyureido(ornithine-*co*-lysine) (PVP-*b*-PUOL) was synthesized *via* ring opening polymerization followed by post-polymerization functionalization with ureido groups as reported earlier.[120] The final product of PVP_{162}-*b*-$PUOL_{513}$ had the number-average molecular weight M_n of 233,000 g mol^{-1} and a polydispersity index of 1.17. This polymer forms spherical BCMs in solutions at temperatures lower than ambient.[120] Temperature of 10 °C was used for construction of LbL films of BCM and TA using the dip-deposition technique. In order to deposit BCM/TA films onto surfaces, first a priming layer of BPEI was deposited at pH 9 for 30 min from 0.2 mg mL^{-1} solution. Afterwards, alternating layers of TA (pH 7.4, 0.2 mg mL^{-1}) and BCM (pH 7.4, 0.5 mg mL^{-1}) were deposited for 30 min at 10 °C so that the final coating had BPEI, TA, BCM, TA (1.5 bilayers) coated on top. Control coatings of PVP and TA were deposited in an analogous manner with PVP solution (pH 7.4, 0.5 mg mL^{-1}) replacing the BCM solution. For ease of characterization of the micellar coatings, 3.5-bilayer films (capped with TA) were also deposited on flat substrates (Si wafers). For surface coverage studies, samples were prepared with varying deposition times of the

BCM layer but constant deposition times for the other layers. To monitor coating deposition, SEM performed with a JEOL JSM-7500F instrument was used for imaging, after sputter coating samples with 3 nm Pt/Pd alloy. Static contact angle measurements were taken using an Optical Contact Angle and Surface Tension Meter CAM 101 (KVS Instrument Inc.) with pH 7.4 PBS. Prior to bacterial and cell culture, samples were sterilized with UV irradiation for 15 min on each side for NF substrates or 30 min for Si wafer substrates. A control test on Si wafers showed that film swelling (determined with a spectroscopic ellipsometry (M-2000, J.A. Woollam) as described in next section) before and after UV sterilization remained constant, suggesting negligible effects of UV on film function.

4.3.3. Degradation Studies on Flat and Structured Substrates

4.3.3.1. Flat Substrates

Two 3.5-bilayer films of BCM/TA on Si wafers were exposed to 5 mL of collagenase (0.1%) or trypsin (0.25%) in PBS at 37 °C. At designated time points, films were removed from solution, washed with pH 7.4 PBS, and dried with nitrogen gas. Dry thicknesses of coatings on Si wafers were measured with spectroscopic ellipsometry (M-2000, J.A. Woollam) at angles of incidence 45, 55, 65 and 75°. A Cauchy layer model was used for analysis with A set to 1.5, which allowed for automatic calculation of the best fit thickness. After measurements, samples were returned to and kept in fresh solutions of collagenase or trypsin until the next measurement.

4.3.3.2. Nanofiber Substrates

To perform degradation studies, 1.5-bilayer BCM/TA coated nanofibers (together with the paper rings) were soaked in 1 mL of sterilized PBS containing trypsin-EDTA (0.25%) in a 12-well plate and incubated at 37 °C under shaking (40 ± 1 rpm). The solution was refreshed every three days. All samples were vigorously washed with deionized water twice and dried at room temperature. For SEM imaging, the samples were examined with a LEO 982 FEG SEM.

4.3.4. Bacterial Studies

4.3.4.1. Antibiotic Loading

3.5-bilayer films of BCM/TA and control polymeric layers without micellar cores (PVP/TA) were loaded with gentamicin (1 mg mL^{-1}, pH 7.5 aqueous solution) at 4 °C for 20 h. Bare PCL/Coll NFs and BCM/TA-coated PCL/Coll NFs were loaded with clindamycin hydrochloride (1 mg mL^{-1}, pH 7.5 aqueous solution) at 4 °C for 20 h after UV irradiation. All samples were washed with pH 7.5 aqueous solution to remove excess antibiotic and then dried (with nitrogen gas for silicon wafers or air dried for nanofiber samples).

4.3.4.2. Bacterial Strain and MIC Assays

For all bacterial studies, *Staphylococcus aureus* (*S. aureus*, ATCC 12600) was streaked on TSB agar plates from a frozen glycerol stock, incubated at 37 °C for 16 h to obtain single colonies, and stored at 4 °C before bacterial cultures. All cultures were started with

colonies from plates of less than a week old. The MIC of clindamycin hydrochloride for *S. aureus* was determined by the antibiotic concentration at which no growth in the main streak was observed upon streaking TSB agar plates with different antibiotic concentrations. The MIC of gentamicin was 12.5 μg mL^{-1} as previously measured by us.[217]

4.3.4.3. Petrifilm Assay

For Petrifilm (3M Petrifilm Aerobic Count Plates, Nelson Jameson, Marshfield, WI, USA) assays, a single colony from the agar plate was inoculated in 2 mL of TSB and grown overnight at 37 °C with shaking (250 rpm). Afterwards, the optical density at 600 nm (OD_{600}) of the culture was measured and used as a guideline to prepare cultures containing 10^9, 10^7 and 10^5 CFU mL^{-1} via dilution with TSB. Petrifilm plates were treated with 1 mL of sterilized DI water for 30 min to hydrate the plate. Si wafers coated with 3.5-bilayer BCM/TA films were placed face up on the hydrated Petrifilms and 10 μL of bacterial suspension was placed onto each sample and incubated at 37 °C for 48 h. After 48 h, the bacterial colonies appearing on top of the samples were counted.

4.3.4.4. Zone of Inhibition Assay

To perform ZOI assays, 4 mL of TSB was inoculated with 5 single colonies from the TSB agar plate and then grown for 17 h. The OD_{600} of the culture was measured and diluted in TSB to ~10^5 CFU mL^{-1}. For ZOI agar plates, 20 mL of TSB was dried overnight, pre-heated at 37 °C for 2 h, and then exposed to bare or BCM-coated PCL/Coll NFs (with and without clindamycin loading) for 1 h (unless otherwise noted). Afterwards, the NF

samples were removed, and the agar plate was streaked three times with a sterile cotton swab from a 10^5 CFU mL^{-1} culture, rotating the plate 60° between each streak. Plates were allowed to dry for 5 min and incubated at 37 °C for 24 h and used for zone of inhibition measurements.

4.3.4.5. Optical Density and CFU mL^{-1} Assay

For OD_{600} measurements as a function of time, 5 single colonies in 4 mL of TSB were grown for 17 h at 37 °C with shaking (250 rpm). 50 mL of TSB was inoculated with 80 μL of the overnight culture at 37 °C with shaking (250 rpm). Cultures were grown for 3 h and then NF samples placed into the culturing flask. At each time point, 0.5 mL of the culture was collected and used for OD_{600} measurements and plated at various dilutions in duplicate to measure cellular counts in solution. Plates were grown for 20 h and colonies were counted manually.

4.3.5. Human Cell Studies

For human cell studies, PCL/Coll NFs with or without TGF-β1 on glass coverslips and 1.5 bilayer BCM/TA-coated or bare PCL/Coll NFs on paper rings were used.

4.3.5.1. Cell Seeding and Culture

Primary normal human skin fibroblasts (NHDFs) from newborn foreskin (R2F) were a gift from Dr. James G. Rheinwald of the Harvard NIH Skin Disease Research Center. The cells were grown in monolayer culture in Dulbecco's modified Eagle media (DMEM, low

glucose) supplemented with 10% FBS and 1% penicillin and streptomycin (Sigma) at 37 °C in a humidified 5% CO_2 atmosphere. Cells were routinely subcultured and used at passages 7-10. For each experiment, 500 µL of cell suspension (4×10^4 cells/mL) was carefully added onto the coverslips coated with nanofibers to avoid any spillage over the edge of the coverslips. The seeded cells were then incubated for 60 min prior to the addition of fully supplemented media. Cells were cultured up to 7 days and media was refreshed every 2-3 days.

4.3.5.2. Cell Proliferation

Cell proliferation was determined using the CyQUANT® Cell Proliferation Assay Kit (Molecular Probes, Inc., Eugene, OR) following the manufacturer's manual. Briefly, cell culture samples (in triplicate, n=3) were harvested on day 1, 4 and 7, respectively. After removal of media and rinsing with pH 7.4 PBS, the samples were snap-frozen and stored at -80 °C. All the samples were lysed in CyQUANT® cell-lysis buffer for 1 h at room temperature and then 200 µL of CyQUANT® GR dye/cell- lysis buffer was added to each sample and incubated for 2-5 min at room temperature in the dark. The fluorescence intensity of cell lysates was measured using the multi-mode BioTek microplate reader (Synergy™ HT, BioTek Instruments Inc., Winooski, VT) at 480 nm ex./520 nm em.

4.3.5.3. Live/Dead Cell Staining

Viability of NHDFs on NFs was determined by fluorescent staining with a Live-Dead Assay Cytotoxicity Kit (Thermo Fisher Sceintific). Specifically, NHDF-seeded NFs after

culture for 1 day were incubated with 4 mM calceinacetoxymethyl ester-AM (stains the cytoplasm of live cells green) and 4 mM ethidiumhomodimer (stains the nuclei of dead cells red) for 5 min at room temperature. After rinsing with PBS, the stained samples were visualized with a Nikon Eclipse 80i fluorescence microscope.

4.3.5.4. Immunofluorescent Staining

Immunofluorescent staining of cells was performed as previously described.[29] Briefly, cultured cells were fixed in 4% paraformaldehyde for 10 min and then permeabilized with 0.2% Triton X-100 in PBS. Primary antibodies used were: phalloidin-FITC (Sigma, 1:500), anti-α-smooth muscle actin, anti-vinculin (Sigma, 1:200), and anti-focal adhesion kinase (Sigma 1:1000). The cells were further incubated with goat anti-mouse or goat anti-rabbit TRITC conjugated IgG secondary antibody (Caltag, 1:400). Cell nuclei were stained with DAPI (Sigma, 1:1000). The staining was examined under a Nikon Eclipse 80i fluorescence microscope.

4.3.5.5. Cell Migration

Migration of fibroblasts on PCL/Coll NFs with and without TGF-β1 was monitored using time-lapse microscopy. Briefly, the culture was placed in a climate-controlled incubator (temperature- and CO_2-controlled chamber) under the eclipse Ti Nikon fluorescence microscope. Each sample was imaged at 10-min intervals for 5 h. Acquired images were analyzed by ImageJ to track at least 10 cells per condition and calculate the mean displacement per 10-min time lapse interval for each cell. To evaluate the migratory

activity of NHDFs in relation to wound healing, in vitro CytoSelect™ 24-Well Wound Healing Assay Kit (Cell Biolabs Inc., San Diego, CA) was used. Briefly, 2×10^5 NHDFs suspended in the culture media were seeded onto the surfaces of NFs with the insert in place. After 24 h, the insert was removed to generate a consistent 0.9-mm-wound gap among the cells. Cells were allowed to migrate into the wound gap for 24 and 72 h. After staining the cells with 0.1% methylene blue, images of the wound gap were taken to analyze the gap distance (n=3).

4.3.5.6. Cell Susceptibility to Clindamycin Hydrochloride in Solution

Cell susceptibility to clindamycin hydrochloride was determined via MTT assay after 24-h culture in a 6-well plate with a series of clindamycin hydrochloride dilutions (0.0625, 0.125, 0.25, 0.5, and 1 μg mL^{-1}) added to the culture media, respectively. Briefly, the culture was incubated with thiazolyl blue tetrazolium bromide (MTT; Sigma, St. Louis, MO) solution (0.5 mg mL^{-1} in culture media) at 37 °C in the dark for 4 h. Upon removal of the nonreacted dye, the formazan product was extracted with DMSO and 100 μL of the extract was transferred to a 96-well plate for absorbance measurement. The absorbance was measured at a wavelength of 570 nm with a Synergy HT Multi-Detection Microplate Reader (BioTek Instruments, Winooski, VT).

4.3.6. Statistical Analysis

All data are expressed as the mean ± SD. For cell studies, each experiment was repeated at least 3 times on different days. All the cell proliferation, migration, and gene expression

were collected at least in triplicate for each group. For bacterial studies, each experiment was repeated at least twice on different days with data collected in at least duplicate for each group. An unpaired student t-test was used to evaluate the significance among experimental groups. A value of $p < 0.05$ was considered statistically significant.

4.4. Results and Discussion

4.4.1. Comparing BCM/TA Coatings on Flat and Nanofibrous Substrates

Polyvinylpyrrolidone-*b*-polyureido(ornithine-*co*-lysine) (PVP-*b*-PUOL), a block copolymer that exhibits upper critical solution temperature (UCST) behavior, forms BCMs above 33 °C.[120] Previously, we reported on the assembly of these BCMs with TA on flat substrates. Here, we explore the possibility of depositing this micellar system onto the surfaces of electrospun PCL/Coll NFs. In contrast to planar surfaces, assembly onto 3D substrates is highly challenging due to the intrinsically uneven topography. After successful deposition, the ability of such BCM-coated NFs to uptake antibiotics and efficacy of antibiotic-loaded BCM/TA-coated NFs to simultaneously prevent bacterial colonization and control cell migration was explored.

To deposit micelles onto planar surfaces (Si wafers) and 3D substrates (PCL/Coll NFs), a priming layer of branched polyethylenimine (BPEI) was used. BCMs (0.5 mg mL^{-1}, pH 7.4) were then deposited followed by a top coat of TA (0.2 mg mL^{-1}, pH 7.4). TA hydrogen bonds with the outer shell of the micelles (composed of PVP), which enables TA to secure the micelles onto the surface. We have previously shown that deposition of

a top coat over stimuli-responsive micelles prevents the desorption of micelles while enabling retention of their morphology and responsive behavior.[60,161]

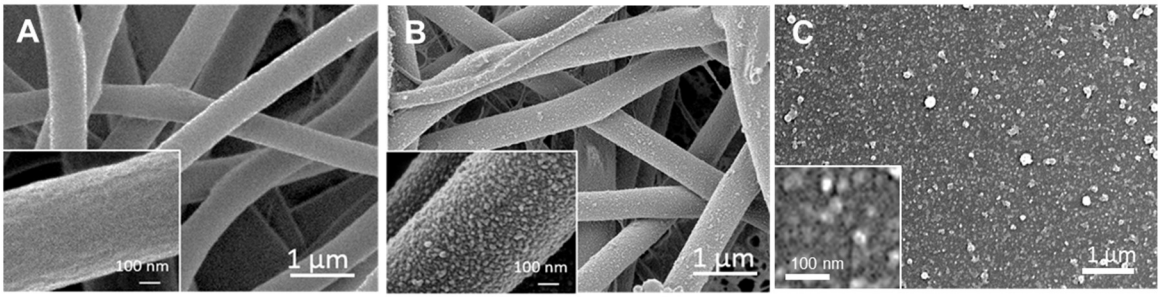

Figure 4-2. SEM images of bare PCL/Coll NFs (A), 1.5-bilayer BCM/TA-coated PCL/Coll NFs (B) and 2.5-bilayer BCM/TA films on a silicon wafer (C). Reprinted with permission from [43] Copyright 2018 John Wiley & Sons, Inc.

We first investigated whether the chemistry of the nanofibers and their surface curvature had any effects on micellar deposition. The PCL/Coll NFs in the electrospun matrices were randomly organized with an average fiber diameter of 482 ± 6 nm. Figure 4-2 shows the surface morphology of bare (A) or BCM/TA-modified PCL/Coll NFs (B) as well as surface morphology of BCM/TA coatings on Si wafers (C). When BCM/TA coatings were deposited at the surface of Si wafers, the average micelle diameter was 36 ± 14 nm as quantified by ImageJ analysis of scanning electron microscopy (SEM) images.[120] Depositing the same micellar system on PCL/Coll NFs resulted in a similar average micelle diameter of 34 ± 19 nm. Thus, curvature of the substrate had no effect on micellar flattening upon adhesion to the surface.

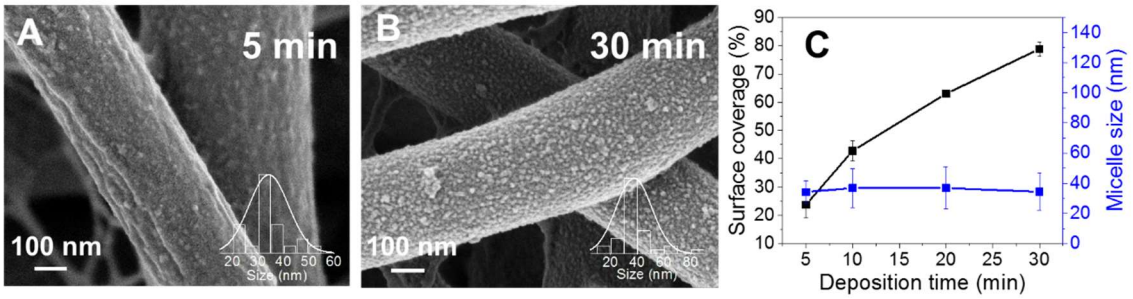

Figure 4-3. Surface coverage of BCM on PCL/Coll NFs depends on deposition time while average micellar size does not. Morphology of PCL/Coll NFs after 1.5 bilayers of BCM/TA deposited for 5 min (A) or 30 min (B). Surface coverage and average micellar size as a function of deposition time (C). Data presented as mean ± SD, n=2. Reprinted with permission from [43] Copyright 2018 John Wiley & Sons, Inc.

Figure 4-3 shows that surface coverage of BCMs on PCL/Coll NFs could be controlled by deposition time, with increasing time leading to an increase in coverage. The micelle coverage was 23 ± 4%, 42 ± 3% and 78 ± 2% for 5, 10, and 30 min deposition times, respectively, as determined by ImageJ software threshold analysis (five randomly selected areas per image were analyzed, the total surface area was approximately 400 μm^2). Similarly, the micellar coverage of planar Si wafer substrate was also quantified, reaching 67 ± 4% after 30-min deposition. The increased micellar coverage on NFs may partly come from the easy access of BCMs to nanofiber surfaces as a result of the open interfiber space. Since electrospun matrices generally have a wide distribution of fiber diameters, it was interesting to see whether such variation of fiber diameter influenced the micellar coating. Quantification of the micellar coverage on individual fibers with different diameters (482 ± 6 nm vs. 259 ± 13 nm) revealed a slightly higher occupancy of micelles on larger fibers (78 ± 2%) than smaller ones (62 ± 8%). Such a noted difference suggests to a certain degree that fiber diameter influences micellar adhesion. Theoretically, all the

fiber diameters are large enough for BCMs to attach, however, finer fibers have a higher curvature, which could impede BCM adhesion and lead to lower coverage.

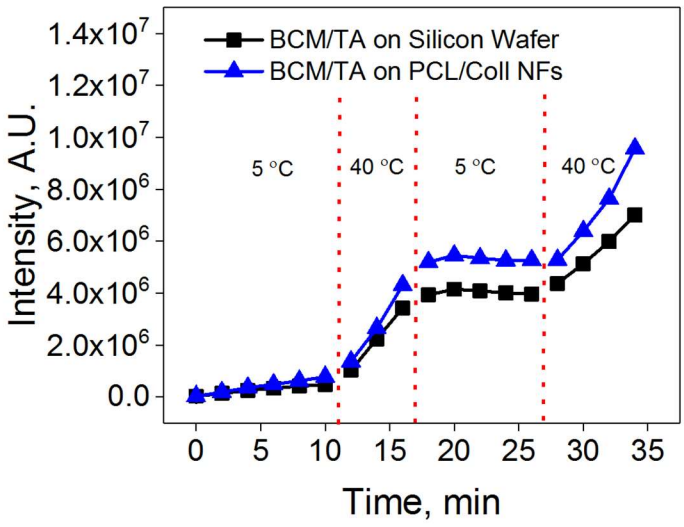

Figure 4-4. Temperature-triggered release of pyrene into PBS (pH 7.4) from 2.5-bilayer BCM/TA films on a silicon wafer and 1.5-bilayer BCM/TA-coated PCL/Coll NFs as measured via fluorescence emission intensity at 371 nm from supernatant. Reprinted with permission from [43] Copyright 2018 John Wiley & Sons, Inc.

In recognition of the effect of nanofiber curvature on micellar deposition, it is necessary to determine whether such curvature could potentially alter the responsive function of micelles. Temperature-responsive release of a model drug (pyrene) into phosphate buffered saline (PBS, pH 7.4) from BCMs immobilized on either Si wafer or PCL/Coll NFs was determined via measuring the fluorescence intensity at 371 nm of the collected PBS samples. To achieve on-demand, pulsated release, the temperature of the release solution was switched between 5 °C and 40 °C, which were below and above the micellar UCST, respectively. Figure 4-4 shows the cumulative continuous release of

pyrene from BCM/TA films on Si wafers and PCL/Coll NFs. For both substrates, an on-off pyrene release was observed, with the release occurring exclusively at 40 °C. These results suggest that the curvature of the NFs exhibits minimal effects on micellar response.

The attachment of BCMs onto the fiber surface relied exclusively on non-covalent hydrogen bonding interactions; however, the micellar coatings were robust and did not decompose or desorb from the fiber surface even after 21 days of exposure to physiological conditions (37 °C, PBS, pH 7.4, with 250 rpm shaking) as can be seen in Figure 4-5A, top row. Moreover, the binding of TA with micellar corona enabled the retention of micellar structure even after exposure to temperatures higher than UCST (Figure 4-4A, top row). Considering the primary purpose of this study was to create multifunctional wound dressings, it was of paramount importance that the BCM/TA-coated NFs could survive the enzymes commonly found in chronic wounds, such as collagenase.[218-220] Based on image analysis, micellar coatings showed stability upon exposure to collagenase (more details can be found in the following section).

4.4.1.1. Degradability of BCM/TA Films on Planar and NF Substrates

Since the goal of this work is to create scaffolds that can be used in wound dressings, it is of paramount importance that the proposed system will not prematurely degrade in the presence of enzymes commonly found in wounds, such as collagenase.[219,221,222] To assess coating stability, films were deposited on NFs and imaged at several time points (Figure 4-5), as well as on planar substrates (silicon wafers) with dry thickness of the coating measured over time to obtain quantitative data (Figure 4-5B).

As can be seen in Figure 4-5, BCM/TA films were stable against collagenase but susceptible to trypsin. Trypsin degrades the polyamino acid backbone by cleaving at the C-terminus of lysine bonds[223] and, therefore, caused clear morphological differences in the BCM/TA coatings attached to NFs after 10 days (Figure 4-5, bottom row) and decreased the thickness of BCM/TA coatings deposited on Si wafers after less than 1 day (Figure 4-5B). The increased rate of degradation of the coatings on planar substrates versus NFs is probably due to the differences in surface area of the coatings.

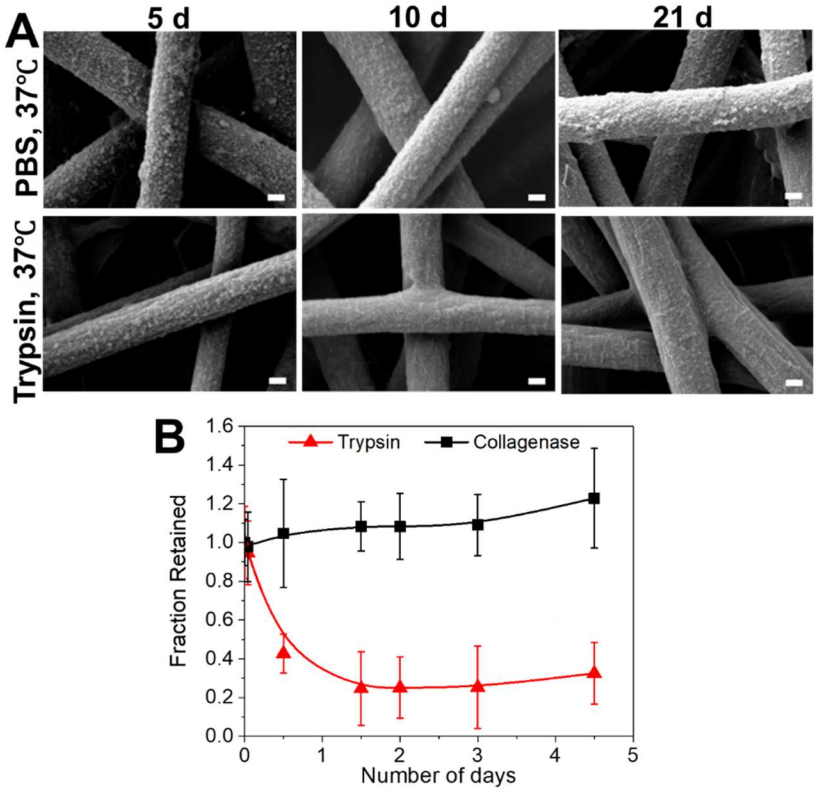

Figure 4-5.(A) Surface morphology of 1.5-bilayer BCM/TA-coated PCL/Coll NFs after 5, 10, and 21 days of exposure to PBS and trypsin at 37 °C. (B) Normalized dry thickness of 3.5-bilayer BCM/TA coatings on silicon wafers as measured by ellipsometry after exposure to trypsin or collagenase. Data presented as mean ± SD, n=2. Reprinted with permission from [43] Copyright 2018 John Wiley & Sons, Inc.

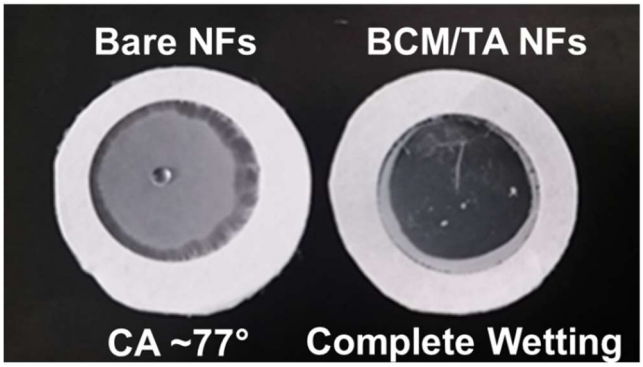

Figure 4-6. Images of PCL/Coll NFs and 1.5-bilayer BCM/TA-coated PCL/Coll NFs after the addition of a droplet of PBS (pH 7.4). PCL/Coll NFs showed a contact angle (CA) of 77 ± 13° while BCM/TA-coated NFs displayed complete wetting. Reprinted with permission from [43] Copyright 2018 John Wiley & Sons, Inc.

Ability to absorb water is also an important parameter for wound dressings.[224] As shown in Figure 4-6, deposition of BCM/TA coatings on PCL/Coll NFs drastically improved the wettability of the substrates. In contrast to the limited wettability of uncoated PCL/Coll NFs (i.e., a contact angle of 77 ± 13°), BCM/TA-coated NFs showed complete wetting by PBS (pH 7.4). The complete wetting capacity of BCM/TA-coated NFs is most likely due to the high hydrophilicity of BCM/TA coatings, which were demonstrated in our previous study to have high swelling ratios in PBS[120] and displayed complete surface wetting when on Si wafers (data not shown).

4.4.2. Cytocompatibility and Cell Migration on BCM/TA-modified NFs

Upon modification with BCM/TA coatings, the surface of PCL/Coll NFs became topographically rougher with secondary nanosized attributes (i.e., micelles) (see Figure 4-2) despite overall morphologic similarity. While it was not possible to measure the

surface roughness of BCM/TA-coated NFs, a root-mean-square roughness of 4.2 ± 1.5 was observed for 2.5-bilayer micellar films on planar substrates.[120] Such nanofeatured surfaces differentially regulate cellular responses, especially those related to wound healing.[225] Thus, bare and BCM/TA-modified PCL/Coll NFs were compared side-by-side for their influence on the attachment, proliferation and migration of NHDFs. After 24 h culture, NHDFs were stained for viability or processed for SEM examination. As shown in Appendix B, NHDFs attached to bare and BCM/TA-modified NFs in a similar fashion, that is, developing strong cell-fiber connections and exhibiting a spindle-like shape. Staining the cultured NHDFs with a live/dead kit showed negligible cell death on both NFs (Appendix B), suggesting the cytocompatibility of BCM/TA coatings with NHDFs. Interestingly, although BCM/TA-coated NFs retained a random orientation, NHDFs on such modified matrices somehow displayed a more aligned, elongated morphology, which was typically observed only on anisotropically aligned PCL/Coll NFs.[29] Further staining the cells for vinculin and FAK affirmed such observation (Appendix B), in which focal adhesion complex (vinculin) distributed primarily on the elongated filopodia. While the cause of such cell orientation is still under investigation, clearly the BCM/TA coating plays a significant role. Proliferation of NHDFs on both PCL/Coll NFs was determined by DNA assay for up to 7 days (Appendix B). Significant stimulation of cell proliferation was observed on BCM/TA-modified NFs, especially for prolonged culture duration (day 4 and 7).

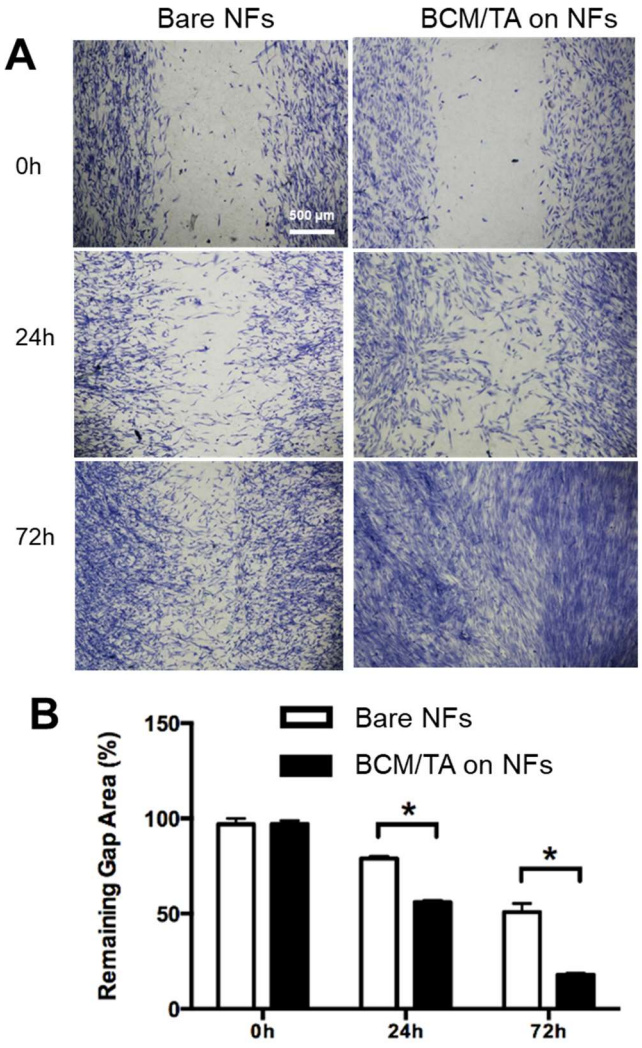

Figure 4-7. BCM/TA coatings enhance NHDFs migration rate and proliferation on PCL/Coll NFs. (A) NHDFs (2×10^5 per matrix) were seeded on either bare or BCM/TA coated PCL/Coll NFs with an insert in the middle. After 24 h, the insert was removed to generate a 0.9-mm wound gap. Cells were allowed to migrate into the wound gap, and visualized after 24 and 72 h using methylene blue staining. (B) Quantification of the distance between the front lines of migrating NDHFs. Data presented as mean ± SD, n=3, *p*-values are calculated using an unpaired student t-test, *p <0.05. Reprinted with permission from [43] Copyright 2018 John Wiley & Sons, Inc.

In recognition of the elongated cell morphology – normally associated with facilitated cell migration – an in vitro wound-healing assay was performed to evaluate the migratory activity of NHDFs on bare and BCM/TA-coated PCL/Coll NFs. Staining the culture after 24 and 72 h with methylene blue revealed that the ability of NHDFs to bridge the model wound gap greatly depended on the substrate. On bare PCL/Coll NFs, the migration of NHDFs into the gap was moderate and only achieved approximately 20% and 50% closure by 24 h and 72 h, respectively (Figure 4-7). In contrast, on the BCM/TA-coated PCL/Coll NFs, NHDF migration into the gap was significantly enhanced and reached approximately 60% and 80% closure by 24 h and 72 h, respectively (Figure 4-7). This trend also agrees with the increased cell proliferation on BCM/TA-coated PCL/Coll NFs (Appendix B). Therefore, we believe that the combination of unique surface topography of BCM/TA coating and increased cell number account for the differences in migration rates. Taken together, BCM/TA-coated PCL/Coll NFs create a favorable environment for NDHFs to migrate and proliferate, two necessary requirements for wound-healing.

4.4.3. Antibacterial Performance of Antibiotic-loaded BCM/TA Coatings

Ability of wound healing materials to prevent bacterial infection is of paramount importance. Therefore, we aimed to explore the capability of BCM/TA-coated NFs to act as cargo holders for biomolecules using two model antibiotics: gentamicin, a bactericidal aminoglycoside, and clindamycin, a bacteriostatic antibiotic. Gentamicin works by binding to the 30S ribosomal subunit, thus preventing bacterial protein synthesis,[226] while

clindamycin works by binding to the 50S ribosomal subunit, causing dissociation of peptidyl-tRNAs from the ribosome.[227] Clindamycin is particularly attractive because it is widely used in clinics for its effectiveness against some strains of methicillin-resistant *S. aureus* (MRSA), which is the most common cause of skin infections.[228]

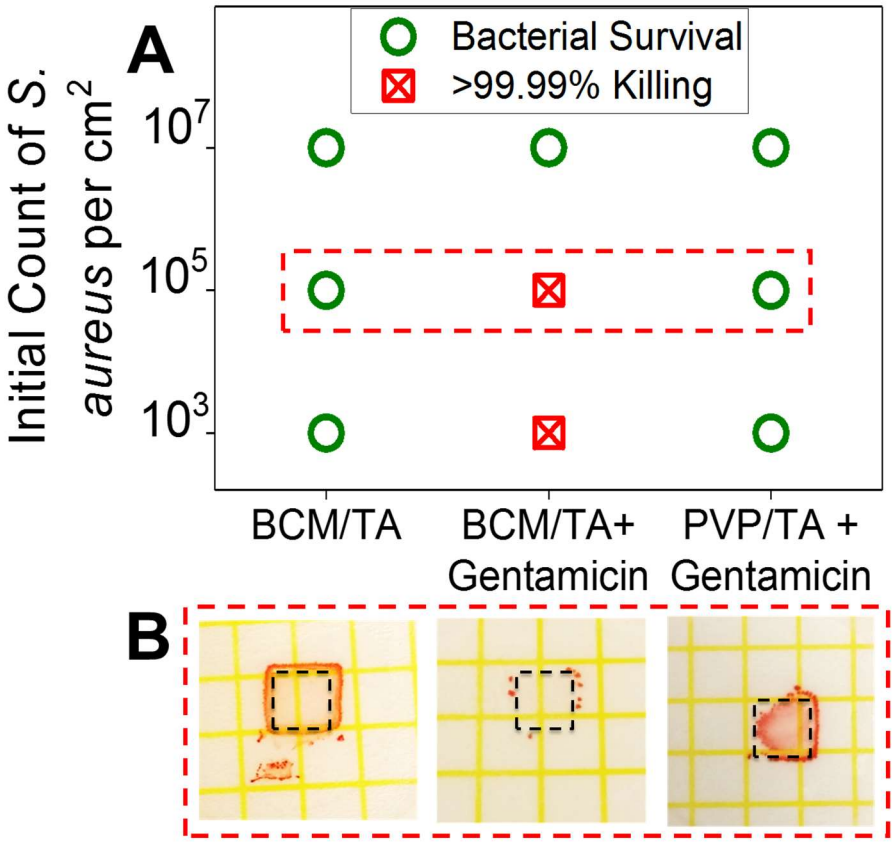

Figure 4-8. BCM/TA coatings on Si wafers can be loaded with gentamicin and prevent bacterial growth. (A) 3.5 bilayer PVP/TA or BCM/TA coatings loaded and unloaded with gentamicin were inoculated with 10^3, 10^5, 10^7 CFU cm^{-2} of *S. aureus* ATCC 12600 and the growth of bacteria enumerated using Petrifilm plates (B). Reprinted with permission from [43] Copyright 2018 John Wiley & Sons, Inc.

To determine the efficiency of assembled micellar films in loading and release of antibiotics, 3.5-bilayer films of BCM/TA were built on Si wafers and loaded with gentamicin (1 mg mL^{-1}, pH 7.5 aqueous solution) at 4 °C for 20 h. This concentration of gentamicin was reported to have no effect on NHDF growth.[229] Gentamicin-loaded and unloaded films were challenged with 10^3, 10^5, and 10^7 CFU cm^{-2} of *S. aureus* ATCC 12600, and the growth of bacteria was enumerated using Petrifilm plates (Figure 4-8) after 48 h. The Si wafers coated with unloaded films did not demonstrate significant prevention of bacterial growth, while wafers with gentamicin-loaded BCM/TA films were able to kill >99.99% of *S. aureus* for a relatively high number of bacteria, 10^5 CFU cm^{-2}. A control group with polymeric layers (3.5 bilayers of PVP/TA) not containing micelles showed negligible antibiotic uptake and no impact on bacterial CFUs. These results indicate that micellar films can be loaded with antibiotics at concentrations above the minimum inhibitory concentration (MIC) (12.5 μg mL^{-1}) and that micellar cores can act as cargo holders for antibiotics. Because LbL deposition was used for micellar coating construction, the amount of antibiotics included in the film can be easily increased by increasing the number of layers in the film.[151,217,230]

We then tested the antibacterial efficacy of the BCM/TA coatings deposited on PCL/Coll NFs. Hypothetical release of antimicrobials into tissues was mimicked in vitro using zone of inhibition (ZOI) assays (Figure 4-8). Prior to bacterial assays, bare PCL/Coll NFs and BCM/TA-coated PCL/Coll NFs were sterilized via UV irradiation and loaded with clindamycin hydrochloride (1 mg mL^{-1}, pH 7.5 aqueous solution) at 4 °C for 20 h. Clindamycin was measured to have an MIC of 0.25 μg mL^{-1} (Appendix B). Figure 4-9 A-

C show that bare NFs had a 28% smaller ($p < 0.02$) ZOI than BCM/TA-coated NFs (ZOI diameters of ~23 ± 9 mm and ~32 ± 6 mm, respectively). By estimating the mass ratios of micelles to nanofibers, micelles were calculated to be approximately 10 times more efficient in absorbing antibiotics than bare NFs. Ability of wound dressings to be fabricated and stored for long periods of time before use is of paramount importance for application in clinics. BCM/TA-coated NFs displayed such an ability as demonstrated by ZOI diameters produced by clindamycin-loaded coatings after 20 weeks of storage of similar size to those observed with fresh BCM/TA-coated NFs (Figure 4-9A). This suggests high robustness of BCM/TA-coated NFs as a platform for antibiotic delivery and a high level of potential for clinical application.

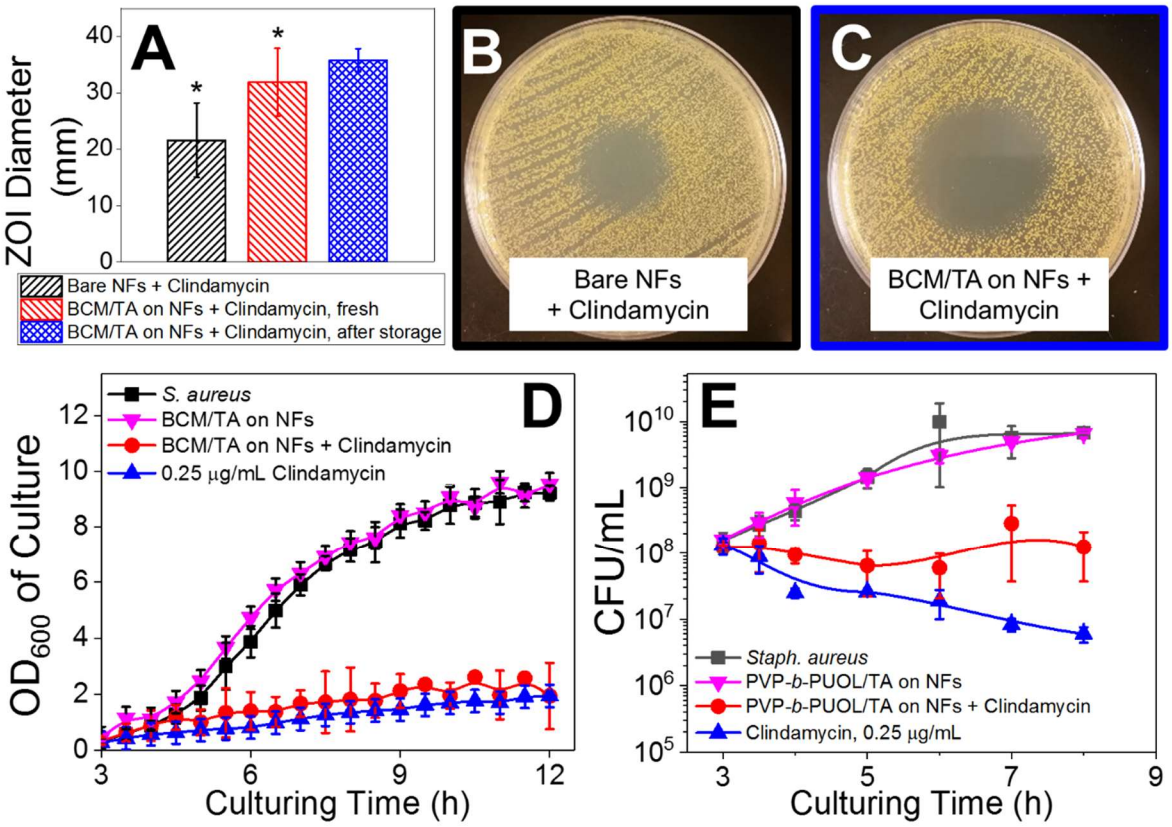

Figure 4-9. BCM/TA coatings on PCL/Coll NFs inhibit growth of *S. aureus* on agar plates and in TSB solution. ZOI diameter in mm (A) and images of ZOIs from bare (B) and BCM/TA-coated (C) PCL/Coll NFs loaded with clindamycin. ZOIs for BCM/TA-coated PCL/Coll NFs loaded with clindamycin are shown for freshly prepared samples (red) as well as samples after 20-weeks of storage at 5 °C (blue). OD of bacterial culture (D) and CFU per mL (E) over time show that clindamycin-loaded BCM/TA coatings on NFs significantly reduce OD and CFU. Data presented as mean ± SD, n=12 for A, n = 2 for D and E, p-values are calculated using an unpaired student t-test, *p <0.02. Reprinted with permission from [43] Copyright 2018 John Wiley & Sons, Inc.

To better mimic bacterial contamination in real wounds, *S. aureus* ATCC 12600 was cultured in large volumes of growth media (tryptic soy broth, TSB) with shaking in the presence of BCM/TA-coated NFs loaded with clindamycin. As controls, clindamycin-free fibers and free clindamycin solutions (MIC, 0.25 μg mL^{-1}) were used. A separate study to

evaluate the correlation of clindamycin concentrations with NHDF growth showed that clindamycin at and above the MIC had minimal effect on NHDF growth (Appendix B). As can be seen in Figure 4-9, all control experiments result in an increase of optical density (OD) of the culture along with an increase in bacterial cellular counts, suggesting that *S. aureus* grew normally in the presence of micellar scaffolds without antibiotics. On the other hand, adding clindamycin to the solution or adding the BCM/TA-coated NFs loaded with clindamycin minimized increases in OD and cellular counts. Specifically, over a culturing period of 5 h, a two-log reduction in bacterial counts was observed for clindamycin-loaded, BCM/TA-coated NFs and was similar to that observed with free clindamycin in solution. This finding suggests that BCM/TA coatings on PCL/Coll NFs could uptake at least 12.5 μg of clindamycin, considering that the culturing volume was 50 mL and the MIC was 0.25 μg mL^{-1}. It is possible that the actual amount of loaded antibiotic was higher, since a further reduction in OD and cellular counts could not be observed for higher concentrations of clindamycin because of its bacteriostatic nature (Figure 4-10).

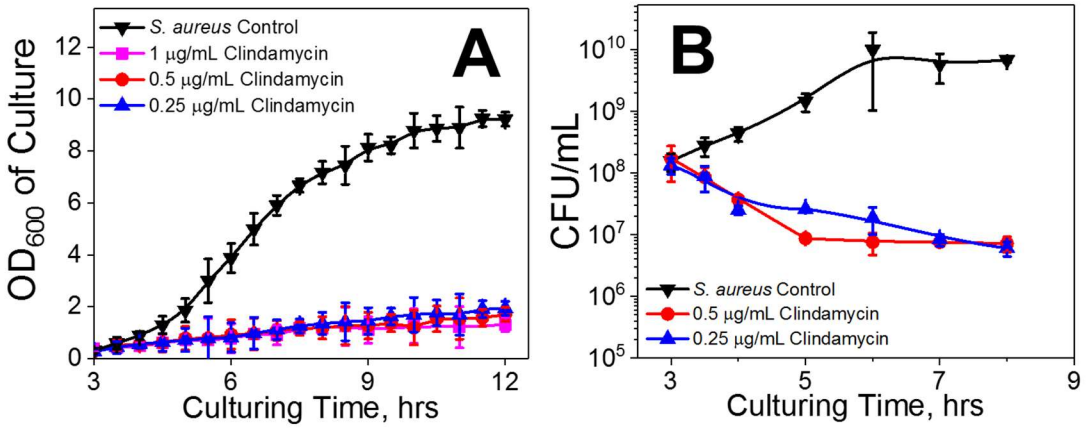

Figure 4-10. OD_{600} of *S. aureus* ATCC 12600 bacterial culture (A) and CFU per mL (B) over time when grown in 50 mL TSB at 37 °C with 250 rpm shaking in the presence of clindamycin in solution. Data presented as mean ± SD, n=2. Reprinted with permission from [43] Copyright 2018 John Wiley & Sons, Inc.

4.4.4. Functionality of Stacking Multiple NFs

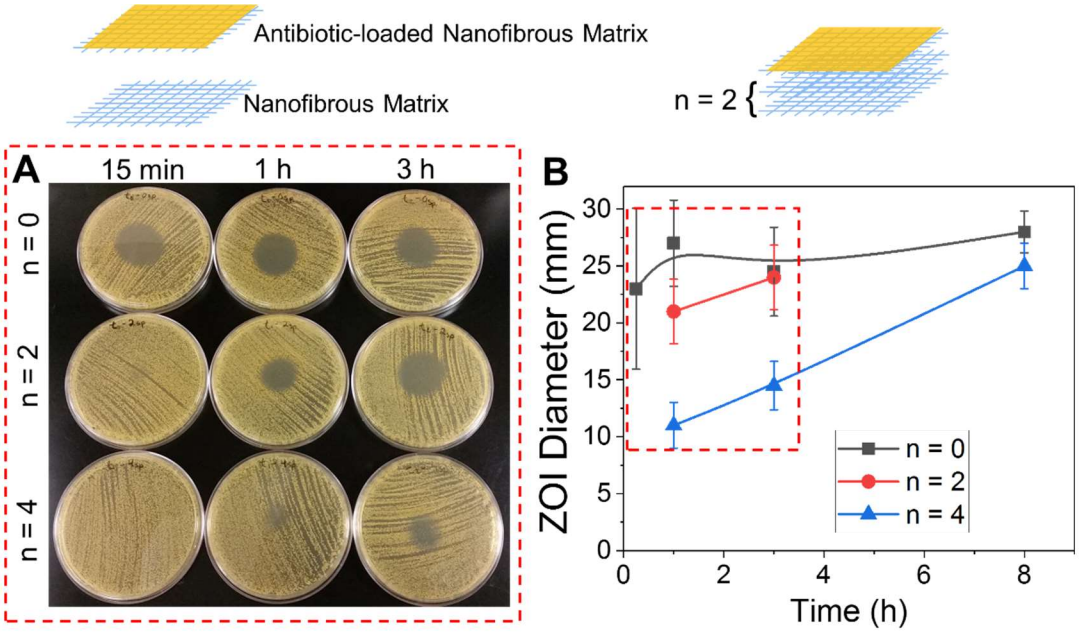

Figure 4-11. Highly tunable inhibition of *S. aureus* from clindamycin-loaded coatings on PCL/Coll NFs via a modular approach. (A) Images of zones of inhibition from clindamycin-loaded coatings on NFs with 0, 2 and 4 spacer layers at time points, 15 min, 1 and 3 h. (B) Quantification of zones of inhibition from clindamycin-loaded coatings on NFs with 0, 2 and 4 spacer layers. Data presented as mean ± SD, n=2. Reprinted with permission from [43] Copyright 2018 John Wiley & Sons, Inc.

In response to the need to deliver multiple biomolecules into chronic wounds, multi-modular matrices containing stacked NFs were designed. This approach takes advantage of the surface functionalization of NFs, and combines them with other types of matrices to create multifunctional matrices as illustrated in Figure 4-11, top. Combination of multiple matrices is advantageous for two reasons. First, this strategy enables control over the delivery rate of bioactive molecules through introduction of spacer layers (n; n=2 is shown in Figure 4-11, top). Second, multiple matrices can be fabricated and functionalized separately to enable dual-agent or multiple-agent release capability.

Here, we demonstrated the feasibility of the first strategy in such a system, in which spacer layers were introduced to enable control over timing of antibiotic delivery. Specifically, 2 and 4 spacer layers (n=2 and n=4) of Whatman filter paper were added between the antibiotic-loaded NFs and agar, which equates to approximately a thickness of 0.5 mm and 1 mm, respectively. Clindamycin-loaded NF samples with and without spacers were exposed to preheated (at 37 °C) agar for various times (15 min, or 1, 3 or 8 h). After this time, the samples were removed and *S. aureus* streaked onto the agar plate from a ~10^5 CFU mL^{-1} TSB culture as described in the experimental section. Without the addition of spacers, one antibiotic-loaded layer appears to completely empty its contents within <1 h, as the ZOI remained the same even for the longest time point (8 h). On the other hand, samples with 2 or 4 spacers (which are 'empty' and do not contain antibiotic) demonstrated pronounced delays in the antibiotic delivery rate to a several-hour scale, as seen by smaller ZOIs at shorter time points (Figure 4-11). Assuming that the antibiotic diffusion coefficient is ~10^{-6} cm^2 s^{-1} (i.e. similar to that of a small fluorescent dye[231]), it is expected to take ~42 min and ~2.8 h for clindamycin, released from the coatings to diffuse through 0.5 and 1 mm, respectively. The observed results match closely with expectations. Importantly, the final zone size after 3 and 8 h, for both the 2 and 4 spacer systems, was the same as the zone generated by a sample without spacers, which suggests no loss of antibiotics into the spacer layers. These results suggest that by strategically assembling NFs together, the delivery time and the effective concentration delivered can be easily tuned. Such a strategy can be readily applied to NFs infiltrated with other biomolecules such as TGF-β1. This approach also can be utilized to develop multifunctional constructs,

e.g. by combining TGF-β1-infilitrated PCL/Coll NFs with antibiotic-loaded BCM-modified PCL/Coll NFs.

4.5. Conclusions

We report direct coating of micellar nanocarriers onto electrospun nanofibers to achieve a hierarchical structure in which the micellar compartments provide significant benefits for controlling interactions with bacteria and mammalian cells. TGF-β1 was directly incorporated into PCL/Coll NFs via electrospinning and stimulated the fibroblast-to-myofibroblast differentiation of normal human dermal fibroblasts seeded on top of NFs. At the same time, LbL-enabled micellar coatings on NFs provided several advantageous features. First, the nanostructured landscape of the fiber surfaces, achieved through attachment of micelles, promoted strong fibroblast adhesion, spreading, proliferation, and enhanced migration even in the absence of a cell-stimulating agent. Second, surface-attached micelles could be used as nanocontainers for the incorporation of small bioactive molecules after fabrication of NFs as shown with antibiotics. These nanoscale-thin micellar coatings on nanofibers efficiently mitigated the infection challenge of *S. aureus*. Moreover, the feasibility of tuning the delivery rate of bioactive molecules via a modular approach that involved stacking functionalized NFs has been demonstrated. This highly versatile, flexible approach provides a promising platform that might enable employment and independent control over the delivery rate of multiple bioactive agents.

5. SURFACE MODIFICATION OF NANOFIBROUS MATS WITH POLYMERIC MICELLES

5.1. Introduction

Electrospun fibers are highly attractive materials for a wide variety of applications ranging from wound healing to food packaging. Therefore, facile modification of these materials to impart application specific properties is highly desirable. Much research has worked on modifying the surfaces of nanofibers for tissue engineering and drug delivery applications.[232] For example, biodegradable and non-biodegradable fibers have been grafted with polymer chains to improve hydrophilicity to enhance cellular adhesion, spreading or proliferation. [233,234] Alternatively, layer-by-layer (LbL) coatings of synthetic polymers,[235] nanoparticles,[236] and biomolecule derived materials[237], even DNA,[238] have been deposited on nanofibers to achieve a variety of features. For example, gold nanoparticles and lysozyme have been deposited on fibers to achieve excellent antimicrobial activity against *Escherichia coli* and *Staphylococcus aureus.* [239] LbL coatings on fibers have been used to endow photocatalytic activity[240] or biosensing capabilities.[241]

We recently published the first report, to our knowledge, of nanocontainers deposited on the surface on nanofibers.[43] We showed that micellar coverage of fibers depended on deposition time for the monolayer and that such a layer could enhance cellular migration. Here, we expand this work to multilayer coatings of micelles and explore not only the unique topography this creates but the functionality of these layers in terms of antioxidant capability endowed by using the assembly partner tannic acid.

Tannic acid is a well-known antioxidant material.[242] Here, we study the antioxidant activity of TA incorporated into LbL with micelles on the surface of electrospun fibers. Antioxidant behavior has been reported for fibers before, mostly for the inclusion of small antioxidants into fibers during electrospinning. For example, Xian Jun Loh's group published several papers on antioxidant biodegradable nanofibers containing lignin as the active component. These fibers had 72 h antioxidant activity and were cytocomptaible for a range of cell lines.[243,244] Alternatively, Selvaraj et al. reported silk fibers with fenugreek that had antioxidant activity that not only enhanced fibroblast proliferation on nanofibers but also enhanced wound healing in an *in vivo* rat wound model study.[245] Other reports on the inclusion of chrysin, curcumin, or gallic acid into fibers during spinning, have shown similar enhancement of viability of cells or promotion of wound closure.[246-248] In contrast to prior reports, our work focuses on attaching tannic acid to fibers in a post-spinning assembly. Since tannic acid is deposited using LbL, the antioxidant capability of such fibers is easy to tune.

In this work, we explore multilayers of UCST micelles and tannic acid on polycaprolactone/collagen (PCL/Coll) fibers. First, we show that the growth of these films is robust and enables temperature-responsive swelling in the physiological range. Next, we explore the stability of these materials in dry storage as well as in physiological conditions. Finally, the antioxidant capacity of these materials is explored as a function of number of coating layers as well as over time. Taken together, these materials show much promise for biomedical applications.

5.2. Materials

Branched polyethylenimine (BPEI, weight-average molecular weight M_w ~ 750 kDa), sodium phosphate monobasic dehydrate, polyvinylpyrrolidone (M_w ~ 55 kDa) were purchased from Sigma-Aldrich (Allentown, PA). Hydrochloric acid, sodium hydroxide, and sulfuric acid were obtained from Alfa Aesar (Tewksbury, MA). Ultrapure water from a Milli-Q system (Merck Millipore, Burlington, MA, USA) with a resistivity of 18.2 MΩ was used in all experiments. Boron-doped silicon (Si) wafers were purchased from University Wafer, Inc. Tannic acid (TA) was purchased from Alfa Aesar chemicals (Tewksbury, MA). Polyvinylpyrrolidone-*block*-poly(acrylamide-co-acrylonitrile) (PVP-*b*-P(AAm-co-AN)) reported earlier[165] were used as temperature responsive micelles. ABTS (2,2'-azino-bis(3-ethylbenzothiazoline-6-sulphonic acid) and potassium persulfate were purchased from VWR. All chemicals were purchased from Sigma-Aldrich and used without further modification.

5.3. Methods

5.3.1. Layer-by-Layer deposition

LbL films of UCST micelles (UCSTMs, PVP-*b*-P(AAm-co-AN)) and tannic acid (TA) were deposited using the dip-deposition technique. To measure LbL growth, samples were deposited on Si wafers as a model substrate. For the rest of the studies, LbL films were deposited on polycaprolactone/collagen nanofibers. To prime all samples, a layer of BPEI (pH 9, 0.2 mg/mL) was deposited for 15 minutes followed by a layer of TA (pH 6, 0.5 mg/mL) for 30 minutes as the prime layer. To deposition micelles, alternating layers of

UCSTMs (pH 6, 0.5 mg/mL, 0.01 M phosphate buffer with 0.15 M NaCl) and TA (pH 6, 0.5 mg/mL, water) were deposited for 30 mins at room temperature to ensure deposition of micelles. Between layer depositions, three washing cycles of 5 minutes each in phosphate buffer were used. Control coatings of PVP and TA were deposited in an analogous manner with PVP solution (pH 6, 0.5 mg/mL) replacing the UCSTM solution.

5.3.2. Spectroscopic Ellipsometry

Thicknesses and optical constants of films in dry states were characterized by a variable angle spectroscopic ellipsometer (VASE, M-2000 UV−visible−NIR (240−1700 nm) J. A. Woollam Co., Inc., Lincoln, NE, USA) at four angles of incidence: 45°, 55°, 65° and 75°. For data fitting, polymeric layers were treated as a Cauchy material. In situ ellipsometry was performed at 75^{o} in a liquid cell. More details of specific fitting models and in situ setup can be found in a previously published paper.[44]

5.3.3. Antioxidant Assay

ABTS was reacted with potassium persulfate following guidelines previously published by others[249]. Samples (Bare fibers, 1, 2, or 3 BL of micelles or PVP control with TA) were exposed to 50 mL of ABTS. At each time point, 3 mL of solution was removed from the container, and measured with a Shimadzu UV2600 spectrophotometer. After measuring the absorbance, the aliquot was returned to the container. Each sample type was run in three separate trials and the data represents the average over the three trials with error bars representing the standard deviation.

5.3.4. Scanning Electron Microscopy (SEM) imaging

All images were taken on a JEOL JSM-7500F with 2.0 kV at WD = 4.5 mm. Samples were coated with ~ 3 nm of Pt/Pd before imaging.

5.4. Results and Discussion

5.4.1. Layer-by-Layer Deposition on Flat Substrates

Previously, we reported the deposition of enzymatically degradable, upper critical solution temperature block copolymer micelles (UCSTMs) on nanofibers and showed that the micelles able to uptake and release antibiotics in able to prevent infection.[43] Importantly, we showed that these constructs were cytocompatible and able to stimulate the migration of fibroblasts. Here we aim to explore the antioxidant capabilities and macrophage responses of a non-enzymatically degradable UCST system. Previously, we reported synthesis of UCSTMs with poly(acrylamide-co-acrylonitrile) (poly(AAm-co-AN)) cores and polyvinylpyrrolidone (PVP) coronae (Chemical structure in Figure 5-1).[135] In that work, we showed that micelles have a size of ~ 150 nm regardless of salt concentration and pH. Here, we use these micelles in assembly with tannic acid (TA) to understand how micellar layers with TA can module fiber topography, and antioxidant capability.

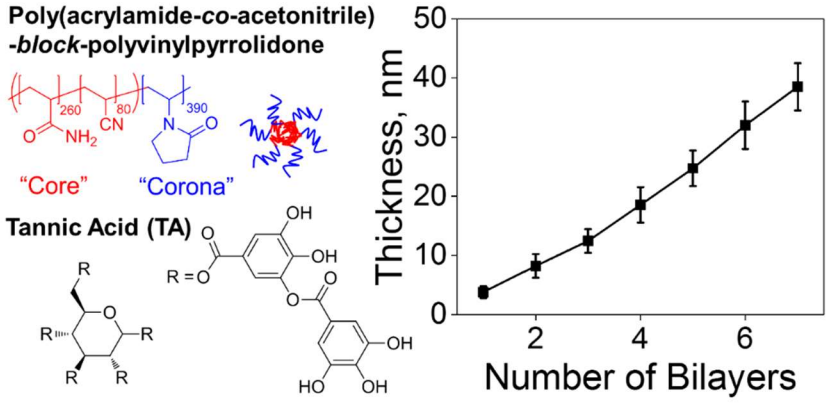

Figure 5-1. Chemical structures of components and LbL growth as measured on Si substrates.

Following the guidelines from our previous work [135] and the pH stability range of collagen,[250] a pH of 6 was chosen for micelle and TA deposition. Before depositing on electrospun polycaprolactone/collagen (PCL/Coll) fibers (NFs) layers were deposited on Si wafer as a model substrate and growth monitored by spectroscopic elliposmetry. As can be seen in Figure 5-1, growth of UCSTMs and TA at pH 6 was linear, indicating strong binding between the components. Such assembly should enable the retention of temperature-responsive behavior of micelles. Indeed, a 6 bilayer film was able to repeatedly show on-off swelling transitions when cycled between 30 and 37 °C in pH 7.5 PBS (Figure 5-2). Moreover, these films are highly stable and can be stored in a refrigerator for up to 4 weeks and still retain their ability to show temperature-induced film swelling. The ability of a material to retain its functionality over a long storage period is essential for biomedical applications.

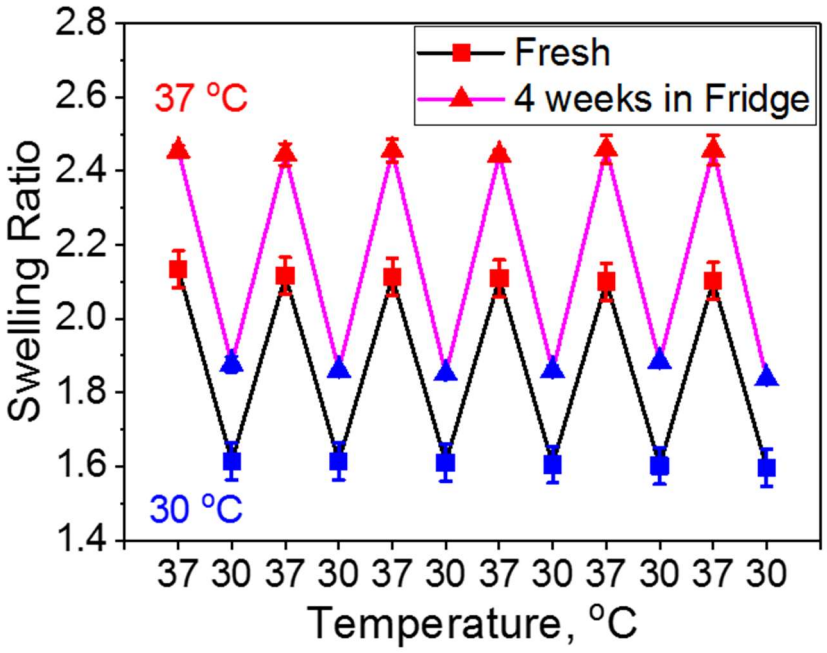

Figure 5-2. Temperature-triggered swelling of UCSTM/TA films on Si wafers for samples as prepared and after 4 weeks of storage at 4 °C.

5.4.2. Layer-by-Layer Deposition on Nanofibers

To deposit micelles and TA on PCL/Coll NFs 30 min deposition cycles were used with the layers always ending with TA to ensure retention of micellar functionality. SEM images of 1, 2, and 3 bilayer UCSTM/TA coatings can be seen in Figure 5-3. Micelles densely cover the surface of nanofibers while not blocking the interfiber pores of the NF mat. Interestingly, 1 bilayer of UCSTM/TA does not completely cover the surface of NFs while 2 bilayers results in a uniform "monolayer" of micelles. This correlates well with previous studies on lower critical solution temperature micelles in films that showed through neutron reflectrometry studies that 2 layers of micelle deposition were required to

achieve a full "monolayer" of micelles.[154] The bumpy morphology shown here is uniquely due to the micelles, as control layers of just PVP and tannic acid are smooth (Figure 5-4).

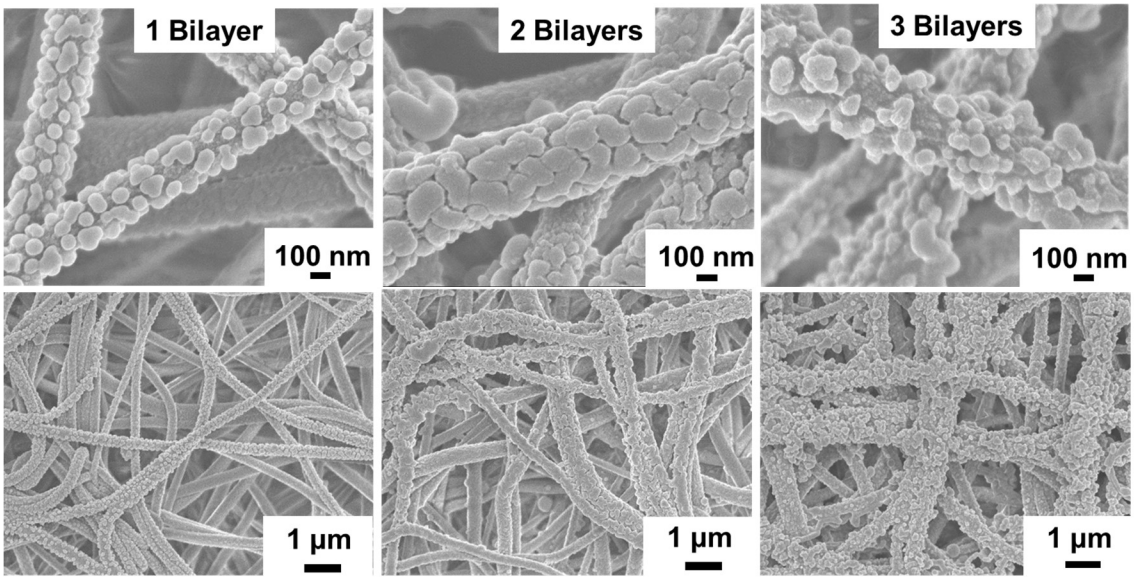

Figure 5-3. SEM images of PCL/Coll NFs coated with 1, 2, or 3 bilayers of UCSTMs/TA.

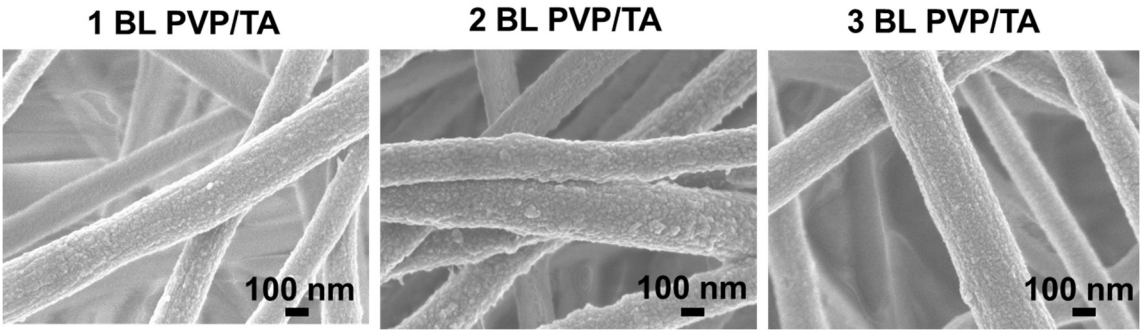

Figure 5-4. SEM images of PCL/Coll NFs coated with 1, 2, or 3 bilayers of PVP/TA.

5.4.3. Antioxidant Activity

Tannic acid is a well-known antioxidant molecule whose antiradical activity can be quantified with several radical scavenging assays.[242] ABTS (2,2'-azino-bis(3-ethylbenzothiazoline-6-sulphonic acid), chemical structure in Figure 5-5) is a well-known radical forming molecule which is commonly used to measure antioxidant capacity.[249] Briefly, ABTS is reacted with potassium persulfate to form radicals, then the rate of radical reduction can be quantified by measuring the decrease in absorbance of $ABTS^{*+}$ solution over time (example in Figure 5-5). Here, we quantified $ABTS^{*+}$ reactivity at 730 nm for UCSTM/TA coated NFs in 50 mL of ABTS solution. As can be seen in Figure 5-6, bare NFs displayed no antioxidant activity. In contrast, 1, 2, and 3 bilayer UCSTM/TA films on PCL/Coll NFs all displayed antioxidant activity with increasing activity being observed for NF mats with more bilayers deposited on them. Interestingly, the antioxidant activity of layers with a linear polymer analog, polyvinylpyrriolodone (PVP), instead of micelles, all show approximately the same level of antioxidant activity regardless of layer number (Figure 5-7). This indicates that deposition of micelles uniquely enhances the amount of TA deposited in a single bilayer, making the antioxidant activity of the NF construct easily tunable.

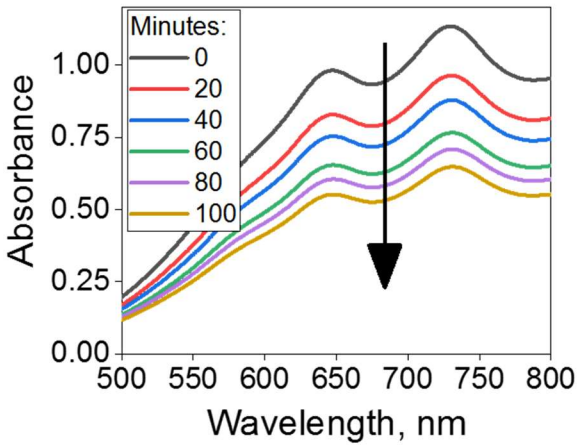

Figure 5-5. UV absorbance of ABTS initially and after reaction with antioxidant material.

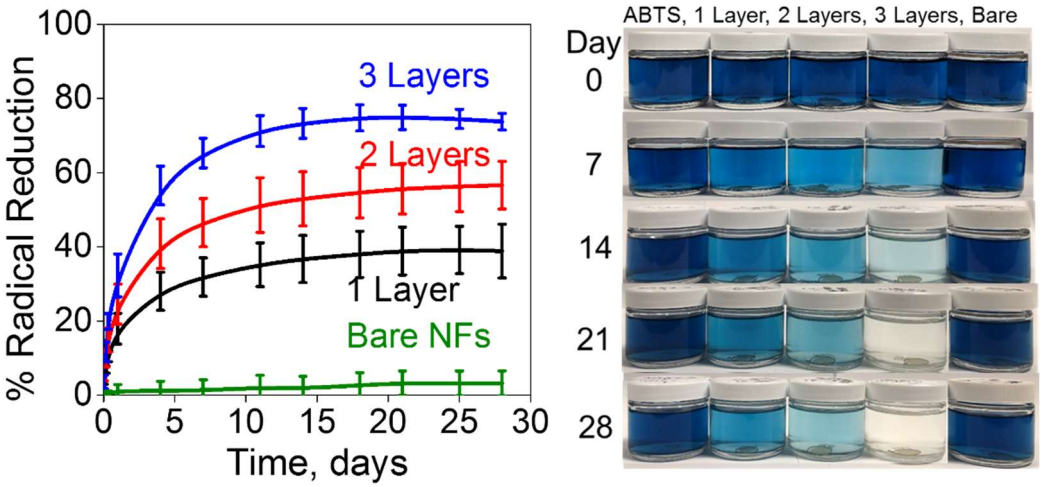

Figure 5-6. Antioxidant activity over time for Bare NFs and NFs coated with 1, 2, or 3 bilayers (BLs) of micelles/tannic acid as measured by reduction of $ABTS^{*+}$ absorption measured with UV-VIS at 730 nm. Images of $ABTS^{*+}$ only, 1 BL, 2 BL, 3 BL, bare NFs in $ABTS^{*+}$ at time points, Day 0, 7, 14, 21, and 28.

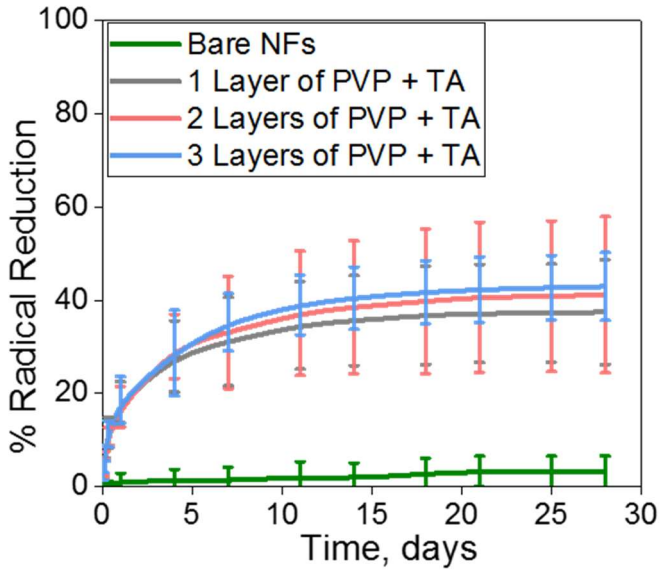

Figure 5-7. Antioxidant activity over time for Bare NFs and NFs coated with 1, 2, or 3 bilayers of PVP/tannic acid as measured by reduction of $ABTS^{*+}$ absorption measured with UV-VIS at 730 nm.

To understand the stability of the micellar coating in physiological conditions, a second assay was done in which fibers were soaked in PBS at 37 °C for days, and then the antioxidant activity of the supernatant solution and the coating was determined. To quantify the surface activity, coatings were placed in $ABTS^{*+}$ and reduction of $ABTS^{*+}$ measured until a plateau was reached (Figure 5-8A) on day 4. Then this maximum activity was taken and compared to the antioxidant activity of the non-soaked sample (Figure 5-8A). For the first five days, only a 20% loss of activity of observed, likely due to desorption of the top layer of tannic acid. A significant loss of activity occurs after 10 days, suggesting that the coating is starting to degrade. To quantify supernatant activity, an aliquot of solution the fibers had been soaking in was taken and reacted with $ABTS^{*+}$. A calibration curve of TA concentration vs. $ABTS^{*+}$ reduction was plotted (Figure 5-8B)

and used to determine the amount of TA released into solution over time. As can be seen in Figure 5-8C, over time TA is released from the fibers, also suggesting the dissolution of the coating. To confirm that coatings dissolve over time in PBS, SEM images of 2 BL micelle/TA coatings were taken after 12 days of exposure. As can be seen in Figure 5-9, many of the micelles have desorbed from the surface of the nanofiber. Moreover, a 6 BL micelle/TA sample on Si wafer was exposed to PBS for 14 days and measured with ellipsometry. The remaining thickness of the coating was close to that of only the prime layer, confirming that the coating desorbs over time.

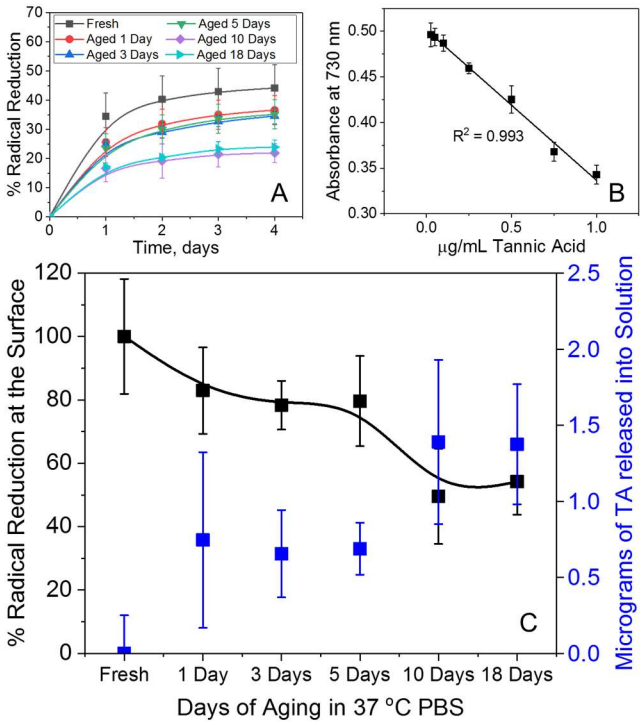

Figure 5-8. (A)% Reduction of ABTS^{*+} radical over time for 2 BL of micelles/TA on glass coverslips as measured by reduction of ABTS^{*+} radical absorption. Data points represent average over two samples and error bars represent standard deviation. (B) Calibration curve of reactivity of tannic acid with ABTS^{*+} (C) Reactivity at the surface and in solution during sample aging.

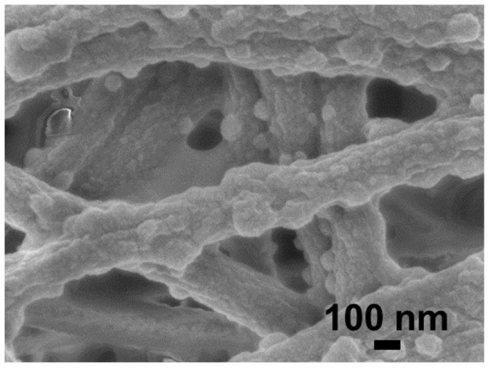

Figure 5-9. SEM image of 2 BL micelles/TA coating on NFs after 12 day exposure to pH 7.5 PBS.

5.5. Conclusions

Multilayers of micelles can be assembled on the surfaces of nanofibers through hydrogen-bonding with tannic acid. Micellar coatings can be stored for up to four weeks at 4 C and still retain temperature-responsive behavior. On fibers, micelle coatings show highly layer dependent surface morphology and antioxidant activity. Previous work has shown that micellar topography can be beneficial for stimulating cellular migration.[43] Additionally, previous work has shown the benefits of antioxidant activity on protection of cells from oxidative stress.[251] Therefore, the materials described here have a lot of potential to be suitable for wound healing applications. Disassembly of coatings begins after about 10 days of exposure to conditions mimicing physiological, suggesting that over time the coating would be biodegradable. Exploring how cells respond to these materials as prepared and after micellar desorption would help better understand the potential of these materials for wound healing applications.

6. SELF-DEFENSIVE ANTIBIOTIC-LOADED LAYER-BY-LAYER COATINGS: IMAGING OF LOCALIZED BACTERIAL ACIDIFICATION AND PH-TRIGGERING OF ANTIBIOTIC RELEASE[3]

6.1. Introduction

Bacterial infection associated with biomaterials implants and devices is a well-known, rapidly growing problem.[1] The traditional treatment of biomaterial-associated infections with systemic antibiotics is often inefficient because of the formation of bacterial biofilms [3,4] in which bacteria are poorly responsive to treatment [5-7]. Prevention of bacterial colonization of surfaces at early stages, *i.e.* upon adhesion of first few bacteria to the implant or device surface, is therefore crucial.

Polymer coatings designed with various molecular architectures have been broadly explored to prevent surfaces from colonization with bacteria. Often, these coatings contain highly hydrated polymers, such as polymer brushes [19] or thin-film hydrogels [17]. The hydrated, open molecular architecture of such coatings can provide them with anti-adhesive properties, and also enable hosting of antibiotics. Several types of antibacterial polymer coatings exist that prevent bacterial adhesion [18], or kill bacteria by either direct contact [21] or through release of antibiotics [26,64,252-254]. Yet, *ad libitum* antibiotic-releasing films often exhibit a burst release followed by a long tail release with sub-lethal

---

[3] Reprinted with permission from Albright, V.; Zhuk, I.; Wang, Y.; Selin, V.; van de Belt-Gritter, B.; Busscher, H. J.; van der Mei, H. C.; Sukhishvili, S. A. Self-defensive antibiotic-loaded layer-by-layer coatings: Imaging of localized bacterial acidification and pH-triggering of antibiotic release. *Acta Biomaterialia* **2017**, *61*, 66-74.

concentrations, leading to the development of antibiotic resistance in bacterial strains [24]. To avoid this, coatings that respond to an external stimulus such as light [30], and electrical pulses [26] have been designed. These coatings release antimicrobials on-demand and therefore are expected to slow down the increasing emergence of antibiotic resistance [24]. One attractive type of such coatings responds to the presence of adhering bacteria to release antibacterial content.

Recently, a series of such "self-defensive", bacterially-triggered coatings has been developed, responding to bacterial presence only when and where needed [63,66,255,256]. Both enzymes [255,257] and acids [33,34] excreted by bacteria have been used as triggers for antimicrobial release to combat adhering bacteria. Recently, our group has developed several types of self-defensive coatings, which take advantage of the layer-by-layer (LbL) polymer deposition technique [35,63,66]. Among these pH-responsive coatings are LbL coatings assembled from montmorillonite clay nanoplatelets and polyacrylic acid and subsequently loaded with antibiotics [63], as well as coatings produced by the direct assembly of tannic acid and antibiotics [66]. Of specific relevance to this work are antibiotic-hosting [258] and antibiotic-free thin-film hydrogels [17], which both demonstrated significant pH-triggered antibacterial activity. In all cases, the pH-responsive 'activation' of the coatings was clearly demonstrated when the coating was exposed to the bacterial strains of *Staphylococcus aureus* or *Escherichia coli*, which are known to acidify the medium in which they grow as a result of secretion of lactic and acetic acid, respectively [33,34].

Although several types of pH- and otherwise bacterially-triggered polymer coatings have been developed, a direct link between bacterial presence and pH activation

through localized acidification has never been demonstrated. One outstanding question is whether bacteria adhering to such coatings produce acidification and trigger antibiotic release at early stages of surface colonization, *i.e.* under physiological conditions when the bulk pH of the surrounding medium remains constant because of its buffering capability, and often while being exposed to fluid flow. Here, localized interfacial acidification induced by adhering bacteria is demonstrated and correlated with pH-triggered release of gentamicin and polymyxin B, by making use of antibiotic-loaded poly(methacrylic acid) (PMAA) hydrogel coatings.[62,258,259] PMAA hydrogel coatings contain primary amino groups as a result of one-end attachment of a diamine crosslinker [260], that enable covalent attachment of a pH-sensitive fluorescent dye for imaging of local acidification from adhering bacteria. Efficacy of the hydrogel coatings is evaluated against a Gram-positive *S. aureus* and a Gram-negative *E. coli* strain, both known to form biofilms on biomaterial implants and devices.[3,4,261]

6.2. Materials

Poly(glycidyl methacrylate) (PGMA, M_n: 20,000), sodium phosphate monobasic, and ethylene diamine (EDA) were obtained from Sigma Aldrich. Branched poly(ethylenimine) (BPEI, 50% aq, M ~750,000) was obtained from Aldrich Chemical Company, Inc., poly(vinyl caprolactam) (PVCL, M_w = 1800) from Polymer Source, Inc., and poly(methacrylic acid) (PMAA) ($M_{Polymer}$ ~80,000) from Scientific Polymer Products, Inc. 1-(3-Dimethylaminopropyl)-3-ethylcarbodiimide hydrochloride (ACT), hydrochloric acid, sodium hydroxide and sulfuric acid were obtained from Alfa Aesar. SNARF-1

carboxylic acid, acetate, succinimidyl ester (SNARF-1) was obtained from Thermo Fisher Scientific. All chemicals were used without further modification. Millipore (Milli-Q system) filtered water with a resistivity of 18.2 MΩ was used. Phosphate buffered saline (PBS) was prepared from 0.01 M sodium phosphate monobasic with 0.2 M NaCl for all experiments unless otherwise noted. Fisher Chemical™ Permount™ Mounting Medium was used for mounting all samples for imaging.

6.3. Methods

6.3.1. Preparation of Hydrogel-like Coatings

Silicon wafers were cleaned as described previously [258]. A prime layer of PGMA, BPEI, and PMAA was deposited following a modified version of the procedure described by Wang *et al.* [262]. Briefly, the wafer was soaked for 15 min in 0.5 mg/mL PGMA in acetone, baked at 110 ^{0}C for 1 h, soaked in 1.0 mg/mL BPEI in methanol for 15 min, baked at 70 ^{0}C for 3 h, soaked in 1.0 mg/mL PMAA in methanol for 15 min and baked at 125 ^{0}C for 1 h. After deposition of the prime layer, alternating layers of PVCL and PMAA were added *via* spin-assisted deposition from 0.2 mg/mL methanol solutions at 3000 rpm to the desired layer number, varying from 6 to 18 bilayers. PMAA/PVCL LbL films assembled in a linear manner with an increase of 2.7 ± 0.1 nm per bilayer as measured by dry ellipsometry. In order to create hydrogel-like thin films, after assembly, the LbL films were crosslinked *via* ethylenediamine using carbodiimide chemistry, *i.e.* by activation of PMAA carboxylic groups with 9 mg/mL of ACT for 15 min and crosslinking with 3 mg/mL EDA for 1 h both in 0.01 M phosphate buffer at pH 5.2. After crosslinking, PVCL

was released by slowly adjusting the pH of the solution to 8, and exposing the LbL films to 0.01 M phosphate buffer solutions at pH 8 overnight to completely release PVCL and form PMAA hydrogel-like coatings. After crosslinking and PVCL release, the dry thickness of all films decreased by ~40%, which is similar with the data on release of a neutral hydrogen-bonding polymer from previously reported PMAA hydrogel-like coatings.[258]

6.3.2. Physicochemical Coating Properties

6.3.2.1. ***Film thickness and wettability:*** All thickness measurements, dry and *in situ*, were taken using a custom-made phase modulated ellipsometer, which enabled the simultaneous determination of refractive index and film thickness. [263] For ellipsometry measurements, a single layer model was used to fit the data. For dry measurements, the refractive index for all coatings was fixed at 1.5 while for wet measurements, the refractive index was measured and decreased to values below 1.5 due to water uptake in the film. All static contact angle measurements were taken using an Optical Contact Angle and Surface Tension Meter CAM 101 (KVS Instrument Inc.). For each dry pH specific measurement, the sample was rinsed with PBS of the corresponding pH and then dried under a flow of nitrogen before the measurement was taken. For *in situ* swelling measurements, each sample was soaked in PBS at the specified pH for 10 min at which point the samples were fully equilibrated.

6.3.2.2. ***Loading and Release of Antibiotics:*** Two common antibiotics were chosen: (1), gentamicin, a broad spectrum antibiotic aminoglycoside, which is a class of drugs that binds to the 30S subunit of ribosomes thus preventing bacterial protein synthesis [264] and (2) polymyxin B, a cyclic cationic polypeptide, which is commonly used against Gram-negative bacteria, that works by disrupting the bacterial cell membrane [265]. Gentamicin and polymyxin B were loaded into the hydrogel by allowing the film to soak in a 0.1 mg/mL of the bioactive molecule in 0.01 M phosphate buffer at pH 7.5 for 2 h then washed three times in 0.01 M phosphate buffer at pH 7.5 to remove excess antibiotic bound to the surface. For testing the release of antibiotics as a function of pH, each sample was soaked in PBS solution of that pH for 2 h. The sample was then rinsed with phosphate buffer at the same pH, dried, and thickness measured by ellipsometry.

6.3.3. Bacterially-Induced pH Changes and Killing Assays

6.3.3.1. Bacterial Culturing: *S. aureus* ATCC 12600 and *E. coli* O2K2 were inoculated on blood agar plates from frozen stock, incubated at 37˚C overnight, and stored in a refrigerator for a maximum of 2 weeks. Single colonies from the blood agar plates were inoculated in 10 mL of growth medium (tryptic soy broth (TSB, OXOID, Basingstoke, UK) for *S. aureus*, and brain heart infusion (BHI, OXOID) for *E. coli.* and grown overnight at 37°C, as the preculture. For the main culture, the preculture was inoculated in 200 mL of the appropriate growth medium, and grown overnight.

6.3.3.2. ***Minimal Inhibitory Concentration Determination****:* To determine the MIC of gentamicin for *S. aureus* ATCC 12600 and of polymyxin B for *E. coli* O2K2, diluted bacterial precultures were added to 150 µL of serially diluted antibiotic concentrations (256 µg/mL to 0.0078 µg/mL) in TSB or BHI for *S. aureus* and *E. coli,* respectively, in a 96-well plates and incubated aerobically at 37°C for 24 h. The MIC-value was taken as the lowest antibiotic concentration at which bacterial growth was visually absent.

6.3.3.3. ***Bacterial Killing Assays:*** For Petrifilm (3 M Petrifilm Aerobic Count Plates, Nelson-Jameson, Marshfield, WI, USA) experiments, bacterial suspension from the preculture were used in different concentrations. Petrifilms were treated with 1 mL of sterilized demineralized water for 30 min to hydrate the nutrient loaded gel layer. Silicon wafers with different numbers (6, 12 and 18) of LbL layers and loaded with or without gentamicin or polymyxin B were placed face up on hydrated Petrifilms and 10 µL of bacterial suspension was placed onto the hydrogel coated wafers and incubated at 37°C for 48 h. After 48 h, the bacterial colonies were counted on the Petrifilms. The antibiotic loaded LbL layers were also tested in multiple cycles in the Petrifilm in order to determine the bacterial efficiency of the LbL layers when fresh bacteria were added to used LbL layers.

For bacterial adhesion experiments, bacteria from the main culture were harvested by centrifugation at 5,000 g for 5 min at 10°C, and washed twice with PBS (0.01M potassium phosphate and 0.15 M NaCl, pH 7.0). Bacteria were counted and diluted to a concentration of 3 x 10^8 CFU (colony forming units)/mL in PBS. Bacterial suspensions of

S. aureus ATCC 12600 and *E. coli* O2K2 were flown through a parallel plate flow chamber as previously described [42]. Briefly, the hydrogel coated silicon samples with different numbers of bilayers and both antibiotics were inserted in the poly(methyl methacrylate) bottom plate of the flow chamber which had a glass plate on top. The flow chamber was then rinsed with PBS to remove all air bubbles from the system, before the start of the adhesion experiment. The bacterial suspension was flowed through the flow chamber for 2 h at a rate of 1 mL/min. After 2 h, fresh PBS buffer was run through the flow chamber to remove non-adhered bacteria and then live/dead stain was injected into the flow chamber to image the adhering bacteria. Live/dead stain of SYTO® 9 nucleic acid (green fluorescent) and propidium iodide (red fluorescent) with a volume ratio of 1:1 was used (*Bac*Light, Invitrogen, Breda, The Netherlands) with 3 μL of stain diluted in 1 mL of demineralized water. After allowing the stain to react with the sample for 15 min in the dark, the samples were imaged using a fluorescence microscope (Leica DM4000B, Leica Microsystems GmbH, Heidelberg, Germany) with a 40x water lens and GFP and N21 filters. Five fluorescent images were taken at different spots on each sample. The total number of adhering live and dead bacteria as well as the percent surface coverage was quantified using ImageJ software.

6.3.3.4. ***Visualization of Local, Bacterially-Induced Acidification:*** For visualization studies, SNARF-1 was covalently bound to PMAA coatings by soaking the films in a solution of SNARF-1 dye dissolved in 0.01 M phosphate buffer for 2 h. After loading the dye, each sample was thoroughly washed in 0.01 M phosphate buffer to remove any dye

that was not covalently attached. For calibration measurements of SNARF-1 labeled hydrogel-like coatings, samples were placed into PBS at the desired pH for 60 min and then gently dried with a flow of nitrogen and imaged with a confocal scanning laser microscope (5 PASCAL laser scanning microscope, Zeiss, Germany) with a C-Apochromat 60X/1.4 oil immersion objective. Samples were excited by a laser at λ= 543 nm (except for a control sample, which was excited at 488 nm) and emission intensities were collected using a LP 560 filter. All imaging parameters, such as exposure time, pinhole size, color contrast and color balance were held constant during data collection. Specifically, for generation of the calibration curve, imaging of local acidification. and comparison of emission intensity of the background hydrogel versus SNARF-1 emission, all parameters were held constant at the following values: exposure time = 1.28 μs, laser power = 1 mW, transmission % = 25, pinhole = 106 μm, detector gain = 957, amplifier gain = 1.00 and amplifier offset = -0.24 V. For comparison of emission intensities profiles of bacteria residing on SNARF-free hydrogels at two different excitation wavelengths, parameters were held constant at the aforementioned values except for the following: exposure time = 1.60 μs, laser power = 1 mW for 543 nm excitation and 25 mW for 488 nm excitation, and transmission % = 25 for 543 nm excitation and 10 for 488 nm excitation. The average intensities of each image of the SNARF-1 labeled hydrogel-like coatings at each pH were determined using ImageJ [36, 37].

To image local acidification, a colony from a tryptic soy broth agar plate that was prepared as described above was placed into 2 mL of TSB and grown overnight. After incubation, bacteria were counted and were diluted in TSB to a concentration of ~10^4

CFU/mL. 5 mL of this mixture was placed into a well-plate containing a hydrogel-like coating, which was sterilized in a 70% ethanol/water mixture, and then incubated for 2 or 4 h. To image the local bacterially-induced acidification, the same CSLM that was used for generating the calibration curve was used under the same conditions. Auto-fluorescence of bacteria was measured by exciting the bacteria at λ= 543 nm and 488 nm and comparing the emission intensities collected by a LP 560 filter. The average intensities of each image of the bacteria and SNARF-1 labeled hydrogel-like coatings were determined using ImageJ. To assess the local pH accurately, the autofluorescence of bacteria (λ= 543 nm) was subtracted from the fluorescence intensities of SNARF-1 (λ= 543 nm) at the locations of bacteria.

6.3.4. Statistical Analysis

All data points indicate the mean over at least three measurements per sample (unless described otherwise below) while error bars reflect the standard deviation of the sample as calculated using STDEV.S in Excel. To generate the calibration curve, intensity measurements were taken at three locations on a sample with each location providing 100 data points. For surface coverage and live/dead analysis, five images were taken per sample and the three most representative images were chosen for processing. Four experiments with different bacterial cultures and separately prepared coatings were run per each sample. Differences in percentage dead bacteria adhering to unloaded and gentamicin-loaded PMAA coatings were assessed with a paired Student's t test and were significant with a p-value <0.05 using Minitab 18 software.

6.4. Results and Discussion

To explore the ability of hydrogel-like thin polymer coatings to uptake and release antibiotics in response to a pH trigger, coatings were constructed from PMAA, which has a high content of carboxylic groups that can act as negative charges and thus be used as binding centers for positively charged antibiotics. Importantly, these thin-film hydrogels also enable facile modification with a pH-sensitive fluorescent label for imaging of bacteria-induced local acidification.

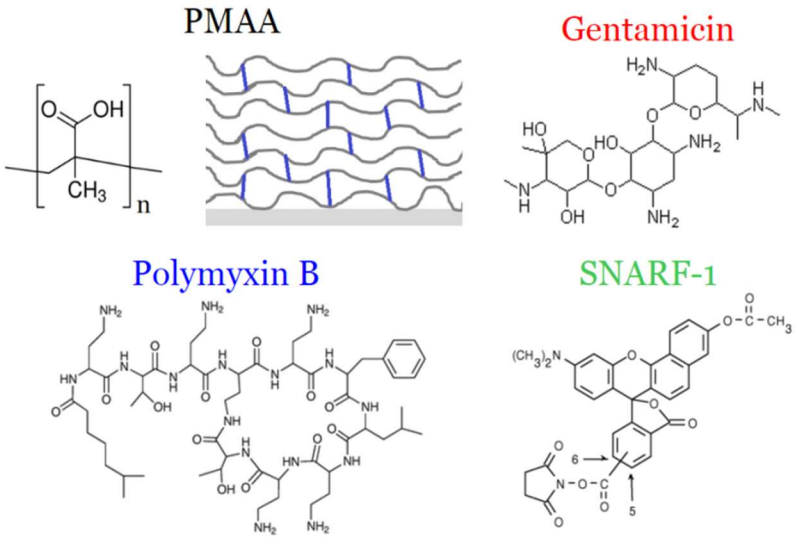

Figure 6-1. Chemical structures and schematic presentation of poly(methacrylic acid), PMAA, hydrogel-like coating with crosslinking segments indicated in blue, two antibiotics (gentamicin and polymyxin B), as well as a reactive label (SNARF-1 carboxylic acid, acetate, succinimidyl ester). Reprinted with permission from [82]. Copyright 2017 Acta Materialia Inc. Published by Elsevier Ltd.

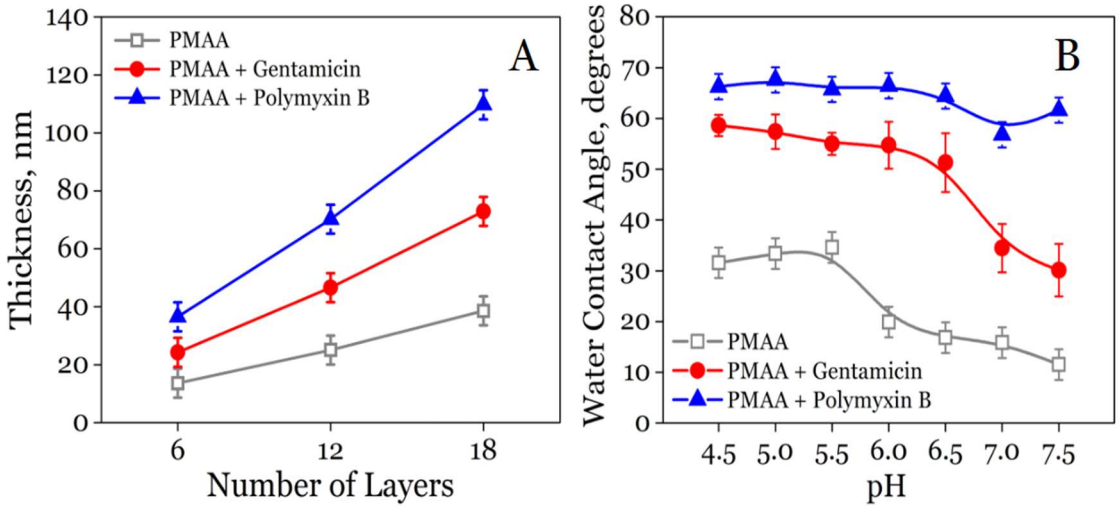

Figure 6-2. (A) Dry thicknesses of PMAA coatings before and after loading gentamicin and polymyxin B as measured by ellipsometry. (B) Surface wettability determined by water contact angle measurements for 18-layer PMAA coatings, unloaded, loaded with gentamicin or loaded with polymyxin B as measured in PBS. Reprinted with permission from [82]. Copyright 2017 Acta Materialia Inc. Published by Elsevier Ltd.

To form PMAA LbL coatings, hydrogen-bonded PMAA/polycaprolactam (PVCL) multilayers were deposited *via* spin-assisted deposition and chemically crosslinked followed by the release of PVCL using a procedure similar to that described previously [258]. Figure 6-2 shows dry thicknesses of PMAA LbL coatings, which increase linearly as a function of number of layers, with the thickness of priming layers (9.6 ± 3.4 nm) subtracted from all the data. To load antibiotics into the coatings, the negatively charged coatings were soaked in antibiotic solutions at pH 7.5 for 2 h. After exposure to positively charged gentamicin and polymyxin B (Figure 6-1), the dry thickness of the antibiotic-loaded coatings increased, indicating antibiotic uptake within the entire thickness of the coatings (Figure 6-2). Calculation of film charge balance (data not shown) suggested that the inclusion of both positively-charged antibiotics resulted in charge neutralization in the

film, therefore suggesting that binding mainly occurs through electrostatic interactions. Assuming a density of 1 g/cm^3 for the antibiotic-loaded hydrogel coating, an 18-layer PMAA film was able to load 10 ± 4 μg/mm^3 of gentamicin. As has been observed earlier [63,151] and can also be seen in Figure 6-2, increasing the number of layers deposited increased the amount of antibiotic that can be hosted in the film. Therefore, the dosage provided by this coating system is highly tunable by simple variation of the number of polymer layers used to create the film.

In addition to the amount of antibiotics absorbed within the coating, wettability and swelling are important factors that may affect antibacterial performance of the coatings. Before antibiotic loading, PMAA films were hydrophilic (Figure 6-2), with its water contact angle decreasing from 32 degrees to 12 degrees between pH 4.5 and 7.5. Upon incorporation of antibiotics, the coating became more hydrophobic. Consistent with the previous observation that drug hydrophobicity affects the wettability of weak polyacid hydrogels [266], polymyxin B, which is more hydrophobic than gentamicin [66], caused a larger increase in water contact angle of the films (Figure 6-2).

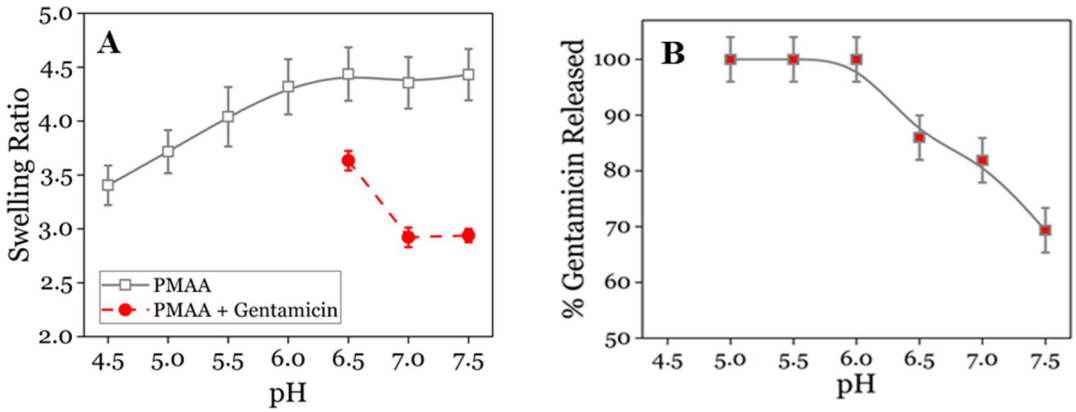

Figure 6-3. *In situ* ellipsometry data for the swelling ratios for unloaded and gentamicin-loaded 18-layer PMAA coatings in PBS as a function of pH (A) and percentage gentamicin released as measured by decrease in dry film thickness using ellipsometry after sequential 2 h exposures of the coatings to PBS with decreasing pH (B). Reprinted with permission from [82]. Copyright 2017 Acta Materialia Inc. Published by Elsevier Ltd.

Figure 6-3 shows *in situ*, ellipsometrically measured swelling of hydrogel coatings in PBS after an equilibration period. Importantly, exposure of unloaded PMAA coatings to pHs from 4.5 to 7.5 overnight does not result in a change in the dry film thickness and thus indicates the coatings are stable over this pH range as observed previously in our earlier works.[62,258,267] From the measured swelling of the films, the crosslinking density was calculated using a previously reported procedure [259], applying 0.985 cm^3/g for the specific volume, 0.598 [259] as χ and 80,000 Da as the molecular weight before crosslinking. The volume fraction of polymer in the swollen gel was 0.42 as calculated from the swelling ratio at pH 4.5. Based on these assumptions, M_c was calculated to be 498 Da or ~5.8 monomer units between crosslinks for PMAA coatings. Such a crosslinking degree was sufficiently low to allow inclusion of antibiotics within

the entire bulk of the hydrogel films. Loading antibiotics that carry positive charge into the negatively charged coatings decreased the LbL film swelling degree because of charge compensation and ion pairing of antibiotics with the carboxylate groups in the coatings [258].

To monitor the pH responsive release of gentamicin from the coatings, the thickness of the coatings after exposure to PBS solutions at decreasing pH values was measured *via* ellipsometry, under the assumption that loss of film thickness is due to the release of gentamicin from the coating. Gentamicin and polymyxin B contain 4 to 5 positive charges at pH 7.5 [268] and form ionic pairs with MAA units, resulting in release that is solely dependent on the ionization degree of PMAA. Importantly, no release of antibiotics was observed when hydrogels containing antibiotics were copiously rinsed with a buffer at a constant pH. The percentage gentamicin released was calculated as $\frac{t_{pH} - t_0}{t_L - t_0} \cdot 100\%$, where t_{pH} and t_L are dry thicknesses of the antibiotic-loaded coatings after exposure to PBS at a specific pH and immediately post-loading at pH 7.5 (low salt), respectively, and t_0 is the dry thickness of antibiotic-free coatings. Figure 6-3 shows that when the pH of the PBS surrounding a film is lowered, the percentage of antibiotic released increases as measured for release of gentamicin from an 18 layer PMAA film. pH-triggered release profiles were similar for gentamicin from coatings of 6 and 12 layers as well as polymyxin B from coatings of all thicknesses (data not shown). In agreement with our prior findings [66], pH-triggered antibiotic release from the coating was fast, and no long-term release occurred at a constant pH (data not shown). This is consistent with

electrostatic retention of antibiotics, and absence of diffusional constrains to drug release from the coatings.

6.4.1. Imaging of Local Acidification Induced by Bacteria

After demonstrating pH-responsive antibiotic release from the coatings, we aimed to verify that bacteria adhering to the hydrogel coatings were able to locally acidify the medium sufficiently to 'send' a release signal to the coating. *S. aureus* and *E. coli* are both known to acidify growth medium as a result of secretion of lactic and acetic acid, respectively [33,34]. Mature biofilms formed by several bacterial strains [269,270], including *S. aureus* [271] have been demonstrated to be acidic, but acidity of the environment around adhering individual bacteria has never been shown. To visualize the areas of acidification on the coatings during bacterial adhesion, a pH sensitive, ratiometric fluorescent probe (see Figure 6-1) was covalently bound to PMAA films. This probe enables the imaging of local pH changes in the hydrogel coating surrounding adhering bacteria *via* fluorescence emission selectively emerging in response to a decreased pH. Specifically, a reactive SNARF-1 label (SNARF-1 carboxylic acid, acetate, succinimidyl ester, Molecular Probes [272,273], see Experimental Section) was covalently attached to the amino groups of the ethylenediamine (EDA) crosslinker, which are approximately 50% one-end attached after crosslinking using carbodiimide chemistry [260]. Unlike exposure to antibiotics, SNARF-tagging did not result in a dry thickness change of the film. SNARF-1 has a pK_a of ~7.5, and emits red fluorescence ($\lambda_{em,\ max}$ = 640 nm) in its deprotonated form at high pH, and green fluorescence ($\lambda_{em,\ max}$ = 580 nm) in its protonated form in an acidic environment.

Figure 6-4 shows combined emission at wavelengths higher than 560 nm (using excitation at 543 nm), as detected during CLSM imaging of SNARF-1-labeled PMAA hydrogel soaked in PBS at varied pH for 1 h in a well plate with no bacteria. The fluorescence was strongly pH dependent, with an almost five-fold increase in green fluorescence between pH 7.5 and 4. Cycling the pH of the solution of the SNARF-1-labeled PMAA hydrogel between pH 4.5 and pH 7.5 showed complete reversibility and fast adjustment of intensity to pH (data not shown) and thus provided evidence that SNARF-1 was covalently attached to the film.

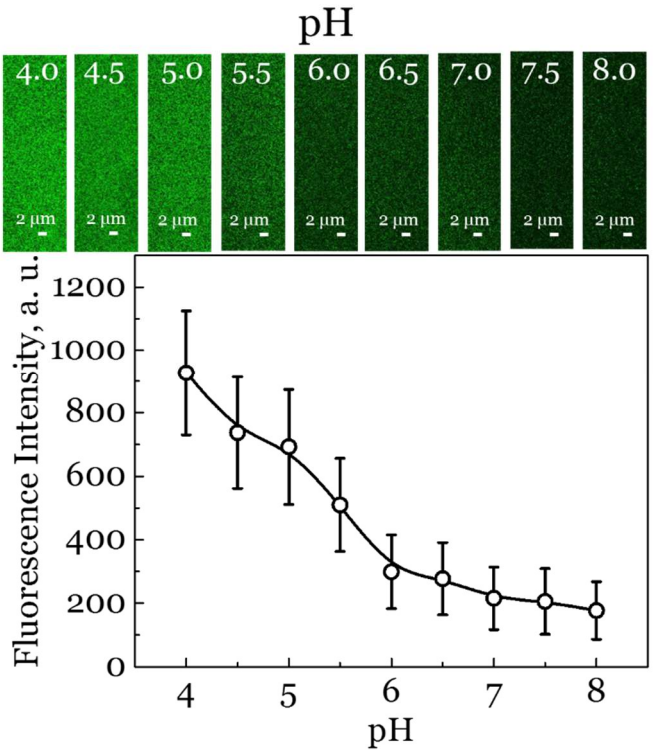

Figure 6-4. The fluorescence intensities (emission above 560 nm using excitation at 543 nm) of SNARF-1-labeled PMAA films as a function of the pH along with representative images. To generate the calibration curve, SNARF-1-containing films were immersed for 60 min in PBS with different pH. Reprinted with permission from [82]. Copyright 2017 Acta Materialia Inc. Published by Elsevier Ltd.

Fluorescence imaging of SNARF-1-labeled hydrogel coatings during bacterial colonization was more challenging than calibrating the fluorescence intensities of the hydrogel in bacteria-free PBS suspensions, since both *S. aureus* and *E. coli* have intrinsic fluorescence due to the amino acid tryptophan (excitation peaks at 230 and 280 nm and an emission peak at 340 nm [274,275]) and cellular metabolites (excitation peaks around 300 to 400 nm and emission peaks from 400 to 500 nm [274,276]). Furthermore, when excited at 410 nm, *E. coli* emits heavily in the range from 500 to 550 nm [277]. Therefore, significant effort was made to avoid interference of the intrinsic fluorescence of bacteria with fluorescence from the hydrogel coating. In a control experiment, bacteria were cultured on SNARF-1-free coatings, and were imaged using excitation at 488 nm and 543 nm (Appendix C). Emissions beyond 560 nm were collected and quantified using ImageJ. Significant green fluorescence from bacteria was observed only after excitation at 488 nm and therefore an excitation wavelength of 543 nm (Appendix C) was chosen for all further experiments.

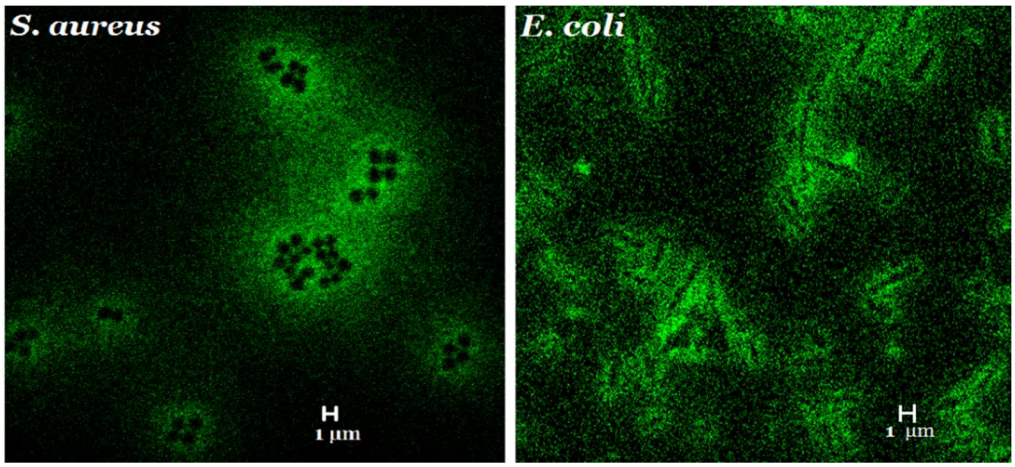

Figure 6-5. Confocal Laser Scanning Microscopy images of *S. aureus* and *E. coli* after 4 h growth on the surface of SNARF-1-labeled 18-layer-PMAA coatings. Images were collected with an excitation wavelength of 543 nm and show fluorescence above 560 nm due to local acidification. Reprinted with permission from [82]. Copyright 2017 Acta Materialia Inc. Published by Elsevier Ltd.

Figure 6-5 shows the results of 4 h culturing of *S. aureus* and *E. coli* on the SNARF-1-labeled PMAA coatings. The local acidification induced by bacteria is clearly seen by the intense green areas around the black spots (bacteria). The local acidification footprint was relatively long-ranged, on a micrometer scale, with *S. aureus* resulting in a larger-sized pH acidification zone than created by *E. coli*. The long range of the fluorescence halo around the bacteria exceeds the electrostatic screening length in culture solutions (7 Å for 0.15 M NaCl) by at least three orders of magnitude and proves that the images reflect excretion of acid around bacteria rather than electrostatic charge renormalization at PMAA carboxylic groups caused by proximity of the charged bacterial wall.

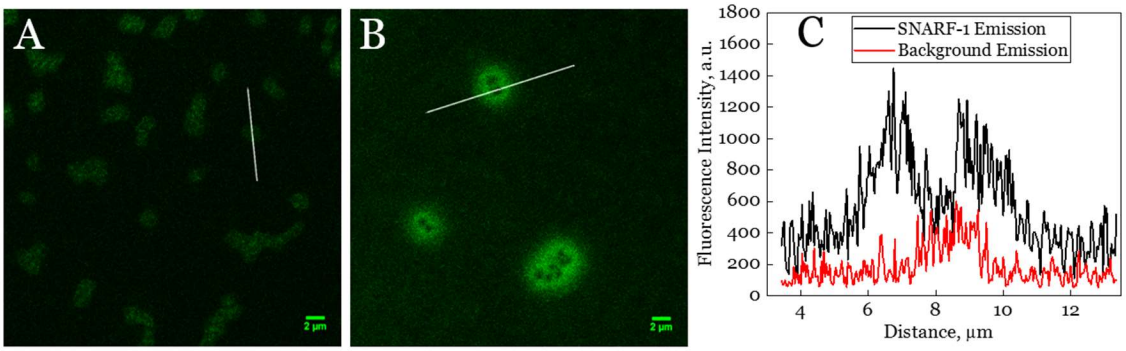

Figure 6-6. Confocal Laser Scanning Microscopy images of *S. aureus* after 4 h growth on the surface of SNARF-free (A) and SNARF-1-labeled (B) 18-layer-PMAA coatings. Images were collected with an excitation wavelength of 543 nm and show fluorescence beyond 560 nm. (C) Crosssectional emission intensities profiles of bacteria residing on a SNARF-free hydrogel (background fluorescence) and on SNARF-1-labeled hydrogel. Reprinted with permission from [82]. Copyright 2017 Acta Materialia Inc. Published by Elsevier Ltd.

The intensity profiles of bacteria residing on SNARF-free and of SNARF-1-tagged hydrogels are shown in Figure 6-6. The cross-sectional emission intensity profiles show that the intensity of SNARF-1 emission directly next to bacteria due to local acidification was significantly higher than the autofluorescence of bacteria in the absence of SNARF. The cross-sectional emission profile of bacteria on a fluorescently tagged hydrogel shows a significant dip in the area over the top of bacteria. From the calibration curve, the pH at the surface near bacteria was estimated to be between pH 5 and pH 5.5. However, precise pH profile determination was prevented due to a high level of noise in the imaging experiments.

6.4.2. Antibacterial Efficacy of Self-Defensive Films in Static, Small Volume and Fluid Flow Conditions

We then aimed to explore how efficient the demonstrated bacterially-triggered acidification was to stimulate antibiotic release and kill adhering Gram-positive, *S. aureus* ATCC 12600, and Gram-negative, *E. coli* O2K2 under static, small volume conditions and under fluid flow, *i.e.* between Petrifilm Aerobic Count Plates and in flow chamber experiments, respectively. PMAA coatings with varying thicknesses (6, 12, or 18 layers) were loaded with either gentamicin or polymyxin B to be evaluated against adhering *S. aureus* or *E. coli*, respectively, while unloaded films of matched thicknesses were used as controls.

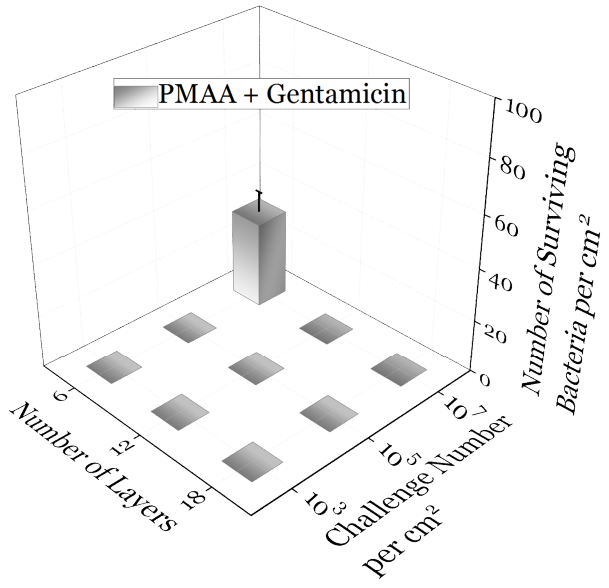

Figure 6-7. The number of surviving *S. aureus* on Petrifilm Aerobic Count Plates *versus* the number of layers of hydrogel films loaded with gentamicin for PMAA films after exposing the samples to various challenge numbers of *S. aureus* and allowing their growth for 48 h at 37˚C. Reprinted with permission from [82]. Copyright 2017 Acta Materialia Inc. Published by Elsevier Ltd.

In Petrifilm assays, antibiotic-free coatings had no effect on the growth of bacteria, whereas the coating became highly efficient in bacterial killing when loaded with corresponding antibiotics. Figure 6-7 shows that PMAA hydrogel films of varied thicknesses loaded with gentamicin were able to completely inhibit bacterial growth at challenge numbers of up to 10^7 *S. aureus* per 1 cm^2 coated sample surface. At a challenge of 10^7 bacteria per cm^2 sample surface, staphylococcal survival was only seen for 6 layer films. The difference in bacterial survival between 6 and 12-layer films can be explained simply from their gentamicin content - about 6.5 and 12.1 μg per cm^2 sample for 6 and 12 layer films, respectively (assuming a density of dry gentamicin of 1 g/cm^3). After release from the coatings in 1.01 mL of liquid employed in Petrifilm assays (1.0 mL to swell the agar plate and 10 μL of bacterial suspension), antibiotic concentrations of about 6.4 and 12.8 μg/mL were established between the Petrifilm Plates for the 6 and 12-layer coatings, respectively. These values are below and above the minimum inhibitory concentration (MIC) of gentamicin (12.5 μg/mL for this *S. aureus* strain), thus explaining the results in Figure 6-7.

Polymyxin B-loaded PMAA coatings demonstrated even higher antibacterial efficacy in the Petrifilm experiments when tested with *E. coli* O2K2. Specifically, the coatings completely inhibited bacterial growth for all film thicknesses even when exposed to the highest bacterial challenge of 10^7 bacteria per cm^2 sample surface (data not shown). This is likely due to the much lower MIC of polymyxin B against *E. coli* O2K2 (0.25 μg/mL). After complete release of polymyxin B from the smallest coatings in 1.01 mL

volume of buffer between the Petrifilm plates, polymyxin B concentration reached 14 μg/mL, *i.e.* well above the MIC of polymyxin B against *E. coli* O2K2.

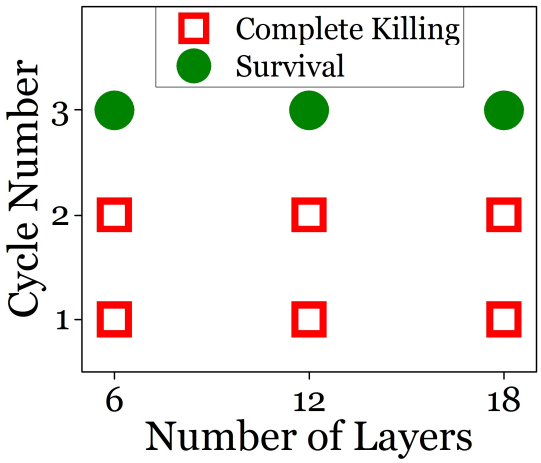

Figure 6-8. Prevention of bacterial growth by polymyxin B-loaded LbL films of varied thickness in Petrifilm experiments during several cycles of exposure to *E. coli* (bacterial challenge 10^7 bacteria per cm^2 sample surface). Reprinted with permission from [82]. Copyright 2017 Acta Materialia Inc. Published by Elsevier Ltd.

Because of the high efficacy of polymyxin B-loaded films against *E. coli*, it was examined whether polymyxin B-loaded films could be repeatedly used against *E. coli*, while preserving their high killing efficacy. To investigate this, after exposure to 10^7

bacteria, films were removed from Petrifilm plates and directly placed into fresh Petrifilm plates and re-exposed to a fresh *E. coli* suspension. Figure 6-8 shows that the high efficacy of the films was retained for two complete cycles of exposure to a challenge of 10^7 bacteria per cm^2 sample surface.

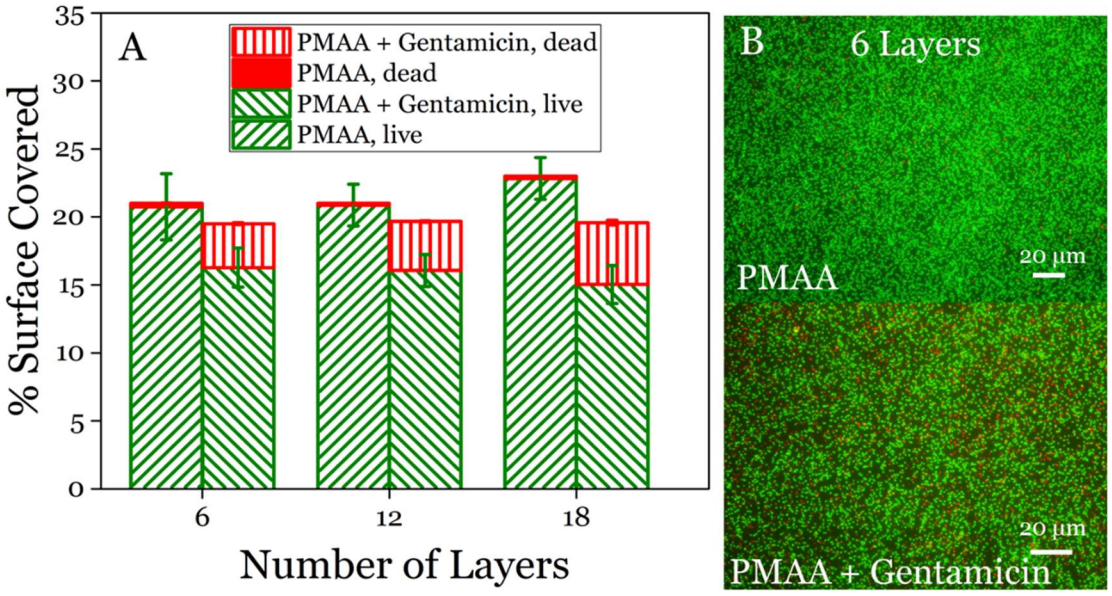

Figure 6-9. (A) Percent surface coverage and viability of *S. aureus* ATCC 12600 adhering from a flowing suspension in PBS (pH 7.0) to unloaded and gentamicin-loaded PMAA coatings with various numbers of layers. (B) Live/Dead images of unloaded (top) and gentamicin-loaded (bottom) 6-layer PMAA hydrogels. Reprinted with permission from [82]. Copyright 2017 Acta Materialia Inc. Published by Elsevier Ltd.

Finally, the efficacy of antibiotic-loaded films was explored in buffer under flow. The presence of flow of buffer through the chamber assures no changes in bulk pH during experiments, and antibiotic-release becomes completely dependent on local acidification by adhering bacteria. In these experiments, a bacterial suspension in PBS was flown over samples at a volumetric flow rate of 1 mL/min for 2 h. *E. coli* could not be used in these experiments because the strain adhered in very low numbers, as previously observed for *E. coli* O2K2 onto negatively charged surfaces [278]. *S. aureus* ATCC 12600, suspended in PBS at a concentration of $3x10^8$ CFU/mL, adhered very well to the coatings regardless of the number of film layers (Figure 6-9). In spite of similar bacterial adhesion, gentamicin-

loaded PMAA films were highly efficient in killing adhering staphylococci when compared to un-loaded PMAA films ($p<0.05$ Student's t-test), with a slight dependence on the number of layers of the film ($p<0.05$ between 6 and 18-layer films but $p>0.05$ between 6 and 12-layer films and 12 and 18-layer films). Further testing with thicker films would need to be conducted to confirm the layer dependence. Nevertheless, this finding confirms that self-defensive coatings remain active even under fluid flow and when the bulk pH is maintained at a constant neutral value.

6.5. Conclusions

In this work, we have demonstrated that coatings composed of a weak polyacid were capable of loading large amounts of positively charged antibiotics primarily through an electrostatic mechanism and released those antibiotics in response to a pH trigger provided by adhering bacteria. Most importantly, our experiments showed that the pH- and bacterially-triggered antibiotic release is highly localized. The LbL technique used to prepare the coatings in this work is attractive for constructing antimicrobials-hosting coatings because of its ability to deposit conformal coatings on a variety of substrates and the ease of control of the antibiotic payload by the number of deposited layers. Combined with the self-defensive mechanism of release of antimicrobials, this approach enables enhancing the antibacterial efficacy of a coating by a simple increase of the number of assembled polymer layers. The simple electrostatics-based mechanism of retention of antimicrobials within the coatings enables their use to host and on-demand deliver, in a

highly localized way, a range of positively charged antibiotics or antimicrobials, including those recently developed to which bacteria are not likely to develop resistance [279].

7. FLUORINATED POLYPHOSPHAZENE COATINGS USING AQUEOUS NANO-ASSEMBLY OF POLYPHOSPHAZENE POLYELECTROLYTES[4]

7.1. Introduction

Polyphosphazenes with fluorinated organic side groups, which comprise some of the most hydrophobic polymers known,[281,282] attract significant interest as materials for a variety of industrial and biomedical applications.[283-285] In particular, poly[bis(trifluoroethoxy)phosphazene], PTFEP and its copolymers have been extensively studied as high-performance elastomers, membranes, and surface coatings.[282-288] As with conventional fluorinated polymers, the high hydrophobicity of PTFEP is owed to fluorine-containing groups, such as the trifluoromethyl group, which tend to minimize the interfacial free energy.[289] However, the inherent flexibility of the polyphosphazene backbone[283] may also play an important role in surface hydrophobicity by allowing the fluoroalkoxy side groups to orient toward the surface and dominate the interfacial properties of the polymer.[290] This assumption is supported by very low glass transition temperatures of PTFEP (-66 °C)[282] and its mixed substituent copolymers (as low as -90 °C).[284,285] Hydrophobic properties of typical solution cast PTFEP surfaces are characterized with contact angles exceeding 100°.[290] Superhydrophobic surface properties of PTFEP can be attained with rough surfaces, for example through forming electrospun

[4] Reprinted in part with permission from Albright, V.; Selin, V.; Hlushko, H.; Palanisamy, A.; Marin, A.; Andrianov, A. K.; Sukhishvili, S. A.: Fluorinated Polyphosphazene Coatings Using Aqueous Nano-Assembly of Polyphosphazene Polyelectrolytes. In Polyphosphazenes in Biomedicine, Engineering, and Pioneering Synthesis; ACS Symposium Series 1298; American Chemical Society, 2018; Vol. 1298; pp 101-118. and Selin, V.; Albright, V.; Ankner, J. F.; Marin, A.; Andrianov, A. K.; Sukhishvili, S. A. Biocompatible Nanocoatings of Fluorinated Polyphosphazenes through Aqueous Assembly. ACS Applied Materials & Interfaces 2018, 10, 9756-9764. Copyright 2018 American Chemical Society.

nanofiber mats of PTFEP, which display contact angles as high as 159°.[290] In the life sciences, PTFEP based coatings are recognized for their outstanding biocompatibility[291] and are important constituents of clinically-validated injectable microspheres[292,293] and medical devices.[294,295]

PTFEP coating deposition is typically achieved *via* heat molding or solution casting,[282,291,296,297] however, these methods allow only limited control over uniformity, thickness, and functionality of the deposited film.[298] In contrast, the layer-by-layer (LbL) deposition technique enables coating substrates of a variety of shapes and surface chemistries with nanoscopically structured films.[35,150] The capability of the LbL technique to generate conformal coatings with programmed thicknesses and diverse compositions has been widely used for functionalization of biomedical devices.[254,291,299] Moreover, the use of water as a solvent[300] makes LbL assembly environmentally benign and aids in preserving the native structure and activity of biomolecules incorporated into films.[301] While water solubility is a common feature of a wide range of ionic macromolecules, endowing this capability to fluorinated polyphosphazenes has been challenging.

The present chapter investigates the feasibility of LbL deposition of fluorinated ionic polyphosphazenes nanofilms, and explores some of the key features of these coatings.

7.2. Results and Discussion

7.2.1. LbL Polymer/Polymer Assemblies

Thus far, fluorinated polyphosphazenes containing carboxylic and sulfonic groups have been successfully synthesized, both of which can provide negative charges to utilize

for electrostatic LbL deposition with polycations. Electrostatic deposition of multilayers is controlled by many factors including the concentration of salt in deposition solution,[302] charge density of polymers,[303,304] and other secondary interactions such as hydrophobicity and hydrogen bonding.[305] In general, it is accepted that there are two modes of growth of LbL films, linear, in which polymers are highly layered due to tight binding, and supralinear or exponential, in which polymer "layers" are highly intermixed due to weak interactions. Mode of growth can be regulated by a large variety of factors including deposition pH,[306] layer number[307] or deposition method (spin- vs. dip-assisted),[308] among others. Below, the assembly and properties of LbL assemblies of carboxylic acid containing, fluorinated polyphosphazenes are discussed. LbL assemblies with sulfonic acid derivatives of fluorinated polyphosphazenes remain unexplored. However, the differences in LbL assemblies due to changing interaction strength (carboxylic vs. sulfonic acid) will be interesting to study in future work.

7.2.1.1. Effects of fluorination degree on assembly thickness and water uptake.

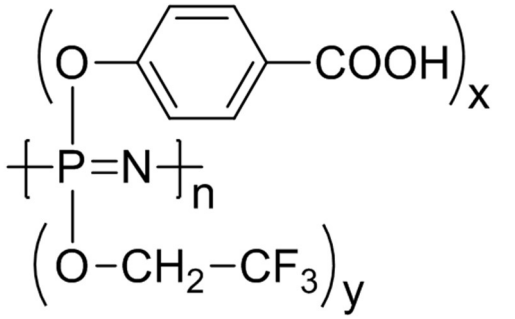

Non-fluorinated (PCPP), y (%) = 0

Fluorinated (FPy), y = 20, 60, 77, 86

Figure 7-1. Chemical structures of PPzs used in this work.

PCPP is a weak polyelectrolyte that is almost fully ionized in physiological conditions[309] and thus can easily be used for LbL deposition (chemical structures in Figure 7-1). Interestingly, fluorinated polyphosphazenes with 86 % (mol) fluorine-containing side groups and 14% carboxylic acid moieties have sufficient charge density at physiological pH (pH 7.4) to enable layer-by-layer binding.[310] Ionic fluorinated and non-fluorinated polyphosphazenes are able to form layers with a variety of polycations including synthetic polymers, such as branched polyethyleneimine (BPEI), and quaternized poly(2-(dimethylamino)ethyl methacrylate) and biodegradable polymers including poly-(L)-lysine.[310] Regardless of polycation partner, the degree of fluorination of ionic polyphosphazenes had a dramatic effect on film growth. Non-fluorinated PCPP formed thicker assemblies with BPEI (M_w = 25 kDa) compared to layers of highly fluorinated counterparts (FP60 and FP86) with BPEI, as determined by ellipsometry of dry LbL films (Figure 7-2). For the highly fluorinated polyelectrolytes, the increments of film thickness increase were similar (3.9 to 3.8 nm per bilayer for FP60 and FP86, respectively), but twice thicker films were formed with non-fluorinated PCPP. Such dramatic differences in film thickness per bilayer suggest the largely different strength of polymer-polymer interactions between assemblies of non-fluorinated and fluorinated polyphosphazenes, which is attributed to the likely enhancement of electrostatic pairing by hydrophobic groups of fluorinated polyions – FP60 and FP86. When deposition of BPEI with a polyphosphazene that has a low degree of fluorination (FP20) is explored, exponential growth similar to that of PCPP/BPEI is observed. This suggests that a certain

threshold exists for fluorination degree to induce film growth to transition from linear to exponential. Importantly, this trend of decreasing film thickness with increasing fluorination degree suggests the ability to control film growth and strength of interactions within the film through film component selection.

The strength of polymer-polymer interactions often dictates film properties/behavior. For example, increased strength of ionic pairing has been shown to enhance stability of electrostatic films in salt solutions.[308] The strength of polymer-polymer interactions exhibits itself in the degree of film swelling. PCPP/BPEI films swelled significantly in water (~45% film thickness increase due to water uptake), while water content in FP86/BPEI multilayers was extremely low, and did not exceed ~6% of their mass when exposed to phosphate buffer at pH 7.4 (Figure 7-2). Weaker bound PCPP/BPEI multilayers formed 'fluffier' layers, which were easily swollen in water due to the intrinsic hydrophilicity of the unbound polymer units, the osmotic pressure created by the counterions, and the electrostatic repulsion between excessive charges in the loops. In contrast, hydrophobic FP60 and F86 strongly contributed to expulsion of water from the film by creating a low-dielectric-constant environment.[311]

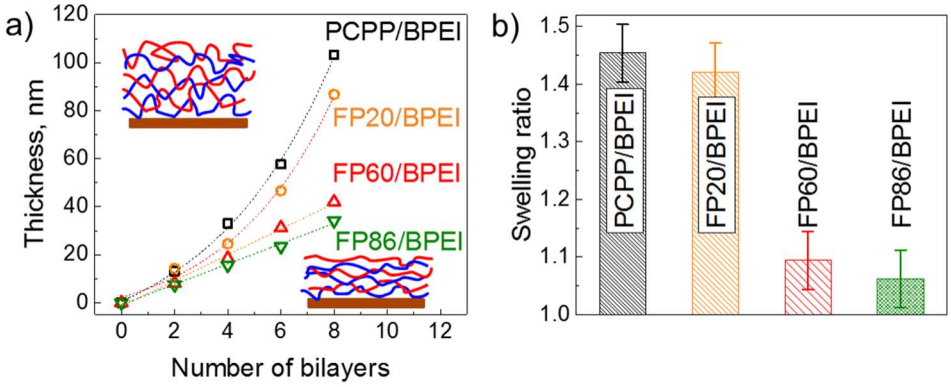

Figure 7-2. Deposition of LbL films with polyphosphazenes of varied hydrophilicity/hydrophobicity on silicon substrates (a), and comparison of LbL film swelling in 0.01 M phosphate buffer at pH 7.4 (b). Reprinted with permission from [280] Copyright 2018 American Chemical Society.

7.2.1.2. Film hydrophobicity and deposition on various substrates.

For biomedical applications, coatings need to be deposited onto substrates of various chemistries and arbitrary shapes with control over surface hydrophobicity. However, controlling surface hydrophobicity is challenging due to the tendency of hydrophobic groups to reorient into films upon exposure to water.[312] Surprisingly, fluorinated multilayers showed large oscillations of water contact angle depending on capping layer[310] and fluorinated content. When a polyphosphazene layer was on top of a polyphosphazene/BPEI film, contact angles of ~95, 80, and 60° were observed for FP86, FP60, and FP20 assemblies, respectively. All of these values are much higher than the value (40°) observed for films capped with PCPP on silicon wafers. On the other hand, when BPEI was on top, contact angles dropped significantly to ~55° for multilayers containing fluorinated polyphosphazenes. By increasing the content of fluorinated side groups, the amplitude of contact angle oscillations can be controlled.

Importantly, fluorinated polyphosphazenes can be coated onto materials such as titanium and polyester felt, which are used commonly for orthopedic implants[313] and medical device applications,[314] respectively. Similarly to those deposited on silicon substrates, FP-capped films coated on other substrates demonstrated high hydrophobicity. While the contact angle for an FP60/BPEI film (capped with FP60) deposited on a titanium foil substrate was similar to that for a film on a silicon wafer (~75°), the film on the porous surgical mesh had an enhanced value of contact angle (130°) as a result of the unique porous structure of the polyester surgical felt, which enhanced substrate roughness (Figure 7-3).[315] Thus, the developed coatings can be used to efficiently tune the wettability of surfaces.

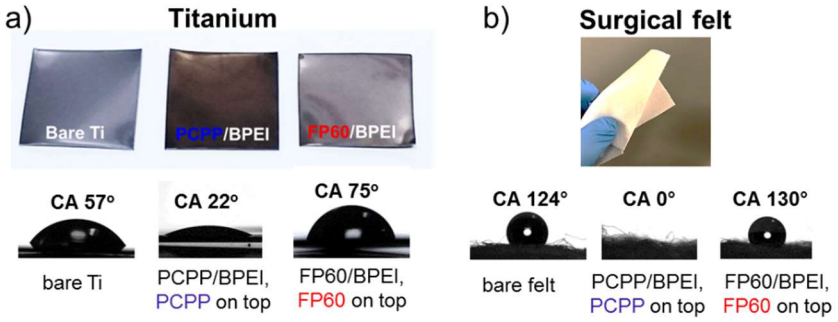

Figure 7-3. Images and water contact angles of LbL films of PCPP/BPEI and FP60/BPEI deposited on titanium foil (a) and polyester surgical felt (b). Reprinted with permission from [280] Copyright 2018 American Chemical Society.

7.2.1.2.1. Unique Oscillating Contact Angles(Adapted from paper)*

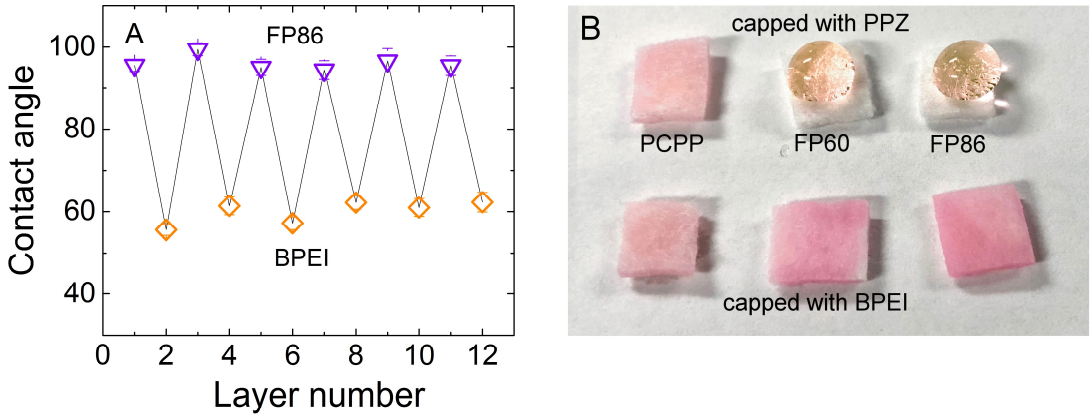

Figure 7-4.Contact angle oscillations as a function of layer number for FP86/BPEI system on Ti foil (A). Polyester surgical felt (B) coated with 6 or 7 (terminated with BPEI or PPz, respectively) layers of PPz-containing films with a droplet of Rhodamine 6G solution (capping layer is denoted below each pad). Reprinted with permission from [44] Copyright 2018 American Chemical Society.

Importantly, similarly to FP86/BPEI multilayers on Si substrates,[44] the contact angle oscillations with films deposited on Ti foil and polyester surgical felt were highly repeatable for a large number of deposition steps. Therefore, an important feature of the PPz-containing coatings is its independence of surface wettability on the film thickness. Figure 7-4 illustrates the wettability properties of LbL-coated polyester surgical felt, and contrasts the use of fluorinated and non-fluorinated PPzs in these coatings. In these experiments, a small amount of Rhodamine 6G (~0.05 mg/mL) was added to water to enhance droplet visibility. In all cases where the LbL coatings were terminated with polycation (BPEI), a droplet of Rhodamine 6G aqueous solution completely soaked the mesh pad. Switching the capping layer to a PPz had a dramatically different effect on wettability in the cases of non-fluorinated and fluorinated PPzs. The use of PCPP as a

capping layer did not change the pad hydrophobicity. In contrast, polyester surgical felt coated with FP-containing film and terminated with either FP60 or FP86 were highly hydrophobic and retained a droplet of Rhodamine 6G at the surface of the sample. Thus, the developed coatings can be used to efficiently tune the wettability of surfaces. In addition, the inclusion of small molecules, illustrated here with a model Rhodamine 6G molecule, was enhanced within FP/BPEI films as compared to the LbL films of non-fluorinated PCPP (Figure 7-4), probably due to the additional contribution of hydrophobic interactions to small molecule absorption.

7.2.2. Functional properties of FP LbL nanofilms: Biocompatibility

Good biocompatibility is the first major prerequisite for materials intended for life science applications.[316-318] To explore the potential of LbL nanocoatings of ionic fluorinated polyphosphazenes for applications in cardiovascular stents or catheters, the hemocompatibility of 200 nm films was evaluated using the common hemolysis test with dilute whole rabbit blood.[316,319] Hemolysis %, which represents an increase in the content of free hemoglobin in blood after incubation with the tested material, was dependent on fluorination degree of polyphosphazene (Figure 7-5). Importantly, LbL films containing FP86 demonstrated hemolysis extent comparable to that of a PTFEP coating. Hemocompatibility of clinically validated PTFEP[293-295] has been correlated with its ability to selectively and irreversibly adsorb human serum albumin (HSA) from blood plasma.[291] Moreover, irreversible adsorption of HSA has been previously related to passivation of surfaces against platelet adhesion.[291] Selective adsorption of HSA from human plasma

onto the polyphosphazene-containing multilayers was dramatically increased on FP/BPEI multilayers. Importantly, these coatings outperform not only non-fluorinated PCPP coatings but also nonionic PTFEP coatings. Therefore, ultrathin LbL films of fluorinated polyphosphazenes constructed in aqueous solutions can potentially achieve similar to or even higher hemocompatibility than that observed for clinically validated solution-cast nonionic PTFEP coatings.

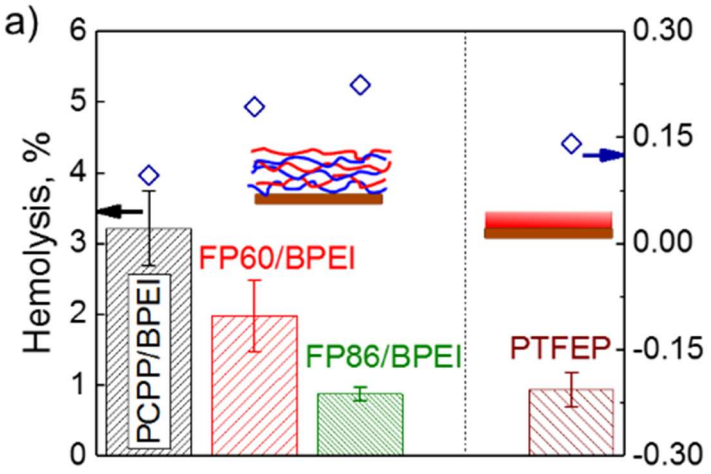

Figure 7-5. Functional properties of LbL films of fluorinated polyphosphazenes: (a) Hemolysis percentage of whole rabbit blood (columns, left axis) and irreversible adsorption of HSA from human plasma (dots, right axis) on FP/BPEI multilayers and control solution-cast PTFEP coatings. Reprinted with permission from [280] Copyright 2018 American Chemical Society.

Therefore, fluorinated polyphosphazenes with ionic carboxylic groups can be assembled into thin films from aqueous solutions using the LbL technique. Film properties can be modulated by the degree of fluorination of polyphosphazene as well as by the capping layer of the film. These films display a high degree of hydrophobicity, are

biocompatible. The next section will explore LbL assembly of these same polymers with small molecules.

7.2.3. LbL Coatings with Small Molecules

While depositing polymers using the LbL technique is commonly successful because of strong multisite interactions between polymer partners, trapping small molecules within LbL films has been challenging due to the smaller number of binding sites between the small molecules and polymers. To combat this, unique strategies such as complexing small molecules directly with other small molecules[66] or depositing small molecules in tetralayers with three other polymers were explored.[65,320] The tetralayer strategy was suggested to work by a combination of electrostatic and non-electrostatic interactions.[65,320] In our work, fluorinated ionic polyphosphazenes exhibited high efficiency in binding and trapping small molecule cationic antibiotics within LbL nanocoatings, a unique capability that is likely due to the high degree of flexibility of polyphosphazene backbones. The use of ionic hydrophobic polyphosphazenes for trapping small molecules within LbL coatings was successful even in the case of gentamicin – a hydrophilic small antibiotic with only ~3.5 positive charges at pH 7.5.[321] One notable difference between polymer-polymer assemblies and coatings with small molecules is the thickness deposited per bilayer. While FP60/BPEI coatings displayed a thickness of ~ 4.8 nm per bilayer, FP60/gentamicin coatings displayed only a thickness of ~1.3 nm per bilayer. To confirm that gentamicin was in the coatings, x-ray photoelectron spectroscopy (XPS), a highly sensitive method that enables resolution of the chemical composition of a coating within a penetration depth

of 3-10 nm, was used with the reference peak of carbon set to 284.9 eV. Comparing the nitrogen (N 1s) binding energies of a spun-cast monolayer of FP60 (Figure 7-6) and a 20-bilayer FP60/gentamicin film (Figure 7-6) clearly shows the emergence of two new peaks at ~400 and ~402 eV corresponding to $-NH_2$ and $-NH_3^+$, respectively, which confirms the presence of gentamicin in the coatings. Activity of gentamicin in the LbL coatings was tested via bacterial cultures of *Staphylococcus aureus,* a gram-positive strain known to form biofilms on biomaterial implants and devices.[3] LbL-assembles containing gentamicin were able to inhibit growth of ~3.5 x 10^3 CFU/cm^2 (Figure 7-6).

One common problem with electrostatic trapping of small molecules in LbL coatings has been the rapid release of antibiotics on exposure to salt containing solutions.[82,258] However, assemblies of gentamicin with fluorinated ionic polyphosphazenes were able to retain antibiotics after one-hour exposure to PBS (pH 7.5, 0.15 M NaCl), as demonstrated for 20-bilayer FP60/gentamicin coatings using XPS (Figure 7-6). On the other hand, assemblies of gentamicin and non-fluorinated ionic polyphosphazene (PCPP) lost ~20% of gentamicin after exposure to the same conditions. Such a difference is likely due to the additional hydrophobic interactions brought by fluorinated groups, which enabled retention of antibiotics even in salt solutions. These data suggest a facile way to incorporate a large variety of cationic small molecules into LbL assemblies at physiological pH without loss of efficacy. This strategy is highly attractive as fluorinated polyphosphazenes have been shown to be biocompatible[291,294] and polyphosphazene polyelectrolytes can be engineered to degrade within a certain time frame.[69,322] For

example, to increase degradation rate, pendant pyrrolidone groups can be added to enhance hydrophilicity and biodegradation.[322]

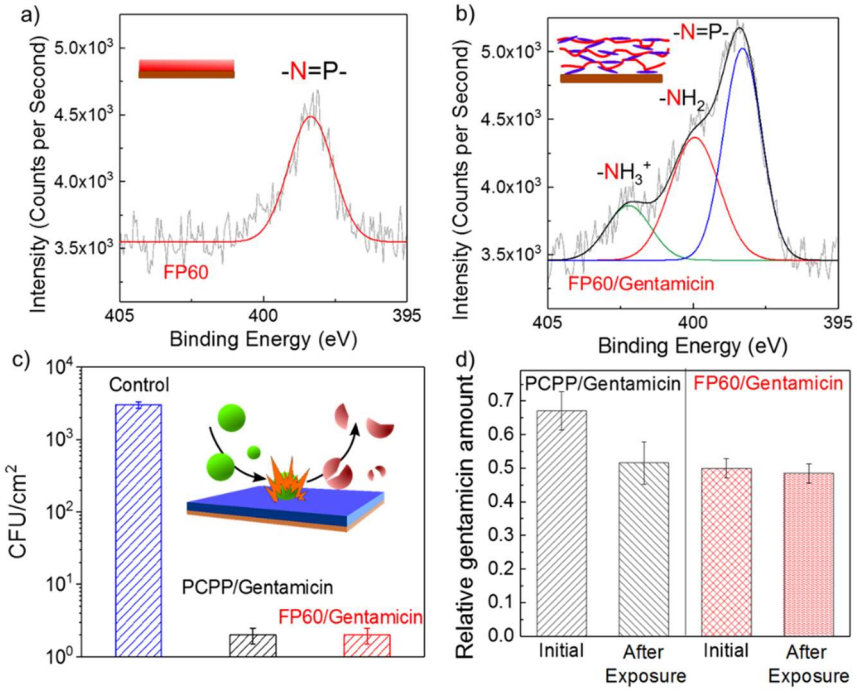

Figure 7-6. XPS analysis showing nitrogen (N 1s) binding energy in an FP60 monolayer (a) and in 20-bilayers of FP60/Gentamicin (b). (c) 35 nm PCPP/Gentamicin and FP60/Gentamicin films are able to prevent the growth of 10^3 colony forming units (CFU) of Staphylococcus aureus per cm^2. (d) Comparison of peak areas of nitrogen from XPS analysis reveals ~20% loss of gentamicin from PCPP/Gentamicin films after 1 hour exposure to PBS (pH 7.5, 0.15 M NaCl) while FP60/Gentamicin retains gentamicin. Reprinted with permission from [280] Copyright 2018 American Chemical Society.

7.3. Conclusions

Polyphosphazenes with fluorine-containing side groups are fiber-, film- and elastomer forming materials, which display high hydrophobicity and superb biocompatibility. A novel class of fluorinated polyphosphazenes has been introduced, which incorporates

ionic functionalities in their macromolecular structure. These mixed-substituent copolymers are water-soluble in their ionized salt form, but become highly hydrophobic when converted to a non-ionic state. Importantly, fluorinated copolymers maintain some of the most important features of polyelectrolytes, such as the ability to form complexes with ionic polymers of the opposite charge or produce ionotropic hydrogels through cross-linking with multivalent ions. The exceptional combination of properties of these macromolecules enables application of advanced aqueous-based methods for the deposition of highly hydrophobic and biocompatible fluorinated coatings. Here, the LbL technique was employed to engineer nanostructured films of fluorinated polyphosphazene polyelectrolytes. The resulting hydrophobic coatings displayed in vitro biocompatibility, which was comparable or better than biocompatibility of a clinically validated fluorinated polyphosphazene - PTFEP. Yet, LbL films of polyphosphazenes display significant advantages over nonionic PTFEP coatings in terms of both environmentally friendly processing conditions and multifunctionality of the resultant films. Specifically, LbL films have easily controlled film thickness and hydrophobicity, can easily be deposited on a wide range of substrates, and can be fabricated to include bioactive molecules, including bactericidal agents. Moreover, nano-layered fluorinated coatings demonstrated the ability to self-heal at near physiological conditions. The versatility of fluorinated polyelectrolytes suggests a wide spectrum of potential applications in life sciences ranging from biocompatible nanoparticle delivery systems to coatings for coronary stents and various implants.

8. A NEW FAMILY OF WATER-SOLUBLE SULFO-FLUORO POLYPHOSPHAZENES AND THEIR ASSEMBLY WITHIN HEMOCOMPATIBLE NANOCOATINGS[5]

8.1. Introduction

Fluorinated polymers and materials possess a range of unmatched properties for life science applications.[324] Outstanding biological inertness, stability, superhydrophobicity, and excellent biocompatibility are among their unique characteristics.[324-326] Taken together, these characteristics provide an abiotic tool for developing supramolecular constructs as well as a means to enable selective interactions with biological targets. Fluoropolymers find applications in medicine as coatings for cardiac stents,[327] such as XIENCE V™ - poly(vinylidene fluoride-co-hexafluoropropylene)[328] and Cobra PzF - poly[di(trifluoroethoxyphosphazene)],[329] as surface modifiers to make infection resistant biomaterials,[330] as nanoparticles for ^{19}F MRI tracking,[331,332] as well as for various uses in ophthalmology and reconstructive surgery.[324] However, the non-ionic nature and poor solubility of the currently used fluorinated polymers restricts their processing to standard melt-processing techniques[325] and prevents their self-assembly into advanced functional coatings. Incorporation of ionic functionalities in these hydrophobic polymers results in ionomers and enables important new features, which so far have been mostly used to develop industrial proton-conducting

---

[5] Reprinted in part with permission from Albright, V.; Marin, A., Kaner, P.; Sukhishvili, S. A.; Andrianov, A. K. New Family of Water-Soluble Sulfo–Fluoro Polyphosphazenes and Their Assembly within Hemocompatible Nanocoatings. ACS Applied Bio Materials 2019, 2, 3897-3906. Copyright 2019 American Chemical Society.

membranes. Along with highly commercially successful Nafion,[333,334] water insoluble fluorinated ionomers include various sulfonated block copolymers of poly(arylene ether),[335-339] and a few polymers with inorganic backbones, produced through multi-step post-synthetic derivatization procedures.[340,341]

Polyphosphazenes (PPzs) – hybrid inorganic-organic synthetic polymers with a phosphorus-nitrogen backbone and organic pendant groups - draw significant attention as macromolecules for biomedical applications.[342-345] They are characterized by a highly flexible backbone, a unique repeat unit that enables high charge density, and "dial-in" biodegradability.[342] We have recently introduced water-soluble, fluorinated PPz polyelectrolytes, which can be employed in all-aqueous assembly of hydrophobic fluorinated coatings.[44,280,346] These copolymers were based on a combination of trifluoroethoxy- and carboxylatophenoxy- pendant groups.[346] However, the narrow pH range of their water-solubility, along with weak acidity of carboxyl groups may impose limitations on the utility of these important macromolecular systems. Therefore, in this work, we explore water-soluble, fluorinated and sulfonated PPzs in solution and as building blocks for macromolecular self-assembly into nanostructured coatings.

Self-assembly can be achieved through the layer-by-layer (LbL) assembly technique, which utilizes oppositely charged ionic macromolecules to create nanoscopic coatings on surfaces of a variety of shapes and chemistries.[150] In particular, the LbL method has been widely explored to functionalize the surface of biomedical devices to control cellular adhesion and modulate delivery of bioactive molecules.[254,291,299] The integration of LbL assembly with the unique material properties of fluorinated systems

can open new prospects for the development of biosurfaces with highly sophisticated sets of characteristics, including controlled nanostructure, hydrophobicity, and/or biofunctionality.

The present paper describes the synthesis and characterization of a new family of fluorinated PPzs bearing sulfonic acid functionalities. The introduction of ionic groups in the polymer structure was achieved through a macromolecular substitution reaction of polydichlorophosphazene with a non-covalently protected sulfonic acid containing nucleophile - a method that avoids the use of harsh sulfonation conditions and eliminates the risk of introducing undesirable polymer irregularities.[347] Copolymers bearing either trifluoroethoxy or trifluoromethylphenoxy side groups displayed water-solubility in a broad pH range and demonstrated low cytotoxicity and high affinity for binding human serum albumin (HSA) – an important parameter in predicting potential biocompatibility of fluorinated materials.[291,327] PPzs assembled in films with branched polyethyleneimine (PEI) through the LbL technique and the resulting hydrophobic nanocoatings display excellent stability in solutions with high ionic strength and high hemocompatibility when tested with whole rabbit blood.

8.2. Materials

Sodium phosphate monobasic dihydrate, potassium chloride, branched polyethylene imine (PEI) of two molecular weights (M_w ~750 kDa and ~25 kDa), human serum albumin (Sigma-Aldrich, St. Louis, MO), porcine red blood cells (RBCs) (Innovative Technology Inc., Novi, MI), and rabbit blood (Rockland Immunochemicals, Inc., Limerick, PA 19468)

were used as received. Silicon wafers (100 orientation, P/B doped) were purchased from Wafer Pro Inc. Ultrapure Milli-Q water (Millipore, resistivity of 18.2 MΩ*cm) was used in all experiments.

8.2.1. Polyphosphazenes

Polydichlorophosphazene (PDCP) was synthesized as described previously.[348] Poly[di(phenoxyphosphazenesulfonic acid)] (SP) was synthesized using noncovalent protection of 4-hydroxybenzenesulfonic acid with tetraalkylammonium salts.[347] PPz containing 20% (mol/mol) of trifluoroethoxy groups and 80% (mol/mol) of carboxylatophenoxy groups (FP20) was synthesized using a previously described method.[346] For this work, two new polyphosphazenes were synthesized by Prof. Andrianov's group. Full details of synthesis and characterization can be found in our publication[349] or in Appendix D. Briefly, PPzs were synthesized to contain p-sulfophenoxy-, ethylphenoxy- and trifluoroethoxy- or trifluoromethylphenoxy- side groups. Specifically, FESP contained ~25% p-sulfophenoxy-, ~55% ethylphenoxy- and ~20% trifluoroethoxy- side groups. Specifically, FPSP contained ~28% p-sulfophenoxy-, ~55% ethylphenoxy- and ~17% trifluoromethylphenoxy- side groups.

8.3. Methods

8.3.1. Film Deposition

Layer-by-layer (LbL) films were assembled on silicon wafers that were cut into 1x1 cm^2 pieces. Prior to deposition, silicon wafers were cleaned *via* overnight treatment with UV

light and followed by exposure to sulfuric acid for 40 min as described elsewhere.[350] Samples were primed with a monolayer of PEI (M_w of ~750 kDa, pH 9, 0.2 mg/ml) by soaking substrates for 15 min in BPEI solution, washing with 0.01 M phosphate buffer (PB), and drying with nitrogen. LbL films were dip deposited with 5 min dipping cycles in 0.2 mg/mL aqueous solutions of either PPz or PEI of M_w ~25 kDa both at pH 7.5 with a wash (0.01 M PB, pH 7.5) in between each dipping cycle and dried with a gentle flow of nitrogen after the desired bilayer number was reached.

8.3.2. Film Characterization

8.3.2.1. Scanning Electron Microscopy

(SEM) was performed on samples sputter coated with ~2 nm of Pt/Pd alloy using a JEOL JSM-7500F.

8.3.2.2. Contact Angle Measurements

Contact angles were collected with an Imagine Source camera on a KSV Instruments Ltd. Setup. Contact angle measurements were performed with 5 μL, droplets of Milli-Q water and analyzed by One Attension software. Contact angle values were measured with ~100-nm thick films using three separate locations on each film.

8.3.2.3. Spectroscopic Ellipsometry Measurements

Spectroscopic ellipsometry was used to characterize film thickness and optical constants in both dry and swollen states using a M-2000 (J. A. Woollam Co., Inc., Lincoln, NE,

USA). Four angles of incidence: 45°, 55°, 65°, and 75° were used to analyze dry films while *in situ* measurements were carried out at 75°. For *in situ* measurements, samples were swollen in 0.01 M PB at pH 7.4 for 5 min before measurement. More details of fitting models used can be found in a previously published manuscript.[351]

8.3.2.4. Salt Stability

Coatings of ~100-nm thickness deposited on silicon wafers were exposed to 5 mL of increasing concentrations of potassium chloride in 0.01 M PB at pH 7.4 for 1 h. After exposure, samples were washed with 0.01 M PB to remove excess salt adhering to the coating and dried with nitrogen. The thickness of coatings was measured in two spots with ellipsometry, and the results were averaged.

8.3.2.5. Hemocompatibility Studies of Polymer Coatings

Hemocompatibility tests of ~100-nm coatings were carried out using whole rabbit blood as described previosuly.[319,351] Briefly, polymer coated silicon wafers (1x1 $cm^{2;}$ ~ 100-nm film thickness) were incubated (37 °C; 4 h) with diluted blood (1.0 mL, 2 mg/mL hemoglobin). Supernatant was isolated by centrifugation (14,000 rpm; 5 min) and the content of hemoglobin was measured by UV-VIS spectrophotometry. Analysis was conducted in duplicates. The difference between percent of free hemoglobin in the blood before and after incubation with coatings was reported as a percent of hemolysis.

8.4. Results and Discussion

8.4.1. Nanoassembly and Physico-Chemical Properties of Polyphosphazene Coatings.

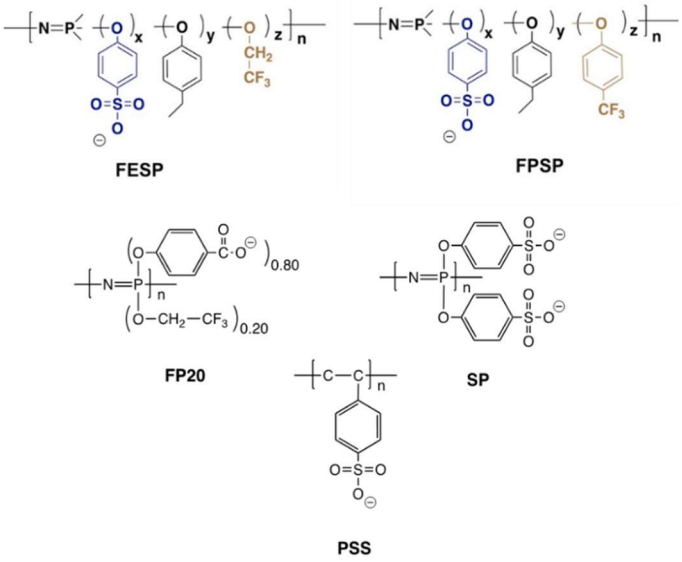

Figure 8-1. Chemical structures of anionic polymers used in this chapter.

Layer-by-layer (LbL) films were assembled in aqueous solutions using PEI as a polycation and silicon wafers as substrates. Figure 8-2 compares deposition of LbL assemblies of PPzs that are fluorinated and non-fluorinated containing sulfonic acid groups (FESP and FPSP vs. SP) and a non-PPz polyelectrolyte, poly(styrene sulfonic acid) (PSS). Chemical structures of all polyanions used are shown in Figure 8-1. The growth observed for all polymers containing sulfonic acid groups (FESP, FPSP, SP, and PSS) was linear with a constant increment of ~4.5-7.5 nm deposited per bilayer. Linear LbL film growth indicated strong ionic pairing between sulfonated polymers and PEI, flattening of polymer chains upon adsorption, and suggested little to no influence of fluorination or

backbone type on binding strength of polymer layers. The slight difference in the mass deposited for different system can likely be accounted for by the differences in the molecular mass of the polymer units. To understand the effect of chemistry of acidic units on polymer assembly, fluorinated PPzs with carboxylic acid (FP20) were deposited with PEI. In this case, significantly thicker films were formed, indicating weaker ionic pairing with positively charged PEI units, which is not surprising as the weaker ionic binding of carboxylic *vs* sulfo- groups is well known.[352,353]

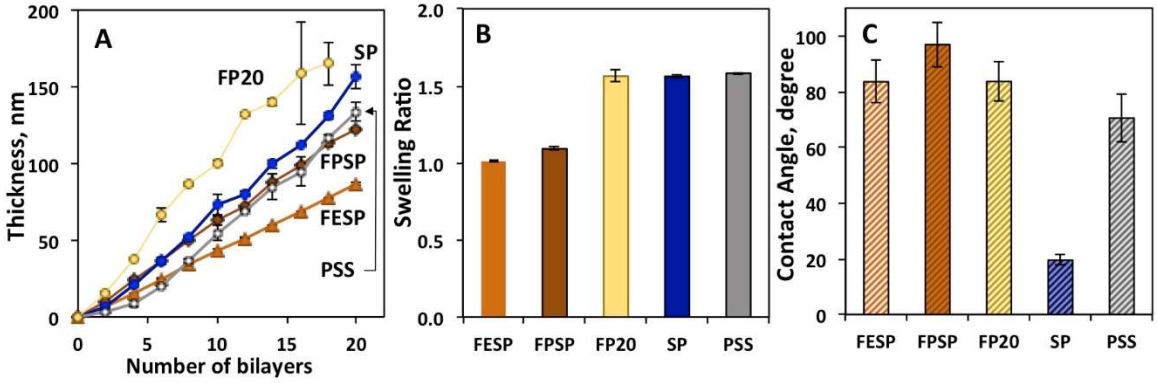

Figure 8-2. (A) Thicknesses of LbL films of PPzs or carbon-chain PSS formed by deposition with PEI as measured by spectroscopic ellipsometry. (B) Swelling ratios of ~100-nm coatings of PPzs or PSS with PEI as measured in 0.01 MPB, pH 7.4. (C) Contact angles of ~100-nm coatings of PPzs or PSS with PEI as measured with Milli-Q water. Reprinted with permission from [323] Copyright 2019 American Chemical Society.

We then explored the effect of chemistry of ionic groups, degree of fluorination, and backbone chemical composition on the capability to swell and control hydrophobicity of the nanocoatings. Figure 8-2 shows that films containing sulfo-fluoro PPzs (FESP and FPSP) did not swell (swelling degree ~1) when exposed to 0.01 M PB (pH 7.4), likely due to their strong binding and high hydrophobicity. In contrast, FP20, SP, and PSS coatings

all displayed relatively high swelling ratios of about 1.6. Significant uptake of water within films of PEI and FP20 probably results from its relatively weak ionic pairing with PEI. Unlike FP20, SP and PSS form strong ionic pairs with PEI, due to their sulfonated groups and high charge density.[352,353] However, both SP and PSS lack fluorinated moieties which provide resistance to water uptake. The contact angles of water for fluorinated nanocoatings containing FESP, FPSP or FP20 were, as expected, much higher than for the coating assembled with non-fluorinated PPz, SP (Figure 8-2). At the same time, the contact angle on the PSS and PEI film was significantly higher than that for the SP and PEI film, indicating a possible contribution of the hydrophobic carbon-based polymer chain to film hydrophobicity.

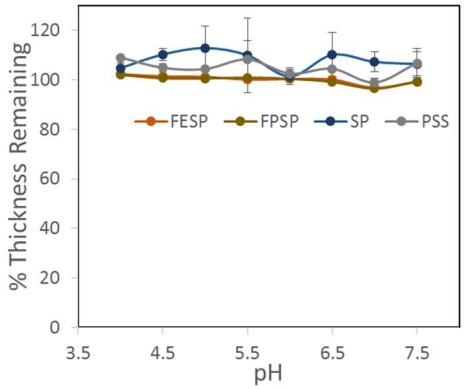

Figure 8-3. Remaining thickness of ~100-nm nanocoatings after exposure to 5 mL of 0.01 M phosphate buffer at pH X for 1 h. Reprinted with permission from [323] Copyright 2019 American Chemical Society.

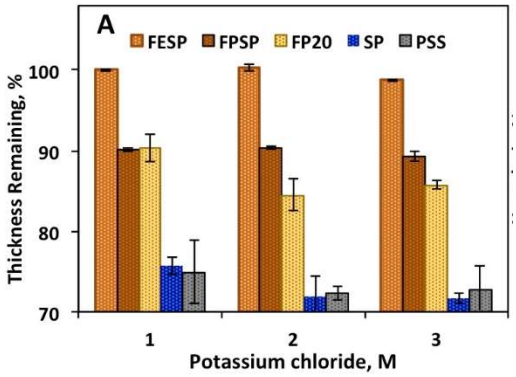

Figure 8-4. Remaining thickness of 100-nm films of PEI and PPzs or PSS after exposure to 1M, 2M, and 3M concentrations of KCl in 0.01 M PB at pH 7.4 for 1 h. Reprinted with permission from [323] Copyright 2019 American Chemical Society.

Stability of LbL films in various environmental conditions (salt and pH) is important for their suitability for biomedical applications. All nanocoatings constructed using sulfonated polyelectrolytes were stable (showing <10% thickness loss) in solutions with pHs ranging from 7.5 down to 4 (Figure 8-3). It is, however, well known that electrostatic pairing can be disrupted by small ions.[354] Thus stability of the nanocoatings was investigated in concentrated solutions of potassium chloride. Sodium chloride was avoided due to previously reported unusual solubility behavior of PPzs in this salt[355] and the observed decrease in solubility of FPSP. Coatings formed by sulfo-fluoro PPzs showed minimal loss of their original thickness, with no mass loss for FESP/PEI and ~10% loss for FPSP/PEI films even in high ionic strength 3M KCl solutions (Figure 8-4) and little change in coating morphology (Figure 8-5). Films of fluorinated carboxylic acid derivative FP20 with PEI were slightly less stable, losing about 15% of their original thickness in 3M KCl solutions. Interestingly, non-fluorinated films with sulfo groups in every polymer repeat unit but different backbone chemistry (SP and PSS, respectively)

lost 20-25% of polymer mass (probably due to dissociation of the top layers of the film) even in 1M salt solutions. Additionally, for SP coatings there was a very distinct change in film morphology from very smooth to spinodal-like dewetting (Figure 8-5).[356] These results demonstrate the importance of fluorinated groups in protecting nanocoatings against dissociation in concentrated salt solutions and also suggest that sulfonic acid functionalities may offer better stability in high ionic strength environment.

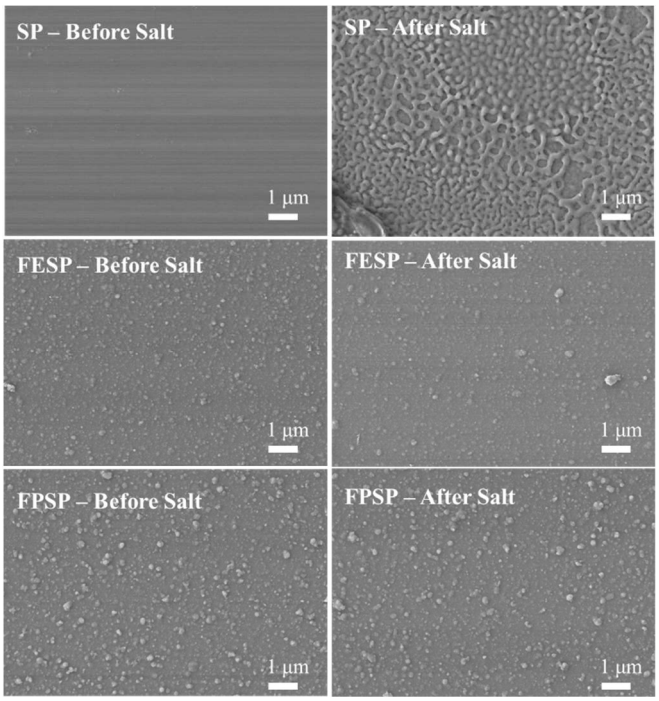

Figure 8-5. SEM images of ~100-nm nanocoatings before (left) and after (right) exposure to 4 M KCl. Images obtained at a WD of 15.4 mm, 3.0 kV, x10,000 zoom and with a 1 micron scalebar shown. Reprinted with permission from [323] Copyright 2019 American Chemical Society.

8.4.2. Hemocompatibility of Nanocoatings.

Adequate biocompatibility is one of the main requirements for materials designed for life sciences applications.[316-318] Therefore, PPz coatings were evaluated for hemolytic

activity using dilute whole rabbit blood test (American Society for Testing and Materials).[316,357] Figure 8-6 presents the results of this test for coatings with matched thicknesses and PPzs as the top layer. Remarkably, both sulfonated PPzs with fluorinated side groups (FESP and FPSP) showed levels of hemolysis less than 1%. Low hemolytic activity was also observed for fluorinated PPz containing carboxylic acid groups - FP20 (1%). Sulfonated PPz containing only ionic groups (SP) display a slightly higher activity (~2%), whereas coatings formed using PSS were the most active inducing about 6% hemolysis. These results show the importance of fluorination for decreasing hemolysis, which correlates well with hemolysis studies of water-soluble components observed earlier in this study, as well as with our previously published report on LbL with PPzs containing fluorinated and carboxylic groups.[44] Moreover, these PPzs demonstrate excellent biocompatibility for both LbL films and their macromolecular components in environments containing blood.

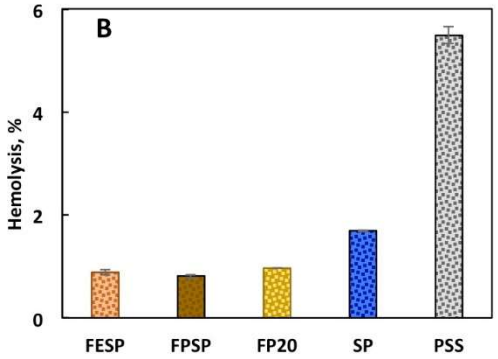

Figure 8-6. Hemolysis percentage of dilute whole rabbit blood after 4 h exposure (37 °C) to ~100 nm films of PEI and PPzs or PSS. Reprinted with permission from [323] Copyright 2019 American Chemical Society.

8.5. Conclusions

Two novel sulfo-fluoro polymers were synthesized using macromolecular substitution of polydichlorophosphazene with nucleophilic reagents, in which the sulfonic acid functionality was protected non-covalently by forming a salt with tertiary alkyl ammonium ions. Polyacids, which contained approximately 20% of either trifluoroethoxy or trifluoromethylphenoxy groups and about 25% of sulfonic acid functionalities, displayed excellent solubility in aqueous solutions over a broad pH range. Their polyelectrolyte behavior was confirmed by forming interpolymer complexes with oppositely charged PEI in aqueous solutions, which occurred even in the presence of 4% (w/w) of sodium chloride. Sulfo-fluoro PPzs and their water-soluble complexes with PEI showed low hemolytic activity and demonstrated the ability to bind HSA, which in the case of fluorinated macromolecules can serve as an indicator of their potential biocompatibility. Using the LbL technique, novel sulfo-fluoro PPzs were assembled with PEI into robust nanocoatings. The resulting nanofilms showed a range of properties, which make them promising candidates for further exploration as prospective biomaterials. These properties include higher hydrophobicity, lower swelling ratio, high stability in salt solutions, and superior hemocompatibility with whole rabbit blood as compared with control LbL films of non-fluorinated sulfonated PPzs or sulfonated carbon-chain polymers.

9. FLUORINATED POLYPHOSPHAZENES ENABLE HEMOCOMPATIBLE, HIGHLY-EFFICIENT ANTIBACTERIAL COATINGS

9.1. Introduction

Preventing bacterial colonization of surfaces in a controlled manner is highly desired for biomedical materials ranging from wound dressings to catheters.[1,358,359] As such, many bactericidal coatings to prevent such colonization have been developed that either use cationic [360]or anionic[17] bacteria killing polymers or that release antibiotics.[361] In terms of antibiotic-releasing coatings, stimuli-responsive coatings that kill bacteria upon their arrival due to a stimulus such as pH,[63,66,217,256] enzymes,[255] or direct contact[362] are highly attractive as they do not continuously elute antibiotics. This may prevent pre-mature depletion of the coatings and the development of bacterial resistance to antibiotics due to unnecessary, low dose antibiotic exposure. One attractive way to make such coatings is to use the layer-by-layer (LbL) method, invented by Decher,[35] which enables all aqueous deposition of coatings onto substrates of a variety of shapes and chemistries.

While many self-defensive LbL coatings have been engineered,[42,66,82,255] direct LbL of small molecules (*i.e.* cationic antibiotics) has been difficult to achieve with traditional anionic polyelectrolytes such as polymethacrylic acid or polyacrylic acid. Chaung *et al*. reported quadlayers of polyacrylic acid, poly(beta-amino esters), and gentamicin which showed tunable release of gentamicin driven by the degradation of the polyesters.[64] While such coatings showed efficacy against *Staphylococcus aureus* in a rabbit bone model,[65] the release was continuous and not “on-demand”. In contrast, our group recently reported multilayers of tannic acid, a small polyphenol, with cationic

antibiotics (tobramycin, gentamicin, and polymyxin B), which showed high loading capacity and non-toxicity towards osteoblasts.[66] While tannic acid can build coatings, it is a natural, small molecule which did not allow for pre-programming its interactions with antibiotics thus antibiotics delivery. Here, we introduced fluorinated PPzs as versatile binding partners of antibiotics, whose fluorination degree efficiently controls binding strength with antibiotics, and thus precisely pre-programs antibiotic delivery. We explore the effect of fluorination, which has been shown to increase biocompatibility,[44,363] of ionic polyphosphazenes in order to create coatings with advanced drug release profiles.

Polyphosphazenes (PPzs) are a unique class of polymers with an inorganic backbone and organic side groups. PPzs facile tunability of their side groups offers control over their degradation rate into generally physiologically benign degradation products.[69-71] PPzs have a proven record of preclinical and clinical safety for stent applications,[72,74-77,364] and therefore, are likely to be safe for other blood-contacting applications such as wound dressings. The ease of varying the side groups of PPzs makes them excellent candidates for systemically exploring the combined effects of electrostatic and hydrophobic interactions on antibiotic retention and release. Non-fluorinated and fluorinated PPzs have be shown to form ionic complexes with mono-valent, di-valent, and multivalent salts depending on fluorination degree,[365-367] suggesting their capability to bind small molecule antibiotics. We recently reported multilayers of fluorinated, ionic polyphosphazenes with several different cationic polymers.[310] These coatings showed tunable hydrophobicity based on polymer-coating top layer and polymer fluorination degree. Importantly, these coatings demonstrated low levels of hemolysis, suggesting their

potential hemocompatibility. Biocompatibility is an important aspect of any biomaterial, yet it is often understudied for antibacterial coatings. While several reports have studied cytotoxicity of antibacterial coatings, only a few[368,369] have considered how blood will react to the surface (hemolysis). In this work, we aim to bridge this gap in the knowledge base by systematically comparing the effect of PPz fluorination degree on antibacterial activity, cytotoxicity, and hemolysis.

Here, we explore direct LbL deposition of cationic small molecule polymyxin B with ionic, fluorinated PPzs (FPy, in which y represents the % of fluorinated substituent groups) and ionic, non-fluorinated poly[di(carboxylatophenoxy)phosphazene] (PCPP). Poly B, a cyclic cationic polypeptide, was chosen for study since it has several positive charges at neutral pH. While Poly B was originally left behind for its less-than-desirable side effects, it is now making a resurgence as an option for treating highly drug resistant gram-negative bacteria.[370] Unlike our previous work, which explored the effect of hydrophobicity of antibiotics on antibiotic delivery,[66] here we aim to control antibiotics delivery through a degree of fluorination of PPzs. Specifically, the influence of fluorination of PPz, which creates local hydrophobic microenvironments with enhanced charge-charge interactions, on binding of antibiotics is explored. We show that fluorination degree and thickness of coatings modulate antibiotic content, and examine the surface activity and non-leachability of coatings against *E. coli* with 3M™ Petrifilm™ and zone of inhibition (ZOI) assays. Furthermore, hemolysis (with rabbit and porcine blood) and cytocompatibility (with NIH 3T3 fibroblasts) is shown.

9.2. Materials

Tryptic soy broth (TSB) powder was obtained from MP biomedicals (Solon, OH). Difco™ Technical Agar was obtained from BD Biosciences (San Jose, CA). Polymyxin B, branched polyethylenimine (BPEI, weight-average molecular weight M_w of 750,000 g/mol), sodium phosphate monobasic dihydrate were purchased from Sigma-Aldrich (Allentown, PA). Hydrochloric acid, sodium hydroxide, and sulfuric acid were obtained from Alfa Aesar (Tewksbury, MA). Ultrapure water from a Milli-Q system (Merck Millipore, Burlington, MA, USA) with a resistivity of 18.2 MΩ was used in all experiments. Boron-doped silicon (Si) wafers were purchased from University Wafer, Inc. All other chemicals were purchased from Sigma-Aldrich and used without further modification. This work uses several ionic, fluorinated polyphosphazenes, which were synthesized by our collaborators and reported earlier.[44,280,348,355,367] M_ws were 800 kDa for PCPP, 140 kDa for FP20, 246 kDa for FP60, and 200 kDa for FP77.

9.3. Methods

9.3.1. Layer-by-Layer Deposition

Films of PPzs and Poly B were deposited using the dip-deposition technique. In order to deposit PPzs/Poly B films onto surfaces, first a priming layer of BPEI (M_W = 750 kDa, pH 9, 0.2 mg/mL) was deposited for 15 min followed by a priming layer of PPz (pH 7.5, 0.01 M phosphate buffer (PB), 0.4 mg/mL) deposited for 10 minutes. Afterwards, alternating layers of PPzs (pH 7.5, 0.4 mg/mL) and Poly B (pH 7.5, 0.5 mg/mL) were deposited for 10 min.

9.3.2. Dry and Wet Thickness Measurements

Thicknesses and optical constants in dry states were characterized by a variable angle spectroscopic ellipsometer (M-2000 UV−visible−NIR (240−1700 nm) J. A. Woollam Co., Inc., Lincoln, NE, USA) equipped with a temperature-controlled liquid cell. Dry measurements were carried out at four angles of incidence: 45°, 55°, 65°, and 75°. For data fitting, polymeric layers were treated as a Cauchy material of thickness d with refractive index A. Both parameters were fit simultaneously. In situ ellipsometry was conducted at an angle of 75° with a liquid cell and temperature controller. Samples were run in PBS at pH 7.5 at 37 °C for 1 hour. To calculate swelling ratio, the wet thickness for the last ten minutes (*i.e.* minutes 50 to 60) were used in order to provide enough time to make sure the film was at equilibrium. More details for fitting models can be found in an earlier publication.[44]

9.3.3. Degradation/stability at 37 °C studies

100-nm coatings on 1x1 cm^2 Si wafers were first washed with PBS at pH 7.5, dried, and thickness measured to separate the effect of salt on the coatings from the effects of pH and temperature. Afterwards, samples were exposed to 10 mL of PBS at pH 7.5 or 5.5. After the desired soak time, samples were washed with pH matched 0.01 M PB, dried with nitrogen, and returned to the same solution. Samples were run in duplicate.

9.3.4. Contact Angle

Contact angle was measured using a KSV Instruments Ltd. Setup equipped with an Imagine Source camera. 5 µL droplets of DI water were placed on coatings of ~ 30 nm in three separate locations. Two separate sets of samples were analyzed using One Attension software and averaged together for the final value.

9.3.5. Liquid Chromatography-Mass Spectrometry (LC-MS)

For LC-MS analysis, 1 x 1 cm^2 samples were exposed to 0.5 mL of PBS at pH 7.5, 6.5, 5.5, 4.5, and 12 consecutively, for 1 hour each and solutions used for LC-MS analysis at the Integrated Metabolomics Analysis Core. After exposure to a certain pH, samples were rinsed with phosphate buffer at matched pH, dried, and thickness measured with ellipsometry. Duplicate sample sets were used to ensure reproducibility. The target compounds from the collected PBS samples were detected and quantified on a triple quadrupole mass spectrometer (Altis, Thermo Scientific, Waltham, MA) coupled to a binary pump HPLC (Vanquish, Thermo Scientific). MS parameters were optimized for the target compound under direct infusion at 5 µL/min to identify the SRM transitions (precursor/product fragment ion pair) with the highest intensity (Table 9-1) Samples were maintained at 4 °C on an autosampler before injection. The injection volume was 10 µL. Chromatographic separation was achieved on a Hypersil Gold 5 µm 50 x 3 mm column (Thermo Scientific) maintained at 30 °C using a solvent gradient method. Solvent A was water (0.1% formic acid). Solvent B was acetonitrile (0.1% formic acid). The gradient method used was 0-1min (20% B to 60% B), 1-1.5 min (60% B to 95% B), 1.5-3 min

(95% B), 3-4.1 min (95% B to 20% B), 4.1-5 min (20% B). The flow rate was 0.5 mL/min. Sample acquisition and analysis was performed with TraceFinder 4.1 (Thermo Scientific).

Table 9-1: Quantitative SRM Transitions for compounds

Compound	Polarity	Precursor (m/z)	Product (m/z)	Collision Energy (V)	RF Lens (V)
Polymyxin B1 2+	Negative	603.0	593.6	16.52	162
Polymyxin B1 3+	Negative	403.0	396.7	10.23	79
Polymyxin B2 2+	Negative	596.8	587.4	16.26	174
Polymyxin B2 3+	Negative	398.0	391.8	10.23	84

9.3.6. Bacterial Studies

Bacterial strains in this work include *Escherichia coli* (*E. coli*) ATCC 25922. *E. coli* was streaked on TSB agar plates from a frozen glycerol stock, incubated at 37 °C for 16 h (hours) to obtain single colonies, and stored at 4˚C before bacterial culture. All cultures were started with colonies from plates of less than one week old.

9.3.6.1. Minimum Inhibitory Concentration (MIC) Assays

The MICs of Poly B for *E. coli* was determined by the standard method of measuring optical density at 600 nm (OD_{600}). Specifically, a single colony was isolated and grown overnight in TSB for 16 h at 37 °C, 250 rpm. Afterwards, OD_{600} was measured and used to calculate the CFU/mL and the culture was diluted to the desired concentration (2 x, 10^3,

10^5 or 10^7 CFU/mL) in TSB. 100 µL of bacterial culture was added to 100 µL of antibiotic in various concentrations and cultured for 24 h in 37 °C (static). OD_{600} of the culture was measured after 24 h. Each antibiotic concentration was tested in triplicate against each bacterial concentration. Three dilutions of each bacterial culture used were plated to verify the count (CFU/mL) used in the test. TSB and bacteria only tubes were used as controls.

9.3.6.2. Growth Curves

A single colony of *E. coli* was isolated and grown overnight in 3 mL of TSB for 16 h at 37 °C, 250 rpm. Afterwards, OD_{600} was measured and used to calculate the CFU/mL and the culture was diluted to 10^5 CFU/mL in TSB. 12 mL of 10^5 CFU/mL in TSB was placed in a 6 well plate with either nothing (control), various concentrations of Poly B, or PPz/Poly B samples on 1x1 cm^2 Si wafers. A volume of 12 mL was chosen so that a maximum concentration less than MIC could be achieved assuming the worst case scenario in which all Poly B was released from the most potent coating PCPP/Poly B 200 nm, which contains ~20 µg of Poly B. OD_{600} was measured every 2 hours starting at hour 4 until 14 hrs. All samples were run in triplicate. Data show represent averages of three data sets with error bars representing the standard.

9.3.6.3. Petrifilm Assays

For Petrifilm assays, a single colony was inoculated in 3 mL of TSB and grown overnight at 37 °C, 250 rpm. Afterwards, the OD_{600} of the culture was measured and used as a guideline to prepare cultures containing 10^9 and 10^7 CFU/mL *via* dilution with TSB. 3M™

Petrifilm™ *E. coli* count plates were treated with 1 mL of sterilized DI water for 30 min to hydrate the nutrient loaded gel layer. PPz + Poly B coated silicon wafers were placed face up on the hydrated Petrifilms and 5 µL of bacterial suspension was placed onto the sample and incubated at 37 °C for 24 h. After 24 h, the bacterial colonies appearing on top of the samples were counted while bacteria off the edges of the sample were not counted. All samples were tested in duplicate.

9.3.6.4. Zone of Inhibition Assay

A single colony was isolated and grown overnight in 3 mL of TSB for 16 h at 37 °C, 250 rpm. Afterwards, OD_{600} was measured and used to calculate the CFU/mL and the culture was diluted to 10^5 CFU/mL. *E. coli* was streaked onto 20 mL TSB agar plates from the stock solution, three times with 60 degree rotation each time. A 1x1 cm^2 sample on Si wafer was placed face down on the agar and the plate incubated for 24 hrs at 37˚C. Samples were run in duplicate with PCPP and FP77 + Poly B coatings of either 100 or 200 nm.

9.3.7. Fibroblast Cell Studies

NIH/3T3 fibroblasts were purchased from the American Type Culture Collection (ATCC, USA). Cells were cultured in Dulbecco's modified Eagle's medium (HyClone) supplemented with 10% fetal bovine serum (v/v) (Atlanta Biologicals), 1% Non-Essential Aminoacids (HyClone), 10 uM HEPES (HyClone) and 1% penicillin/streptomycin (Corning). Cells were propagated following ATCC standard protocols. Prior to cell

studies, samples were sterilized with UV light inside a biosafety cabinet for 10 minutes per side.

For culturing, samples were placed inside a 24-well plate, covered with a cell suspension at a seeding density of 10^4 cells/cm^2 in 1 mL of fresh media, and incubated at 37 °C in a 10% CO_2 atmosphere for 2 or 4 days. For Live/Dead staining, the media was removed, samples were washed with 250 uL of 1X Phosphate-Buffered Saline (PBS) at room temperature, and they were overlaid with a staining solution of 2 uM Calcein AM (Enzo Life Sciences) and 3 uM Propidium Iodine (Enzo Life Sciences) in PBS. A positive control (cells grown without exposure to sample) and negative control (cells fixed with 70% ethanol in water for 30 minutes at 4 °C before staining) were included. After 30 minutes of incubation at room temperature while protected from light, each sample was imaged using confocal microscopy (Leica DMi8) at five independent regions in the surface. Total cell count per region was calculated using ImageJ.

9.3.8. Hemolysis Studies

Hemocompatibility tests were conducted using modified hemolysis test with Red blood cells, RBCs (1% suspension in PBS, 2 h incubation at 37° C)[371-374] and using whole rabbit blood (1.0 mL, 2 mg/mL hemoglobin, 4 h incubation at 37° C).[319,351]

9.4. Results and Discussion

9.4.1. Physiochemical Characterization

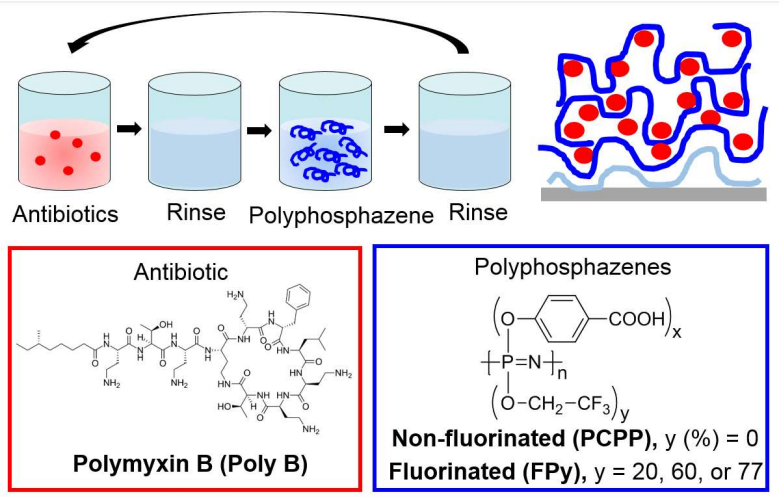

Figure 9-1. Schematic representation of LbL assembly and chemical structures of LbL components.

Inspired by polyphosphazenes's (PPzs) ability to form ionotropic gels with multivalent ions, such as calcium or spermine, which physically resemble calcium alginate hydrogels[375,376] and the preclinical safety record of fluorinated PPzs for blood contacting applications,[329] here, we explore layer-by-layer films of cationic antibiotics with PPzs of various fluorination degrees. The structures of Poly B, non-fluorinated poly[di(carboxylatophenoxy)phosphazene] (PCPP) and fluorinated PPzs (FPy, in which y represents the % of fluorinated substituent groups) are shown in Figure 9-1. LbL assembly was conducted at pH 7.5 with 10 min dipping cycles, as illustrated in Figure 9-1, and measured by spectroscopic ellipsometry **(**Figure 9-2A). Strikingly, all PPzs, even a fluorination degree of 77% can support film growth. This is in sharp contrast to traditional polyelectrolytes (PAA, PMAA, etc.), which are unable to support LbL growth of cationic

antibiotics at neutral pH. All films deposited in an exponential-like manner suggesting intermixing of film components. FP20 + Poly B system shows slightly thinner growth than the rest of the films, likely due to slightly lower M_w.

To explore the influence of molecule weight, PCPP of various molecular weights was deposited with Poly B (Figure 9-3A). Interestingly, PCPP with M_w of 200 kDa or greater enabled film growth while PCPP of M_w of 60 kDa or less prevented film deposition. It has been observed with long chain polyelectrolytes that low molecular weight anions and cations can "strip" each other off of the surface and prevent film growth because they have a propensity to form polyelectrolyte complexes due to their interaction energy.[377] It has been found that ionic crosslinking of alginic acid is molecular weight dependent and if the polymer length is too short, crosslinks do not form,[378] which correlates well with what we observe here for short chain PCPP. Therefore, the thinner coatings of FP20, which has a Mw of ~140 kDa, is likely due to the shorter chains.

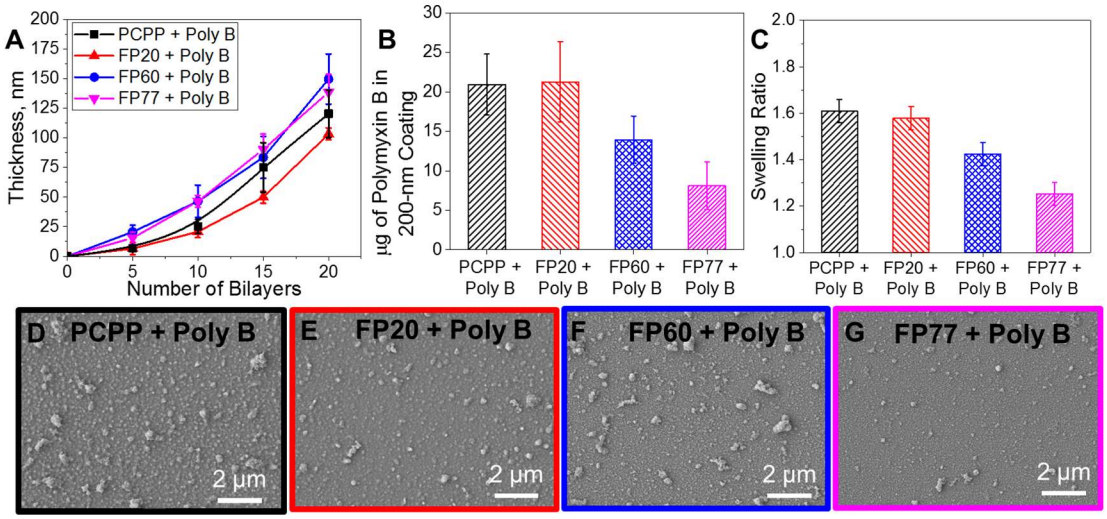

Figure 9-2. (A) Dry thicknesses of layer-by-layer films as measured by spectroscopic ellipsometry for assembly of polymyxin B (Poly B) with PPzs with various fluorination degrees, (B) Micrograms of Poly B in a 200 nm film on a 1x1 cm^2 wafer as measured by LC-MS for dissolved films. (C) Swelling ratio of PPz + Poly B films measured in PBS at pH 7.5 at 37 ˚C. (D-G) SEM images of 100 nm PPz + Poly B films.

To quantify the amount of Poly B retained in the LbL assemblies, coatings were dissolved in basic conditions and resulting solution analyzed *via* liquid chromatography-mass spectrometry to determine the concentration of Poly B. LC-MS detection of Poly B was done on a triple quadrupole with the 2+ and 3+ ions of Poly B. Since Poly B is actually a mixture of five different variations with slightly different R groups, with Poly B1 and B2 being the major components, the 2+ and 3+ ions of Poly B1 and Poly B2 were tracked for analysis. The specific m/z product and parent ions monitored are listed in Table 9-1 in the Materials & Methods section along with more details about the LC-MS method used. Measured concentrations of Poly B as well as release volumes were used to calculate antibiotic content in the films and then normalized by film thickness. Comparing normalized data for 200 nm films on 1 x 1 cm^2 wafers (Figure 9-2B), PCPP and FP20

films contain ~ 21± 4 and 21±5 μg of Poly B, respectively, while 20 while FP60 and FP77 contain ~ 14±3 and 8±3 μg of Poly B, respectively. This confirms that antibiotics were bound within the film by electrostatic interactions. To explore effect of M_w on amount of drug loaded, the content of a film assembled with PCPP-200 kDa was compared to the content of a film assembled with PCPP-800 kDa. (Figure 9-3B). Both values are within error of each other, suggesting that molecular weight does not play a large role on antibiotic content. This confirms that the differences observed between films with different fluorination degrees were due to PPz fluorination degree and not molecular weight.

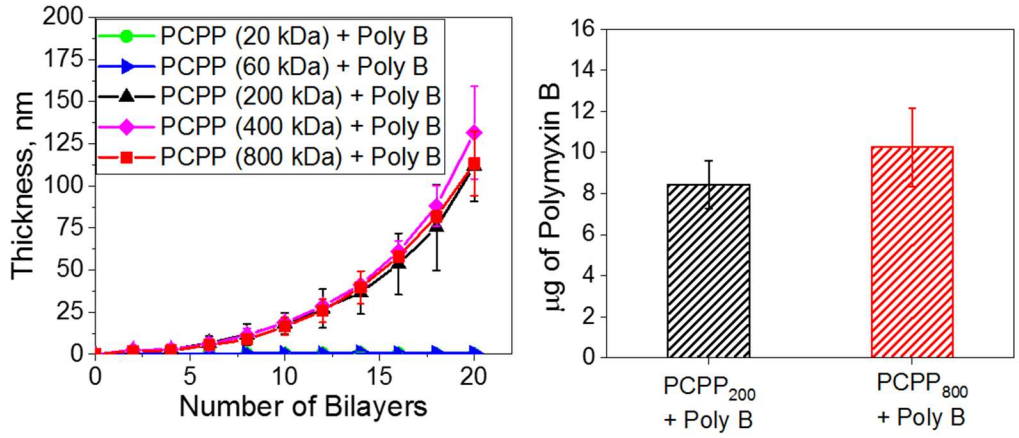

Figure 9-3. (A) Dry thicknesses of layer-by-layer films as measured by spectroscopic ellipsometry for assembly of polymyxin B (Poly B) with various PCPP molecular weights. Films were deposited from 0.5 mg/mL Poly B in DI water and 0.4 mg/mL PPz in 0.01 M PB at pH 7.5 with 10 min dipping cycles. (B) Calculated micrograms of Poly B in a 100 nm film on a 1x1 cm^2 wafer. PPz + Poly B films were dissolved in pH 12 PBS and concentration of Poly B released measured by LC-MS.

In our prior work on PPz coatings with branched polyethylene imine, we compared PCPP *vs.* FP60 and observed a strong effect of fluorination on the swelling of LbL

assemblies.[44] Specifically, increasing fluorination degree decreased overall film swelling ratio (~1.45 to ~1.1 for PCPP and FP60, respectively). Swelling of Poly B films in 0.01 M phosphate buffer (PB) with 0.15 M NaCl (PBS) at pH 7.5 was conducted at 37 °C to mimic physiological conditions (Figure 9-2C). Here, PCPP + Poly B films swell the most while the fluorinated films swell less, as would be expected for polymers of increasing hydrophobicity and agreeing with our previous finding.[44] Interestingly, SEM of coatings (Figure 9-2D-G) reveals that all coatings have a similar bumpy topography, with FP77 + Poly B coatings having a slightly less bumpy morphology.

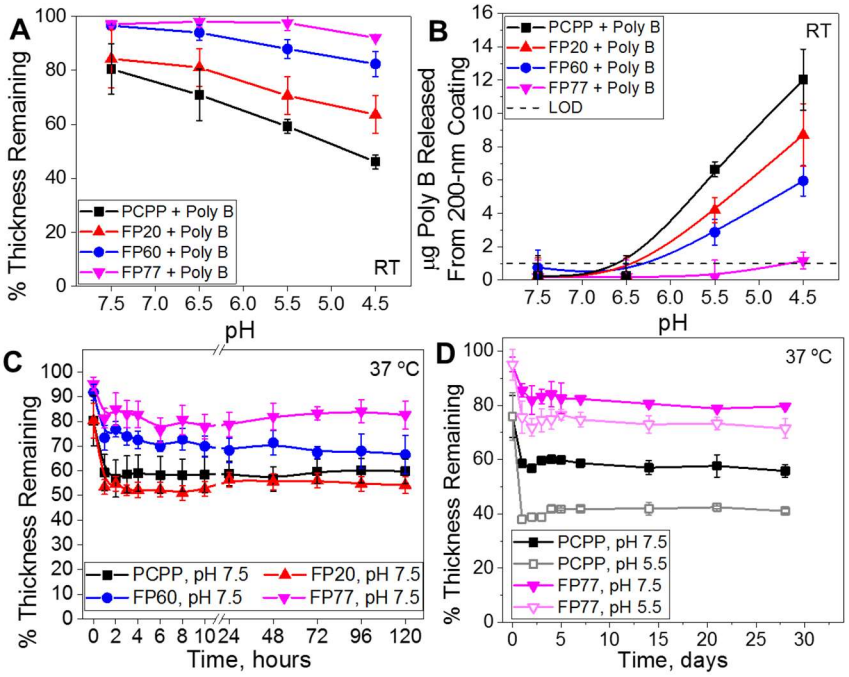

Figure 9-4. Decrease in film thickness (A) and percentage of antibiotic released (B) after 1 hour exposure to PBS at room temperature. Thickness was measured by spectroscopic ellipsometry after a wash with 0.01 M PB and drying with nitrogen. Antibiotic release into PBS was measured by LC-MS for films of ~200 nm. Decrease in film thickness after exposure to pH 7.5 PBS at 37 °C during the first day of exposure (C) and to pH 5.5 or pH 7.5 PBS at 37 °C for 30 days (D). Thickness was measured by spectroscopic ellipsometry after a wash with 0.01 M PB and drying with nitrogen.

We then aimed to understand how coatings would perform under conditions similar to those of bacterial colonization. To that end, coatings were exposed to decreasing pHs as *Staphylococcus aureus* and *Escherichia coli* are known to acidify the medium in which they grow as a result of secretion of lactic and acetic acid, respectively.[33,34] Specifically, to understand the pH-responsive behavior of these films, they were exposed to PBS at decreasing pHs (7.5, 6.5, 5.5, 4.5) for 1 hour, the coating thickness measured with ellipsometry (Figure 9-4A) and the supernatant solutions analyzed by LC-MS (Figure 9-4B). With a decrease of pH, a systematic mass loss of the film occurred (Figure 9-4A) as a result of pH-triggered charge balance in the films, which correlated with antibiotic release in solution as measured by LC-MS (Figure 9-4B). All PPz + Poly B coatings released antibiotics in response to decreasing pH, and the release was dependent on the amplitude of pH decrease. Unlike previous reports, however, antibiotic dose released could be controlled by the degree of PPz fluorination (Figure 9-4A&B). Highly fluorinated coatings displayed little decrease in thickness and little antibiotic release likely due to low overall antibiotic content as well as hydrophobic interactions between the polymer and antibiotic. Importantly, the pH triggered release of antibiotics from coatings was pulsatile and remained constant for 30 days (Figure 9-4D), similar to other self-defensive coatings.[66]

Coating performance in physiological conditions is paramount for clinical translation. To mimic physiological conditions, coatings were exposed to pH 7.5, PBS at 37 °C and thickness measured over time (Figure 9-4C&D). As shown in Figure 9-4, fluorinated coatings displayed only a slight mass loss and low antibiotic release upon

exposure to salt at a constant pH 7.5, while non-fluorinated coatings showed a more significant ~20% loss of thickness. Such a loss upon exposure to salt is common for electrostatic coatings which contain small molecules, because of the ease of disruption of their ionic pairing with polymers.[82] However, loss in the film mass was much less than previously observed for cationic antibiotics trapped in anionic surface attached hydrogels built from non-PPz molecules.[82] Importantly, Figure 9-4A shows that for highly fluorinated FP60 and FP77, dissociation of antibiotics from the coating in PBS at pH 7.5 was almost completely suppressed. This result illustrates that increased polymer hydrophobicity strengthened ionic binding within the film and increases film stability in salt solutions at a constant pH. Upon exposure to 37 °C, Poly B coatings with PCPP and FP20 display ~ 40-50% loss in thickness while FP60 and FP77 coatings display ~30% and ~20% thickness loss. (Figure 9-4C). This loss occurred during the first hour of heating samples, after which samples are stabile for at least 5 days. For PCPP+Poly B and FP77+Poly B coatings, coatings were stable for at least up to 30 days of exposure (Figure 9-4D).

9.4.2. Hemocompatiblity and Cytocompatibility

An important, yet often disregarded, aspect of antibacterial coatings is their interact with blood upon implantation into the body. Materials based on fluorinated PPzs have previously been shown to display superior biocompatibility.[329] To test such properties, coatings of PCPP with various thicknesses (10, 50 or 100 nm) and matched thickness (100 nm) but various fluorination degrees were assembled to enable us to

distinguish between the influence of Poly B content, film thickness, and effect of fluorination degree. Solution cast films of poly[bis(trifluoroethoxyphosphazene)], PTFEP were used as a control as hemocompatibility of this fluorinated PPz has been clinically proven and it is currently employed as a coating material for two US Food and Drug Administration approved products – coronary stents and embolic microbeads.[329] Two well-established hemolytic activity tests were employed (Figure 9-6A) – using whole rabbit blood[319,351] and with porcine red blood cells.[371-374] The results of both studies demonstrated exceptionally low hemolytic activity of all films (less than 1%) regardless of degree of fluorination (Figure 9-6A) and thickness of the coating (data not shown). In solution, all polymers showed no hemolytic activity (less than 0.1 %) while Poly B showed concentration dependent hemolysis with a maximum hemolysis degree of 2% being reached for a very high concentration of 10 ug/mL (data not shown). Therefore, the fact that there is no thickness vs. hemolysis relationship for PCPP coatings shows the remarkable hemocompatibility of these constructs. Importantly, the hemocompatibility of all Poly B containing nanocoatings was at least at the same level than that of PTEFP – a material with well-established performance both in animal experiments and clinical trials.

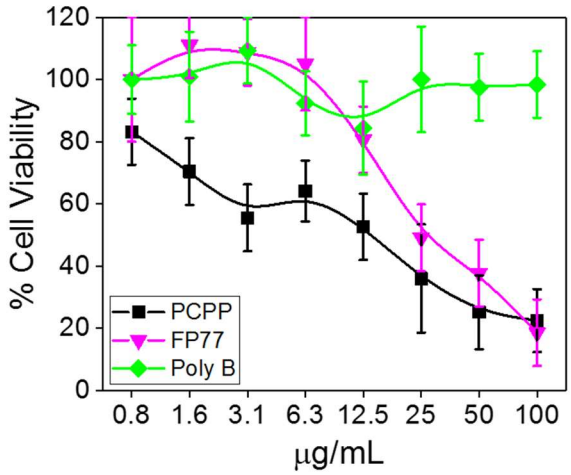

Figure 9-5. MTT assay with Fibroblast NIH 3T3 and Poly B, PCPP, or FP77 in solution.

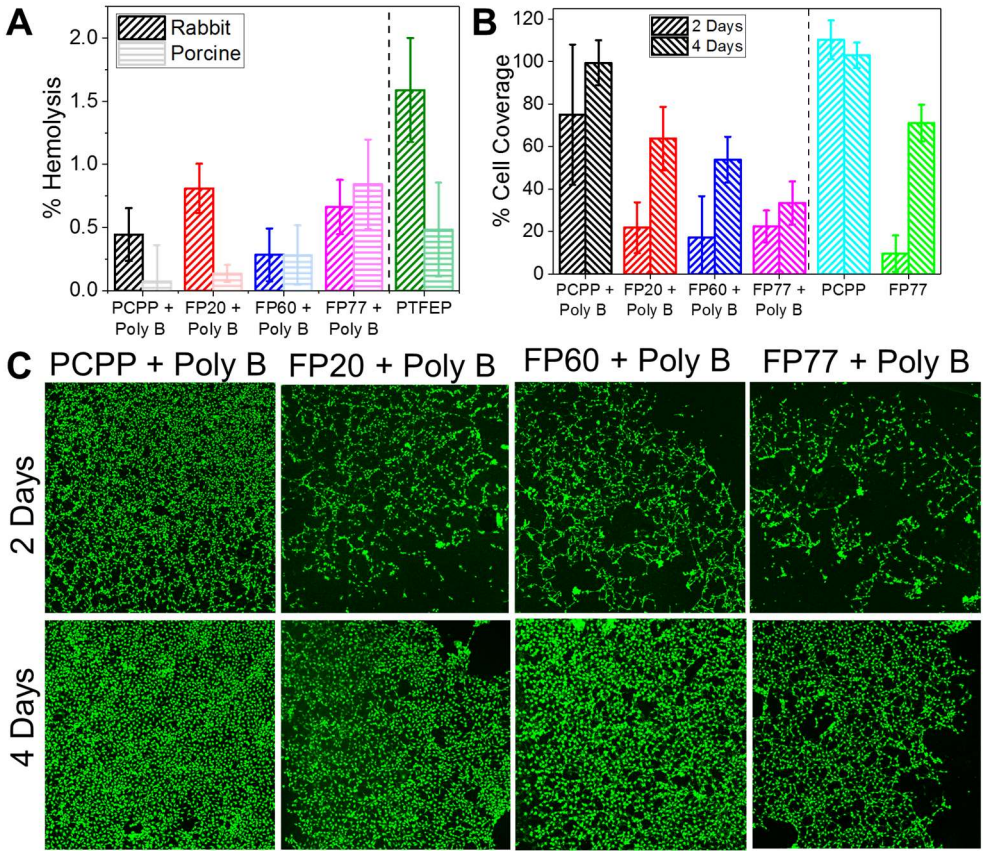

Figure 9-6. (A) Hemocompatibility studies of coatings using whole rabbit blood and porcine red blood cell tests. (B) Cytotoxicity of coatings was tested with NIH 3T3 Fibroblast cells. Cells were incubated with 100 nm coatings for 2 and 4 days for various fluorination degree coatings. (C) Representative images of surfaces at 2 and 4 days.

Cytocompatibility is an important aspect of any biomaterial. To assess cytocompatibility PPz + Poly B coatings, NIH 3T3 fibroblasts were used. First, fibroblasts were exposed to various concentrations of polymers on extreme ends of fluorination degree (PCPP and FP77) as well as Poly B in solution (Figure 9-5). We find that after 24 hr culture, Poly B shows negligible toxicity in all concentrations tested. In contrast, PCPP causes a distinct drop in cellular metabolism at all concentration ranges, even causing a 20% drop at a low concentration of 0.8 μg/mL, likely due to the charged groups as seen before for anionic hydrogels.[17] Interestingly, FP77 causes no decrease in cellular activity for concentrations up to 6.3 μg/mL. Fibroblasts were incubated with matched thickness (100 nm) Poly B coatings with various fluorination degrees (Figure 9-6B&C). Comparing equal thickness coatings and various fluorination degrees, after 2 days of culture, highly fluorinated FP60 and FP77 have less cells adhered than PCPP and FP20. Interestingly, all 100-nm coatings show approximately the same level of cellular coverage on day 4. Importantly, few, if any, dead cells were observed on coatings. These results indicate the PPz + Poly B coatings are non-toxic and that fluorination degree can be used to tune cellular adhesion during the early days of culturing.

9.4.3. Antibacterial Activity

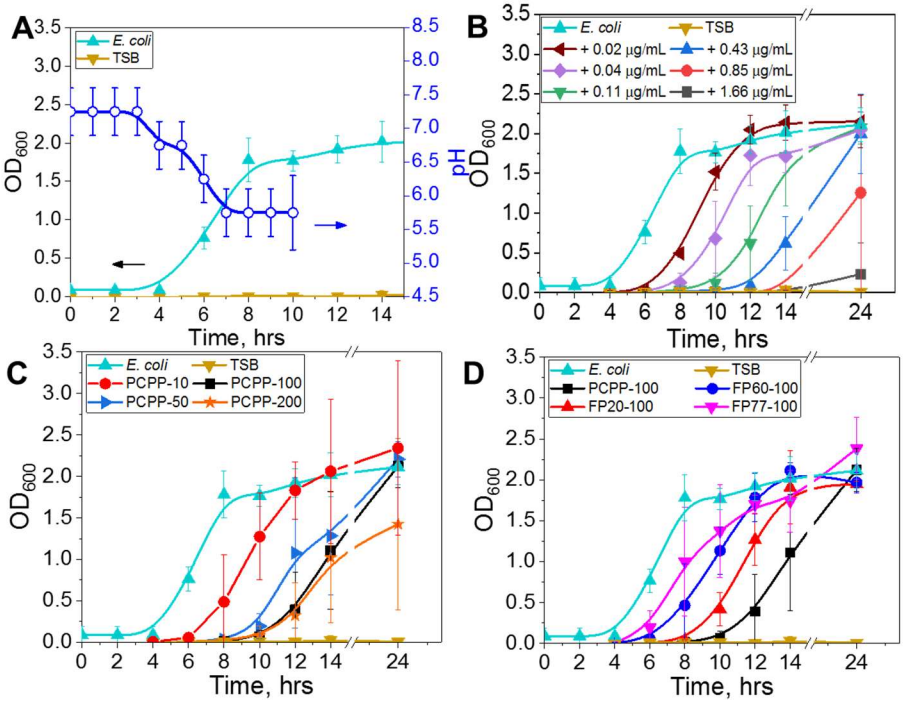

Figure 9-7. Optical density of *E. coli* growing in 12 mL culture of TSB at 37 °C (A) in the presence of various concentrations of Poly B in solution (B), PPz + Poly B coatings of (C) one PPz (PCPP) at a variety of thicknesses or (D) a set thickness (100 nm) of various PPzs on 1x1 cm^2 Si wafers. Starting concentration of *E. coli* was ~ 10^5 CFU/mL. pH of culture was measured over time with pH paper. Samples run in triplicate.

Antibacterial performance of coatings was then evaluated against *E. coli* ATCC 25922 in measurements of bacterial concentrations in solution (Figure 9-7). *E. coli* is well known to grow in TSB at 37 °C and display typical growth phases of lag-log-stationary as determined by measuring the optical density (OD_{600}) of culture over time. The growth data of *E. coli* in TSB (Figure 9-7) matches well with that observed by others previously.[379] As expected, *E. coli* reduces the culture pH over time (Figure 9-7A), which agrees with our previous results.[82] Interestingly, *E. coli* is highly sensitive to sub-minimum inhibitory concentrations (MIC) Poly B concentrations during its growth (Figure 9-7B). Therefore,

this technique provides an easy way to detect release of Poly B from coatings in low concentrations. To understand release of Poly B from coatings, coatings were exposed to a large volume of TSB to ensure that release amount would be sub-MIC. MIC was determined to be CFU dependent with MICs of 2, 2, and 4 μg/mL, being observed for 10^3, 10^5, and 10^7 CFU/mL cultures (Figure 9-8), which is close to the range previously observed by others.[380] Coatings of various thicknesses (10, 50, 100, and 200 nm) were compared for polymer coatings of various fluorination degrees (PCPP, FP20, FP60, FP77) all constructed with Poly B and run in triplicate with a starting concentration of ~10^5 CFU/mL of *E. coli*. As controls, prime layers (a monolayer of BPEI and PPz) were exposed to *E. coli*, with no appreciable difference being observed in the growth pattern (Figure 9-8). This is as expected since previous reports only showed mild antibacterial activity of PPzs.[381,382]

From Figure 9-7**,** it is clear that by increasing the thickness of the coating, the time it took for bacteria to reach the log phase increased. This result indicates that thicker LbL coatings contained more antibiotics, and that more antibiotic was released from the bulk of the film when triggered by bacteria-growth induced pH decrease. Comparing polymer coatings of the same thickness (100 nm) but different fluorination degrees **(**Figure 9-7D) reveals that the amount of antibiotic released decreased for films built from highly fluorinated PPzs. This trend is in part due to the overall different content of antibiotics in the films. Figure 9-9 shows that the trend of increasing amounts of antibiotic released from films of increasing film thickness is true for all PPzs.

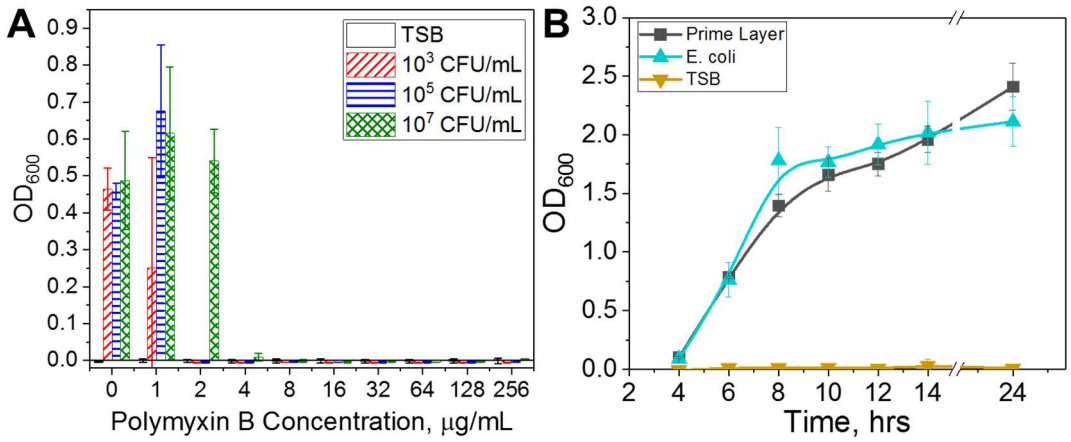

Figure 9-8. (A) Minimum inhibitory concentration of Poly B for *E. coli* is dependent on starting cell concentration. OD600 measured by 96 well plate reader after 24 hr culture at 37 °C. (B) Optical density of *E. coli* growing in 12 mL culture of TSB at 37 °C in the presence of prime layer controls of PPzs. Starting concentration of *E. coli* was ~ 10^5 CFU/mL. Samples run in triplicate. Prime layer samples consist of a layer of BPEI and PPz. Note: Prime layer samples were only run in duplicate.

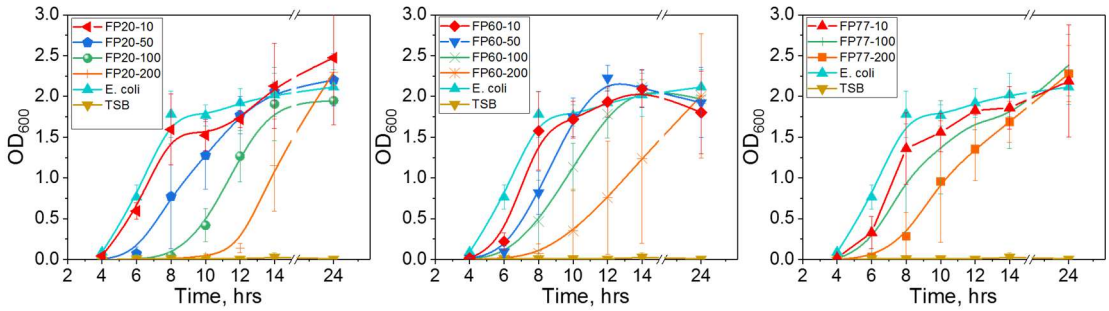

Figure 9-9. Optical density of *E. coli* growing in 12 mL culture of TSB at 37 °C in the presence of PPz + Poly B coatings of a variety of thicknesses for various PPzs on 1x1 cm^2 Si wafers. Starting concentration of *E. coli* was ~ 10^5 CFU/mL. Samples run in triplicate.

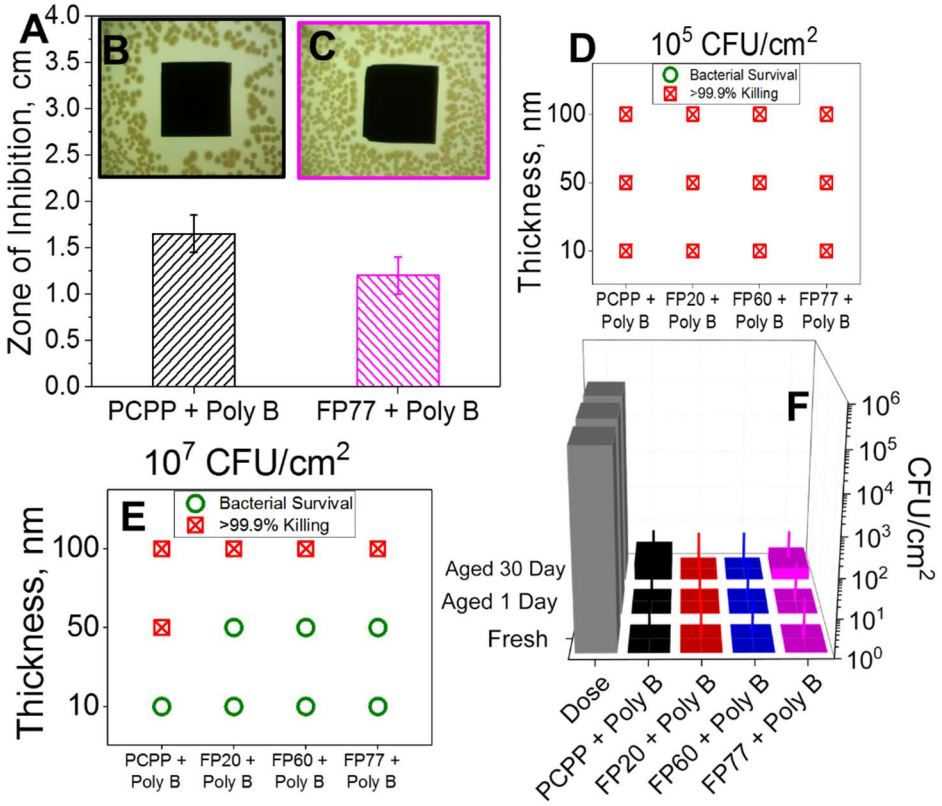

Figure 9-10. (A) Zones of inhibition (ZOI) of 100 nm coatings of either PCPP or FP77 with Poly B as tested with *E. coli*. Samples of 1x1 cm^2 on Si wafer were tested in duplicate. Images of ZOIs for Poly B coatings with PCPP of 100 (B) or FP77 of 100 nm (C). (D &E) Petrifilm™ assay results demonstrating the effect of coating thickness and composition on bacterial death or survival. Assay run with 10^5 (D) or 10^7 (E) CFU of *E. coli* on 1x1 cm^2 Si wafer with PPz + Poly B coatings of a variety of thicknesses and incubated for 24 hrs at 37˚C on a 3M™ Petrifilm™ E. coli Count Plate. Images of Petrifilm plates for FP77 + Poly B of 100 nm (F) and 10 nm (G) show complete inhibition on the surface and total bacterial coverage, respectively. Samples were tested in duplicate. (H) Petrifilm™ assay results demonstrating the effect of sample aging on bacterial death or survival. Assay run with 10^5 or 10^7 CFU of *E. coli* on 100 nm coatings.

After understanding release mechanisms of antibiotics from the coatings in solution, we aimed to demonstrate antibacterial performance of surfaces coated with PPz + Poly B coatings against bacterial challenge. To understand how much of the antibiotics elute out of the coatings, zone of inhibition (ZOI) assays were conducted with 100 nm coatings of polymers on extreme ends (non-fluorinated PCPP and highly fluorinated

FP77) as can be seen in Figure 9-10**.** Although, Poly B is known to diffuse slowly through agar plates which can present challenges for quantification,[380] all coatings displayed small ZOIs with PCPP coatings having larger ZOIs. This is suggestive of more antibiotics being released from PCPP coatings, which correlates well with the result in Figure 9-7. To understand the maximum potency of coatings, coatings were challenged with extremely high concentrations of bacteria directly applied to the surface. Specifically, a small droplet (5 µl) of *E. coli* at the desired concentration was placed on top of a on 1x1 cm^2 Si wafer and incubated for 24 hrs at 37˚C on a 3M™ Petrifilm™ *E. coli* Count Plate. Coatings of three different thicknesses (10, 50, and 100 nm) and four different fluorination degrees (PCPP, FP20, FP60, and FP77) were tested for comparison in duplicate. All coatings can prevent the growth of 10^5 CFU per sample (Figure 9-10D). However, for 10^7 CFU per sample, thicker coatings (100 nm) are able to prevent growth while 10 nm coatings fail (Figure 9-10E). Interestingly, at 50 nm, PCPP coatings are able to prevent bacterial growth while the other PPzs fail to do so. This is likely due to the higher content of Poly B in PCPP coatings. To understand the long term efficacy of coatings, 100 nm PPz + Poly B coatings were aged in PBS at 37 °C for 1 day or 30 days and then challenged with a bacterial dose of 10^5 CFU per sample. All coatings, even those soaked for 30 days in physiological conditions, were able to completely prevent a bacterial challenge of 10^5 CFU (Figure 9-10F).

9.4.4. Versatility

After in depth studies on one antibiotic, we wondered whether this approach was feasible for other cationic antibiotics. To this end, we assembled several polymyxins and aminoglycosides into coatings with PCPP and FP77. In addition to poly B, both polymers are able to support growth with gentamicin (Gent), neomycin, and colistin as shown in Figure 9-11. The minimum inhibitory concentrations of all four antibiotics was measured against *S. aureus* and *E. coli* (Table 9-2). As all antibiotics here are well known to treat gram-negative bacteria, it is not surprising that MICs for all antibiotics are relatively low against *E. coli*.

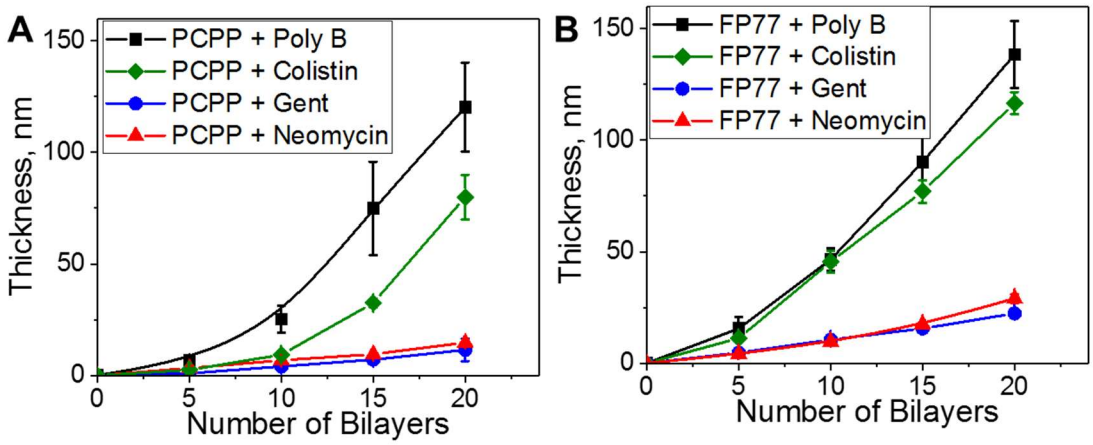

Figure 9-11. Dry thicknesses of layer-by-layer films for assembly of various antibiotics with PCPP (A) and FP77 (B).

Table 9-2. Minimum Inhibitory Concentrations (MICs, µg/mL) of *E. coli* and *S. aureus* at various concentrations (CFU/mL) against various antibiotics.

	Poly B	Col	Gent	Neo
E. coli, 10^3	2	2	<1	4
E. coli, 10^5	2	2	<1	4-8
E. coli, 10^7	4-8	8-16	2	8-16
S. aureus, 10^3	64	>64	<1	2-4
S. aureus, 10^5	64	>64	<1	4-8
S. aureus, 10^7	>64	>64	2	4-8

Finally, we challenged 10 nm coatings of non-fluorinated and highly fluorinated PPzs with various antibiotics with *E. coli* and *S. aureus* as various concentrations (Figure 9-12). Regardless of antibiotic, all coatings were able to prevent a bacterial challenge of 10^3 CFU per cm^2. In contrast, Gent coatings were able to prevent a challenge of 10^5 but not 10^7 while Neomycin coatings were unable to prevent anything higher than 10^3. In contrast, Poly B coatings were able to prevent up to 10^5 while Colistin coatings were able to prevent up to 10^7. Such results are not surprising considering the MICs of these compounds. No large differences were observed between the non-fluorinated and fluorinated PPz coatings. Therefore, these coatings are highly versatile and can be used with not only multiple antibiotics but also to treat a variety of bacterial strains.

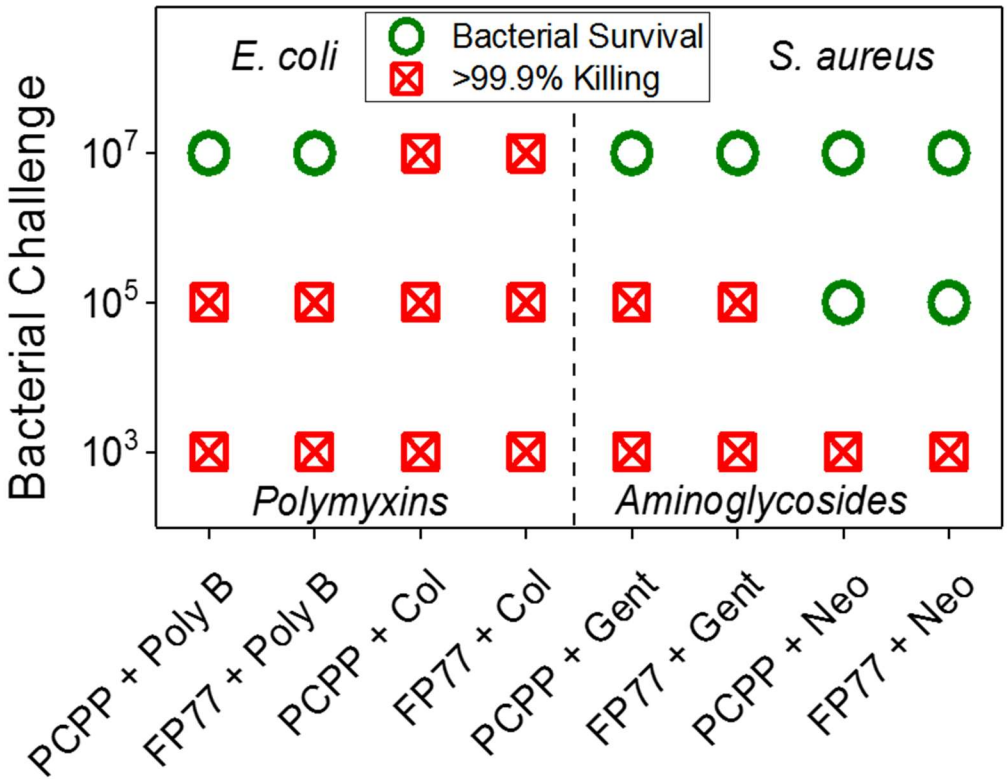

Figure 9-12. Antibacterial activity of 10 nm coatings of PPzs plus various antibiotics against *E. coli* and *S. aureus* at various concentrations (CFU/cm^2).

9.5. Conclusions

In conclusion, we have shown direct assembly of antibiotics with polymers, for the first time to our knowledge. Fluorination degree of PPz can be used to tune antibiotic content and antibiotic release profiles. Moreover, all coatings are highly hemocompatible and cytocompatible. Coatings are active against large numbers of bacteria in a thickness dependent manner and remain active for at least 30 days. Moreover, a large variety of cationic antibiotics can be used for assembly, demonstrating the versatility of the system.

10. CONCLUSIONS

10.1. Temperature-Responsive Coatings

Temperature-responsive block copolymer micelles are promising building blocks for next generation surface coatings. UCST micelle coatings can be LbL assembled with a variety of hydrogen-bonding materials ranging from synthetic polymers like poly(methacrylic acid) to natural, small molecules like tannic acid. Deposition of coatings is possible on both flat substrates and the curved surfaces of nanofibers. Deposition conditions can be used to tune the strength of interaction between the binding partner and micelles, thus modulating the micellar response to changes in temperature. Drug release from UCST micellar LbL films is temperature-responsive and repeatable for small hydrophobic molecules. Moreover, micelles can load antimicrobial agents and prevent the growth of bacteria on surfaces. Additionally, the texture that micellar coatings provide can be used to tune interactions with cells. By choosing tannic acid as a binding partner, multilayer coatings of micelles can display layer-dependent antioxidant behavior. Taken together, such coatings are promising for drug delivery and wound healing applications.

10.2. pH-Responsive Coatings

For the first time, the direct local acidification has been imaged for bacteria. Such acidification can be used as a trigger to release antimicrobials from pH-responsive polymer coatings. One promising coating type is polyacid surface attached hydrogels whose pH-responsive release profiles can be tuned by polymer pKa and still remain active under challenging conditions (flowing buffer) in which bulk pH changes do not occur.

Fluorinated, ionic polyphosphazenes (PPzs) are a new class of polymers that are promising for life science applications. PPzs enable deposition on a variety of substrates including biomedically relevant titanium and polyester fibers. Importantly, fluorinated, ionic polyphosphazenes enable highly hemocompatible LbL assemblies that can even surpass the hemocompatibility level of a currently used standard. The strength of such assemblies can be tuned by PPz fluorination degree or ionic group type, resulting in highly tunable film wettability and swelling degree. Using ions that form strong ionic pairs, like sulfonated groups, can enable coatings with low swelling degrees that are very stable in high salt concentrations and therefore could potentially be used to prevent salt-induced corrosion. Moreover, these unique hybrid molecules enable direct LbL deposition with a wide range of small molecules, even those with only ~3+ charges. Antimicrobial PPz coatings are pH-responsive and highly efficient in preventing the growth of bacteria. Importantly, such coatings remain active for at least 30 days, are cytocompatible for fibroblasts, and hemocompatible. Taken together, these coatings show promise for advanced antibacterial and blood-contacting applications.

REFERENCES

(1) Busscher, H. J.; van der Mei, H. C.; Subbiahdoss, G.; Jutte, P. C.; van den Dungen, J. J. A. M.; Zaat, S. A. J.; Schultz, M. J.; Grainger, D. W. Biomaterial-Associated Infection: Locating the Finish Line in the Race for the Surface. *Science Translational Medicine* **2012**, *4*, 153rv110.

(2) Donlan, R. M. Biofilms: microbial life on surfaces. *Emerg Infect Dis* **2002**, *8*.

(3) Barth, E.; Myrvik, Q. M.; Wagner, W.; Gristina, A. G. In vitro and in vivo comparative colonization of Staphylococcus aureus and Staphylococcus epidermidis on orthopaedic implant materials. *Biomaterials* **1989**, *10*, 325-328.

(4) Wenzel, R. P. Minimizing Surgical-Site Infections. *New England Journal of Medicine* **2010**, *362*, 75-77.

(5) Stewart, P. S.; William Costerton, J. Antibiotic resistance of bacteria in biofilms. *The Lancet* **2001**, *358*, 135-138.

(6) Hall-Stoodley, L.; Costerton, J. W.; Stoodley, P. Bacterial biofilms: from the Natural environment to infectious diseases. *Nat Rev Micro* **2004**, *2*, 95-108.

(7) Dunne, W. M. Bacterial Adhesion: Seen Any Good Biofilms Lately? *Clinical Microbiology Reviews* **2002**, *15*, 155-166.

(8) Wolcott, R. D.; Rhoads, D. D.; Bennett, M. E.; Wolcott, B. M.; Gogokhia, L.; Costerton, J. W.; Dowd, S. E. Chronic wounds and the medical biofilm paradigm. *Journal of Wound Care* **2010**, *19*, 45.

(9) Robson, M. C. WOUND INFECTION. *Surgical Clinics of North America* **1997**, *77*, 637-650.

(10) Bozic, K. J.; Ries, M. D. The Impact of Infection After Total Hip Arthroplasty on Hospital and Surgeon Resource Utilization. *The Journal of Bone & Joint Surgery* **2005**, *87*, 1746-1751.

(11) Maunders, E.; Welch, M. Matrix exopolysaccharides; the sticky side of biofilm formation. *FEMS Microbiology Letters* **2017**, *364*.

(12) Kumar, V.; Rauscher, H.; Brétagnol, F.; Arefi-Khonsari, F.; Pulpytel, J.; Colpo, P.; Rossi, F.: Preventing Biofilm Formation on Biomedical Surfaces. In *Plasma Technology for Hyperfunctional Surfaces*, 2010.

(13) Chen, M.; Yu, Q.; Sun, H. Novel Strategies for the Prevention and Treatment of Biofilm Related Infections. *International Journal of Molecular Sciences* **2013**, *14*, 18488-18501.

(14) Shah, S. R.; Tatara, A. M.; D'Souza, R. N.; Mikos, A. G.; Kasper, F. K. Evolving strategies for preventing biofilm on implantable materials. *Materials Today* **2013**, *16*, 177-182.

(15) Rodrigues, L. R.: Inhibition of Bacterial Adhesion on Medical Devices. In *Bacterial Adhesion: Chemistry, Biology and Physics*; Linke, D., Goldman, A., Eds.; Springer Netherlands: Dordrecht, 2011; pp 351-367.

(16) Kyomoto, M.; Shobuike, T.; Moro, T.; Yamane, S.; Takatori, Y.; Tanaka, S.; Miyamoto, H.; Ishihara, K. Prevention of bacterial adhesion and biofilm formation on

a vitamin E-blended, cross-linked polyethylene surface with a poly(2-methacryloyloxyethyl phosphorylcholine) layer. *Acta Biomaterialia* **2015**, *24*, 24-34.

(17) Lu, Y.; Wu, Y.; Liang, J.; Libera, M. R.; Sukhishvili, S. A. Self-defensive antibacterial layer-by-layer hydrogel coatings with pH-triggered hydrophobicity. *Biomaterials* **2015**, *45*, 64-71.

(18) Boulmedais, F.; Frisch, B.; Etienne, O.; Lavalle, P.; Picart, C.; Ogier, J.; Voegel, J. C.; Schaaf, P.; Egles, C. Polyelectrolyte multilayer films with pegylated polypeptides as a new type of anti-microbial protection for biomaterials. *Biomaterials* **2004**, *25*, 2003-2011.

(19) Murata, H.; Koepsel, R. R.; Matyjaszewski, K.; Russell, A. J. Permanent, non-leaching antibacterial surfaces—2: How high density cationic surfaces kill bacterial cells. *Biomaterials* **2007**, *28*, 4870-4879.

(20) Tiller, J. C.; Liao, C.-J.; Lewis, K.; Klibanov, A. M. Designing surfaces that kill bacteria on contact. *Proceedings of the National Academy of Sciences of the United States of America* **2001**, *98*, 5981-5985.

(21) Wong, S. Y.; Li, Q.; Veselinovic, J.; Kim, B.-S.; Klibanov, A. M.; Hammond, P. T. Bactericidal and virucidal ultrathin films assembled layer by layer from polycationic N-alkylated polyethylenimines and polyanions. *Biomaterials* **2010**, *31*, 4079-4087.

(22) Huang, X.; Brazel, C. S. On the importance and mechanisms of burst release in matrix-controlled drug delivery systems. *Journal of Controlled Release* **2001**, *73*, 121-136.

(23) Pan, C.; Zhou, Z.; Yu, X. Coatings as the useful drug delivery system for the prevention of implant-related infections. *J. Orthop. Surg. Res.* **2018**, *13*, 220.

(24) Taubes, G. The Bacteria Fight Back. *Science* **2008**, *321*, 356-361.

(25) Kelley, E. G.; Albert, J. N. L.; Sullivan, M. O.; Epps, T. H. Stimuli-responsive copolymer solution and surface assemblies for biomedical applications. *Chemical Society reviews* **2013**, *42*, 7057-7071.

(26) Schmidt, D. J.; Moskowitz, J. S.; Hammond, P. T. Electrically Triggered Release of a Small Molecule Drug from a Polyelectrolyte Multilayer Coating. *Chemistry of Materials* **2010**, *22*, 6416-6425.

(27) Gao, H.; Wen, D.; Tarakina, N. V.; Liang, J.; Bushby, A. J.; Sukhorukov, G. B. Bifunctional ultraviolet/ultrasound responsive composite TiO2/polyelectrolyte microcapsules. *Nanoscale* **2016**, *8*, 5170-5180.

(28) Lentacker, I.; De Geest, B. G.; Vandenbroucke, R. E.; Peeters, L.; Demeester, J.; De Smedt, S. C.; Sanders, N. N. Ultrasound-Responsive Polymer-Coated Microbubbles That Bind and Protect DNA. *Langmuir* **2006**, *22*, 7273-7278.

(29) Li, Y.; Ding, J.; Zhu, J.; Tian, H.; Chen, X. Photothermal Effect-Triggered Drug Release from Hydrogen Bonding-Enhanced Polymeric Micelles. *Biomacromolecules* **2018**.

(30) Anandhakumar, S.; Raichur, A. M. Polyelectrolyte/silver nanocomposite multilayer films as multifunctional thin film platforms for remote activated protein and drug delivery. *Acta Biomaterialia* **2013**, *9*, 8864-8874.

(31) Zhuk, A.; Pavlukhina, S.; Sukhishvili, S. A. Hydrogen-Bonded Layer-by-Layer Temperature-Triggered Release Films. *Langmuir* **2009**, *25*, 14025-14029.

(32) Ward, M. A.; Georgiou, T. K. Thermoresponsive Polymers for Biomedical Applications. *Polymers* **2011**, *3*.

(33) Smith, S. M. D-lactic acid production as a monitor of the effectiveness of antimicrobial agents. *Antimicrobial Agents and Chemotherapy* **1991**, *35*, 237-241.

(34) Andersen, K. B.; von Meyenburg, K. Are growth rates of Escherichia coli in batch cultures limited by respiration? *Journal of Bacteriology* **1980**, *144*, 114-123.

(35) Decher, G.; Hong, J.-D. Buildup of ultrathin multilayer films by a self-assembly process, 1 consecutive adsorption of anionic and cationic bipolar amphiphiles on charged surfaces. *Makromolekulare Chemie. Macromolecular Symposia* **1991**, *46*, 321-327.

(36) Decher, G.; Hong, J. D. In *Tilte*1990.

(37) Zhao, S.; Caruso, F.; Dähne, L.; Decher, G.; De Geest, B. G.; Fan, J.; Feliu, N.; Gogotsi, Y.; Hammond, P. T.; Hersam, M. C.; Khademhosseini, A.; Kotov, N.; Leporatti, S.; Li, Y.; Lisdat, F.; Liz-Marzán, L. M.; Moya, S.; Mulvaney, P.; Rogach, A. L.; Roy, S.; Shchukin, D. G.; Skirtach, A. G.; Stevens, M. M.; Sukhorukov, G. B.; Weiss, P. S.; Yue, Z.; Zhu, D.; Parak, W. J. The Future of Layer-by-Layer Assembly: A Tribute to ACS Nano Associate Editor Helmuth Möhwald. *ACS Nano* **2019**, *13*, 6151-6169.

(38) Sukhishvili, S. A. Responsive polymer films and capsules via layer-by-layer assembly. *Current Opinion in Colloid & Interface Science* **2005**, *10*, 37-44.

(39) Tang, Z.; Wang, Y.; Podsiadlo, P.; Kotov, N. A. Biomedical Applications of Layer-by-Layer Assembly: From Biomimetics to Tissue Engineering. *Advanced Materials* **2006**, *18*, 3203-3224.

(40) Richardson, J. J.; Cui, J.; Björnmalm, M.; Braunger, J. A.; Ejima, H.; Caruso, F. Innovation in Layer-by-Layer Assembly. *Chemical Reviews* **2016**, *116*, 14828-14867.

(41) Kharlampieva, E.; Kozlovskaya, V.; Sukhishvili, S. A. Layer-by-Layer Hydrogen-Bonded Polymer Films: From Fundamentals to Applications. *Advanced Materials* **2009**, *21*, 3053-3065.

(42) Hizal, F.; Zhuk, I.; Sukhishvili, S.; Busscher, H. J.; van der Mei, H. C.; Choi, C.-H. Impact of 3D Hierarchical Nanostructures on the Antibacterial Efficacy of a Bacteria-Triggered Self-Defensive Antibiotic Coating. *ACS Applied Materials & Interfaces* **2015**, *7*, 20304-20313.

(43) Albright, V.; Xu, M.; Palanisamy, A.; Cheng, J.; Stack, M.; Zhang, B.; Jayaraman, A.; Sukhishvili, S. A.; Wang, H. Micelle-Coated, Hierarchically Structured Nanofibers with Dual-Release Capability for Accelerated Wound Healing and Infection Control. *Advanced Healthcare Materials* **2018**, *7*, 1800132.

(44) Selin, V.; Albright, V.; Ankner, J. F.; Marin, A.; Andrianov, A. K.; Sukhishvili, S. A. Biocompatible Nanocoatings of Fluorinated Polyphosphazenes through Aqueous Assembly. *ACS Applied Materials & Interfaces* **2018**, *10*, 9756-9764.

(45) Ren, K.-f.; Hu, M.; Zhang, H.; Li, B.-c.; Lei, W.-x.; Chen, J.-y.; Chang, H.; Wang, L.-m.; Ji, J. Layer-by-layer assembly as a robust method to construct extracellular

matrix mimic surfaces to modulate cell behavior. *Progress in Polymer Science* **2019**, *92*, 1-34.

(46) Park, S.; Han, U.; Choi, D.; Hong, J. Layer-by-layer assembled polymeric thin films as prospective drug delivery carriers: design and applications. *Biomaterials Research* **2018**, *22*, 29.

(47) Keeney, M.; Jiang, X. Y.; Yamane, M.; Lee, M.; Goodman, S.; Yang, F. Nanocoating for biomolecule delivery using layer-by-layer self-assembly. *J Mater Chem B* **2015**, *3*, 8757-8770.

(48) Stebbins, N. D.; Ouimet, M. A.; Uhrich, K. E. Antibiotic-containing polymers for localized, sustained drug delivery. *Advanced drug delivery reviews* **2014**, *78*, 77-87.

(49) Croy, S. R.; Kwon, G. S. Polymeric micelles for drug delivery. *Current pharmaceutical design* **2006**, *12*, 4669-4684.

(50) Caminade, A.-M.; Turrin, C.-O. Dendrimers for drug delivery. *Journal of Materials Chemistry B* **2014**, *2*, 4055-4066.

(51) Loftsson, T.; Jarho, P.; Másson, M.; Järvinen, T. Cyclodextrins in drug delivery. *Expert Opinion on Drug Delivery* **2005**, *2*, 335-351.

(52) Kim, B.-S.; Park, S. W.; Hammond, P. T. Hydrogen-Bonding Layer-by-Layer-Assembled Biodegradable Polymeric Micelles as Drug Delivery Vehicles from Surfaces. *ACS Nano* **2008**, *2*, 386-392.

(53) Smith, R. C.; Riollano, M.; Leung, A.; Hammond, P. T. Layer-by-layer platform technology for small-molecule delivery. *Angewandte Chemie (International ed. in English)* **2009**, *48*, 8974-8977.

(54) Xu, L.; Zhu, Z.; Borisov, O. V.; Zhulina, E. B.; Sukhishvili, S. A. pH-triggered block copolymer micelle-to-micelle phase transition. *Phys Rev Lett* **2009**, *103*, 118301.

(55) Xu, L.; Zhu, Z.; Sukhishvili, S. A. Polyelectrolyte Multilayers of Diblock Copolymer Micelles with Temperature-Responsive Cores. *Langmuir* **2011**, *27*, 409-415.

(56) Erel, I.; Zhu, Z.; Sukhishvili, S.; Patyukova, E.; Potemkin, I.; Kramarenko, E. Two Types of Block Copolymer Micelles with Ion-Containing Cores. *Macromolecular Rapid Communications* **2010**, *31*, 490-495.

(57) Erel, I.; Zhu, Z.; Zhuk, A.; Sukhishvili, S. A. Hydrogen-bonded layer-by-layer films of block copolymer micelles with pH-responsive cores. *Journal of Colloid and Interface Science* **2011**, *355*, 61-69.

(58) Kim, B.-S.; Lee, H.-i.; Min, Y.; Poon, Z.; Hammond, P. T. Hydrogen-bonded multilayer of pH-responsive polymeric micelles with tannic acid for surface drug delivery. *Chemical Communications* **2009**, 4194-4196.

(59) Zhu, Z.; Gao, N.; Wang, H.; Sukhishvili, S. A. Temperature-triggered on-demand drug release enabled by hydrogen-bonded multilayers of block copolymer micelles. *Journal of Controlled Release* **2013**, *171*, 73-80.

(60) Zhu, Z.; Sukhishvili, S. A. Temperature-Induced Swelling and Small Molecule Release with Hydrogen-Bonded Multilayers of Block Copolymer Micelles. *ACS Nano* **2009**, *3*, 3595-3605.

(61) Zhu, Z.; Sukhishvili, S. A. Layer-by-layer films of stimuli-responsive block copolymer micelles. *Journal of Materials Chemistry* **2012**, *22*, 7667-7671.

(62) Kharlampieva, E.; Erel-Unal, I.; Sukhishvili, S. A. Amphoteric Surface Hydrogels Derived from Hydrogen-Bonded Multilayers: Reversible Loading of Dyes and Macromolecules†. *Langmuir* **2007**, *23*, 175-181.

(63) Pavlukhina, S.; Zhuk, I.; Mentbayeva, A.; Rautenberg, E.; Chang, W.; Yu, X.; van de Belt-Gritter, B.; Busscher, H. J.; van der Mei, H. C.; Sukhishvili, S. A. Small-molecule-hosting nanocomposite films with multiple bacteria-triggered responses. *NPG Asia Mater* **2014**, *6*, e121.

(64) Chuang, H. F.; Smith, R. C.; Hammond, P. T. Polyelectrolyte Multilayers for Tunable Release of Antibiotics. *Biomacromolecules* **2008**, *9*, 1660-1668.

(65) Moskowitz, J. S.; Blaisse, M. R.; Samuel, R. E.; Hsu, H.-P.; Harris, M. B.; Martin, S. D.; Lee, J. C.; Spector, M.; Hammond, P. T. The effectiveness of the controlled release of gentamicin from polyelectrolyte multilayers in the treatment of Staphylococcus aureus infection in a rabbit bone model. *Biomaterials* **2010**, *31*, 6019-6030.

(66) Zhuk, I.; Jariwala, F.; Attygalle, A. B.; Wu, Y.; Libera, M. R.; Sukhishvili, S. A. Self-Defensive Layer-by-Layer Films with Bacteria-Triggered Antibiotic Release. *ACS Nano* **2014**, *8*, 7733-7745.

(67) Allcock, H. R. Polyphosphazene elastomers, gels, and other soft materials. *Soft Matter* **2012**, *8*, 7521-7532.

(68) Allcock, H. R. Chemistry and Applications of Polyphosphazenes. *Wiley* **2002**, 725.

(69) DeCollibus, D. P.; Marin, A.; Andrianov, A. K. Effect of Environmental Factors on Hydrolytic Degradation of Water-Soluble Polyphosphazene Polyelectrolyte in Aqueous Solutions. *Biomacromolecules* **2010**, 487-492.

(70) Andrianov, A. K.; Marin, A. Degradation of polyaminophosphazenes: Effects of hydrolytic environment and polymer processing. *Biomacromolecules* **2006**, *7*, 1581-1586.

(71) Allcock, H. R.; Pucher, S. R.; Scopelianos, A. G. Poly[(amino acid ester)phosphazenes]: Synthesis, Crystallinity, and Hydrolytic Sensitivity in Solution and the Solid State. *Macromolecules* **1994**, *27*, 1071-1075.

(72) Cutlip, D. E.; Garratt, K. N.; Novack, V.; Barakat, M.; Meraj, P.; Maillard, L.; Erglis, A.; Jauhar, R.; Popma, J. J.; Stoler, R.; Silber, S. 9-Month Clinical and Angiographic Outcomes of the COBRA Polyzene-F NanoCoated Coronary Stent System. *JACC: Cardiovascular Interventions* **2017**, *10*, 160-167.

(73) CeloNova Biosciences Receives FDA Approval of COBRA PzFTM Stent System. http://celonova.com/wp-content/uploads/2016/09/COBRA-PzF-FDA-Approval-Press-Release-APM-0219-Rev-B.pdf.

(74) U.S. Food & Drug Administration Premarket Approval (PMA). https://www.accessdata.fda.gov/scripts/cdrh/cfdocs/cfPMA/pma.cfm?id=P160014.

(75) Styllou, P.; Silber, S. A case report of the new Polyzene™-F COBRA PzF™ Nanocoated Coronary Stent System (NCS): Addressing an unmet clinical need. *Cardiovascular Revascularization Medicine* **2016**, *17*, 209-211.

(76) Verret, V.; Wassef, M.; Pelage, J. P.; Ghegediban, S. H.; Jouneau, L.; Moine, L.; Labarre, D.; Golzarian, J.; Schwartz-Cornil, I.; Laurent, A. Influence of degradation on inflammatory profile of polyphosphazene coated PMMA and trisacryl gelatin microspheres in a sheep uterine artery embolization model. *Biomaterials* **2011**, *32*, 339-351.

(77) Thongcharoen, P.; Suriyanon, V.; Paris, R. M.; Khamboonruang, C.; de Souza, M. S.; Ratto-Kim, S.; Karnasuta, C.; Polonis, V. R.; Baglyos, L.; El Habib, R. A Phase 1/2 Comparative Vaccine Trial of the Safety and Immunogenicity of a CRF01_AE (Subtype E) Candidate Vaccine: ALVAC-HIV (vCP1521) Prime With Oligomeric gp160 (92TH023/LAI-DID) or Bivalent gp120 (CM235/SF2) Boost. *JAIDS Journal of Acquired Immune Deficiency Syndromes* **2007**, *46*, 48.

(78) Albright, V.; Palanisamy, A.; Zhou, Q.; Selin, V.; Sukhishvili, S. A. Functional Surfaces through Controlled Assemblies of Upper Critical Solution Temperature Block and Star Copolymers. *Langmuir* **2019**, *35*, 10677-10688.

(79) Zheng, J.; Xiao, P.; Le, X.; Lu, W.; Theato, P.; Ma, C.; Du, B.; Zhang, J.; Huang, Y.; Chen, T. Mimosa inspired bilayer hydrogel actuator functioning in multi-environments. *Journal of Materials Chemistry C* **2018**, *6*, 1320-1327.

(80) So, S.; Hayward, R. C. Tunable Upper Critical Solution Temperature of Poly(N-isopropylacrylamide) in Ionic Liquids for Sequential and Reversible Self-Folding. *ACS Applied Materials & Interfaces* **2017**, *9*, 15785-15790.

(81) Hu, X.; McIntosh, E.; Simon, M. G.; Staii, C.; Thomas, S. W. Stimuli-Responsive Free-Standing Layer-By-Layer Films. *Advanced Materials* **2016**, *28*, 715-721.

(82) Albright, V.; Zhuk, I.; Wang, Y.; Selin, V.; van de Belt-Gritter, B.; Busscher, H. J.; van der Mei, H. C.; Sukhishvili, S. A. Self-defensive antibiotic-loaded layer-by-layer coatings: Imaging of localized bacterial acidification and pH-triggering of antibiotic release. *Acta Biomaterialia* **2017**, *61*, 66-74.

(83) Brockgreitens, J.; Abbas, A. Responsive Food Packaging: Recent Progress and Technological Prospects. *Comprehensive Reviews in Food Science and Food Safety* **2015**, *15*, 3-15.

(84) Crespy, D.; Rossi, R. M. Temperature-responsive polymers with LCST in the physiological range and their applications in textiles. *Polymer International* **2007**, *56*, 1461-1468.

(85) Maeda, Y.; Higuchi, T.; Ikeda, I. Change in Hydration State during the Coil−Globule Transition of Aqueous Solutions of Poly(N-isopropylacrylamide) as Evidenced by FTIR Spectroscopy. *Langmuir* **2000**, *16*, 7503-7509.

(86) Grosberg, A. Y.; Kuznetsov, D. V. Single-chain collapse or precipitation? Kinetic diagram of the states of a polymer solution. *Macromolecules* **1993**, *26*, 4249-4251.

(87) Dormidontova, E. E. Role of Competitive PEO−Water and Water−Water Hydrogen Bonding in Aqueous Solution PEO Behavior. *Macromolecules* **2002**, *35*, 987-1001.

(88) Smith, G. D.; Bedrov, D. Roles of Enthalpy, Entropy, and Hydrogen Bonding in the Lower Critical Solution Temperature Behavior of Poly(ethylene oxide)/Water Solutions. *The Journal of Physical Chemistry B* **2003**, *107*, 3095-3097.

(89) Galamba, N. Water's Structure around Hydrophobic Solutes and the Iceberg Model. *The Journal of Physical Chemistry B* **2013**, *117*, 2153-2159.

(90) Bischofberger, I.; Calzolari, D. C. E.; De Los Rios, P.; Jelezarov, I.; Trappe, V. Hydrophobic hydration of poly-N-isopropyl acrylamide: a matter of the mean energetic state of water. *Scientific Reports* **2014**, *4*, 4377.

(91) Hou, L.; Wu, P. On the abnormal "forced hydration" behavior of P(MEA-co-OEGA) aqueous solutions during phase transition from infrared spectroscopic insights. *Physical Chemistry Chemical Physics* **2016**, *18*, 15593-15601.

(92) Heyda, J.; Soll, S.; Yuan, J.; Dzubiella, J. Thermodynamic Description of the LCST of Charged Thermoresponsive Copolymers. *Macromolecules* **2014**, *47*, 2096-2102.

(93) Karjalainen, E.; Aseyev, V.; Tenhu, H. Upper or lower critical solution temperature, or both? Studies on cationic copolymers of N-isopropylacrylamide. *Polymer Chemistry* **2015**, *6*, 3074-3082.

(94) Teotia, A. K.; Sami, H.; Kumar, A.: 1 - Thermo-responsive polymers: structure and design of smart materials. In *Switchable and Responsive Surfaces and*

Materials for Biomedical Applications; Zhang, Z., Ed.; Woodhead Publishing: Oxford, **2015**; pp 3-43.

(95) Yamauchi, H.; Maeda, Y. LCST and UCST Behavior of Poly(N-isopropylacrylamide) in DMSO/Water Mixed Solvents Studied by IR and Micro-Raman Spectroscopy. *The Journal of Physical Chemistry B* **2007**, *111*, 12964-12968.

(96) Fujishige, S.; Kubota, K.; Ando, I. Phase transition of aqueous solutions of poly(N-isopropylacrylamide) and poly(N-isopropylmethacrylamide). *The Journal of Physical Chemistry* **1989**, *93*, 3311-3313.

(97) Mah, E.; Ghosh, R. Thermo-Responsive Hydrogels for Stimuli-Responsive Membranes. *Processes* **2013**, *1*, 238.

(98) Roth, P. J.; Davis, T. P.; Lowe, A. B. Comparison between the LCST and UCST Transitions of Double Thermoresponsive Diblock Copolymers: Insights into the Behavior of POEGMA in Alcohols. *Macromolecules* **2012**, *45*, 3221-3230.

(99) Yasushi, M.; Hiroki, M.; Isao, I. Hydration Changes during Thermosensitive Association of a Block Copolymer Consisting of LCST and UCST Blocks. *Macromolecular Rapid Communications* **2004**, *25*, 1330-1334.

(100) Seuring, J.; Bayer, F. M.; Huber, K.; Agarwal, S. Upper Critical Solution Temperature of Poly(N-acryloyl glycinamide) in Water: A Concealed Property. *Macromolecules* **2012**, *45*, 374-384.

(101) Huang, G.; Li, H.; Feng, S. T.; Li, X. Q.; Tong, G. Q.; Liu, J.; Quan, C. Y.; Jiang, Q.; Zhang, C.; Li, Z. P. Self-assembled UCST-Type Micelles as Potential Drug Carriers for Cancer Therapeutics. *Macromol Chem Phys* **2015**, *216*, 1014-1023.

(102) Li, W.; Huang, L.; Ying, X.; Jian, Y.; Hong, Y.; Hu, F.; Du, Y. Antitumor Drug Delivery Modulated by A Polymeric Micelle with an Upper Critical Solution Temperature. *Angewandte Chemie International Edition* **2015**, *54*, 3126-3131.

(103) Wu, C.; Zhou, S. Q. Laser-Light Scattering Study of the Phase-Transition of Poly(N-Isopropylacrylamide) in Water .1. Single-Chain. *Macromolecules* **1995**, *28*, 8381-8387.

(104) Tavagnacco, L.; Zaccarelli, E.; Chiessi, E. On the molecular origin of the cooperative coil-to-globule transition of poly(N-isopropylacrylamide) in water. *Phys. Chem. Chem. Phys.* **2018**, *20*, 9997-10010.

(105) Shimada, N.; Ino, H.; Maie, K.; Nakayama, M.; Kano, A.; Maruyama, A. Ureido-Derivatized Polymers Based on Both Poly(allylurea) and Poly(L-citrulline) Exhibit UCST-Type Phase Transition Behavior under Physiologically Relevant Conditions. *Biomacromolecules* **2011**, *12*, 3418-3422.

(106) Fujihara, A.; Itsuki, K.; Shimada, N.; Maruyama, A.; Sagawa, N.; Shikata, T.; Yusa, S. I. Preparation of Ureido Group Bearing Polymers and Their Upper Critical Solution Temperature in Water. *Journal of Polymer Science, Part A: Polymer Chemistry* **2016**, *54*, 2845-2854.

(107) Winnik, F. M. Fluorescence studies of aqueous solutions of poly(N-isopropylacrylamide) below and above their LCST. *Macromolecules* **1990**, *23*, 233-242.

(108) Richardson, J. J.; Cui, J.; Björnmalm, M.; Braunger, J. A.; Ejima, H.; Caruso, F. Innovation in Layer-by-Layer Assembly. *Chemical Reviews* **2016**.

(109) Osypova, A.; Magnin, D.; Sibret, P.; Aqil, A.; Jerome, C.; Dupont-Gillain, C.; Pradier, C. M.; Demoustier-Champagne, S.; Landoulsi, J. Dual stimuli-responsive coating designed through layer-by-layer assembly of PAA-b-PNIPAM block copolymers for the control of protein adsorption. *Soft Matter* **2015**, *11*, 8154-8164.

(110) Nash, M. E.; Healy, D.; Carroll, W. M.; Elvira, C.; Rochev, Y. A. Cell and cell sheet recovery from pNIPAm coatings; motivation and history to present day approaches. *Journal of Materials Chemistry* **2012**, *22*, 19376-19389.

(111) Schmidt, S.; Zeiser, M.; Hellweg, T.; Duschl, C.; Fery, A.; Möhwald, H. Adhesion and Mechanical Properties of PNIPAM Microgel Films and Their Potential Use as Switchable Cell Culture Substrates. *Advanced Functional Materials* **2010**, *20*, 3235-3243.

(112) Bertrand, O.; Vlad, A.; Hoogenboom, R.; Gohy, J.-F. Redox-controlled upper critical solution temperature behaviour of a nitroxide containing polymer in alcohol-water mixtures. *Polymer Chemistry* **2016**, *7*, 1088-1095.

(113) Zhang, Q.; Hoogenboom, R. Polymers with upper critical solution temperature behavior in alcohol/water solvent mixtures. *Progress in Polymer Science* **2015**, *48*, 122-142.

(114) Fu, W.; Luo, C.; Morin, E. A.; He, W.; Li, Z.; Zhao, B. UCST-Type Thermosensitive Hairy Nanogels Synthesized by RAFT Polymerization-Induced Self-Assembly. *ACS Macro Letters* **2017**, *6*, 127-133.

(115) Ge, C.; Liu, S.; Liang, C.; Ling, Y.; Tang, H. Synthesis and UCST-type phase behavior of [small alpha]-helical polypeptides with Y-shaped and imidazolium pendants. *Polymer Chemistry* **2016**, *7*, 5978-5987.

(116) Liu, W.; Zhu, M.; Xiao, J.; Ling, Y.; Tang, H. Synthesis and UCST-type phase behavior of polypeptide with alkyl side-chains in alcohol or ethanol/water solvent mixtures. *Journal of Polymer Science Part A: Polymer Chemistry* **2016**, *54*, 3425-3435.

(117) Seuring, J.; Agarwal, S. Polymers with Upper Critical Solution Temperature in Aqueous Solution. *Macromolecular Rapid Communications* **2012**, *33*, 1898-1920.

(118) Zhu, Y.; Noy, J.-M.; Lowe, A. B.; Roth, P. J. The synthesis and aqueous solution properties of sulfobutylbetaine (co)polymers: comparison of synthetic routes and tuneable upper critical solution temperatures. *Polymer Chemistry* **2015**, *6*, 5705-5718.

(119) Jia, X.; Chen, D.; Jiang, M. Preparation of PEO-b-P2VPH+-S2O82- micelles in water and their reversible UCST and redox-responsive behavior. *Chemical Communications* **2006**, 1736-1738.

(120) Palanisamy, A.; Albright, V.; Sukhishvili, S. A. Upper Critical Solution Temperature Layer-by-Layer Films of Polyamino acid-Based Micelles with Rapid, On-Demand Release Capability. *Chem. Mat.* **2017**, *29*, 9084-9094.

(121) Seuring, J.; Agarwal, S. Polymers with Upper Critical Solution Temperature in Aqueous Solution: Unexpected Properties from Known Building Blocks. *ACS Macro Letters* **2013**, *2*, 597-600.

(122) Aoki, T.; Kawashima, M.; Katono, H.; Sanui, K.; Ogata, N.; Okano, T.; Sakurai, Y. Temperature-Responsive Interpenetrating Polymer Networks Constructed with Poly(acrylic acid) and Poly(N,N-dimethylacrylamide). *Macromolecules* **1994**, *27*, 947-952.

(123) Jiang, Z.; You, Y.; Gu, Q.; Hao, J.; Deng, X. Effect of Microstructures on the Phase Transition Behavior of P(CL-GL)-PEG-P(CL-GL) Triblock Copolymer Aqueous Solutions. *Macromolecular Rapid Communications* **2008**, *29*, 1264-1268.

(124) Shimada, N.; Saito, M.; Shukuri, S.; Kuroyanagi, S.; Kuboki, T.; Kidoaki, S.; Nagai, T.; Maruyama, A. Reversible Monolayer/Spheroid Cell Culture Switching by UCST-Type Thermoresponsive Ureido Polymers. *ACS Applied Materials & Interfaces* **2016**, *8*, 31524-31529.

(125) Seuring, J.; Agarwal, S. First Example of a Universal and Cost-Effective Approach: Polymers with Tunable Upper Critical Solution Temperature in Water and Electrolyte Solution. *Macromolecules* **2012**, *45*, 3910-3918.

(126) Roth, P. J. Composing Well-Defined Stimulus-Responsive Materials Through Postpolymerization Modification Reactions. *Macromol Chem Phys* **2014**, *215*, 825-838.

(127) Ustoglu, C.; Cagli, E.; Erel-Goktepe, I. Layer-by-layer films of block copolymer micelles with cores exhibiting upper critical solution temperature behaviour. *European Polymer Journal* **2017**, *96*, 278-294.

(128) Chen, L.; Honma, Y.; Mizutani, T.; Liaw, D. J.; Gong, J. P.; Osada, Y. Effects of polyelectrolyte complexation on the UCST of zwitterionic polymer. *Polymer* **2000**, *41*, 141-147.

(129) Fangyao, L.; Seema, A. Thermoresponsive Gold Nanoparticles with Positive UCST-Type Thermoresponsivity. *Macromolecular Chemistry and Physics* **2015**, *216*, 460-465.

(130) Housni, A.; Zhao, Y. Gold nanoparticles functionalized with block copolymers displaying either LCST or UCST thermosensitivity in aqueous solution. *Langmuir* **2010**, *26*, 12933-12939.

(131) Tao, H.; Galati, E.; Kumacheva, E. Temperature-Responsive Self-Assembly of Nanoparticles Grafted with UCST Polymer Ligands. *Macromolecules* **2018**, *51*, 6021-6027.

(132) Weaver, J. V. M.; Armes, S. P.; Butun, V. Synthesis and aqueous solution properties of a well-defined thermo-responsive schizophrenic diblock copolymer. *Chemical Communications* **2002**, 2122-2123.

(133) Dimitrov, I.; Trzebicka, B.; Müller, A. H. E.; Dworak, A.; Tsvetanov, C. B. Thermosensitive water-soluble copolymers with doubly responsive reversibly interacting entities. *Progress in Polymer Science* **2007**, *32*, 1275-1343.

(134) Zhang, Q.; Hong, J.-D.; Hoogenboom, R. A triple thermoresponsive schizophrenic diblock copolymer. *Polymer Chemistry* **2013**, *4*, 4322-4325.

(135) Palanisamy, A.; Sukhishvili, S. A. Swelling Transitions in Layer-by-Layer Assemblies of UCST Block Copolymer Micelles. *Macromolecules* **2018**, *51*, 3467-3476.

(136) Zhang, H.; Tong, X.; Zhao, Y. Diverse Thermoresponsive Behaviors of Uncharged UCST Block Copolymer Micelles in Physiological Medium. *Langmuir* **2014**, *30*, 11433-11441.

(137) Qi, M. W.; Li, K.; Zheng, Y. L.; Rasheed, T.; Zhou, Y. F. Hyperbranched Multiarm Copolymers with a UCST Phase Transition: Topological Effect and the Mechanism. *Langmuir* **2018**, *34*, 3058-3067.

(138) Zhou, Q.; Palanisamy, A.; Albright, V.; Sukhishvili, S. A. Enzymatically degradable star polypeptides with tunable UCST transitions in solution and within layer-by-layer films. *Polymer Chemistry* **2018**, DOI 10.1039/C1038PY00939B.

(139) Da-Peng, Y.; Linn, O. M. N. N.; Roshan, D. G.; Zibiao, L.; Jun, L. X. Nano-Star-Shaped Polymers for Drug Delivery Applications. *Macromolecular Rapid Communications* **2017**, *38*, 1700410.

(140) Fujihara, A.; Shimada, N.; Maruyama, A.; Ishihara, K.; Nakai, K.; Yusa, S.-i. Preparation of upper critical solution temperature (UCST) responsive diblock copolymers bearing pendant ureido groups and their micelle formation behavior in water. *Soft Matter* **2015**, *11*, 5204-5213.

(141) Abbott, L. J.; Tucker, A. K.; Stevens, M. J. Single Chain Structure of a Poly(N-isopropylacrylamide) Surfactant in Water. *The Journal of Physical Chemistry B* **2015**, *119*, 3837-3845.

(142) Zajforoushan Moghaddam, S.; Thormann, E. Hofmeister Effect on PNIPAM in Bulk and at an Interface: Surface Partitioning of Weakly Hydrated Anions. *Langmuir* **2017**, *33*, 4806-4815.

(143) Wang, L.; Maji, S. K.; Sawaya, M. R.; Eisenberg, D.; Riek, R. Bacterial inclusion bodies contain amyloid-like structure. *PLoS Biology* **2008**, *6*, e195.

(144) Fandrich, M.; Dobson, C. M. The behaviour of polyamino acids reveals an inverse side chain effect in amyloid structure formation. *EMBO Journal* **2002**, *21*, 5682-5690.

(145) Wang, R.; Xu, N.; Du, F. S.; Li, Z. C. Facile control of the self-assembled structures of polylysines having pendent mannose groups via pH and surfactant. *Chemical Communications* **2010**, *46*, 3902-3904.

(146) Shen, J.; Han, K.; Martin, E. J.; Wu, Y. Y.; Kung, M. C.; Hayner, C. M.; Shull, K. R.; Kung, H. H. Upper-critical solution temperature (UCST) polymer functionalized graphene oxide as thermally responsive ion permeable membrane for energy storage devices. *Journal of Materials Chemistry A* **2014**, *2*, 18204-18207.

(147) Azzaroni, O.; Brown Andrew, A.; Huck Wilhelm, T. S. UCST Wetting Transitions of Polyzwitterionic Brushes Driven by Self-Association. *Angewandte Chemie International Edition* **2006**, *45*, 1770-1774.

(148) Xue, X.; Thiagarajan, L.; Braim, S.; Saunders, B. R.; Shakesheff, K. M.; Alexander, C. Upper critical solution temperature thermo-responsive polymer brushes and a mechanism for controlled cell attachment. *Journal of Materials Chemistry B* **2017**, *5*, 4926-4933.

(149) Minko, S.: Grafting on Solid Surfaces: “Grafting to” and “Grafting from” Methods. In *Polymer Surfaces and Interfaces: Characterization, Modification and*

Applications; Stamm, M., Ed.; Springer Berlin Heidelberg: Berlin, Heidelberg, 2008; pp 215-234.

(150) Decher, G.: Layer-by-Layer Assembly (Putting Molecules to Work). In *Multilayer Thin Films*; Wiley-VCH Verlag GmbH & Co. KGaA, 2012; pp 1-21.

(151) Pavlukhina, S. V.; Kaplan, J. B.; Xu, L.; Chang, W.; Yu, X.; Madhyastha, S.; Yakandawala, N.; Mentbayeva, A.; Khan, B.; Sukhishvili, S. A. Noneluting Enzymatic Antibiofilm Coatings. *ACS Applied Materials & Interfaces* **2012**, *4*, 4708-4716.

(152) Zhu, Z. C.; Sukhishvili, S. A. Layer-by-layer films of stimuli-responsive block copolymer micelles. *J Mater Chem* **2012**, *22*, 7667-7671.

(153) Tan, W. S.; Cohen, R. E.; Rubner, M. F.; Sukhishvili, S. A. Temperature-Induced, Reversible Swelling Transitions in Multilayers of a Cationic Triblock Copolymer and a Polyacid. *Macromolecules* **2010**, *43*, 1950-1957.

(154) Zhuk, A.; Xu, L.; Ankner, J. F.; Sukhishvili, S. A. Selective water uptake within micelle-containing layer-by-layer films of various architectures: a neutron reflectometry study. *Soft Matter* **2013**, *9*, 410-417.

(155) Erel-Unal, I.; Sukhishvili, S. A. Hydrogen-bonded multilayers of a neutral polymer and a polyphenol. *Macromolecules* **2008**, *41*, 3962-3970.

(156) Kozlovskaya, V.; Kharlampieva, E.; Drachuk, I.; Cheng, D.; Tsukruk, V. V. Responsive microcapsule reactors based on hydrogen-bonded tannic acid layer-by-layer assemblies. *Soft Matter* **2010**, *6*, 3596-3608.

(157) Kozlovskaya, V.; Zavgorodnya, O.; Chen, Y.; Ellis, K.; Tse, H. M.; Cui, W.; Thompson, J. A.; Kharlampieva, E. Ultrathin polymeric coatings based on hydrogen-

bonded polyphenol for protection of pancreatic islet cells. *Advanced functional materials* **2012**, *22*, 3389-3398.

(158) Albright, V.; Xu, M.; Palanisamy, A.; Cheng, J.; Stack, M.; Zhang, B.; Jayaraman, A.; Sukhishvili Svetlana, A.; Wang, H. Micelle-Coated, Hierarchically Structured Nanofibers with Dual-Release Capability for Accelerated Wound Healing and Infection Control. *Advanced Healthcare Materials* **2018**, *7*, 1800132.

(159) Zhou, Q.; Palanisamy, A.; Albright, V.; Sukhishvili, S. A. Enzymatically degradable star polypeptides with tunable UCST transitions in solution and within layer-by-layer films. *Polymer Chemistry* **2018**, *9*, 4979-4983.

(160) Zhou, Q.; Zhang, L.; Yang, T.; Wu, H. Stimuli-responsive polymeric micelles for drug delivery and cancer therapy. *International journal of nanomedicine* **2018**, *13*, 2921-2942.

(161) Erel, I.; Zhu, Z.; Zhuk, A.; Sukhishvili, S. A. Hydrogen-bonded layer-by-layer films of block copolymer micelles with pH-responsive cores. *Journal of colloid and interface science* **2011**, *355*, 61-69.

(162) Xu, L.; Zhu, Z.; Sukhishvili, S. A. Polyelectrolyte multilayers of diblock copolymer micelles with temperature-responsive cores. *Langmuir* **2011**, *27*, 409-415.

(163) Zhu, Z.; Sukhishvili, S. A. Temperature-induced swelling and small molecule release with hydrogen-bonded multilayers of block copolymer micelles. *ACS Nano* **2009**, *3*, 3595-3605.

(164) Albright, V.; Palanisamy, A.; Zhou, Q.; Selin, V.; Sukhishvili, S. A. Functional Surfaces through Controlled Assemblies of Upper Critical Solution Temperature Block and Star Copolymers. *Langmuir* **2018**.

(165) Palanisamy, A.; Sukhishvili, S. A. Swelling Transitions in Layer-by-Layer Assemblies of UCST Block Copolymer Micelles. *Macromolecules* **2018**.

(166) Sen, C. K.; Gordillo, G. M.; Roy, S.; Kirsner, R.; Lambert, L.; Hunt, T. K.; Gottrup, F.; Gurtner, G. C.; Longaker, M. T. Human skin wounds: a major and snowballing threat to public health and the economy. *Wound Repair Regen* **2009**, *17*, 763-771.

(167) Markova, A.; Mostow, E. N. US Skin Disease Assessment: Ulcer and Wound Care. *Dermatologic Clinics* **2012**, *30*, 107-111.

(168) Frykberg, R. G.; Banks, J. Challenges in the Treatment of Chronic Wounds. *Adv Wound Care (New Rochelle)* **2015**, *4*, 560-582.

(169) Panuncialman, J.; Falanga, V. The science of wound bed preparation. *Clin Plast Surg* **2007**, *34*, 621-632.

(170) Dickinson, L. E.; Gerecht, S. Engineered Biopolymeric Scaffolds for Chronic Wound Healing. *Front Physiol* **2016**, *7*, 341.

(171) Zhong, S. P.; Zhang, Y. Z.; Lim, C. T. Tissue scaffolds for skin wound healing and dermal reconstruction. *Wiley interdisciplinary reviews. Nanomedicine and nanobiotechnology* **2010**, *2*, 510-525.

(172) Hinderer, S.; Layland, S. L.; Schenke-Layland, K. ECM and ECM-like materials - Biomaterials for applications in regenerative medicine and cancer therapy. *Adv Drug Deliv Rev* **2016**, *97*, 260-269.

(173) Wang, K.; Xu, M.; Zhu, M.; Su, H.; Wang, H.; Kong, D.; Wang, L. Creation of macropores in electrospun silk fibroin scaffolds using sacrificial PEO-microparticles to enhance cellular infiltration. *J Biomed Mater Res A* **2013**, *101*, 3474-3481.

(174) Chou, S. F.; Carson, D.; Woodrow, K. A. Current strategies for sustaining drug release from electrospun nanofibers. *J Control Release* **2015**, *220*, 584-591.

(175) Wang, Z.; Qian, Y.; Li, L.; Pan, L.; Njunge, L. W.; Dong, L.; Yang, L. Evaluation of emulsion electrospun polycaprolactone/hyaluronan/epidermal growth factor nanofibrous scaffolds for wound healing. *Journal of Biomaterials Applications* **2016**, *30*, 686-698.

(176) Nwachukwu, C. C.; Einstein, G. P.; Tulp, O. L. Electrospun Nanofibers as Scaffolds for Wound Healing. *The FASEB Journal* **2017**, *31*, 333.332.

(177) Chen, S.; Liu, B.; Carlson, M. A.; Gombart, A. F.; Reilly, D. A.; Xie, J. Recent advances in electrospun nanofibers for wound healing. *Nanomedicine (London, England)* **2017**, *12*, 1335-1352.

(178) Liu, M.; Duan, X. P.; Li, Y. M.; Yang, D. P.; Long, Y. Z. Electrospun nanofibers for wound healing. *Mater Sci Eng C Mater Biol Appl* **2017**, *76*, 1413-1423.

(179) Venugopal, J. R.; Zhang, Y.; Ramakrishna, S. In vitro culture of human dermal fibroblasts on electrospun polycaprolactone collagen nanofibrous membrane. *Artificial organs* **2006**, *30*, 440-446.

(180) Yang, X.; Shah, J. D.; Wang, H. Nanofiber enabled layer-by-layer approach toward three-dimensional tissue formation. *Tissue engineering. Part A* **2009**, *15*, 945-956.

(181) Chen, X.; Fu, X.; Shi, J.-g.; Wang, H. Regulation of the osteogenesis of pre-osteoblasts by spatial arrangement of electrospun nanofibers in two- and three-dimensional environments. *Nanomedicine: Nanotechnology, Biology and Medicine* **2013**, *9*, 1283-1292.

(182) Pakyari, M.; Farrokhi, A.; Maharlooei, M. K.; Ghahary, A. Critical Role of Transforming Growth Factor Beta in Different Phases of Wound Healing. *Adv Wound Care (New Rochelle)* **2013**, *2*, 215-224.

(183) Diegelmann, R. F.; Evans, M. C. Wound healing: an overview of acute, fibrotic and delayed healing. *Frontiers in bioscience : a journal and virtual library* **2004**, *9*, 283-289.

(184) Crowe, M. J.; Doetschman, T.; Greenhalgh, D. G. Delayed wound healing in immunodeficient TGF-beta 1 knockout mice. *J Invest Dermatol* **2000**, *115*, 3-11.

(185) Fu, X.; Xu, M.; Jia, C.; Xie, W.; Wang, L.; Kong, D.; Wang, H. Differential regulation of skin fibroblasts for their TGF-β1-dependent wound healing activities by biomimetic nanofibers. *Journal of Materials Chemistry B* **2016**, *4*, 5246-5255.

(186) Hinz, B.; Celetta, G.; Tomasek, J. J.; Gabbiani, G.; Chaponnier, C. Alpha-smooth muscle actin expression upregulates fibroblast contractile activity. *Mol Biol Cell* **2001**, *12*, 2730-2741.

(187) Desmouliere, A.; Geinoz, A.; Gabbiani, F.; Gabbiani, G. Transforming growth factor-beta 1 induces alpha-smooth muscle actin expression in granulation tissue myofibroblasts and in quiescent and growing cultured fibroblasts. *The Journal of cell biology* **1993**, *122*, 103-111.

(188) Ronnov-Jessen, L.; Petersen, O. W. Induction of alpha-smooth muscle actin by transforming growth factor-beta 1 in quiescent human breast gland fibroblasts. Implications for myofibroblast generation in breast neoplasia. *Lab Invest* **1993**, *68*, 696-707.

(189) Wukich, D. K.; Ahn, J.; Raspovic, K. M.; Gottschalk, F. A.; La Fontaine, J.; Lavery, L. A. Comparison of Transtibial Amputations in Diabetic Patients With and Without End-Stage Renal Disease. *Foot Ankle Int* **2017**, *38*, 388-396.

(190) Sanchez-Sanchez, M.; Cruz-Pulido, W. L.; Bladinieres-Camara, E.; Alcala-Duran, R.; Rivera-Sanchez, G.; Bocanegra-Garcia, V. Bacterial Prevalence and Antibiotic Resistance in Clinical Isolates of Diabetic Foot Ulcers in the Northeast of Tamaulipas, Mexico. *Int J Low Extrem Wounds* **2017**, *16*, 129-134.

(191) Maruccia, M.; Onesti, M. G.; Sorvillo, V.; Albano, A.; Dessy, L. A.; Carlesimo, B.; Tarallo, M.; Marcasciano, M.; Giudice, G.; Cigna, E.; Ribuffo, D. An Alternative Treatment Strategy for Complicated Chronic Wounds: Negative Pressure Therapy over Mesh Skin Graft. *Biomed Res Int* **2017**, *2017*, 8395219.

(192) Rahim, K.; Saleha, S.; Zhu, X.; Huo, L.; Basit, A.; Franco, O. L. Bacterial Contribution in Chronicity of Wounds. *Microb Ecol* **2017**, *73*, 710-721.

(193) Gjødsbøl, K.; Christensen, J. J.; Karlsmark, T.; Jørgensen, B.; Klein, B. M.; Krogfelt, K. A. Multiple bacterial species reside in chronic wounds: a longitudinal study. *International Wound Journal* **2006**, *3*, 225-231.

(194) ALEXANDER, J. W.; MACMILLAN, B. G.; LAW, E. J.; KRUMMEL, R. Prophylactic Antibiotics as an Adjunct for Skin Grafting in Clean Reconstructive Surgery following Burn Injury. *Journal of Trauma and Acute Care Surgery* **1982**, *22*, 687-690.

(195) Robson, M. C. Wound infection. A failure of wound healing caused by an imbalance of bacteria. *Surg Clin North Am* **1997**, *77*, 637-650.

(196) Kuijpers, D.; Smeets, N.; Lapière, K.; Thissen, M.; Krekels, G.; Neumann, H. Do systemic antibiotics increase the survival of a full thickness graft on the nose? *Journal of the European Academy of Dermatology and Venereology* **2006**, *20*, 1296-1301.

(197) Taubes, G. The bacteria fight back. *Science* **2008**, *321*, 356-361.

(198) Gao, Y.; Bach Truong, Y.; Zhu, Y.; Louis Kyratzis, I. Electrospun antibacterial nanofibers: Production, activity, and in vivo applications. *Journal of Applied Polymer Science* **2014**, *131*.

(199) Dave, R.; Jayaraj, P.; Ajikumar, P. K.; Joshi, H.; Mathews, T.; Venugopalan, V. P. Endogenously triggered electrospun fibres for tailored and controlled antibiotic release. *Journal of biomaterials science. Polymer edition* **2013**, *24*, 1305-1319.

(200) Bakhsheshi-Rad, H. R.; Hadisi, Z.; Hamzah, E.; Ismail, A. F.; Aziz, M.; Kashefian, M. Drug delivery and cytocompatibility of ciprofloxacin loaded gelatin nanofibers-coated Mg alloy. *Materials Letters* **2017**, *207*, 179-182.

(201) Zupancic, S.; Sinha-Ray, S.; Sinha-Ray, S.; Kristl, J.; Yarin, A. L. Controlled Release of Ciprofloxacin from Core-Shell Nanofibers with Monolithic or Blended Core. *Molecular pharmaceutics* **2016**, *13*, 1393-1404.

(202) Kenawy el, R.; Bowlin, G. L.; Mansfield, K.; Layman, J.; Simpson, D. G.; Sanders, E. H.; Wnek, G. E. Release of tetracycline hydrochloride from electrospun poly(ethylene-co-vinylacetate), poly(lactic acid), and a blend. *Journal of controlled release : official journal of the Controlled Release Society* **2002**, *81*, 57-64.

(203) Xu, X.; Zhong, W.; Zhou, S.; Trajtman, A.; Alfa, M. Electrospun PEG–PLA nanofibrous membrane for sustained release of hydrophilic antibiotics. *Journal of Applied Polymer Science* **2010**, *118*, 588-595.

(204) Chen, X. N.; Gu, Y. X.; Lee, J. H.; Lee, W. Y.; Wang, H. J. Multifunctional surfaces with biomimetic nanofibres and drug-eluting micro-patterns for infection control and bone tissue formation. *European cells & materials* **2012**, *24*, 237-248.

(205) Yang, G.; Wang, J.; Li, L.; Ding, S.; Zhou, S. Electrospun micelles/drug-loaded nanofibers for time-programmed multi-agent release. *Macromolecular bioscience* **2014**, *14*, 965-976.

(206) Yang, G.; Wang, J.; Wang, Y.; Li, L.; Guo, X.; Zhou, S. An implantable active-targeting micelle-in-nanofiber device for efficient and safe cancer therapy. *ACS Nano* **2015**, *9*, 1161-1174.

(207) Zhu, Z.; Gao, N.; Wang, H.; Sukhishvili, S. A. Temperature-triggered on-demand drug release enabled by hydrogen-bonded multilayers of block copolymer micelles. *Journal of controlled release : official journal of the Controlled Release Society* **2013**, *171*, 73-80.

(208) Tan, W. S.; Zhu, Z.; Sukhishvili, S. A.; Rubner, M. F.; Cohen, R. E. Effect of Block Copolymer Architecture on the Thermally Induced Swelling of Micelle-Containing Multilayer Thin Films. *Macromolecules* **2011**, *44*, 7767-7774.

(209) Kim, B. S.; Park, S. W.; Hammond, P. T. Hydrogen-bonding layer-by-layer-assembled biodegradable polymeric micelles as drug delivery vehicles from surfaces. *ACS Nano* **2008**, *2*, 386-392.

(210) Bertrand, P.; Jonas, A.; Laschewsky, A.; Legras, R. Ultrathin polymer coatings by complexation of polyelectrolytes at interfaces: suitable materials, structure and properties. *Macromolecular Rapid Communications* **2000**, *21*, 319-348.

(211) Hammond, P. T. Form and Function in Multilayer Assembly: New Applications at the Nanoscale. *Advanced Materials* **2004**, *16*, 1271-1293.

(212) Richardson, J. J.; Cui, J.; Bjornmalm, M.; Braunger, J. A.; Ejima, H.; Caruso, F. Innovation in Layer-by-Layer Assembly. *Chemical reviews* **2016**, *116*, 14828-14867.

(213) Ninan, N.; Forget, A.; Shastri, V. P.; Voelcker, N. H.; Blencowe, A. Antibacterial and Anti-Inflammatory pH-Responsive Tannic Acid-Carboxylated Agarose Composite Hydrogels for Wound Healing. *ACS Appl Mater Interfaces* **2016**, *8*, 28511-28521.

(214) Kozlovskaya, V.; Xue, B.; Lei, W.; Padgett, L. E.; Tse, H. M.; Kharlampieva, E. Hydrogen-Bonded Multilayers of Tannic Acid as Mediators of T-Cell Immunity. *Advanced Healthcare Materials* **2015**, *4*, 686-694.

(215) Tarnuzzer, R. W.; Schultz, G. S. Biochemical analysis of acute and chronic wound environments. *Wound repair and regeneration : official publication of the Wound Healing Society [and] the European Tissue Repair Society* **1996**, *4*, 321-325.

(216) Zhang, Y. Z.; Venugopal, J.; Huang, Z. M.; Lim, C. T.; Ramakrishna, S. Characterization of the surface biocompatibility of the electrospun PCL-collagen nanofibers using fibroblasts. *Biomacromolecules* **2005**, *6*, 2583-2589.

(217) Albright, V.; Zhuk, I.; Wang, Y.; Selin, V.; van de Belt-Gritter, B.; Busscher, H. J.; van der Mei, H. C.; Sukhishvili, S. A. Self-defensive antibiotic-loaded layer-by-layer coatings: Imaging of localized bacterial acidification and pH-triggering of antibiotic release. *Acta Biomaterialia* **2017**, *61*, 66-74.

(218) Schultz, G. S.; Sibbald, R. G.; Falanga, V.; Ayello, E. A.; Dowsett, C.; Harding, K.; Romanelli, M.; Stacey, M. C.; Teot, L.; Vanscheidt, W. Wound bed preparation: a systematic approach to wound management. *Wound repair and regeneration : official publication of the Wound Healing Society [and] the European Tissue Repair Society* **2003**, *11 Suppl 1*, S1-28.

(219) Saarialho-Kere, U. K.; Kovacs, S. O.; Pentland, A. P.; Olerud, J. E.; Welgus, H. G.; Parks, W. C. Cell-matrix interactions modulate interstitial collagenase expression by human keratinocytes actively involved in wound healing. *The Journal of clinical investigation* **1993**, *92*, 2858-2866.

(220) Schiffer, D.; Blokhuis-Arkes, M.; van der Palen, J.; Sigl, E.; Heinzle, A.; Guebitz, G. M. Assessment of infection in chronic wounds based on the activities of elastase, lysozyme and myeloperoxidase. *The British journal of dermatology* **2015**, *173*, 1529-1531.

(221) Schultz, G. S.; Sibbald, R. G.; Falanga, V.; Ayello, E. A.; Dowsett, C.; Harding, K.; Romanelli, M.; Stacey, M. C.; Teot, L.; Vanscheidt, W. Wound bed preparation: a systematic approach to wound management. *Wound Repair and Regeneration* **2003**, *11*, S1-S28.

(222) Schiffer, D.; Blokhuis-Arkes, M.; van der Palen, J.; Sigl, E.; Heinzle, A.; Guebitz, G. M. Assessment of infection in chronic wounds based on the activities of elastase, lysozyme and myeloperoxidase. *British Journal of Dermatology* **2015**, *173*, 1529-1531.

(223) Olsen, J. V.; Ong, S.-E.; Mann, M. Trypsin Cleaves Exclusively C-terminal to Arginine and Lysine Residues. *Molecular & Cellular Proteomics* **2004**, *3*, 608-614.

(224) Ousey, K.; Cutting, K. F.; Rogers, A. A.; Rippon, M. G. The importance of hydration in wound healing: reinvigorating the clinical perspective. *Journal of wound care* **2016**, *25*, 122, 124-130.

(225) Yim, E. K. F.; Leong, K. W. Significance of synthetic nanostructures in dictating cellular response. *Nanomedicine: Nanotechnology, Biology and Medicine* **2005**, *1*, 10-21.

(226) McCoy, L. S.; Xie, Y.; Tor, Y. Antibiotics that target protein synthesis. *Wiley interdisciplinary reviews. RNA* **2011**, *2*, 209-232.

(227) Tenson, T.; Lovmar, M.; Ehrenberg, M. The mechanism of action of macrolides, lincosamides and streptogramin B reveals the nascent peptide exit path in the ribosome. *Journal of molecular biology* **2003**, *330*, 1005-1014.

(228) King, M. D.; Humphrey, B. J.; Wang, Y. F.; Kourbatova, E. V.; Ray, S. M.; Blumberg, H. M. Emergence of community-acquired methicillin-resistant Staphylococcus aureus USA 300 clone as the predominant cause of skin and soft-tissue infections. *Annals of internal medicine* **2006**, *144*, 309-317.

(229) Goetz, I. E.; Moklebust, R.; Warren, C. J. Effects of some antibiotics on the growth of human diploid skin fibroblasts in cell culture. *In vitro* **1979**, *15*, 114-119.

(230) Pavlukhina, S.; Zhuk, I.; Mentbayeva, A.; Rautenberg, E.; Chang, W.; Yu, X.; van de Belt-Gritter, B.; Busscher, H. J.; van der Mei, H. C.; Sukhishvili, S. A. Small-molecule-hosting nanocomposite films with multiple bacteria-triggered responses. *Npg Asia Materials* **2014**, *6*, e121.

(231) Pristinski, D.; Kozlovskaya, V.; Sukhishvili, S. A. Fluorescence correlation spectroscopy studies of diffusion of a weak polyelectrolyte in aqueous solutions. *The Journal of chemical physics* **2005**, *122*, 14907.

(232) Yoo, H. S.; Kim, T. G.; Park, T. G. Surface-functionalized electrospun nanofibers for tissue engineering and drug delivery. *Advanced Drug Delivery Reviews* **2009**, *61*, 1033-1042.

(233) Park, K.; Ju, Y. M.; Son, J. S.; Ahn, K. D.; Han, D. K. Surface modification of biodegradable electrospun nanofiber scaffolds and their interaction with fibroblasts. *J Biomater Sci Polym Ed* **2007**, *18*, 369-382.

(234) Ma, Z.; Kotaki, M.; Yong, T.; He, W.; Ramakrishna, S. Surface engineering of electrospun polyethylene terephthalate (PET) nanofibers towards development of a new material for blood vessel engineering. *Biomaterials* **2005**, *26*, 2527-2536.

(235) Ding, B.; Fujimoto, K.; Shiratori, S. Preparation and characterization of self-assembled polyelectrolyte multilayered films on electrospun nanofibers. *Thin Solid Films* **2005**, *491*, 23-28.

(236) Ogawa, T.; Ding, B.; Sone, Y.; Shiratori, S. Super-hydrophobic surfaces of layer-by-layer structured film-coated electrospun nanofibrous membranes. *Nanotechnology* **2007**, *18*, 165607.

(237) Deng, H.; Zhou, X.; Wang, X.; Zhang, C.; Ding, B.; Zhang, Q.; Du, Y. Layer-by-layer structured polysaccharides film-coated cellulose nanofibrous mats for cell culture. *Carbohydrate Polymers* **2010**, *80*, 474-479.

(238) Müller, K.; Quinn, J. F.; Johnston, A. P. R.; Becker, M.; Greiner, A.; Caruso, F. Polyelectrolyte Functionalization of Electrospun Fibers. *Chemistry of Materials* **2006**, *18*, 2397-2403.

(239) Zhou, B.; Li, Y.; Deng, H.; Hu, Y.; Li, B. Antibacterial multilayer films fabricated by layer-by-layer immobilizing lysozyme and gold nanoparticles on nanofibers. *Colloids and Surfaces B: Biointerfaces* **2014**, *116*, 432-438.

(240) Sui, C.; Wang, C.; Wang, Z.; Xu, Y.; Gong, E.; Cheng, T.; Zhou, G. Different coating on electrospun nanofiber via layer-by-layer self-assembly for their

photocatalytic activities. *Colloids and Surfaces A: Physicochemical and Engineering Aspects* **2017**, *529*, 425-433.

(241) Wang, X.; Kim, Y.-G.; Drew, C.; Ku, B.-C.; Kumar, J.; Samuelson, L. A. Electrostatic Assembly of Conjugated Polymer Thin Layers on Electrospun Nanofibrous Membranes for Biosensors. *Nano Letters* **2004**, *4*, 331-334.

(242) Gülçin, İ.; Huyut, Z.; Elmastaş, M.; Aboul-Enein, H. Y. Radical scavenging and antioxidant activity of tannic acid. *Arabian Journal of Chemistry* **2010**, *3*, 43-53.

(243) Kai, D.; Zhang, K.; Jiang, L.; Wong, H. Z.; Li, Z.; Zhang, Z.; Loh, X. J. Sustainable and Antioxidant Lignin–Polyester Copolymers and Nanofibers for Potential Healthcare Applications. *ACS Sustainable Chemistry & Engineering* **2017**, *5*, 6016-6025.

(244) Kai, D.; Ren, W.; Tian, L.; Chee, P. L.; Liu, Y.; Ramakrishna, S.; Loh, X. J. Engineering Poly(lactide)–Lignin Nanofibers with Antioxidant Activity for Biomedical Application. *ACS Sustainable Chemistry & Engineering* **2016**, *4*, 5268-5276.

(245) Selvaraj, S.; Fathima, N. N. Fenugreek Incorporated Silk Fibroin Nanofibers—A Potential Antioxidant Scaffold for Enhanced Wound Healing. *ACS Applied Materials & Interfaces* **2017**, *9*, 5916-5926.

(246) Deldar, Y.; Pilehvar-Soltanahmadi, Y.; Dadashpour, M.; Montazer Saheb, S.; Rahmati-Yamchi, M.; Zarghami, N. An in vitro examination of the antioxidant, cytoprotective and anti-inflammatory properties of chrysin-loaded nanofibrous mats for potential wound healing applications. *Artificial Cells, Nanomedicine, and Biotechnology* **2018**, *46*, 706-716.

(247) Mei, L.; Fan, R.; Li, X.; Wang, Y.; Han, B.; Gu, Y.; Zhou, L.; Zheng, Y.; Tong, A.; Guo, G. Nanofibers for improving the wound repair process: the combination of a grafted chitosan and an antioxidant agent. *Polymer Chemistry* **2017**, *8*, 1664-1671.

(248) Aytac, Z.; Kusku, S. I.; Durgun, E.; Uyar, T. Encapsulation of gallic acid/cyclodextrin inclusion complex in electrospun polylactic acid nanofibers: Release behavior and antioxidant activity of gallic acid. *Materials Science and Engineering: C* **2016**, *63*, 231-239.

(249) Re, R.; Pellegrini, N.; Proteggente, A.; Pannala, A.; Yang, M.; Rice-Evans, C. Antioxidant activity applying an improved ABTS radical cation decolorization assay. *Free Radical Biology and Medicine* **1999**, *26*, 1231-1237.

(250) Hayashi, T.; Nagai, Y. Effect of pH on the stability of collagen molecule in solution. *Journal of biochemistry* **1973**, *73*, 999-1006.

(251) Kozlovskaya, V.; Xue, B.; Lei, W.; Padgett, L. E.; Tse, H. M.; Kharlampieva, E. Hydrogen-Bonded Multilayers of Tannic Acid as Mediators of T Cell Immunity. *Advanced healthcare materials* **2015**, *4*, 686-694.

(252) Min, J.; Braatz, R. D.; Hammond, P. T. Tunable staged release of therapeutics from layer-by-layer coatings with clay interlayer barrier. *Biomaterials* **2014**, *35*, 2507-2517.

(253) Pérez-Anes, A.; Gargouri, M.; Laure, W.; Van Den Berghe, H.; Courcot, E.; Sobocinski, J.; Tabary, N.; Chai, F.; Blach, J.-F.; Addad, A.; Woisel, P.; Douroumis, D.; Martel, B.; Blanchemain, N.; Lyskawa, J. Bioinspired Titanium Drug Eluting

Platforms Based on a Poly-β-cyclodextrin–Chitosan Layer-by-Layer Self-Assembly Targeting Infections. *ACS Applied Materials & Interfaces* **2015**, *7*, 12882-12893.

(254) Pavlukhina, S.; Sukhishvili, S. Polymer assemblies for controlled delivery of bioactive molecules from surfaces. *Advanced Drug Delivery Reviews* **2011**, *63*, 822-836.

(255) Cado, G.; Aslam, R.; Séon, L.; Garnier, T.; Fabre, R.; Parat, A.; Chassepot, A.; Voegel, J. C.; Senger, B.; Schneider, F.; Frère, Y.; Jierry, L.; Schaaf, P.; Kerdjoudj, H.; Metz-Boutigue, M. H.; Boulmedais, F. Self-Defensive Biomaterial Coating Against Bacteria and Yeasts: Polysaccharide Multilayer Film with Embedded Antimicrobial Peptide. *Advanced Functional Materials* **2013**, *23*, 4801-4809.

(256) Komnatnyy, V. V.; Chiang, W.-C.; Tolker-Nielsen, T.; Givskov, M.; Nielsen, T. E. Bacteria-Triggered Release of Antimicrobial Agents. *Angewandte Chemie International Edition* **2014**, *53*, 439-441.

(257) Francesko, A.; Fernandes, M. M.; Ivanova, K.; Amorim, S.; Reis, R. L.; Pashkuleva, I.; Mendoza, E.; Pfeifer, A.; Heinze, T.; Tzanov, T. Bacteria-responsive multilayer coatings comprising polycationic nanospheres for bacteria biofilm prevention on urinary catheters. *Acta Biomaterialia* **2016**, *33*, 203-212.

(258) Pavlukhina, S.; Lu, Y.; Patimetha, A.; Libera, M.; Sukhishvili, S. Polymer Multilayers with pH-Triggered Release of Antibacterial Agents. *Biomacromolecules* **2010**, *11*, 3448-3456.

(259) Kozlovskaya, V.; Kharlampieva, E.; Mansfield, M. L.; Sukhishvili, S. A. Poly(methacrylic acid) Hydrogel Films and Capsules: Response to pH and Ionic Strength, and Encapsulation of Macromolecules. *Chemistry of Materials* **2006**, *18*, 328-336.

(260) Kozlovskaya, V.; Sukhishvili, S. A. Amphoteric Hydrogel Capsules: Multiple Encapsulation and Release Routes. *Macromolecules* **2006**, *39*, 6191-6199.

(261) Kaplan, J. B. Biofilm Dispersal: Mechanisms, Clinical Implications, and Potential Therapeutic Uses. *Journal of Dental Research* **2010**, *89*, 205-218.

(262) Wang, Y.; Kozlovskaya, V.; Arcibal, I. G.; Cropek, D. M.; Kharlampieva, E. Highly swellable ultrathin poly(4-vinylpyridine) multilayer hydrogels with pH-triggered surface wettability. *Soft Matter* **2013**, *9*, 9420-9429.

(263) Pristinski, D.; Kozlovskaya, V.; Sukhishvili, S. A. Determination of film thickness and refractive index in one measurement of phase-modulated ellipsometry. *J. Opt. Soc. Am. A* **2006**, *23*, 2639-2644.

(264) McCoy, L. S.; Xie, Y.; Tor, Y. Antibiotics that target protein synthesis. *Wiley Interdisciplinary Reviews: RNA* **2011**, *2*, 209-232.

(265) Falagas, M. E.; Kasiakou, S. K.; Saravolatz, L. D. Colistin: The Revival of Polymyxins for the Management of Multidrug-Resistant Gram-Negative Bacterial Infections. *Clinical Infectious Diseases* **2005**, *40*, 1333-1341.

(266) Constantin, M.; Bucatariu, S.; Harabagiu, V.; Popescu, I.; Ascenzi, P.; Fundueanu, G. Poly(N-isopropylacrylamide-co-methacrylic acid) pH/thermo-responsive porous hydrogels as self-regulated drug delivery system. *European Journal of Pharmaceutical Sciences* **2014**, *62*, 86-95.

(267) Kozlovskaya, V.; Sukhishvili, S. A. pH-Controlled Permeability of Layered Hydrogen-Bonded Polymer Capsules. *Macromolecules* **2006**, *39*, 5569-5572.

(268) Zhuk, I.; Jariwala, F.; Attygalle, A. B.; Wu, Y.; Libera, M. R.; Sukhishvili, S. A. Self-Defensive Layer-by-Layer Films with Bacteria-Triggered Antibiotic Release. *ACS Nano* **2014**.

(269) Schlafer, S.; Garcia, J. E.; Greve, M.; Raarup, M. K.; Nyvad, B.; Dige, I. Ratiometric Imaging of Extracellular pH in Bacterial Biofilms with C-SNARF-4. *Applied and Environmental Microbiology* **2015**, *81*, 1267-1273.

(270) Hunter, R. C.; Beveridge, T. J. Application of a pH-Sensitive Fluoroprobe (C-SNARF-4) for pH Microenvironment Analysis in Pseudomonas aeruginosa Biofilms. *Applied and Environmental Microbiology* **2005**, *71*, 2501-2510.

(271) Dige, I.; Baelum, V.; Nyvad, B.; Schlafer, S. Monitoring of extracellular pH in young dental biofilms grown in vivo in the presence and absence of sucrose. *2016* **2016**, *8*.

(272) Whitaker, J. E.; Haugland, R. P.; Prendergast, F. G. Spectral and photophysical studies of benzo[c]xanthene dyes: Dual emission pH sensors. *Analytical Biochemistry* **1991**, *194*, 330-344.

(273) Haugland, R. P.; Whitaker, J.: Xanthene dyes having a fused (C) benzo ring. Google Patents, 1990.

(274) Dartnell, L. R.; Roberts, T. A.; Moore, G.; Ward, J. M.; Muller, J.-P. Fluorescence Characterization of Clinically-Important Bacteria. *PLoS ONE* **2013**, *8*, e75270.

(275) Alimova, A.; Katz, A.; Savage, H. E.; Shah, M.; Minko, G.; Will, D. V.; Rosen, R. B.; McCormick, S. A.; Alfano, R. R. Native fluorescence and excitation spectroscopic changes in Bacillus subtilis and Staphylococcus aureus bacteria subjected to conditions of starvation. *Appl. Opt.* **2003**, *42*, 4080-4087.

(276) Estes, C.; Duncan, A.; Wade, B.; Lloyd, C.; Ellis Jr, W.; Powers, L. Reagentless detection of microorganisms by intrinsic fluorescence. *Biosensors and Bioelectronics* **2003**, *18*, 511-519.

(277) Giana, H. E.; Silveira, L.; Zângaro, R. A.; Pacheco, M. T. T. Rapid Identification of Bacterial Species by Fluorescence Spectroscopy and Classification Through Principal Components Analysis. *Journal of Fluorescence* **2003**, *13*, 489-493.

(278) Gottenbos, B.; Grijpma, D. W.; van der Mei, H. C.; Feijen, J.; Busscher, H. J. Antimicrobial effects of positively charged surfaces on adhering Gram-positive and Gram-negative bacteria. *Journal of Antimicrobial Chemotherapy* **2001**, *48*, 7-13.

(279) Ling, L. L.; Schneider, T.; Peoples, A. J.; Spoering, A. L.; Engels, I.; Conlon, B. P.; Mueller, A.; Schaberle, T. F.; Hughes, D. E.; Epstein, S.; Jones, M.; Lazarides, L.; Steadman, V. A.; Cohen, D. R.; Felix, C. R.; Fetterman, K. A.; Millett, W. P.; Nitti, A. G.; Zullo, A. M.; Chen, C.; Lewis, K. A new antibiotic kills pathogens without detectable resistance. *Nature* **2015**, *517*, 455-459.

(280) Albright, V.; Selin, V.; Hlushko, H.; Palanisamy, A.; Marin, A.; Andrianov, A. K.; Sukhishvili, S. A.: Fluorinated Polyphosphazene Coatings Using Aqueous Nano-Assembly of Polyphosphazene Polyelectrolytes. In *Polyphosphazenes in*

Biomedicine, Engineering, and Pioneering Synthesis; ACS Symposium Series 1298; American Chemical Society, 2018; Vol. 1298; pp 101-118.

(281) Allcock, H. R.; Steely, L. B.; Singh, A. Hydrophobic and superhydrophobic surfaces from polyphosphazenes. *Polymer International* **2006**, *55*, 621-625.

(282) Allcock, H. R.; Steely, L.; Singh, A.; Hindenlang, M. Hydrophobic and superhydrophobic polyphosphazenes. *J. Adhes. Sci. Technol.* **2009**, *23*, 435-445.

(283) Allcock, H. R. Chemistry and Applications of Polyphosphazenes. *Wiley* **2002**, 725 p.

(284) Gleria, M.; Bertani, R.; De Jaeger, R. Fluorinated Polyphosphazenes: A Survey. *J. Inorg. Organomet. Polym.* **2004**, *14*, 1-28.

(285) Gleria, M.; Bertani, R.; Jaeger, R. D.; Lora, S. Fluorine containing phosphazene polymers. *J. Fluorine Chem.* **2004**, *125*, 329-337.

(286) Allcock, H. R.; Kugel, R. L. Synthesis of High Polymeric Alkoxy- and Aryloxyphosphonitriles. *Journal of the American Chemical Society* **1965**, *87*, 4216-4217.

(287) Tur, D. R.; Koršak, V. V.; Vinogradova, S. V.; Dobrova, N. B.; Novikova, S. P.; Il'ina, M. B.; Sidorenko, E. S. Investigation of the thermostability of poly[bis(trifluoroethoxy)phosphazene]. *Acta Polym.* **1985**, *36*, 627-631.

(288) Tur, D. R.; Koršak, V. V.; Vinogradova, S. V.; Slonimskij, G. L.; Il'Ina, M. N.; Dubovik, I. I.; Provotorova, N. P.; Dobrova, N. B.; Smurova, E. V. Investigation of the effects of biological environment on the properties of poly-bis-(trifluoroethoxy)phosphazene (r). *Acta Polym.* **1986**, *37*, 203-208.

(289) Nishino, T.; Meguro, M.; Nakamae, K.; Matsushita, M.; Ueda, Y. The Lowest Surface Free Energy Based on −CF3 Alignment. *Langmuir* **1999**, *15*, 4321-4323.

(290) Singh, A.; Steely, L.; Allcock, H. R. Poly[bis(2,2,2-trifluoroethoxy)phosphazene] Superhydrophobic Nanofibers. *Langmuir* **2005**, *21*, 11604-11607.

(291) Welle, A.; Grunze, M.; Tur, D. Plasma Protein Adsorption and Platelet Adhesion on Poly[bis(trifluoroethoxy)phosphazene] and Reference Material Surfaces. *Journal of Colloid and Interface Science* **1998**, *197*, 263-274.

(292) Smeets, A. J.; Nijenhuis, R. J.; van Rooij, W. J.; Lampmann, L. E. H.; Boekkooi, P. F.; Vervest, H. A. M.; De Vries, J.; Lohle, P. N. M. Embolization of Uterine Leiomyomas with Polyzene F–coated Hydrogel Microspheres: Initial Experience. *J. Vasc. Interv. Radiol.* **2010**, *21*, 1830-1834.

(293) Stampfl, U.; Radeleff, B.; Sommer, C.; Stampfl, S.; Dahlke, A.; Bellemann, N.; Kauczor, H.-U.; Richter, G. M. Midterm results of uterine artery embolization using narrow-size calibrated embozene microspheres. *Cardiovasc. Intervent. Radiol.* **2011**, *34*, 295-305.

(294) Styllou, P.; Silber, S. A case report of the new Polyzene™-F COBRA PzF™ Nanocoated Coronary Stent System (NCS): Addressing an unmet clinical need. *Cardiovasc. Revasc. Med.* **2016**, *17*, 209-211.

(295) Cutlip, D. E.; Garratt, K. N.; Novack, V.; Barakat, M.; Meraj, P.; Maillard, L.; Erglis, A.; Jauhar, R.; Popma, J. J.; Stoler, R.; Silber, S. 9-Month Clinical and

Angiographic Outcomes of the COBRA Polyzene-F NanoCoated Coronary Stent System. *Cardiovasc. Interventions* **2017**, *10*, 160-167.

(296) Lanzer, P.; Sternberg, K.; Schmitz, K.-P.; Kolodgie, F.; Nakazawa, G.; Virmani, R. Drug-Eluting Coronary Stent Very Late Thrombosis Revisited. *Herz Kardiovaskuläre Erkrankungen* **2008**, *33*, 334-342.

(297) Lei, L.; Guo, S.-R.; Chen, W.-L.; Rong, H.-J.; Lu, F. Stents as a platform for drug delivery. *Expert Opinion on Drug Delivery* **2011**, *8*, 813-831.

(298) Saylor, D. M.; Guyer, J. E.; Wheeler, D.; Warren, J. A. Predicting microstructure development during casting of drug-eluting coatings. *Acta Biomaterialia* **2011**, *7*, 604-613.

(299) Liu, X.; Han, F.; Zhao, P.; Lin, C.; Wen, X.; Ye, X. Layer-by-layer self-assembled multilayers on PEEK implants improve osseointegration in an osteoporosis rabbit model. *Nanomedicine: Nanotechnology, Biology and Medicine* **2017**, *13*, 1423-1433.

(300) Schönhoff, M. Layered polyelectrolyte complexes: physics of formation and molecular properties. *J. Phys.: Condens. Matter* **2003**, *15*, R1781.

(301) Pace, C. N.; Trevino, S.; Prabhakaran, E.; Scholtz, J. M. Protein structure, stability and solubility in water and other solvents. *Philos. Trans. R. Soc., B* **2004**, *359*, 1225-1235.

(302) Ladam, G.; Schaad, P.; Voegel, J. C.; Schaaf, P.; Decher, G.; Cuisinier, F. In Situ Determination of the Structural Properties of Initially Deposited Polyelectrolyte Multilayers. *Langmuir* **2000**, *16*, 1249-1255.

(303) Shiratori, S. S.; Rubner, M. F. pH-Dependent Thickness Behavior of Sequentially Adsorbed Layers of Weak Polyelectrolytes. *Macromolecules* **2000**, *33*, 4213-4219.

(304) Yoo, D.; Shiratori, S. S.; Rubner, M. F. Controlling Bilayer Composition and Surface Wettability of Sequentially Adsorbed Multilayers of Weak Polyelectrolytes. *Macromolecules* **1998**, *31*, 4309-4318.

(305) Hammond, P. T. Recent explorations in electrostatic multilayer thin film assembly. *Current Opinion in Colloid & Interface Science* **1999**, *4*, 430-442.

(306) Xu, L.; Pristinski, D.; Zhuk, A.; Stoddart, C.; Ankner, J. F.; Sukhishvili, S. A. Linear versus Exponential Growth of Weak Polyelectrolyte Multilayers: Correlation with Polyelectrolyte Complexes. *Macromolecules* **2012**, *45*, 3892-3901.

(307) Porcel, C.; Lavalle, P.; Decher, G.; Senger, B.; Voegel, J. C.; Schaaf, P. Influence of the Polyelectrolyte Molecular Weight on Exponentially Growing Multilayer Films in the Linear Regime. *Langmuir* **2007**, *23*, 1898-1904.

(308) Zhuk, A.; Selin, V.; Zhuk, I.; Belov, B.; Ankner, J. F.; Sukhishvili, S. A. Chain Conformation and Dynamics in Spin-Assisted Weak Polyelectrolyte Multilayers. *Langmuir* **2015**, *31*, 3889-3896.

(309) DeCollibus, D. P.; Marin, A.; Andrianov, A. K. Effect of Environmental Factors on Hydrolytic Degradation of Water-Soluble Polyphosphazene Polyelectrolyte in Aqueous Solutions. *Biomacromolecules* **2010**, *11*, 2033-2038.

(310) Selin, V.; Albright, V.; Ankner, J. F.; Marin, A.; Andrianov, A. K.; Sukhishvili, S. A. Biocompatible Nanocoatings of Fluorinated Polyphosphazenes through Aqueous Assembly. *ACS Applied Materials & Interfaces* **2018**.

(311) Hougham, G.; Tesoro, G.; Viehbeck, A. Influence of Free Volume Change on the Relative Permittivity and Refractive Index in Fluoropolyimides. *Macromolecules* **1996**, *29*, 3453-3456.

(312) Yasuda, H.; Sharma, A. K.; Yasuda, T. Effect of orientation and mobility of polymer molecules at surfaces on contact angle and its hysteresis. *Journal of Polymer Science: Polymer Physics Edition* **1981**, *19*, 1285-1291.

(313) Brunette, D. M.: *Titanium in Medicine: Material Science, Surface Science, Engineering, Biological Responses, and Medical Applications*; Springer, 2001.

(314) Soler, M.; Verhaeghe, P. J.; Stoppa, R.: Polyester (Dacron®) Mesh. In *Abdominal Wall Hernias: Principles and Management*; Bendavid, R., Abrahamson, J., Arregui, M. E., Flament, J. B., Phillips, E. H., Eds.; Springer New York: New York, NY, 2001; pp 266-271.

(315) Jiang, S. X.; Qin, W. F.; Guo, R. H.; Zhang, L. Surface functionalization of nanostructured silver-coated polyester fabric by magnetron sputtering. *Surface and Coatings Technology* **2010**, *204*, 3662-3667.

(316) Braune, S.; Lendlein, A.; Jung, F.: 3 - Developing standards and test protocols for testing the hemocompatibility of biomaterials A2 - Siedlecki, Christopher A. In *Hemocompatibility of Biomaterials for Clinical Applications*; Woodhead Publishing, 2018; pp 51-76.

(317) Xu, L.-C.; Bauer, J. W.; Siedlecki, C. A. Proteins, platelets, and blood coagulation at biomaterial interfaces. *Colloids Surf., B* **2014**, *124*, 49-68.

(318) Stanisławska, A. Biomaterials and implants in cardiac and vascular surgery-review. *Adv. Mater. Sci.* **2014**, *14*, 5-17.

(319) Henkelman, S.; Rakhorst, G.; Blanton, J.; van Oeveren, W. Standardization of incubation conditions for hemolysis testing of biomaterials. *Mater. Sci. Eng.: C Mater. Biol. Appl.* **2009**, *29*, 1650-1654.

(320) Shukla, A.; Avadhany, S. N.; Fang, J. C.; Hammond, P. T. Tunable Vancomycin Releasing Surfaces for Biomedical Applications. *Small* **2010**, *6*, 2392-2404.

(321) Josepovitz, C.; Pastoriza-Munoz, E.; Timmerman, D.; Scott, M.; Feldman, S.; Kaloyanides, G. J. Inhibition of gentamicin uptake in rat renal cortex in vivo by aminoglycosides and organic polycations. *The Journal of pharmacology and experimental therapeutics* **1982**, *223*, 314-321.

(322) Martinez, A. P.; Qamar, B.; Fuerst, T. R.; Muro, S.; Andrianov, A. K. Biodegradable "Smart" Polyphosphazenes with Intrinsic Multifunctionality as Intracellular Protein Delivery Vehicles. *Biomacromolecules* **2017**, *18*, 2000-2011.

(323) Albright, V.; Marin, A.; Kaner, P.; Sukhishvili, S. A.; Andrianov, A. K. New Family of Water-Soluble Sulfo–Fluoro Polyphosphazenes and Their Assembly within Hemocompatible Nanocoatings. *ACS Applied Bio Materials* **2019**, *2*, 3897-3906.

(324) Krafft, M. P.; Riess, J. G. Perfluorocarbons: Life sciences and biomedical uses Dedicated to the memory of Professor Guy Ourisson, a true RENAISSANCE man. *J. Polym. Sci., Part A: Polym. Chem.* **2007**, *45*, 1185-1198.

(325) Gardiner, J. Fluoropolymers: Origin, Production, and Industrial and Commercial Applications. *Aust. J. Chem.* **2015**, *68*, 13-22.

(326) Teo, A. J. T.; Mishra, A.; Park, I.; Kim, Y.-J.; Park, W.-T.; Yoon, Y.-J. Polymeric Biomaterials for Medical Implants and Devices. *ACS Biomater. Sci. Eng.* **2016**, *2*, 454-472.

(327) O'Brien, B.; Carroll, W. The evolution of cardiovascular stent materials and surfaces in response to clinical drivers: A review. *Acta Biomater.* **2009**, *5*, 945-958.

(328) Ding, N.; Pacetti, S. D.; Tang, F.-W.; Gada, M.; Roorda, W. XIENCE V™ Stent Design and Rationale. *J. Interv. Cardiol.* **2009**, *22*, S18-S27.

(329) Bates, M. C.; Yousaf, A.; Sun, L.; Barakat, M.; Kueller, A. Translational Research and Early Favorable Clinical Results of a Novel Polyphosphazene (Polyzene-F) Nanocoating. *Regen. Eng. Transl. Med.* **2019**, 1-13.

(330) Campoccia, D.; Montanaro, L.; Arciola, C. R. A review of the biomaterials technologies for infection-resistant surfaces. *Biomaterials* **2013**, *34*, 8533-8554.

(331) Nurmi, L.; Peng, H.; Seppälä, J.; Haddleton, D. M.; Blakey, I.; Whittaker, A. K. Synthesis and evaluation of partly fluorinated polyelectrolytes as components in 19F MRI-detectable nanoparticles. *Polym. Chem.* **2010**, *1*, 1039-1047.

(332) Battistella, C.; Yang, Y.; Chen, J.; Klok, H.-A. Synthesis and Postpolymerization Modification of Fluorine-End-Labeled Poly(Pentafluorophenyl Methacrylate) Obtained via RAFT Polymerization. *ACS Omega* **2018**, *3*, 9710-9721.

(333) Heitner-Wirguin, C. Recent advances in perfluorinated ionomer membranes: structure, properties and applications. *J. Membr. Sci.* **1996**, *120*, 1-33.

(334) Mauritz, K. A.; Moore, R. B. State of Understanding of Nafion. *Chem. Rev.* **2004**, *104*, 4535-4586.

(335) Miyatake, K.; Oyaizu, K.; Tsuchida, E.; Hay, A. S. Synthesis and Properties of Novel Sulfonated Arylene Ether/Fluorinated Alkane Copolymers. *Macromolecules* **2001**, *34*, 2065-2071.

(336) Lee, H. C.; Hong, H. S.; Kim, Y.-M.; Choi, S. H.; Hong, M. Z.; Lee, H. S.; Kim, K. Preparation and evaluation of sulfonated-fluorinated poly(arylene ether)s membranes for a proton exchange membrane fuel cell (PEMFC). *Electrochim. Acta* **2004**, *49*, 2315-2323.

(337) Mukherjee, R.; Mohanty, A. K.; Banerjee, S.; Komber, H.; Voit, B. Phthalimidine based fluorinated sulfonated poly(arylene ether sulfone)s copolymer proton exchange membranes. *J. Membr. Sci.* **2013**, *435*, 145-154.

(338) Kim, A. R.; Vinothkannan, M.; Yoo, D. J. Sulfonated-fluorinated copolymer blending membranes containing SPEEK for use as the electrolyte in polymer electrolyte fuel cells (PEFC). *Int. J. Hydrogen Energy* **2017**, *42*, 4349-4365.

(339) Yu, X.; Roy, A.; Dunn, S.; Badami, A. S.; Yang, J.; Good, A. S.; McGrath, J. E. Synthesis and characterization of sulfonated-fluorinated, hydrophilic-hydrophobic multiblock copolymers for proton exchange membranes. *JJ. Polym. Sci., Part A: Polym. Chem.* **2009**, *47*, 1038-1051.

(340) He, M.-L.; Xu, H.-L.; Dong, Y.; Xiao, J.-H.; Liu, P.; Fu, F.-Y.; Hussain, S.; Zhang, S.-Z.; Jing, C.-J.; Hao, X.; Zhu, C.-J. Synthesis and Characterization of

Perfluoroalkyl Sulfonic Acid Functionalized Polyphosphazene for Proton-Conducting Membranes. *J. Macromol. Sci., Part A: Pure Appl.Chem.* **2014**, *51*, 55-62.

(341) Fu, F.; Xu, H.; Dong, Y.; He, M.; Zhang, Z.; Luo, T.; Zhang, Y.; Hao, X.; Zhu, C. Design of polyphosphazene-based graft copolystyrenes with alkylsulfonate branch chains for proton exchange membranes. *J. Membr. Sci.* **2015**, *489*, 119-128.

(342) Allcock, H. R.: *Chemistry and Applications of Polyphosphazenes*; Wiley: Hoboken, NJ, 2002.

(343) *Polyphosphazenes for Biomedical Applications*; Andrianov, A. K., Ed.; John Wiley & Sons: Hoboken, New Jersey, 2009, pp 457.

(344) *Polyphosphazenes in Biomedicine, Engineering & Pioneering Synthesis*; Andrianov, A. K.; Allcock, H. R., Eds.; American Chemical Society: Washington, DC, 2018; Vol. 1298, ACS Symposium Series.

(345) Teasdale, I.; Brüggemann, O. Polyphosphazenes: multifunctional, biodegradable vehicles for drug and gene delivery. *Polymers* **2013**, *5*, 161-187.

(346) Andrianov, A. K.; Marin, A.; Peterson, P.; Chen, J. Fluorinated polyphosphazene polyelectrolytes. *J. Appl. Polym. Sci.* **2007**, *103*, 53-58.

(347) Andrianov, A. K.; Marin, A.; Chen, J.; Sargent, J.; Corbett, N. Novel route to sulfonated polyphosphazenes: Single-step synthesis using "noncovalent protection" of sulfonic acid functionality. *Macromolecules* **2004**, *37*, 4075-4080.

(348) Andrianov, A. K.; Chen, J.; LeGolvan, M. P. Poly(dichlorophosphazene) as a precursor for biologically active polyphosphazenes: Synthesis, characterization, and stabilization. *Macromolecules* **2004**, *37*, 414-420.

(349) Albright, V.; Marin, A.; Kaner, P.; Sukhishvili, S. A.; Andrianov, A. K. New Family of Water-Soluble Sulfo–Fluoro Polyphosphazenes and Their Assembly within Hemocompatible Nanocoatings. *ACS Applied Bio Materials* **2019**.

(350) Dubas, S. T.; Schlenoff, J. B. Factors controlling the growth of polyelectrolyte multilayers. *Macromolecules* **1999**, *32*, 8153-8160.

(351) Selin, V.; Albright, V.; Ankner, J. F.; Marin, A.; Andrianov, A. K.; Sukhishvili, S. A. Biocompatible Nanocoatings of Fluorinated Polyphosphazenes through Aqueous Assembly. *ACS Appl. Mater. Interfaces* **2018**, *10*, 9756-9764.

(352) Dubas, S. T.; Schlenoff, J. B. Swelling and Smoothing of Polyelectrolyte Multilayers by Salt. *Langmuir* **2001**, *17*, 7725-7727.

(353) Sukhishvili, S. A.; Kharlampieva, E.; Izumrudov, V. Where Polyelectrolyte Multilayers and Polyelectrolyte Complexes Meet. *Macromolecules* **2006**, *39*, 8873-8881.

(354) Selin, V.; Ankner, J. F.; Sukhishvili, S. A. Diffusional Response of Layer-by-Layer Assembled Polyelectrolyte Chains to Salt Annealing. *Macromolecules* **2015**, *48*, 3983-3990.

(355) Andrianov, A. K.; Svirkin, Y. Y.; LeGolvan, M. P. Synthesis and biologically relevant properties of polyphosphazene polyacids. *Biomacromolecules* **2004**, *5*, 1999-2006.

(356) Xie, R.; Karim, A.; Douglas, J.; C. Han, C.; Weiss, R. A.: *Spinodal Dewetting of Thin Polymer Films*, 1998; Vol. 81.

(357) Henkelman, S.; Rakhorst, G.; Blanton, J.; van Oeveren, W. Standardization of incubation conditions for hemolysis testing of biomaterials. *Mater. Sci. Eng. C.* **2009**, *29*, 1650-1654.

(358) Vasilev, K.; Cook, J.; Griesser, H. J. Antibacterial surfaces for biomedical devices. *Expert Review of Medical Devices* **2009**, *6*, 553-567.

(359) Coad, B. R.; Griesser, H. J.; Peleg, A. Y.; Traven, A. Anti-infective Surface Coatings: Design and Therapeutic Promise against Device-Associated Infections. *PLOS Pathogens* **2016**, *12*, e1005598.

(360) Riga, E. K.; Vöhringer, M.; Widyaya, V. T.; Lienkamp, K. Polymer-Based Surfaces Designed to Reduce Biofilm Formation: From Antimicrobial Polymers to Strategies for Long-Term Applications. *Macromolecular Rapid Communications* **2017**, *38*, 1700216.

(361) Zhu, X.; Jun Loh, X. Layer-by-layer assemblies for antibacterial applications. *Biomaterials Science* **2015**, *3*, 1505-1518.

(362) Liang, J.; Wang, H.; Libera, M. Biomaterial surfaces self-defensive against bacteria by contact transfer of antimicrobials. *Biomaterials* **2019**, *204*, 25-35.

(363) Wen, X.-W.; Pei, S.-P.; Li, H.; Ai, F.; Chen, H.; Li, K.-Y.; Wang, Q.; Zhang, Y.-M. Study on an antifouling and blood compatible poly(ethylene–vinyl acetate) material with fluorinated surface structure. *Journal of Materials Science* **2010**, *45*, 2788-2797.

(364) Zhang, J.; Kou, R.; Liu, G. Effect of Salt Concentration on the pH Responses of Strong and Weak Polyelectrolyte Brushes. *Langmuir* **2017**, *33*, 6838-6845.

(365) Allcock, H. R.; Kwon, S. An ionically crosslinkable polyphosphazene: poly[bis(carboxylatophenoxy)phosphazene] and its hydrogels and membranes. *Macromolecules* **1989**, *22*, 75-79.

(366) Cohen, S.; Bano, M. C.; Visscher, K. B.; Chow, M.; Allcock, H. R.; Langer, R. Ionically crosslinkable polyphosphazene: a novel polymer for microencapsulation. *Journal of the American Chemical Society* **1990**, *112*, 7832-7833.

(367) Andrianov, A. K.; Marin, A.; Peterson, P.; Chen, J. Fluorinated polyphosphazene polyelectrolytes. *J. Appl. Polym. Sci.* **2007**, *103*, 53-58.

(368) Ulusan, S.; Bütün, V.; Banerjee, S.; Erel-Goktepe, I. Biologically Functional Ultrathin Films Made of Zwitterionic Block Copolymer Micelles. *Langmuir* **2019**, *35*, 1156-1171.

(369) He, M.; Wang, Q.; Zhao, W.; Zhao, C. A substrate-independent ultrathin hydrogel film as an antifouling and antibacterial layer for a microfiltration membrane anchored via a layer-by-layer thiol–ene click reaction. *Journal of Materials Chemistry B* **2018**, *6*, 3904-3913.

(370) Garg, S. K.; Singh, O.; Juneja, D.; Tyagi, N.; Khurana, A. S.; Qamra, A.; Motlekar, S.; Barkate, H. Resurgence of Polymyxin B for MDR/XDR Gram-Negative Infections: An Overview of Current Evidence. *Critical Care Research and Practice* **2017**, *2017*, 3635609.

(371) Yessine, M.-A.; Leroux, J.-C. Membrane-destabilizing polyanions: interaction with lipid bilayers and endosomal escape of biomacromolecules. *Adv. Drug Delivery Rev.* **2004**, *56*, 999-1021.

(372) Lackey, C. A.; Murthy, N.; Press, O. W.; Tirrell, D. A.; Hoffman, A. S.; Stayton, P. S. Hemolytic activity of pH-responsive polymer-streptavidin bioconjugates. *Bioconjugate Chem.* **1999**, *10*, 401-405.

(373) Rozema, D. B.; Ekena, K.; Lewis, D. L.; Loomis, A. G.; Wolff, J. A. Endosomolysis by masking of a membrane-active agent (EMMA) for cytoplasmic release of macromolecules. *Bioconjugate Chem.* **2003**, *14*, 51-57.

(374) Andrianov, A. K.; Marin, A.; Fuerst, T. R. Self-assembly of polyphosphazene immunoadjuvant with poly(ethylene oxide) enables advanced nanoscale delivery modalities and regulated pH-dependent cellular membrane activity. *Heliyon* **2016**, *2*, Article e00102.

(375) Andrianov, A. K.; Chen, J.; Payne, L. G. Preparation of hydrogel microspheres by coacervation of aqueous polyphosphazene solutions. *Biomaterials* **1998**, *19*, 109-115.

(376) Andrianov, A. K.; Chen, J. Polyphosphazene microspheres: Preparation by ionic complexation of phosphazene polyacids with spermine. *J. Appl. Polym. Sci.* **2006**, *101*, 414-419.

(377) Sui, Z.; Salloum, D.; Schlenoff, J. B. Effect of Molecular Weight on the Construction of Polyelectrolyte Multilayers: Stripping versus Sticking. *Langmuir* **2003**, *19*, 2491-2495.

(378) Fang, Y.; Al-Assaf, S.; Phillips, G. O.; Nishinari, K.; Funami, T.; Williams, P. A.; Li, L. Multiple Steps and Critical Behaviors of the Binding of Calcium to Alginate. *The Journal of Physical Chemistry B* **2007**, *111*, 2456-2462.

(379) Kubo, M.; Ohshima, Y.; Irie, F.; Mikio, K.; Sawai, J. Disinfection Treatment of Heated Scallop-Shell Powder on Biofilm of Escherichia coli ATCC 25922 Surrogated for E. coli O157:H7. *Journal of Biomaterials and Nanobiotechnology* **2013**, *04*, 10-19.

(380) Poirel, L.; Jayol, A.; Nordmann, P. Polymyxins: Antibacterial Activity, Susceptibility Testing, and Resistance Mechanisms Encoded by Plasmids or Chromosomes. *Clinical Microbiology Reviews* **2017**, *30*, 557.

(381) Allcock, H. R.; Pucher, S. R.; Fitzpatrick, R. J.; Rashid, K. Antibacterial activity and mutagenicity studies of water-soluble phosphazene high polymers. *Biomaterials* **1992**, *13*, 857-862.

(382) Liu, X.; Zhang, H.; Tian, Z.; Sen, A.; Allcock, H. R. Preparation of quaternized organic-inorganic hybrid brush polyphosphazene-co-poly[2-(dimethylamino)ethyl methacrylate] electrospun fibers and their antibacterial properties. *Polymer Chemistry* **2012**, *3*, 2082-2091.

(383) Souza, F. T. S.; Mello, A. S. d.; Michelin, K.; Coelho, J. C. Effect of amikacin, cephalothin, clindamycin and vancomycin on in vitro fibroblast growth. *Genetics and Molecular Biology* **2004**, *27*, 454-459.

(384) Allcock, H. R.; Fitzpatrick, R. J.; Salvati, L. Sulfonation of (aryloxy)-and (arylamino) phosphazenes: small-molecule compounds, polymers, and surfaces. *Chem. Mater.* **1991**, *3*, 1120-1132.

(385) Allcock, H. R.; Klingenberg, E. H.; Welker, M. F. Alkanesulfonation of cyclic and high polymeric phosphazenes. *Macromolecules* **1993**, *26*, 5512-5519.

(386) Wycisk, R.; Pintauro, P. N. Sulfonated polyphosphazene ion-exchange membranes. *J. Membr. Sci.* **1996**, *119*, 155-160.

(387) Guo, Q.; Knight, P. T.; Mather, P. T. Tailored drug release from biodegradable stent coatings based on hybrid polyurethanes. *J. Controlled Release* **2009**, *137*, 224-233.

(388) Ranade, S. V.; Miller, K. M.; Richard, R. E.; Chan, A. K.; Allen, M. J.; Helmus, M. N. Physical characterization of controlled release of paclitaxel from the TAXUS™ Express2™ drug-eluting stent. *J. Biomed. Mater. Res., Part A* **2004**, *71A*, 625-634.

APPENDIX A

SUPPORTING MATERIAL FOR CHAPTER 2

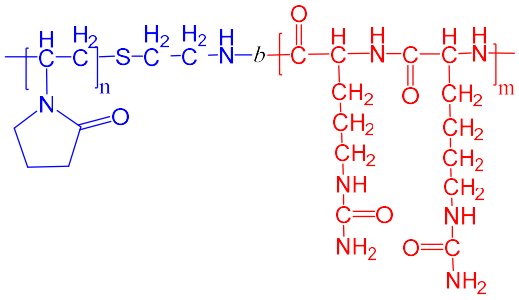

Figure A-1. Chemical structure of polyvinylpyrrolidone-*b*-polyureido(ornithine-co-lysine) (PVP-*b*-PUOL) micelles.

APPENDIX B

SUPPORTING MATERIAL FOR CHAPTER 4

Activity of Clindamycin against *S. aureus* ATCC 12600

To determine the MIC of clindamycin hydrochloride, *S. aureus* was streaked onto 20 mL TSB agar plates containing different concentrations of clindamycin. Plates were incubated for 24 h at 37 °C. The MIC was defined as the lowest concentration at which no bacterial growth was observed. All tests were performed in triplicate. As can be seen in Figure B-1, 0.125 µg/mL displayed minimal bacterial growth, while 0.25 µg/mL completely prevented bacterial growth. Therefore, 0.25 µg/mL was chosen as the MIC.

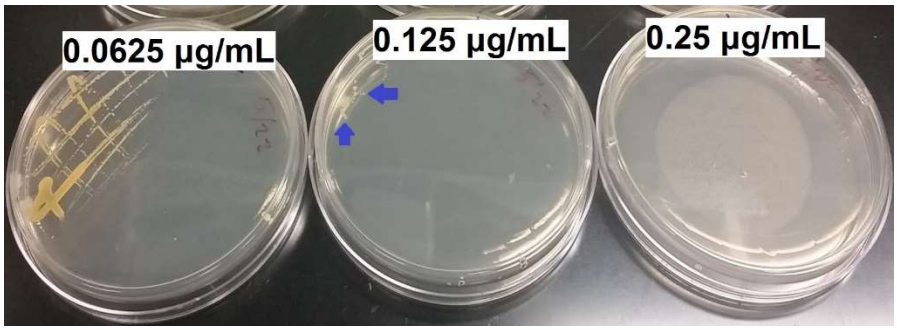

Figure B-1. 20 mL TSB agar plates streaked with *S. aureus* ATCC 12600 containing clindamycin of various concentrations: 0.0625, 0.125, and 0.25 µg mL^{-1}. Hard to see bacterial growth is marked with blue arrows. Reprinted with permission from [43] Copyright 2018 John Wiley & Sons, Inc.

Fibroblast Growth in the Presence of Clindamycin

To explore the effect of clindamycin on fibroblast growth, NDHFs were cultured for 24 h in a 6-well plate with a series of clindamycin hydrochloride dilutions (0.0625, 0.125, 0.25, 0.5, and 1 µg mL^{-1}) added to the culture media. Growth of fibroblasts, quantified by OD_{570}, did not significantly differ for any of the clindamycin concentrations

Figure B-2. This result is in good agreement with previous work that has shown that clindamycin (up to a concentration of 3 μg mL^{-1}) does not impede the growth or alter the viability of fibroblasts.[383]

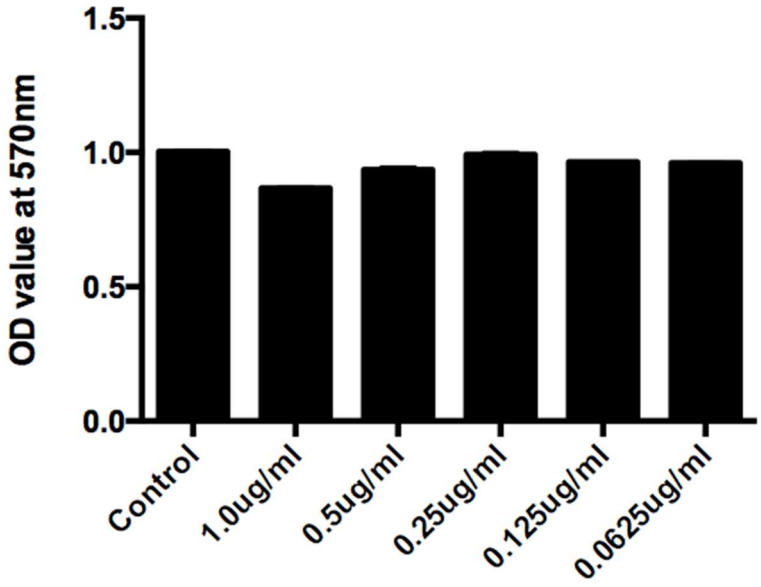

Figure B-2. Clindamycin hydrochloride in bulk solution does not affect the growth of fibroblasts. OD_{570} for fibroblasts after exposure to various concentrations of clindamycin hydrochloride in solution. Data presented as mean ± SD, n=3. Reprinted with permission from [43] Copyright 2018 John Wiley & Sons, Inc.

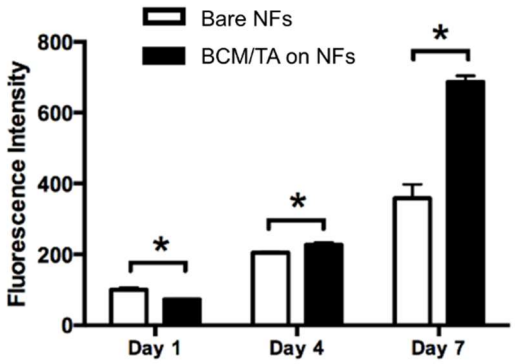

Figure B-3. Fibroblast proliferation on bare or 1.5-bilayer BCM/TA-coated PCL/Coll NFs up to seven days as measured by DNA assay. Data presented as mean ± SD, n=3, p-values are calculated using an unpaired student t-test, *p <0.05. Reprinted with permission from [43] Copyright 2018 John Wiley & Sons, Inc.

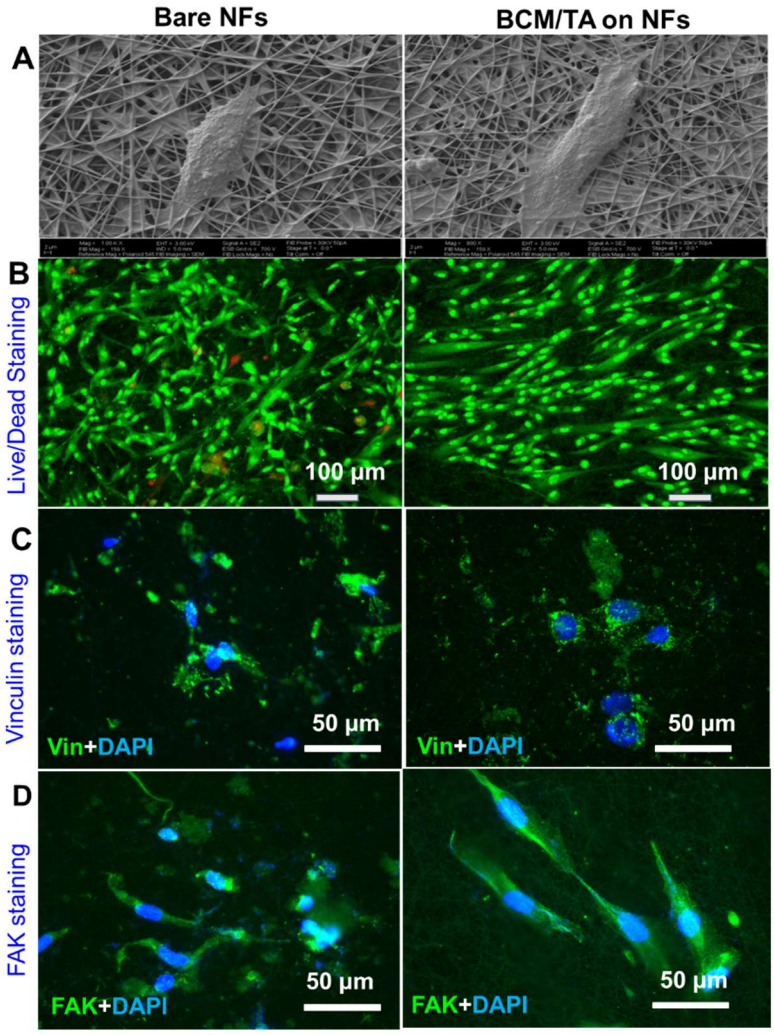

Figure B-4. Bare and BCM/TA-coated PCL/Coll NFs support the growth and attachment of NHDFs. Attachment of NHDFs as imaged by SEM imaging after 24 h culture of 5.0×10^4 cells (A). (B) Live/dead staining of NHDFs after 24 h culture of 5.0×10^4 cells/sample. Immunofluorescent staining of focal adhesion protein vinculin (green) and nuclei with DAPI (blue) (C), and FAK (green) (D) with DAPI (blue) after 48 h culture of 2×10^4 cells/sample. Reprinted with permission from [43] Copyright 2018 John Wiley & Sons, Inc.

APPENDIX C

SUPPORTING MATERIAL FOR CHAPTER 6

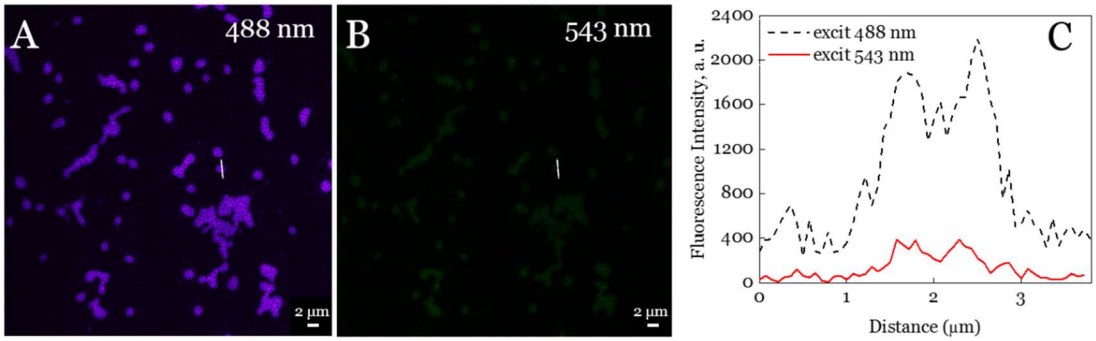

Figure C-1. Confocal Laser Scanning Microscopy images of SNARF-1-free 18-layer-PMAA coatings that had been cultured with 10^4 CFU/mL *S. aureus* for four hours and excited at 488 nm (A) and 543 nm (B) with emission collected beyond 560 nm. (C) Crosssectional emission intensities profiles of bacteria residing on a SNARF-free hydrogels at two different excitation wavelengths. Reprinted with permission from [82]. Copyright 2017 Acta Materialia Inc. Published by Elsevier Ltd.

APPENDIX D

SUPPORTING MATERIAL FOR CHAPTER 8

Synthesis of Trifluoroethoxy (FESP) and Trifluoromethylphenoxy (FPSP) Derivatives of Sulfonated PPzs and Their Physico-Chemical Characterization.

PPzs were designed to have p-sulfophenoxy side groups and either trifluoroethoxy or trifluoromethylphenoxy groups as fluorine containing moieties (Figure D-1). Sulfonated groups were introduced using non-covalent protection of ionic functionalities using alkylammonium salts.[347] This method provides a mild, single-step alternative to the more common technique that uses sulfuric acid or sulfur trioxide,[384-386] which may potentially result in undesirable modification or even degradation of pendant groups. Since many polymers that are used as biomaterials coatings have higher glass transition temperatures[328,387,388] than those of typical fluorinated PPzs, such as poly[bis(trifluoroethoxyphosphazene)], a bulkier substituent – ethylphenoxy group, which is intended to decrease flexibility of the polymer chain, was also introduced.[342] The reaction pathway included macromolecular substitution of polydichlorophosphazene (PDCP) with fluorinated nucleophile – either trifluoroethanol or trifluoromethylphenol, resulting in a partially substituted PPz IA and IB (Figure D-1), followed by the addition of ethylphenol (intermediates IIA and IIB). The sulfonic acid side groups were introduced by further modifying an incompletely substituted PPz with alkylammmonium salt of p-hydroxybenzenesulfonic acid as described previously.[347]

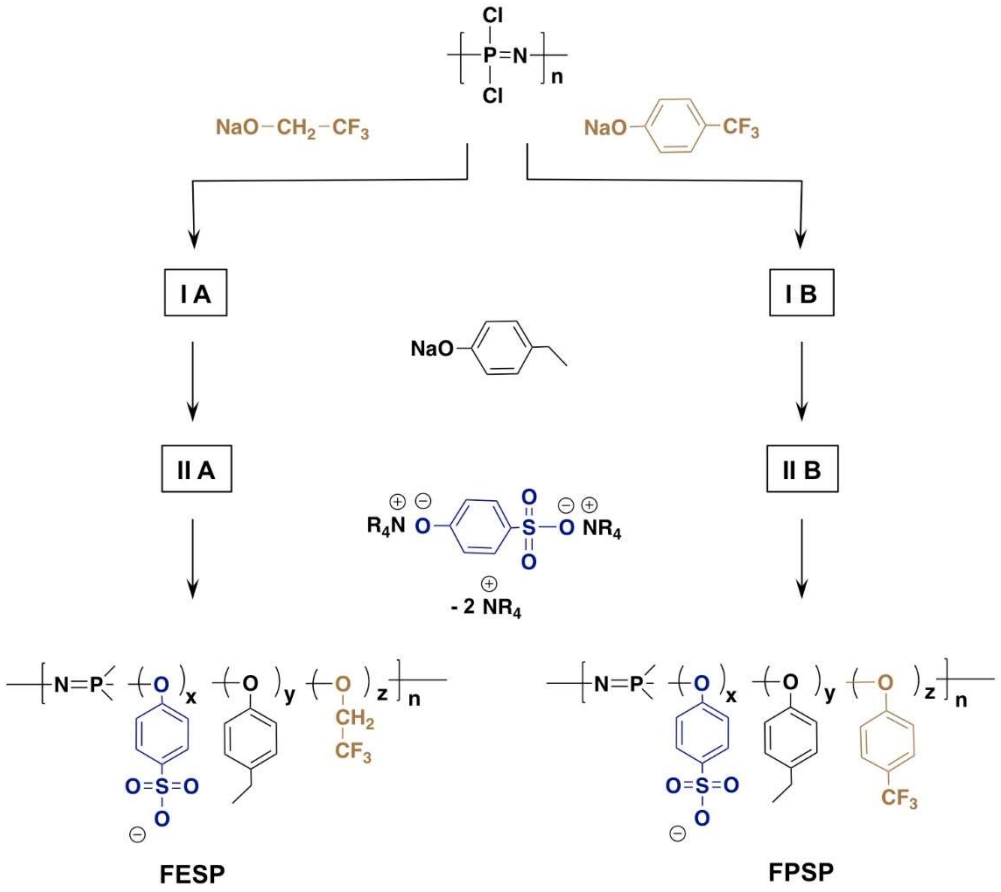

Figure D-1. The reaction pathway to the trifluoroethoxy (FESP) and trifluoromethylphenoxy (FPSP) derivatives of sulfonated PPzs and the schematic representation of their structures. IA, IB, IIA, and IIB are intermediate products - partially substituted PPzs. Reprinted with permission from [323] Copyright 2019 American Chemical Society.

Table D-1 shows data for molecular characteristics of PPzs. Based on ^{1}H NMR for FESP and ^{1}H NMR and ^{13}C NMR for FPSP, both polymers contained approximately 25 % (mol) of sulfonic acid groups and 20 % (mol) of fluorinated pendant groups. Despite the relatively high content of hydrophobic groups, both polymers demonstrated solubility in water in a broad range of pH between 1 and 14. GPC analysis showed single peak

profiles for both polymers, with weight average molar mass of approximately 70,000 g/mol and dispersity of less than 1.5.

Table D-1. Physico-Chemical Characterization of Sulfonated PPzs. Reprinted with permission from [323] Copyright 2019 American Chemical Society.

Polyphosphazene		FESP	FPSP
Content of Pendant Groups* %, mol	p-Sulfophenoxy-	25	28
	Trifluoroethoxy- or Trifluoromethylphenoxy-	20	17
	Ethylphenoxy-	55	55
Molar Masses**	M_w, kg/mol	70.9	69.7
	M_n, kg/mol	44.3	43.4
	Đ	1.43	1.44
D_z,*** nm		49	45

* Based on ^{1}H NMR for FESP and ^{1}H NMR and ^{13}C NMR for FPSP; ** weight-average (M_w), number-average (M_n) molar masses, and dispersity (Đ) were calculated based on gel permeation chromatography (GPC) data; *** z-average hydrodynamic diameter (D_z) was determined by DLS in phosphate buffer (pH 7.4).